UNIVERSITY OF TRENTO

Doctoral School in Civil, Environmental and Mechanical Engineering

Curriculum 3. Modelling and Simulation

Marco Rossi

Dynamics and stability of discrete and continuous structures: flutter instability in piecewise-smooth mechanical systems and cloaking for wave propagation in Kirchhoff plates

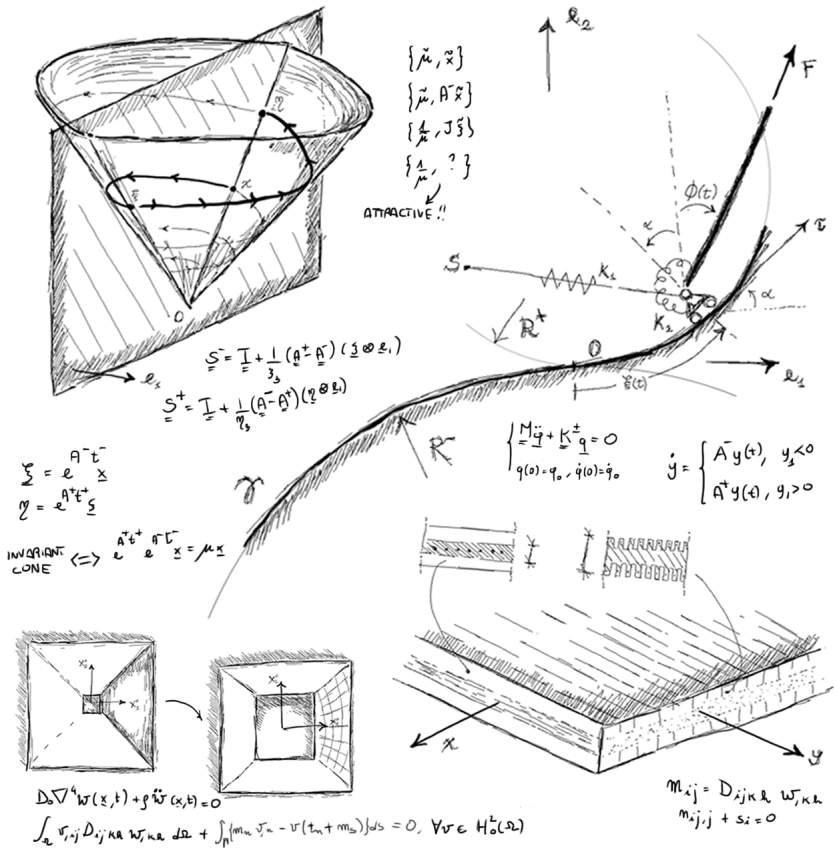

2021 - Doctoral thesis

UNIVERSITY OF TRENTO
DEPARTMENT OF CIVIL, ENVIRONMENTAL, AND MECHANICAL ENGINEERING

DOCTORAL SCHOOL IN
CIVIL, ENVIRONMENTAL, AND MECHANICAL ENGINEERING (DICAM)
Modelling and Simulation – XXXIII cycle

Doctoral Thesis

MARCO ROSSI

Dynamics and stability of discrete and continuous structures: flutter instability in piecewise-smooth mechanical systems and cloaking for wave propagation in Kirchhoff plates

Supervisors:
Prof. D. Bigoni - Prof A. Piccolroaz

San Tomaso Agordino, November 2021

University of Trento
Doctoral School in Civil, Environmental and Mechanical Engineering
http://web.unitn.it/en/dricam
Via Mesiano 77, I-38123 Trento
Tel. +39 0461 282670 / 2611 - *dicamphd@unitn.it*

Dedicated to
my mother Fiorella and my father Tita,
for their example and love

"Benchè le scienze mathematiche siano senza fraude veruna, con tutto ciò sono tanto sagaci, che nascondendosi sotto qualche velo; benchè sottilissimo, fanno parere il negro bianco e il bianco negro, ne quello si può scuoprire con cosa più propria, che con la pratica operando; è ben vero che questa, quando non ha la sua luce, cioè la Theorica, è come cieca e perciò non può scuoprire cosa alcuna"

Tito Livio Burattini *(1617-1681)*
physicist

"Va certo che se un briciolino di tempo mi avanza di buon grado lo spendo, nel poco che valgo, a sbugiardare e distruggere quel: sempre si è fatto così!"

don Antonio Della Lucia *(1824-1906)*
enlightened priest

"E da tosat infin che se vien gris
se cognon vive e mai no sta debant,
el contadin ghe tocca strusià fis,
l'istesso l'artesan sfadiga tant.
Senza patì nogugn va in Paradis:
senza vertù no se deventa Sant:
cossì senza le strussie de la dent,
la tera da so posta no la rent."

Luigi Lazzaris *(1816-1906)*
vernacular poet

Declaration of Authorship

I, Marco Rossi, declare that this Thesis titled, *"Dynamics and stability of discrete and continuous structures: flutter instability in piecewise-smooth mechanical systems and cloaking for wave propagation in Kirchhoff plates"* and the work presented in it are my own. I confirm that:

- This work was done wholly or mainly while in candidature for a research degree at this University.
- Where I have consulted the published work of others, this is always clearly attributed.
- Where I have quoted from the work of others, the source is always given. With the exception of such quotations, this thesis is entirely my own work.
- I have acknowledged all main sources of help.

San Tomaso Agordino, 11th November, 2021

Marco Rossi

ACKNOWLEDGEMENTS

At the end of this wonderful and challenging journey, it's time to thank all the people who accompanied me in this unforgettable adventure in the world of Science.

Traditionally, the first people that must be thanked are the supervisors, Davide Bigoni and Andrea Piccolroaz. Moreover, I express my sincere and profound gratitude to Prof. Massimiliano Gei, not an "official supervisor" but surely a mentor, for his honesty and his support in the second part of this Thesis, dealing with the 'invisibility cloak'. I also thank the other members of the Solid and Structural Mechanics Group, in particular Roberta Springhetti, Diego Misseroni, Fiorella Pantano, and Francesco Dal Corso.

A special thanks goes to the inhabitants of the *Fifth Floor* and the *Independent Reign of Soppalco*, the place where all the ideas on Mechanics are born and developed, an indefatigable smithery of sudden insights, governed by serendipity and strengthened by the logical reasoning of young wonderful guys who do love Science and Research and try to tear the Veil of Maya in *every* field of human knowledge. The mystical beauty of how different thoughts, approaches, perspectives have mixed together and produced sophisticated intellectual outcomes, with no purpose, other than to understand better the world and explain it with mathematical models, was the only thing that help me in the hard moments of my research experience. When you realise that the only fruitful research topic that maximizes your happiness would have been the attempt to freeze the time in order to live these moments forever, you understand that you have found not only colleagues, but friends. I hope that someone, when finally will be conscious of what has been the *Fifth Floor* in the past four years,

will not destroy this indefatigable smithery and try to support it, since this approach leads to relevant results in Research.

I would like to express my sincere gratitude to the "wonderful guys" that I mentioned before: Giovanni, Gianluca, Luca, Riccardo, Alessandro, Matteo, Costanza, Ilaria, Diana, Andrea, Mattia... this journey would not be the same, without you! An additional thanks goes to those who shared with me the pleasant 'scientific dinners', delightful moments in which the problems born in the office were solved in the restaurant, and new and more interesting ones arose (actually, I should also thank the owners of the restaurants, who never closed the door until we finished our discussion!). Therefore, I would like to thank Gianluca, for his contagious optimism and for the infinite amount of chaotic bifurcations that he is able to produce in a single dinner; Luca, for his precious advice and for simply being Luca; Giovanni, who has been an "additional supervisor" as well as a friend, for the long and fruitful discussions regarding every field of human knowledge, from Science to Philosophy, from Politics to Economy, with an only maxim: *don't trust, verify!*

The *Fifth Floor* would not have been the same without the presence of C.d. Ph.D. Eng. Daniele Veber, an "old" mentor for all of us, who naturally passes from complicated functionals for the theoretical definition of computational models to the design of special structural elements, to the classification of all the types of vines cultivations. Thank you, *dear farmer*, for your precious advice, for your suggestions and for being an example for me!

Moreover, other friends accompanied me during these years and I want to sincerely thank Martina, Marco, Piotr, LK, Valentina, Gabriel, Mirko, Zeta, Michele, Daniele, Loris, Nadia, Mary, Rossella, Ilaria, Eleonora, Elena.

A special thanks goes to the friends of the *Coro della Sat*, I am honoured to be a part of this group, to share with other people the atavistic beauty of the ancient music of the mountains.

I would like to express my gratitude to my village, San Tomaso Agordino, perched on the Dolomites in front of the beautiful Civetta, and to all the people living there. The poet J. W. Goethe wrote that *"the mountains are mute masters who make for silent pupils"* and I think that this aphorism really represents my essence. I am a son of the ancient culture of the Dolomites and my behaviour reflects the teachings that I have received in

this wonderful place. Moreover, I would like to thank all the people that in many associations (Pro Loco, Church Choir, etc...) help me to keep my beloved village alive and vital. I would like to express my sincere gratitude to all my relatives and to all the people that always supported me.

Finally, I am immensely indebted to you, Fiorella and Tita, mum and dad, for your unconditional support and constant encouragement during these years, for your love and for being constant examples for me. This thesis is dedicated to you.

San Tomaso Agordino, 11th November, 2021

Marco Rossi
Marote

ABSTRACT

The **first part** of this Thesis deals with the analysis of piecewise-smooth mechanical systems and the definition of special stability criteria in presence of non-conservative follower forces.

To illustrate the peculiar stability properties of this kind of dynamical system, a reference 2 d.o.f. structure has been considered, composed of a rigid bar, with one and constrained to slide, without friction, along a curved profile, whereas the other and is subject to a follower force. In particular, the curved constraint is assumed to be composed of two circular profiles, with different and opposite curvatures, defining two separated subsystems. Due to this jump in the curvature, located at the junction point between the curved profiles, the entire mechanical structure can be modelled by discontinuous equations of motion, the differential equations valid in each subsystem can be combined, leading to the definition of a piecewise-smooth dynamical system.

When a follower force acts on the structure, an unexpected and counterintuitive behaviour may occur: although the two subsystems are stable when analysed separately, the composed structure is unstable and exhibits flutter-like exponentially-growing oscillations. This special form of instability, previously known only from a mathematical point of view, has been analysed in depth from an engineering perspective, thus finding a mechanical interpretation based on the concept of non-conservative follower load.

Moreover, the goal of this work is also the definition of some stability criteria that may help the design of these mechanical piecewise-smooth systems, since classical theorems cannot be used for the investigation of equilibrium configurations located at the discontinuity. In the literature,

this unusual behaviour has been explained, from a mathematical perspective, through the existence of a discontinuous *invariant cone* in the phase space. For this reason, starting from the mechanical system described above, the existence of invariant cones in 2 d.o.f. mechanical systems is investigated through Poincaré maps. A complete theoretical analysis on piecewise-smooth dynamical systems is presented and special mathematical properties have been discovered, valid for generic 2 d.o.f. piecewise-smooth mechanical systems, which are useful for the characterisation of the stability of the equilibrium configurations.

Numerical tools are implemented for the analysis of a 2 d.o.f. piecewise-smooth mechanical system, valid for piecewise-linear cases and extendible to the nonlinear ones. A numerical code has been developed, with the aim of predicting the stability of a piecewise-linear dynamical system *a priori*, varying the mechanical parameters. Moreover, "design maps" are produced for a given subset of the parameters space, so that a system with a desired stable or unstable behaviour can easily be designed.

The aforementioned results can find applications in soft actuation or energy harvesting. In particular, in systems devoted to exploiting the flutter-like instability, the range of design parameters can be extended by using piecewise-smooth instead of smooth structures, since unstable flutter-like behaviour is possible also when each subsystem is actually stable.

The **second part** of this Thesis deals with the numerical analysis of an elastic cloak for transient flexural waves in Kirchhoff-Love plates and the design of special metamaterials for this goal.

In the literature, relevant applications of transformation elastodynamics have revealed that flexural waves in thin elastic plates can be diverted and channelled, with the aim of shielding a given region of the ambient space. However, the theoretical transformations which define the elastic properties of this "invisibility cloak" lead to the presence of a strong compressive prestress, which may be unfeasible for real applications. Moreover, this theoretical cloak must present, at the same time, high bending stiffness and a null twisting rigidity.

In this Thesis, an orthotropic meta-structural plate is proposed as an approximated elastic cloak and the presence of the prestress has been neglected in order to be closer to a realistic design. With the aim of estimating the performance of this approximated cloak, a Finite Element code is

implemented, based on a sub-parametric technique. The tool allows the investigation of the sensitivity of specific stiffness parameters that may be difficult to match in a real cloak design. Moreover, the Finite Element code is extended to investigate a meta-plate interacting with a Winkler foundation, to analyse how the substrate modulus transforms in the cloak region.

This second topic of the Thesis may find applications in the realization of approximated invisibility cloaks, which can be employed to reduce the destructive effects of earthquakes on civil structures or to shield mechanical components from unwanted vibrations.

Acknowledgements:
The author acknowledges Italian Ministry of Education, University and Research (MIUR) for supporting his research under grant PRIN 2015 2015LYYXA8-006.

PUBLISHED PAPERS

The main results presented in this Thesis are summarized in the following papers:

[1] M. Rossi, A. Piccolroaz, and D. Bigoni. "Fusion of two stable elastic structures resulting in an unstable system". *submitted* (2021).

[2] M. Rossi, D. Veber, and M. Gei. "Numerical Assessment of the Performance of Elastic Cloaks for Transient Flexural Waves". *Frontiers in Materials* 7 (2020), p. 603667. DOI: 10.3389/fmats.2020.603667.

Contents

List of Figures

List of Tables

CHAPTER 1

Introduction

"If we knew what we were doing, it wouldn't be called Research"
Albert Einstein

"The truth belongs to those who seek it, not to those who claim to own it"
Nicolas de Caritat, marquis de Condorcet

In the realm of Mechanics, an increasing interest of researchers and engineers is being revealed in the analysis of unexpected mechanical features that dynamical systems may exhibit, concerning both discrete and continuous models for real structures.

In this Thesis, two completely different topics are investigated, from two different perspectives. The first part deals with the theoretical analysis of discrete mechanical systems characterised by an unstable behaviour and presenting a lack of smoothness in the governing differential equations. In the second part, a computational Finite Element model has been developed for the investigation of continuous thin elastic plates, with the aim of shielding a void with respect to flexural waves, using a particular kind of metamaterial that behaves as an "invisibility cloak".

1.1 Part I: stability of piecewise-smooth mechanical systems

1.1.1 State of the art and research challenges

The interest in the analysis of the unstable behaviour of mechanical structures has increased in the last decades, with the double aim of avoiding the

presence of dangerous events, especially in extremely deformable structures which are particularly prone to an abrupt loss of stability, and of realising dynamical systems that exploit the emergence of instability for energy harvesting and soft actuation.

Ziegler [90] described a special form of instability, called *flutter*, which originates in mechanical systems subjected to a particular kind of non-conservative loads: the *follower forces*. Flutter instability, which is defined in the linearised regime for small displacements, is characterised by the presence of oscillations accompanied by an exponential growth in the amplitude. The practical realisation of non-conservative follower forces acting on elastic structures has been investigated in Bigoni *et al.* [6, 7], where experimental results support both the evidence of flutter instability and the so-called "Ziegler's paradox".

From a qualitative and intuitive point of view, the most important feature characterising a follower force is the fact that it is not conservative, since the load depends on the geometry of the current configuration of the analysed system at each time. This special attribute originates the following questions, which are on the basis of the present work:

- *What is the effect of a follower force, when a mechanical system is governed by discontinuous equations of motion?*
- *How can a mechanical system be treated, when the equations of motion are piecewise-smooth?*
- *Can the combination of follower forces with discontinuous systems generate dynamic instability?*
- *Can this combination be used for design purposes?*

The attempt to answer the above-listed questions lead us to the theoretical results on piecewise-smooth dynamical systems found by Carmona *et al.* [16]. In this paper, a counterintuitive and unexpected behaviour is illustrated, namely, a discontinuous set of 3-dimensional first order ODEs showing an unstable behaviour, even when each single subsystem that composes the entire system is stable. The mathematical explanation of this phenomenon is the presence in the state space of a particular invariant set, namely an invariant cone, that describes the behaviour of the system for a given set of initial conditions.

In this Thesis, the link between discontinuous dynamical systems and non-conservative loads is elucidated, with the aim of reproducing in a real mechanical system the unexpected behaviour found by Carmona *et al.* with reference only to purely mathematical systems. In addition, the theoretical investigation of piecewise-smooth dynamical systems allows us to translate the mathematical concepts into mechanical tools that can help engineers to define general instability criteria for at least a subset of piecewise-smooth mechanical systems. Following this idea, we open a new way to the design of structures with peculiar dynamical behaviour, to be used for energy harvesting or as soft devices.

A special 2 d.o.f. mechanical system has been chosen as a reference structure, see Figure 1.1, taking inspiration from the work of Bigoni *et al.* [4] and Misseroni *et al.* [67], where a mechanical system is analysed, characterized by a doubly circular profile as constraint, and subjected to a dead load. The extension of this case to follower forces has been the starting point of the present work on piecewise-smooth systems since the doubly circular profile can be studied as the junction between two separately smooth subsystems.

Two main approaches can be found in the literature concerning the theoretical analysis of piecewise-smooth dynamical systems. The first one regards the exploration of discontinuous phenomena like impact, unilateral constraints, and friction, [1, 9, 38]. This approach has a strong numerical component and its main focus is the identification of the behaviour of complex mechanical systems, with discontinuous constitutive relations, treated via Convex Analysis. The second one, adopted in the present Thesis, is more mathematically oriented, so that an extension is pursued of classical results of analytical dynamics to the case of piecewise dynamical systems. Our focus is the theoretical analysis of simple mechanical systems with few degrees of freedom and the classification of all the possible bifurcation conditions [33, 62, 63].

One of the advantages of this second approach is its versatility, so that many analysed concepts can be adopted in many different fields of application, as for instance electronics [2, 36], or biology [81]. Hence, the problems that have been solved in other fields can be used to guide solutions in mechanics. The main disadvantage of the method is the growth in the number of different configurations emerging already in dynamical system at low dimensions, [28, 29, 80]. The mere classification of the

great number of possible bifurcations may become sometimes even useless, as reported for instance by Glendinning [37]. Therefore we will avoid long classification procedures, preferring to this approach a more practical *modus operandi*, where a few simple cases are involved.

A milestone in the analysis of piecewise-smooth dynamical system is certainly the work of the Russian mathematician Aleksei Fedorovich Filippov, see [32], who gave solid theoretical foundations to the analysis of dynamical systems described by first order ODEs with discontinuous right-hand-side, using concepts from Convex Analysis.

Two main "schools" emerge in the theoretical analysis of piecewise-smooth dynamical systems. The first, represented by Carmona, Freire, Ponce, and Llibre [1] [14, 15, 17, 18, 61, 64, 65], adopts a strict mathematical perspective, thus analysing the theoretical conditions that lead to a particular dynamical behaviour. The second, represented by Küpper, Weiss, and Hosham [41, 51, 52, 86, 87], has developed a more practical approach to the analysis of piecewise-linear and nonlinear system. Actually, both schools deal with the analysis of piecewise systems from a theoretical point of view, but slight differences make one approach or the other preferable in specific cases. In particular, Carmona *et al.* has been followed to define the structure representing our case study, while Küpper *et al.* has been referred for the implementation of the numerical codes developed for solving the structure.

The translation of the above mentioned mathematical tools to the field of mechanics required the non-trivial discovery of a structure behaving in a way compatible with the developed theories. Often the described mathematical approaches are too general on the one hand, while they require fulfilment of other specific properties, not valid for mechanical systems, on the other. For example in [42], a dynamical system with the same dimension of the reference structure is considered, but the results cannot be used directly by us, because of the too strong hypotheses not fulfilled for a mechanical system. Moreover, the purpose of these theoretical works is to *show* a particular interesting behaviour; on the contrary, the aim of this Thesis is the definition of a possible strategy to *design* a mechanical system

[1] I sincerely thank Professor E. Ponce and J. Llibre, together with Professor Marco Sabatini who puts us in contact, for their help and advice on the mathematical part of this topic.

with the required performance.

Analyses of discontinuous mechanical systems completely different from those analysed in this work (for instance referred to unilateral contact or contact with friction) can be found in the literature, see for example [47, 56], and in particular [43, 92] where invariant cones are also addressed. However, the main purpose of this Thesis is to create a link between follower loads and systems with simple discontinuities in the equations of motion, not covered in the aforementioned papers.

1.1.2 Outline of part I

Chapter 2 begins with an introduction on the analysis of smooth systems, necessary to provide a theoretical background, where basic concepts of analytical dynamics are briefly exposed. In the second part of Chapter 2, the theoretical tools for smooth systems are extended to cover also the case of piecewise-smooth mechanics. Some features, typical of discontinuous systems, are described, together with a summary of the general setting proposed by Filippov for the analysis of discontinuous ODEs.

The investigation of dynamical systems showing the unexpected behaviour described by Carmona *et al.* [16] begins with the analysis of a reference structure, presented in Chapter 3. This mechanical system, similar to those studied in [4], is made up of a rigid bar with an end constrained to move, without friction, on a curved constraint, composed of two circular profiles, see Figure 1.1. The other end is subjected to a follower force, remaining always parallel to the bar, and two springs, one longitudinal and one rotational are present to provide an elastic constraint on the structure. The equations of motion for this mechanical system are obtained in a Lagrangian description for a generic smooth curved profile, then the two special cases of circular constraints with positive and negative curvature are investigated, in terms of stability behaviour of the single equilibrium point of the structure. The equations of motion of the piecewise-smooth mechanical system obtained by the composition of the two curved profiles are finally derived, both for the linear and nonlinear case. The equations of motion are also transformed into a Hamiltonian formulation so that the 2 d.o.f. mechanical system can be described by a set of 4-dimensional first order ODEs.

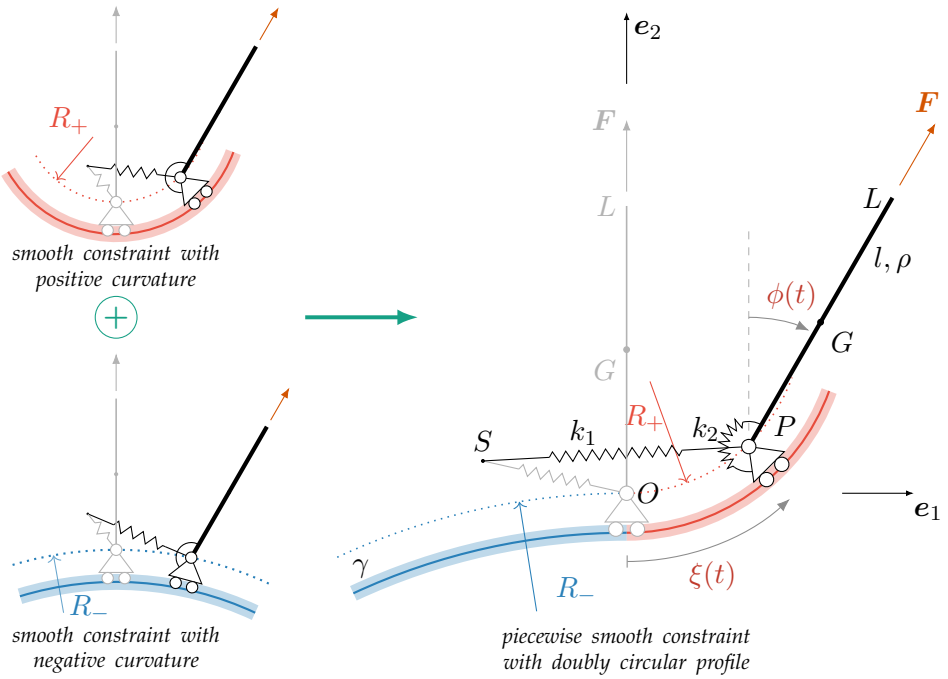

Figure 1.1: The reference piecewise mechanical structure is composed of a rigid bar with one end constrained to move on a doubly circular profile without friction, while the other end is subjected to a follower force. This system can be seen as the composition of two subsystems with smooth profiles having different and opposite curvatures. The stability of an equilibrium configuration located on the discontinuity of the joined system cannot be deduced from the analysis of each single subsystem, since an unstable behaviour of the entire structure is possible also when the subsystems are separately stable.

In Chapter 4, theoretical results are presented on piecewise-linear systems. A generic 2 d.o.f. linear *mechanical* system is considered, derived from the linearisation of the equations of motion for each single subsystem. When the two subsystems are stable, the presence of an unstable behaviour in the assembled structure is associated with the existence of an invariant cone that fulfils certain given properties. These lead to the definition of an instability criterion, valid for 2 d.o.f piecewise-linear mechanical

systems. Moreover, the attractivity of the cone is finally investigated and, in particular, some theoretical results are given.

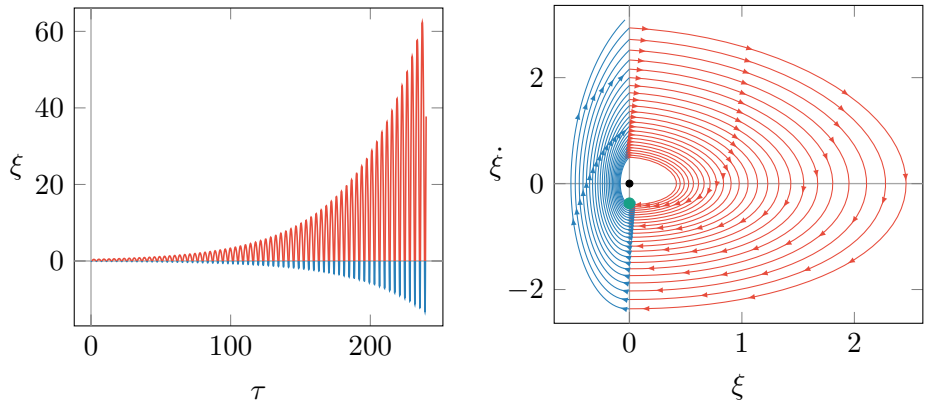

Figure 1.2: Example of the behaviour of the reference mechanical system when an unstable invariant cone is detected, see Section 6.1.1. On the left, the exponential growth in the amplitude of the Lagrangian generalised coordinate ξ is plotted as a function of the non-dimensional time τ. On the right, a phase portrait is depicted, where a projection of the 4D invariant cone onto a 2D plane reveals the unstable behaviour of the equilibrium configuration located at the origin.

The theoretical results are in general valid for 2 d.o.f. mechanical systems, which can be obtained by the merging of two stable subsystems. These results are implemented in a numerical tool in Chapter 5, tailored for the explicit computation of invariant cones. A numerical algorithm for the detection of the aforementioned invariant set is developed and the solutions of some critical aspects of the proposed computational scheme are described and solved. Due to the piecewise-linear structure of the problem, the step-by-step solution of the nonlinear system can be avoided and some results on the existence and properties of invariant cones can be obtained *a priori*. This possibility may greatly help a designer in the realisation of a specific structure with required behaviour, since the space of design parameters can be explored and, at each point, our numerical algorithm is capable of detecting the presence of this particular form of instability.

The mechanical structure defined in Chapter 3 is then analysed in

Chapter 6, where numerical results are presented, obtained using the computational tool developed in Chapter 5. Paradigmatic examples are presented, to show that the algorithm gives results that are in agreement with theoretical predictions and to prove that the considered structure composed of a doubly circular profile is a mechanical system that reveals the unexpected and counterintuitive behaviours described by Carmona [16].

1.2 Part II: cloaking of flexural waves in thin elastic plates

1.2.1 State of the art and research challenges

The control of elastic waves to cloak a region of the ambient space has been shown achievable by transformation elastodynamics, which provides the mechanical properties of the material surrounding the region [11, 66, 72]. A relevant application of this broad area is the control of transverse waves in plates, for which solutions have been proposed mainly based on two approaches: a "passive" one, where the features of the cloak are achieved by a given microstructure [10, 24, 25, 30, 31, 60, 69, 89] and an "active" one, in which tunable quantities depending on the actual mechanical input are employed for the same goal (see e.g. [19, 34, 71, 73]). Experiments have been also proposed to validate some of the previous theoretical proposals [26, 68, 69, 83]. Most of these investigations show that this technique can be feasible and likely to be employed in centimetre-size real-life systems with wave frequencies in the order of a few kHz.

Within the set of attempts based on the "passive" approach, [25] proposed a transformation to conceive a Kirchhoff-Love plate theory for cloaking flexural waves. The resulting governing equations for the thin plate in the transformed domain involve the presence of variable (in space) bending and torsional stiffnesses, and density, in addition to the presence of in-plane body forces and prestresses in the plate. In the same paper, the general framework was specialised to the case of a square cloak composed of four trapezoidal elements (see Figure 1.3) embedded in an isotropic, homogeneous domain. For this geometry, a set of relationships was established to provide explicit expressions of the quantities concerned in each part of the cloak. The broadband effectiveness of the metamaterial plate

cloak was then assessed by means of numerical tests.

The features of the suggested meta-structure can be summarised as follows:

(i) the cloak is locally an orthotropic thin plate with principal directions varying point-to-point. These directions obey the geometric symmetries of the domain (see, e.g., trapezoid $\mathcal{C}^{(1)}$ displayed in Figure 1.3, where the principal directions are sketched with thin lines). In the same figure, the increase of the out-of-alignment of the local principal system with the axis of symmetry towards the diagonals of the cloak can be noticed;

(ii) by investigating how the stiffnesses of the plate in the orthotropic principal system depend on the position and thinking to construct the plate with a homogeneous material, it turns out that the thickness of the plate must assure an increase in bending stiffness along the direction parallel to the inner boundary of the cloak moving away from the axis of symmetry of each trapezoid and a decrease of the bending stiffness along the "radial" direction moving towards the centre of the cloak. These two requirements are apparently in contradiction, but they must be addressed in an effective design;

(iii) the twisting stiffness in the principal system of orthotropy *vanishes* at each point of the domain;

(iv) the mass density of the cloak is not constant and varies with the Jacobian of the transformation; in particular, this quantity decreases by approaching the inner boundary of the cloak;

(v) in-plane body forces and prestresses in the interior of the domain as well as forces per unit length applied along the diagonals of the cloak are necessary to warrant equilibrium. The predicted prestress is compressive in a large part of the domain with values that are likely to exceed the buckling threshold for the thin structure.

The set of listed properties demonstrates that the design and engineering of an effective cloak for flexural waves based on transformation elastodynamics of Kirchhoff-Love plates is an exceptional challenge. Actually, the presence of severe compressive prestresses leads to the conclusion that

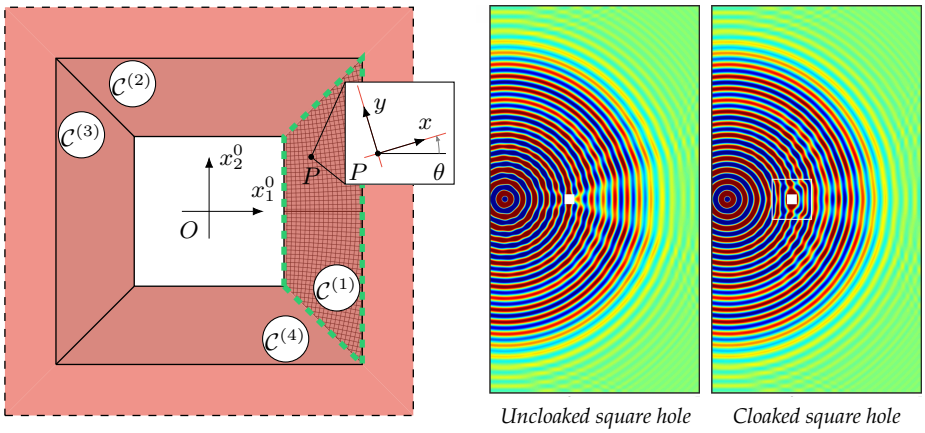

Figure 1.3: On the left, sketch of the reference problem, namely a square hole coated by a square cloak composed of four trapezoids. On the right, numerical results evidencing the effect of the invisibility cloak on the propagation of flexural waves near the hole.

it is impossible to construct a stable, ideal cloak. Therefore, an approach based on carefully considered approximations is required to achieve the goal. In the experimental test conducted by [68], for instance, the design of the approximated cloak has focused mainly on the match of bending stiffnesses along the directions of orthotropy.

Moving from the points raised in the just edited list, the goal of this Thesis is four-fold:

(i) the first aim is to design and implement a fully open in-house FE code, based on a subparametric technique, to simulate transient wave propagation in locally orthotropic Kirchhoff-Love plates;

(ii) the numerical tool is then exploited to assess the performance of meta-structural square cloaks designed by assuming reasonable approximations (prestress free, local twisting stiffness as limited as possible, cross-sections of the plate ensuring the required local bending stiffnesses, non-constant mass density);

(iii) the same tool is employed to investigate the role of certain stiffness parameters, i.e. twisting and coupling bending stiffnesses;

(iv) in addition, a non-secondary purpose of the paper is to propose an extension of the theory to encompass interaction of the cloak with an elastic substrate modelled with a Winkler foundation and assess its effectiveness.

1.2.2 Outline of part II

In the first part of Chapter 7, the theory regarding the application of transformation elastodynamics to the case of thin elastic plates has been introduced, as well as the reference case that will be investigated in depth through the Finite Element Method. Then, all the elastic properties of the cloak are computed from an analytical point of view, for the considered transformation. In the second part of Chapter 7, the application of the Galerkin method for the definition of a Finite Element computational model is outlined. In particular, all the steps required for the passage from the mathematical to the numerical model are described in detail.

The reference problem is then solved in Chapter 8, using the aforementioned computational tool, and the most important features of the solution are investigated. In particular, the displacement field with different values of load frequencies is computed and a sensitivity analysis is performed on the theoretical stiffness parameters. To quantitatively understand the behaviour of the designed approximated cloak, a "quality measure" is introduced and several examples are analysed. Furthermore, the presence of a Winkler's soil is considered, in order to understand the performance of the cloak in a more realistic case. Finally, a first example of a microstructure capable of approximating the features of the theoretically predicted cloak is presented at the end of Chapter 8. This last case must be intended as a starting point for future developments on this interesting topic.

PART I

Flutter instability in piecewise-smooth mechanical systems

CHAPTER 2

Introduction to smooth and non-smooth dynamics

"A scientist worthy of his name, about all a mathematician, experiences in his work the same impression as an artist; his pleasure is as great and of the same nature"

Jules Henri Poincaré

The aim of this introductory Chapter is to provide to the Reader all the theoretical notions useful for the analysis of dynamical systems.

The first Section 2.1 is mainly devoted to the definition of all the general features useful in the investigation of smooth dynamical systems, e.g. the concept of stability and bifurcation of a solution and the definition of invariant set. The themes discussed in this part are classical topics in the field of Analytical Mechanics, see for example [49, 54, 58, 74, 90].

The aforementioned concepts are then extended in the second Section 2.2, to deal with piecewise-smooth and piecewise-linear dynamical systems. As for the mathematical foundations, a reference work is the book written by Filippov [32], while a modern framework on this topic can be found in Simpson [82] and, in particular, in the books of Di Bernardo *et al.* [27] (with a more theoretical perspective) and Leine *et al.* [57] (having a more practical point of view).

2.1 Smooth dynamical systems

2.1.1 Mathematical model of a smooth dynamical system

The evolution in time of a smooth dynamical system can be described by a first order ordinary differential equation of the form

$$\dot{\boldsymbol{y}}(t) = \boldsymbol{f}(t, \boldsymbol{y}), \tag{2.1}$$

with initial conditions

$$\boldsymbol{y}(t_0) = \boldsymbol{y}_0, \tag{2.2}$$

where $\boldsymbol{y}(t) \in \mathbb{R}^n$ is the vector of generalized coordinates, $\dot{\boldsymbol{y}}(t) = d\boldsymbol{y}/dt$ is the derivative with respect to the independent variable time $t \in \mathbb{R}$, $\boldsymbol{f} : \mathbb{R} \times \mathbb{R}^n \to \mathbb{R}^n$ is a non-linear smooth vector function $\boldsymbol{f} \in \mathcal{C}^2$, and t_0 is a reference time in which the value of the coordinate vector $\boldsymbol{y_0}$ is known.

When the vector field $\boldsymbol{f}$ explicitly depends on time, the dynamical system is called *non - autonomous*, otherwise it is defined *autonomous* and it is described by the following Cauchy problem

$$\dot{\boldsymbol{y}}(t) = \boldsymbol{f}(\boldsymbol{y}(t)), \qquad \boldsymbol{y}(0) = \boldsymbol{y}_0. \tag{2.3}$$

In the latter case, the specific value of the reference time t_0 is not important in the description of the solution, therefore a simple time translation can be performed in order to assume, without loss of generality, $t_0 = 0$.

Definition 1 (see [54, 74, 88]). The dynamical system (2.1) is called *linear* if the vector field $\boldsymbol{f}(t, \boldsymbol{y})$ is linear in $\boldsymbol{y}$.

Definition 2 (see [54, 74, 88]). The system (2.1) is called *time periodic* if there exists T such that $\boldsymbol{f}(t + T, \boldsymbol{y}) = \boldsymbol{f}(t, \boldsymbol{y})$, for all t and $\boldsymbol{y}$, and the minimum value of T that fulfils this relation is called *period*.

The solution of (2.1) with initial conditions (2.2) can generally be written as $\boldsymbol{y}(t) = \boldsymbol{\varphi}_t(t_0, \boldsymbol{y}_0)$, where the parametric function $\boldsymbol{\varphi}_t : \mathbb{R} \times \mathbb{R}^n \to \mathbb{R}^n$, calculated for a specific time t is called *evolution operator* (since it describes how the system evolves in time from the initial state $\boldsymbol{y}(t_0) = \boldsymbol{y}_0$ to the considered state $\boldsymbol{y}(t)$ at time t), while the one-parameter family of maps $\boldsymbol{\varphi}_t$ parametrised by t is called *flow*. The set of points

$$\gamma = \{\boldsymbol{\varphi}_t(t_0, \boldsymbol{y}_0) \in \mathbb{R}^n : -\infty < t < \infty\}$$

is called *trajectory* or *orbit* passing through the initial condition $\boldsymbol{y}_0$ at time t_0, see [74]. The *phase portrait* is a graphical representation of the evolution of the dynamical system and it consists of a collection of orbits for given initial conditions.

Definition 3. An *equilibrium point* (also called *fixed point*) $\boldsymbol{y}^*$ of an autonomous system is a particular solution of (2.3), which is constant in time, i.e. $\boldsymbol{y}(t) = \boldsymbol{\varphi}_t(t_0, \boldsymbol{y}^*) = \boldsymbol{y}^*$, for all t.

The vector field calculated in the equilibrium points vanishes, namely $\boldsymbol{f}(\boldsymbol{y}^*) = \boldsymbol{0}$, and this is the condition that generally must be imposed to detect the fixed points.

Definition 4 (see [74])**.** A solution of the autonomous system (2.3) is called a *periodic solution* if $\boldsymbol{\varphi}_{t+T}(\boldsymbol{y}_0) = \boldsymbol{\varphi}_t(\boldsymbol{y}_0)$, for all t, and the minimum T for which this relation is fulfilled is called *period*.

Let's note that all the points on the trajectory describing a periodic solution can be chosen as initial conditions, yielding the same solution. A periodic orbit is defined *isolated* if in the neighbourhood of this orbit no other periodic solutions are present.

Definition 5 (see [74])**.** An isolated periodic orbit of an autonomous dynamical system is also called *limit cycle*.

Definition 6 (see [74])**.** A solution of the autonomous system (2.3) is called a *quasi-periodic solution* if it can be expressed as a countable sum of periodic solutions

$$\boldsymbol{y}(t) = \sum_j \boldsymbol{\psi}_j(t),$$

where each $\boldsymbol{\psi}_j(t)$ has a specific period T_j and frequency $\varphi_j = 1/T_j$. Furthermore, there must exist a finite set of linearly independent base frequencies $\{\hat{\varphi}_1, \hat{\varphi}_2, \dots \hat{\varphi}_k\}$, so that each φ_j can be written as an integer linear combination of the elements of the basis.

The orbits of a $k-$periodic solution (i.e. a quasi-periodic solution with k base frequencies) of a dynamical system describe a $k-$dimensional torus (also called $k-$torus) in the $n-$dimensional phase space, see [54, 74, 88].

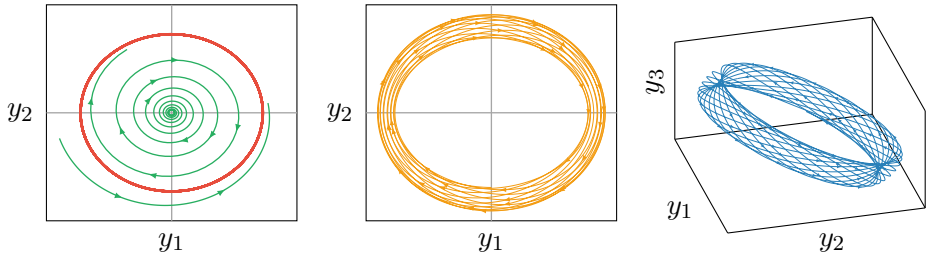

(a) *limit cycle* **(b)** *2D projection of a torus* **(c)** *3D projection of a torus*

Figure 2.1: Examples of possible solutions for an autonomous dynamical system. The red isolated periodic solution in Figure 2.1a is a limit cycle, while the orbits in Figure 2.1b and 2.1c are the 2D and 3D projections of a torus embedded in a 4-dimensional phase space (the single positive system analysed in 6.1.1).

2.1.2 Solution of linear autonomous systems

The solution $\boldsymbol{y}(t) = \boldsymbol{\varphi}_t(\boldsymbol{y}_0)$ of the autonomous dynamical system (2.3) cannot generally be written in a closed-form for a generic vector field $\boldsymbol{f}(\boldsymbol{y})$. However, when the dynamical system is described by a set of linear ODEs, see Definition 1, such that

$$\dot{\boldsymbol{y}}(t) = \boldsymbol{A}\boldsymbol{y}(t), \qquad \boldsymbol{y}(0) = \boldsymbol{y}_0, \tag{2.4}$$

where A is an $n \times n$ time-independent real matrix, the solution can be written as a function of the initial conditions as

$$\boldsymbol{y}(t) = e^{\boldsymbol{A}t}\boldsymbol{y}_0.$$

We introduced the so-called *matrix exponential* $e^{\boldsymbol{A}t}$, which is the analogous of an exponential function in the field of matrices and whose formal definition is

$$e^{\boldsymbol{A}t} := \boldsymbol{I} + \boldsymbol{A}t + \frac{1}{2!}\boldsymbol{A}^2t^2 + \cdots = \sum_{j=0}^{\infty} \frac{1}{j!}\boldsymbol{A}^j t^j, \tag{2.5}$$

see [3, 57, 58]. Let's note that if we apply the definition (2.5) to a diagonal matrix $\boldsymbol{A} = \text{diag}\{a_1, a_2, \ldots, a_n\}$, the result is simply a diagonal matrix, whose elements are the exponentials of the original elements, namely,

$e^{\boldsymbol{A}} = \text{diag}\{e^{a_1}, e^{a_2}, \dots, e^{a_n}\}$. On the contrary, in case of a full matrix, the matrix exponential is not a simple application of the exponential function to each element of the matrix and the definition in (2.5) must be used to determine its form.

For this purpose, the reduction of the matrix $\boldsymbol{A}$ to its canonical Jordan form can be a straightforward way for the explicit calculation of the matrix exponential. In fact, there exists an invertible matrix $\boldsymbol{U} \in \mathbb{C}^{n\times n}$, such that $\boldsymbol{A} = \boldsymbol{U}\overline{\boldsymbol{A}}\boldsymbol{U}^{-1}$, where $\overline{\boldsymbol{A}}$ is the Jordan canonical form of $\boldsymbol{A}$ (see Appendix A for more details)

$$\overline{\boldsymbol{A}} = \begin{bmatrix} \boldsymbol{J}_1 & \boldsymbol{0} & \cdots & \boldsymbol{0} \\ \boldsymbol{0} & \boldsymbol{J}_2 & \cdots & \boldsymbol{0} \\ \vdots & \vdots & \vdots & \vdots \\ \boldsymbol{0} & \boldsymbol{0} & \cdots & \boldsymbol{J}_m \end{bmatrix}.$$

For a matrix expressed in its canonical Jordan form, the following property is fulfilled

$$e^{\boldsymbol{A}t} = \boldsymbol{U}e^{\overline{\boldsymbol{A}}t}\boldsymbol{U}^{-1}$$

and due to the diagonal-block-structure of $\overline{\boldsymbol{A}}$, the matrix exponential $e^{\overline{\boldsymbol{A}}t}$ can easily be computed from the definition (2.5) as

$$e^{\overline{\boldsymbol{A}}t} = \sum_{j=0}^{\infty} \frac{t^j}{j!} \begin{bmatrix} \boldsymbol{J}_1 & \boldsymbol{0} & \cdots & \boldsymbol{0} \\ \boldsymbol{0} & \boldsymbol{J}_2 & \cdots & \boldsymbol{0} \\ \vdots & \vdots & \vdots & \vdots \\ \boldsymbol{0} & \boldsymbol{0} & \cdots & \boldsymbol{J}_m \end{bmatrix}^j = \begin{bmatrix} e^{\boldsymbol{J}_1 t} & \boldsymbol{0} & \cdots & \boldsymbol{0} \\ \boldsymbol{0} & e^{\boldsymbol{J}_2 t} & \cdots & \boldsymbol{0} \\ \vdots & \vdots & \vdots & \vdots \\ \boldsymbol{0} & \boldsymbol{0} & \cdots & e^{\boldsymbol{J}_m t} \end{bmatrix}.$$

Thereby, the computation of the exponential of the entire matrix reduces to the calculation of the exponential of each Jordan block, whose structure has been defined in Appendix A. When the Jordan sub-blocks are diagonal matrices, the computation of the matrix exponential is trivial, otherwise more calculations must be performed.

The q-dimensional non-diagonal Jordan sub-block

$$\boldsymbol{J}_h = \begin{bmatrix} \lambda_h & 1 & 0 & \cdots & 0 & 0 \\ 0 & \lambda_h & 1 & \cdots & 0 & 0 \\ 0 & 0 & \lambda_h & \cdots & 0 & 0 \\ \vdots & \vdots & \vdots & \vdots & \vdots & \vdots \\ 0 & 0 & 0 & \cdots & \lambda_h & 1 \\ 0 & 0 & 0 & \cdots & 0 & \lambda_h \end{bmatrix} \tag{2.6}$$

can be decomposed into the sum

$$\boldsymbol{J}_h = \lambda_h \boldsymbol{I} + \boldsymbol{N},$$

where $\boldsymbol{I}$ is the identity matrix and

$$\boldsymbol{N} = \begin{bmatrix} 0 & 1 & 0 & \cdots & 0 & 0 \\ 0 & 0 & 1 & \cdots & 0 & 0 \\ 0 & 0 & 0 & \cdots & 0 & 0 \\ \vdots & \vdots & \vdots & \vdots & \vdots & \vdots \\ 0 & 0 & 0 & \cdots & 0 & 1 \\ 0 & 0 & 0 & \cdots & 0 & 0 \end{bmatrix}$$

is a nilpotent matrix of order q, i.e. $\boldsymbol{N}^k = 0$, with $k \geq q$. Let's note that for $1 \leq k < q$ the power of the nilpotent matrix $\boldsymbol{N}^k$ is the matrix whose elements are equal to 1 on the k-th superdiagonal, and 0 otherwise.

A fundamental property of a matrix exponential is that, given two matrices $\boldsymbol{A}$ and $\boldsymbol{B}$, if $\boldsymbol{AB} = \boldsymbol{BA}$, then $e^{\boldsymbol{A}+\boldsymbol{B}} = e^{\boldsymbol{A}} e^{\boldsymbol{B}}$. The matrices $\lambda_h \boldsymbol{I}$ and $\boldsymbol{N}$ obviously fulfil this condition, hence

$$e^{\boldsymbol{J}_h t} = e^{\lambda_h t \boldsymbol{I} + \boldsymbol{N} t} = e^{\lambda_h \boldsymbol{I} t} e^{\boldsymbol{N} t} = e^{\lambda_h t} \boldsymbol{I} e^{\boldsymbol{N} t} = e^{\lambda_h t} \sum_{j=0}^{q-1} \frac{t^j}{j!} \boldsymbol{N}^j =$$

$$e^{\lambda_h t} \left[\boldsymbol{I} + t\boldsymbol{N} + \frac{t^2}{2!} \boldsymbol{N}^2 + \cdots + \frac{t^{q-1}}{(q-1)!} \boldsymbol{N}^{q-1} \right],$$

where the properties of a nilpotent matrix of order q have been used to reduce the infinite sum in expression (2.5) to a finite one. Finally, the structure of the powers of the nilpotent matrix $\boldsymbol{N}$ is well-known, so the matrix exponential of the considered Jordan block (2.6) is

$$e^{\boldsymbol{J}_h t} = e^{\lambda_h t} \begin{bmatrix} 1 & t & \frac{t^2}{2!} & \frac{t^3}{3!} & \cdots & \frac{t^{q-2}}{(q-2)!} & \frac{t^{q-1}}{(q-1)!} \\ 0 & 1 & t & \frac{t^2}{2!} & \cdots & \frac{t^{q-3}}{(q-3)!} & \frac{t^{q-2}}{(q-2)!} \\ 0 & 0 & 1 & t & \cdots & \vdots & \frac{t^{q-3}}{(q-3)!} \\ 0 & 0 & 0 & 1 & \cdots & \vdots & \vdots \\ \vdots & \vdots & \vdots & & \vdots & \vdots & \vdots \\ 0 & 0 & 0 & & \cdots & 1 & t \\ 0 & 0 & 0 & & \cdots & 0 & 1 \end{bmatrix}$$

The derivative in time of the matrix exponential defined in (2.5) is equal to

$$\frac{d}{dt}e^{\boldsymbol{A}t} = \boldsymbol{A}e^{\boldsymbol{A}t} = e^{\boldsymbol{A}t}\boldsymbol{A},$$

see [3], therefore it is now clear why an ansatz in the form $\boldsymbol{y}(t) = e^{\boldsymbol{A}t}\boldsymbol{b}$ (where $\boldsymbol{b}$ is an undetermined constant vector) can be chosen as a solution of the linear autonomous system (2.4). Finally, the imposition of initial conditions leads to $\boldsymbol{b} = \boldsymbol{y}_0$.

Let's note that for autonomous systems a shift in time is always allowed, so, in this case, the time t in the matrix exponential actually can be substituted by a time interval from the initial condition. Hence, for a general initial reference time t_0, the correct form for the solution is $\boldsymbol{y}(t) = e^{\boldsymbol{A}(t-t_0)}\boldsymbol{y}(t_0)$.

The determination of the solution of a linear autonomous system can be performed from a more physical point of view (an approach that is common especially in the realm of Structural Analysis for engineers), considering the eigenmodes in which the solution can be decomposed.

If the ansatz $\boldsymbol{y}(t) = c_i e^{\lambda_i t}\boldsymbol{u}_i$ is considered and substituted into the ODEs (2.4), then the following problem must be solved

$$(\boldsymbol{A} - \lambda_i \boldsymbol{I})\,\boldsymbol{u}_i = 0,$$

where clearly the scalars λ_i (the vectors $\boldsymbol{u}_i$) can be interpreted as the eigenvalues (eigenvectors) of the matrix $\boldsymbol{A}$. When an eigenvalue λ_i of $\boldsymbol{A}$ has an algebraic multiplicity r_i greater that 1, the secular terms $t^p e^{\lambda_i t}$ appear in the solution together with the term $e^{\lambda_i t}$, with $p = 1, 2, \ldots, r_i - 1$. According to this approach, a general solution of a linear dynamical system can be interpreted as a sum of fundamental solution, called *eigensolutions*,

$$\boldsymbol{y}(t) = \sum_{i=1}^{n} c_i e^{\lambda_i t}\boldsymbol{u}_i$$

and the coefficients c_i can be determined imposing the fulfilment of initial conditions, see [57].

Actually, this latter interpretation of the solution can be linked to the former that involves the fundamental solution matrix. The n-dimensional linear problem (2.4) admits n linearly independent solutions and the sum

of them is still a solution of the ODEs, due to linearity. These linearly independent solutions can be assumed to be equal to a linear combination of the eigenmodes, i.e. $\boldsymbol{\phi}_i(t) = \sum_{j=1}^{n} b_j e^{\lambda_j t} \boldsymbol{u}_j$, where in this case the coefficients b_j have a different meaning with respect to the previously used c_i coefficients. In fact, while the c_i are fixed by the initial conditions of (2.4) in order to define the combination of modes that produces the complete solution $\boldsymbol{y}(t)$, the b_j are fixed in order to obtain n linearly independent solutions $\boldsymbol{\phi}_i(t)$, since in this case the linear combination of the $\boldsymbol{\phi}_i(t)$ leads the final solution $\boldsymbol{y}(t)$. For example, the b_i can be fixed in order to have $\boldsymbol{\phi}_i(0) = \boldsymbol{e}_i$, where $\boldsymbol{e}_i$ is the unit vector defining an orthonormal basis. If we gather all the independent solutions $\boldsymbol{\phi}_i(t)$ in a matrix by columns

$$\boldsymbol{\Phi}(t) = [\boldsymbol{\phi}_1(t) \quad \boldsymbol{\phi}_2(t) \quad \cdots \quad \boldsymbol{\phi}_n(t)]$$

and we consider the condition presented above for the determination of the b_j, the problem (2.4) becomes

$$\dot{\boldsymbol{\Phi}}(t) = \boldsymbol{A}\boldsymbol{\Phi}(t) \qquad \boldsymbol{\Phi}(0) = \boldsymbol{I} \tag{2.7}$$

and the solution of this matrix ordinary differential equation is the matrix exponential $\boldsymbol{\Phi}(t) = e^{\boldsymbol{A}t}$. Any matrix that fulfils the equation (2.7) is called *fundamental solution matrix* for the linear problem (2.4).

Therefore, the link between the two perspectives presented above for the interpretation of the solution of a linear dynamical system has been clarified, in fact, a different interpretation of the eigenmode method leads to a differential problem whose solution is the matrix exponential $e^{\boldsymbol{A}t}$.

As a final remark, the possibility of computing the solution of a linear system in a closed form is crucial to understand the behaviour of essentially all dynamical systems. In fact, as will be described in depth in Section 2.1.3, both the original differential problem and the associated variational problem that describes the behaviour of a perturbed solution near a reference one (fixed point, limit cycle, ...) can be linearised in a form similar to (2.4). Since the concept of stability of a reference solution is strictly related to the evolution of the perturbed orbits, the linear analysis of the perturbations is enough in most cases for the determination of the qualitative behaviour of a dynamical system.

2.1.3 Stability criteria for fixed points

An important property of a solution of (2.3) is its *stability*, which essentially describes the behaviour of the dynamical system in the neighbourhood of the considered solution, i.e. it defines the qualitative motion of the system for small perturbation of the initial conditions. For this reason, the concept of stability is strictly related to the concept of perturbation of a given solution, see [58].

The easiest solutions for which a stability analysis can be performed are fixed points and this topic will be treated below. In Section 2.1.4 extensions will be provided for the stability of other invariant sets.

Definition 7 (see [49, 54, 74, 88])**.** According to the Liapunov definition of stability, the equilibrium solution $\boldsymbol{y}(t) = \boldsymbol{y}^*$ is *stable* if, $\forall \varepsilon > 0$ there exists a $\delta(\varepsilon) > 0$, function of ε, such that $||\boldsymbol{y}(0) - \boldsymbol{y}^*|| < \delta$ implies $||\boldsymbol{y}(t) - \boldsymbol{y}^*|| < \varepsilon$, for all t.

Definition 8 (see [49, 54, 74, 88])**.** The equilibrium solution $\boldsymbol{y}(t) = \boldsymbol{y}^*$ is called *unstable* according to Liapunov if it is not stable, i.e. if there exist $\varepsilon > 0$ and $t_\delta > 0$ such that at least a solution $\boldsymbol{y}(t)$ exists with $||\boldsymbol{y}(0) - \boldsymbol{y}^*|| < \delta$ and $||\boldsymbol{y}(t_\delta) - \boldsymbol{y}^*|| \geq \varepsilon$, for any $\delta > 0$.

Definition 9 (see [49, 54, 74, 88])**.** The equilibrium solution $\boldsymbol{y}(t) = \boldsymbol{y}^*$ is called *attractive* if there exists $\delta > 0$ such that for all $||\boldsymbol{y}(0) - \boldsymbol{y}^*|| < \delta$ the solution $\boldsymbol{y}(t) = \boldsymbol{\varphi}(\boldsymbol{y}_0)$ is well defined at least for $t \geq 0$ and this solution $\boldsymbol{y}(t)$ tends to the fixed point $\boldsymbol{y}^*$ for $t \to +\infty$, i.e. $\lim_{t \to +\infty} ||\boldsymbol{y}(t) - \boldsymbol{y}^*|| = 0$.

Definition 10 (see [49, 54, 74, 88])**.** An equilibrium point that is both stable and attractive is called *asymptotically stable*.

The previously described approach for the definition of stability can be generalised to cover also the cases of limit cycles and more complex solutions, introducing a geometrical approach in the analysis of stability.

The Liapunov definitions mentioned above define the concept of stability for a fixed point, however their practical application to understand whether or not the considered equilibrium point is stable is not trivial. For this purpose, many theorems have been formulated to operatively determine the stability of a given dynamical system like (2.3), often introducing very strict hypotheses on the vector field $\boldsymbol{f}(\boldsymbol{y})$.

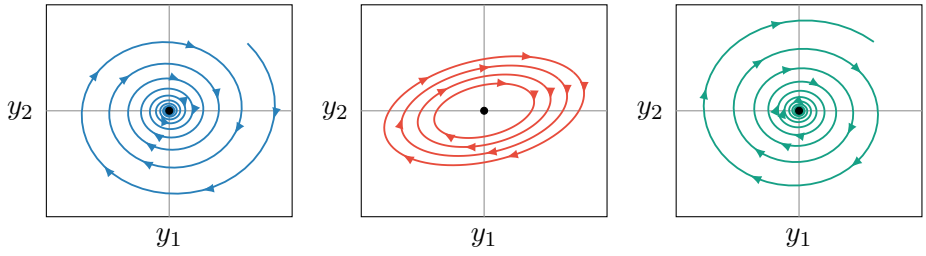

(a) *stable focus* **(b)** *center* **(c)** *unstable focus*

Figure 2.2: Three examples of possible configurations for a fixed point in the origin of a 2D phase space described by the generalised coordinate y_1 and y_2.

One of the most powerful stability criterion is the so-called *direct method of Liapunov*, that has no restrictions in its applicability and can be used for all dynamical systems.

Theorem 1 (Liapunov, see [49, 58])**.** *Considering the autonomous system* (2.3)*, if there exists a positive definite function $V(\boldsymbol{y}) \in \mathcal{C}^1$, such that its derivative along the trajectories is negative semidefinite $\dot{V}(\boldsymbol{y}) \leq 0$, then the equilibrium $\boldsymbol{y} = 0$ is Liapunov stable.*

Let's recall that the scalar function $V(\boldsymbol{y})$ is positive definite in a domain $\mathcal{B}$ if $V(\mathbf{0}) = 0$ and $V(\boldsymbol{y}) > 0$ for $\boldsymbol{y} \in \mathcal{B} \setminus \{\mathbf{0}\}$, while the function $\dot{V}(\boldsymbol{y})$ is negative semidefinite in a domain $\mathcal{B}$ if $\dot{V}(\mathbf{0}) = 0$ and $\dot{V}(\boldsymbol{y}) \leq 0$ for $\boldsymbol{y} \in \mathcal{B} \setminus \{\mathbf{0}\}$. Moreover, the derivative of the function $V(\boldsymbol{y})$ along the trajectories of the system (2.3) can be calculated as

$$\dot{V}(\boldsymbol{y}) = \frac{\partial V(\boldsymbol{y})}{\partial \boldsymbol{y}} \cdot \boldsymbol{f}(\boldsymbol{y}).$$

One must finally note that the equilibrium point in Theorem 1 is the origin of the phase space, but a proper change of coordinates can easily be performed to extend the results of this theorem to a general fixed point $\boldsymbol{y}^*$.

The function $V(\boldsymbol{y})$ is called *Liapunov function* and it is quite hard to determine for generic dynamical systems. For conservative mechanical systems, the mechanical energy is generally a good candidate to be a proper

Liapunov function, but no criteria are available for the definitions of Liapunov function for mechanical structures under general non-conservative actions.

The *linear stability analysis theorem* provides a more useful criterion to determine the stability of a dynamical system, in which the linearisation of the vector field plays an essential role.

Theorem 2 (Liapunov, see [49, 58])**.** *Let's consider the autonomous system* (2.3) *and suppose that* $\boldsymbol{y}^*$ *is an equilibrium point. Let's linearise the vector field* $\boldsymbol{f}(\boldsymbol{y})$ *near the equilibrium point* $\boldsymbol{y}^*$ *and let's consider the Jacobian matrix* $\boldsymbol{A} = \frac{\partial \boldsymbol{f}}{\partial \boldsymbol{y}}(\boldsymbol{y}^*)$*, evaluated in* $\boldsymbol{y}^*$*. The equilibrium point is stable if the condition* $Re\,[\lambda_k] < 0$ *is fulfilled, for all the eigenvalues* λ_k *of the Jacobian matrix* $\boldsymbol{A}$*.*

Definition 11 (see [54])**.** The equilibrium points that have no eigenvalues with a vanishing real part are called *hyperbolic*.

Theorem 2 is the principal mathematical tool that will be used in the next Chapters for the stability analysis of smooth and non-smooth mechanical systems, hence some details on its application must be discussed to better understand all the implications of this criterion.

According to Theorem 2, the following properties can be deduced, see [49, 58, 74]:

- if the original system is *linear*, so $\dot{\boldsymbol{y}}(t) = \boldsymbol{A}\boldsymbol{y}(t)$, the fixed point is stable if $\text{Re}\,[\lambda_k] \leq 0$, while the equilibrium is asymptotically stable if $\text{Re}\,[\lambda_k] < 0$. Hence, for the linear case, the stability of the system can always be assured when eigenvalues with non-positive real part are present; [1]

- the fixed point of the *nonlinear* system $\dot{\boldsymbol{y}}(t) = \boldsymbol{f}(\boldsymbol{y})$ is stable if the associated linearised system near the equilibrium point is described by a Jacobian matrix for which all the eigenvalues have a negative real part, $\text{Re}\,[\lambda_k] < 0$. In this case the stability of the linearised system gives informations on the behaviour of the nonlinear one;

[1] Actually, the existence of a vanishing eigenvalue $\lambda_i = 0$ with an algebraic multiplicity greater than 1 leads to the presence of the secular terms $te^{\lambda_i t}, t^2 e^{\lambda_i t}, \ldots$, that yield to an unstable behaviour in the vicinity of the equilibrium configuration. However, this is considered a pathological case and it is assumed that in the examples described in this Thesis, this specific condition is not present, as can be seen in Section 3.3.2.

- the fixed point of the same *nonlinear* system is unstable when there exists at least one eigenvalue $\overline{\lambda}_k$ of the Jacobian matrix $\boldsymbol{A}$ such that $\text{Re}\left[\overline{\lambda}_k\right] > 0$. Also in this case the nonlinear behaviour can be deduced from the linearised system;

- when the spectrum of the Jacobian matrix $\boldsymbol{A}$ contains eigenvalues for which $\text{Re}\left[\lambda_k\right] \leq 0$, the behaviour of the linear system is known (see the first point), however, the behaviour of the nonlinear system near the equilibrium point cannot be deduced from the previous one. This is a pathological case, not covered by this Theorem, that can be determined with a higher order expansion of the vector field $\boldsymbol{f}$, or using a more general stability criterion.

The conditions in the first point come from the analysis of the exponential solution of a linear dynamical system, already described in Section 2.1.2, while, in the following cases, the results on the linearised system are used to understand the behaviour of the associated nonlinear original one. One must observe that, according to the fourth point, there exists a case, when the real part of the eigenvalues is not positive, for which this theorem cannot predict the behaviour in the nonlinear case.

Some specific criteria for conservative mechanical systems are the *Lagrange - Dirichlet criteria*, see [58, 90], in which the stability of an equilibrium point is determined by the nature of the stationary point of the total potential energy. In particular, if a fixed point of a mechanical system subject only to conservative loads represents a minimum of the total potential energy, the system is stable. These criteria can also be extended, involving the presence of dissipative actions by the *Barbasin-Krasowski theorem* [49, 58], but these methods for detecting the stability of a fixed point are suitable only for mechanical systems without generic non-conservative forces. For this reason, these criteria have only been mentioned here because they are standard tools for the stability analysis, but they will not be used in the discussion below since non-conservative follower forces are present in the structure that will be analysed in the following Chapters.

As a final remark, in this Thesis the concept of stability is sometimes directly associated with the dynamical system, in expressions like "stable system" or "unstable system". For the sake of clarity, we underline that these phrases must be intended as "system in which the considered equilibrium configuration is stable/unstable". Although this linguistic choice

is not formally correct, it has been used for its power of synthesis. However, the precise meaning should not be misunderstood, since the dynamical systems under analysis always reveal the same features, with respect to the presence of fixed points.

2.1.4 Invariant sets and their stability

The description of the evolution of dynamical systems from a geometrical point of view, introduced in the XIX Century, represents a milestone in the realm of Dynamics and Mechanics. According to this interpretation, some specific concepts of Analysis, Geometry, and Topology can be extended, in order to have an overall comprehension of the evolution of dynamical systems.

An *invariant set* of an autonomous dynamical system (2.3) is a subset $\mathcal{S}$ of the phase space, such that $\boldsymbol{y}_0 \in \mathcal{S}$ implies $\boldsymbol{y}(t) = \boldsymbol{\varphi}_t(\boldsymbol{y}_0) \in \mathcal{S}$, for all t, [54]. A single orbit (thus also a fixed point or a limit cycle) is a trivial example of an invariant set, but other more complex sets can be present in the phase space as invariant set, describing the trajectories of families of solutions.

The invariant sets will often be called also *invariant manifolds* in the following Chapters, since all the invariant sets that are considered below are supposed to be sufficiently regular to describe a differentiable manifold. The exact definition of a manifold is quite complex and it goes beyond the purpose of this Chapter. In simple words, a *manifold* is a particular set that has locally the structure of an Euclidean space and that is $\mathcal{C}^r$ differentiable, $r \geq 1$. Hence, a manifold can be thought as a m-dimensional locally differentiable hypersurface embedded in the $\mathbb{R}^n$ phase space.

Definition 12 (see [54])**.** An invariant set $\mathcal{S}$ is *stable* if for any small neighbourhood $\mathcal{U} \supset \mathcal{S}$ there exists a neighbourhood $\mathcal{V} \supset \mathcal{S}$ such that $\boldsymbol{\varphi}_t(\boldsymbol{y}_0) \in \mathcal{U}$ for all $\boldsymbol{y}_0 \in \mathcal{V}$, for all t.

Definition 13 (see [54])**.** An invariant set $\mathcal{S}$ is called *attractive* if there exists a neighbourhood $\mathcal{W}$ such that $\boldsymbol{\varphi}_t(\boldsymbol{y}_0) \to \mathcal{S}$ for all $\boldsymbol{y}_0 \in \mathcal{W}$, as $t \to +\infty$.

Definition 14 (see [54])**.** An invariant set is defined *asymptotically stable* if it is stable and attractive.

From the definitions above, one can see how the concept of Liapunov stability of a fixed point can easily be extended to all kinds of invariant sets and possible orbits describing the solutions of a dynamical system.

2.1.5 Bifurcations of equilibrium points

The concept of *bifurcation of an equilibrium point* can have different definitions in various fields of Mechanics. Typically, for engineers, it is introduced in an intuitive way when the buckling of the Euler's column is considered, and it is associated with a change in the stability behaviour of the structure with the presence of new possible equilibrium configurations, when the load is increased or decreased, see [58, 90]. In the mathematical analysis of dynamical systems, [54, 88], the concept of bifurcation has a more complex but general definition, that will be exposed in this Section.

The fundamental concept on which this topic is based is the equivalence among different dynamical systems. It can be intuitively thought as the similarity in their behaviours, that can be defined in a more rigorous way, considering the orbits and the phase portraits.

Definition 15 (see [54])**.** Two dynamical systems are called *topologically equivalent* if there exists a homeomorphism $h : \mathbb{R}^n \to \mathbb{R}^n$ mapping the orbits of the first system onto the orbit of the second one, preserving the direction of time.

Hence, all topologically equivalent systems have the same qualitative behaviour, despite the trajectories do not exactly coincide. Moreover, some "classes of behaviours" can be defined, i.e. some paradigms that exemplify and fully describe particular kinds of solutions. These classes can be taken as references, their mathematical properties can be analysed, and then the specific behaviour of any general dynamical system can be studied simply considering it as a "distortion" from a reference one.

Let's now consider the autonomous dynamical system in the form (2.3), but let's suppose that the right-hand-side of the differential equation depends on a generic vector of parameters $\boldsymbol{\alpha} \in \mathbb{R}^m$, such that the system can be described by

$$\dot{\boldsymbol{y}}(t) = \boldsymbol{f}(\boldsymbol{y}, \boldsymbol{\alpha}), \qquad \boldsymbol{y}(0) = \boldsymbol{y}_0.$$

For example, in a mechanical structure, the vector $\boldsymbol{\alpha}$ contains all the geometrical, mechanical, or load design parameters that are supposed to vary in the design process.

Definition 16 (see [54])**.** The appearance of a topological non-equivalent phase portrait under variation of parameters is called a *bifurcation*.

This definition of bifurcation is general and it is suitable both for smooth and non-smooth dynamical systems. Particular kinds of bifurcations have been classified in order to better understand how the dynamical systems with given structures in the vector field $\boldsymbol{f}$ evolve, when the bifurcation parameters are changed.

Regarding nonsmooth systems, the classification of all the possible cases is quite cumbersome, due to the complexity in the mathematical description of piecewise systems. This kind of analysis has been performed in recent papers, see [33, 62, 63], in which, under specific hypotheses on the structure of the vector fields, all the possible bifurcation cases are described. However, the analysis performed in the following Chapters on piecewise mechanical systems does not explicitly consider the evolution of the parameters, so the classification of bifurcation in non-smooth structures is beyond the aim of this Thesis. On the contrary, a conceptual description of the most important classes of bifurcations for smooth problems will be presented below, to better understand the link between the structural and mathematical perspectives in the study of dynamical systems and to clarify the procedure performed in Section 3.4 for the calculation of flutter and divergence critical loads.

One must note that Definition 16 cannot be used directly to compute the critical values of the bifurcation parameters. However, the appearance of a topological non-equivalent phase portrait can be clearly associated with a change in the stability behaviour of the solution that is considered. From Theorem 2, the stability of an equilibrium configuration has been associated with the nature of the eigenvalues of the Jacobian matrix, so also the change in the structure of the phase portrait can be linked to the change in the nature of the eigenvalues $\lambda_k(\boldsymbol{\alpha})$, considered as functions of the design parameters.

These intuitive considerations can be investigated in depth from a theoretical point of view, according to the concept of structural stability (a

system described by the vector field $\boldsymbol{f}$ is *structurally stable* if it is topologically equivalent to the system obtained with a small perturbation of $\boldsymbol{f}$ in all the parameters) and applying the theorems that assure the structural instability of a non-hyperbolic fixed point. All the analytical details are omitted due to the descriptive purpose of this paragraph, however the main outcome of this approach is that the qualitative change in the phase portrait occurs only when a system becomes structurally unstable. For this reason, the value of the bifurcation parameters is associated with the presence of a non-hyperbolic equilibrium solution. This implies that at least one of the eigenvalues must have a vanishing real part to have a bifurcation of a fixed point, hence a bifurcation occurs for the values of the parameters $\boldsymbol{\alpha}$, for which at least one of the eigenvalues hits the imaginary axis.

Definition 17 (see [54, 58, 88])**.** The *fold bifurcation* occurs when there exists a change in the phase portrait between a configuration with no equilibrium points and another one with two fixed points. In the switch between the two phase portraits an eigenvalue vanishes.

Definition 18 (see [54, 58, 88])**.** The *transcritical bifurcation* occurs when there exists a change in the phase portrait between a configuration with two fixed points (one is stable and the other is unstable) and another configuration with two fixed points (the stable fixed point becomes unstable and another stable point appears). In the switch between the two phase portraits an eigenvalue vanishes.

Definition 19 (see [54, 58, 88])**.** The *pitchfork bifurcation* occurs when there exists a change in the phase portrait between a configuration with a single stable point and another one with three fixed points (one unstable point and two stable ones). In the switch between the two phase portraits an eigenvalue vanishes.

Let's observe that this kind of bifurcation appears in the discrete version of the classical Euler's column, subject to conservative loads, where the single stable equilibrium branch becomes unstable when the critical load is reached, and two other stable branches originate from the critical point.

Definition 20 (see [54, 58, 88])**.** A *Hopf bifurcation* occurs when there exists a change in the phase portrait between a configuration with a fixed point

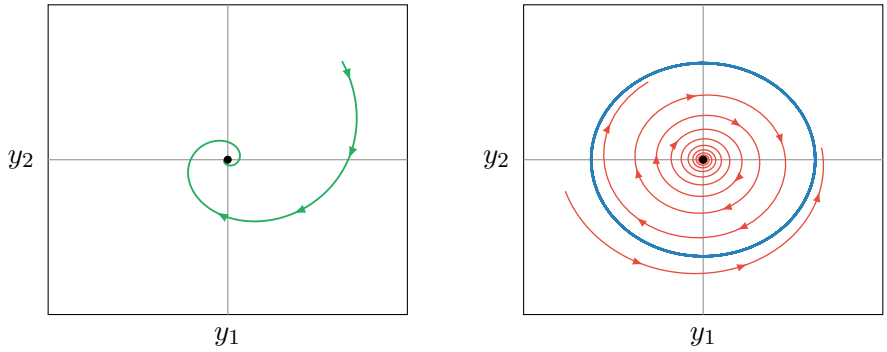

(a) $\alpha < \alpha_{cr}$ **(b)** $\alpha > \alpha_{cr}$

Figure 2.3: Supercritical Hopf bifurcation, with respect to the parameter α. For $\alpha < \alpha_{cr}$ the equilibrium configuration is a stable focus, while for $\alpha > \alpha_{cr}$ the fixed point is unstable and a stable limit cycle appears in the phase portrait.

and another one with a fixed point and a limit cycle. In the switching between the two phase portraits, a couple of purely imaginary eigenvalues appears.

In particular, when the bifurcation reveals a change from a stable fixed point to an unstable fixed point with a stable limit cycle, it is called a *supercritical Hopf bifurcation*. On the contrary, if there is a change from an unstable fixed point to a stable fixed point with an unstable limit cycle, it is called a *subcritical Hopf bifurcation*. From a physical point of view, the Hopf bifurcation is associated with the appearance of flutter instability.

2.1.6 Lagrangian vs. Hamiltonian formulations of the equations of motion

The analysis of dynamical systems has been introduced from a mathematical and geometrical point of view, without any assumption on the structure of the smooth problem, so the formalism described in previous Sections can be adopted in every field of Physics, provided that the dynamical system can be described by a set of first order ordinary differential equations.

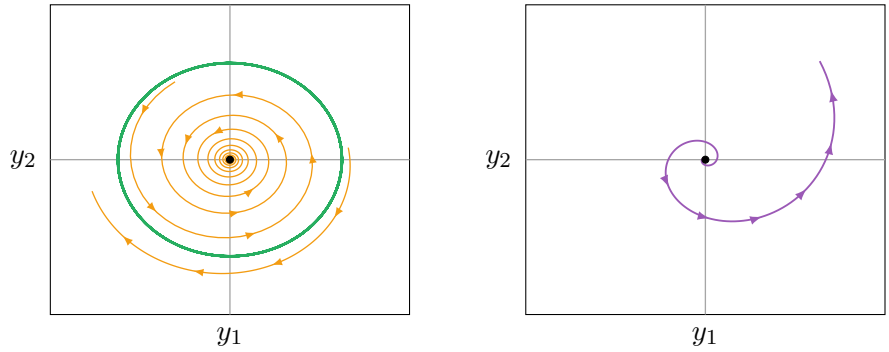

(a) $\alpha < \alpha_{cr}$ **(b)** $\alpha > \alpha_{cr}$

Figure 2.4: Subcritical Hopf bifurcation, with respect to the parameter α. For $\alpha < \alpha_{cr}$ the phase portrait is defined by a stable fixed point and an unstable limit cycle, while for $\alpha > \alpha_{cr}$ an only unstable equilibrium configuration is present.

When the analysis is restricted to the field of Mechanics, different ways in the mathematical description of physical phenomena can be adopted, so they must be reduced to the definition of a first order ODE structure in order to apply the previously described formalism, see [55] .

The most intuitive approach in the analysis of physical structures is the vectorial description of a mechanical system, introduced and formalised by Newton. According to this formulation, the particles that compose the mechanical structure can be described through their geometrical coordinates with a transformation between the real physical space and the Euclidean space. This intuitive and direct approach to the analysis of mechanical systems, which is fundamental to understand the behaviour of physical bodies but hard to apply in complex problems, has been overcome when Lagrange and Euler introduced the calculus of variations, defining an analytical approach in Mechanics.

In this second analytical formulation, the concept of geometrical coordinates describing the degrees of freedom of the particles of a body has been extended to the concept of *generalised coordinates*, which can be defined as any possible set of parameters that can completely characterize the position of a mechanical system. The number of the $\boldsymbol{q}(t)$ generalised

coordinates are equal to the number of degrees of freedom of the mechanical structure and the set of all the $q_1, q_2, \ldots, q_N$ can be interpreted as an N-dimensional space called the *configuration space* in which the position of the system can be represented.

Moreover, in this analytical formulation introduced by Lagrange and Euler, the notion of force, typical of the vectorial approach, is substituted by a single quantity, the *work*, that solely describes all the information about the nature of the forces acting on the system. In particular, through the definition of the work, some *generalised forces* can be defined, which are the dual components of the generalised coordinates q_i. With these theoretical ingredients, a variational formulation for the description of the dynamical system is introduced and the equations describing the Second Principle of Dynamics for each particle of the system are substituted by the condition of minimisation of a properly defined functional.

From the variational principle (weak formulation), the equations of motion expressed as a set of differential equations (strong formulation) can be obtained. One of the possible descriptions of the dynamics of a holonomic mechanical system is given by the well known *Lagrange formulation* of the equations of motion, namely the following set of N *second order* ordinary differential equations

$$\frac{d}{dt}\left(\frac{\partial \mathcal{L}}{\partial \dot{q}_i}\right) - \frac{\partial \mathcal{L}}{\partial q_i} = \mathcal{Q}_i(t, \boldsymbol{q}, \dot{\boldsymbol{q}}), \qquad \forall i = 1, \ldots, N\,, \tag{2.8}$$

where $\mathcal{Q}_i$ is the component of the generalised force that do not have a representation in terms of a potential energy, while the functional $\mathcal{L}(\boldsymbol{q}, \dot{\boldsymbol{q}})$ is called the *Lagrangian function* and is defined as $\mathcal{L}(\boldsymbol{q}, \dot{\boldsymbol{q}}) = \mathcal{T}(\dot{\boldsymbol{q}}) - \mathcal{U}(\boldsymbol{q}, \dot{\boldsymbol{q}})$, where $\mathcal{T}$ is the kinetic energy and $\mathcal{U}$ is the potential energy, see [55].

Another analytical representation is the so-called *Hamiltonian formulation* that can be obtained by a Legendre transformation of the Lagrangian equations of motion, see [55, 58]. The new independent parameters p_i are introduced, called *generalised momenta*, such that

$$p_i = \frac{\partial \mathcal{L}}{\partial \dot{q}_i}, \qquad \forall i = 1, \ldots, N\,, \tag{2.9}$$

which can be substituted into (2.8), obtaining

$$\dot{p}_i = \frac{\partial \mathcal{L}}{\partial q_i} + \mathcal{Q}_i(t, \boldsymbol{q}, \dot{\boldsymbol{q}}), \qquad \forall i = 1, \ldots, N\,. \tag{2.10}$$

The function obtained applying a Legendre transformation to th Lagrangian function $\mathcal{L}(\boldsymbol{q}, \dot{\boldsymbol{q}})$ is called *Hamiltonian function* $\mathcal{H}(\boldsymbol{q}, \boldsymbol{p})$, which can be written as

$$\mathcal{H} = \boldsymbol{p} \cdot \dot{\boldsymbol{q}} - \mathcal{L},$$

and equations (2.9) and (2.10), together with the properties of the Legendre transformation, lead to the so-called *Hamiltonian formulation* of the equations of motion (or *canonical* equations of motion)

$$\dot{q}_i = \frac{\partial \mathcal{H}}{\partial p_i}, \qquad \dot{p}_i = -\frac{\partial \mathcal{H}}{\partial q_i} + \mathcal{Q}_i, \qquad \forall i = 1, \dots, N\,.$$

The transformation from the Lagrangian to the canonical equations of motion implies the introduction of new variables, the momenta p_i, thought as independent from the generalised coordinates q_i. The number of unknown functions is doubled passing from N to $2N$, however, the equations of motion are now *first order* ODEs.

The new $2N$ unknown coordinates $\{q_1, q_2, \dots, q_N, p_1, p_2, \dots, p_N\}$ employed for the description of the motion of a mechanical system are called *phases* and the $2N$-dimensional Euclidean space in which they can be represented is called *phase space*. The representation of the motion of a mechanical system is more convenient in the phase space rather than in the configuration space. In the former space, each curve represents an orbit of the dynamical system, hence it fully describes the motion, while a trajectory in the configuration space is not enough to completely define the evolution of the mechanical system.

In the following Chapters, we will adopt a Hamiltonian description of the behaviour of the considered mechanical system, but the equations of motion have been obtained through the Principle of virtual Power and so they are second order ODEs, analogous to (2.8). In this Thesis, the reduction to the first order ODEs canonical equations of motion has been obtained in a simplified way and without the application of the Legendre transformation, which describes the link between Lagrangian and Hamiltonian systems from a theoretical point of view.

The generalised momenta are simply defined as $p_i = \dot{q}_i$ and the equations of motion have been rewritten with respect to the new vector of unknowns (the vector of phases) $\boldsymbol{y} = [\boldsymbol{q}, \boldsymbol{p}]^{\mathrm{T}} = [\boldsymbol{q}, \dot{\boldsymbol{q}}]^{\mathrm{T}}$, obtaining a set of first

order ordinary differential equation. The initial conditions are then properly changed and rewritten

$$\boldsymbol{q}(0) = \boldsymbol{q}_0 \quad \text{and} \quad \dot{\boldsymbol{q}}(0) = \dot{\boldsymbol{q}}_0 \qquad \longrightarrow \qquad \boldsymbol{y}(0) = \boldsymbol{y}_0,$$

where the vector $\boldsymbol{y}_0 = [\boldsymbol{q}_0, \dot{\boldsymbol{q}}_0]^{\mathrm{T}}$ of the initial phase values has been introduced. This simplified strategy can be adopted because the potential energy is a function of the generalised coordinates $\boldsymbol{q}$ (and not of the velocity $\dot{\boldsymbol{q}}$), so equation (2.9) that defines the momenta simply reduced to $p_i = \dot{q}_i$.

2.1.7 A more general definition of dynamical system

At the beginning of this Chapter, the concept of dynamical system has been introduced simply by defining the first order differential equations that actually represent the mathematical model of a particular kind of dynamical system. However, a more sophisticated definition can be given of the concept of dynamical system itself.

From a more general perspective, a dynamical system can be described by the triple $\{\mathcal{T}, \mathcal{Y}, \boldsymbol{\varphi}_t\}$, where $\mathcal{T}$ is a time set, $\mathcal{Y}$ is called *state space* (or *phase space* in Mechanics) and $\boldsymbol{\varphi}_t$ is an evolution operator, see [54]. The elements $\boldsymbol{y} \in \mathcal{Y}$ represents all the possible states of the dynamical system and must be chosen to be sufficient for the description of both the configurations of the system and its evolution in time.

The systems described by (2.1) are clearly a subset of this wide definition of dynamical systems. In particular, they are called *continuous - time* dynamical system, since it has been assumed that the time set is composed of the elements $t \in \mathcal{T} = \mathbb{R}$. Actually, more general dynamical systems can be defined with a time set $\mathcal{T}$ composed of isolated elements (e.g. $\mathcal{T} = \mathbb{Z}$), that are called *discrete - time* dynamical systems. The latter are generally described by an evolution rule, like

$$\boldsymbol{y}_{k+1} = \boldsymbol{F}(\boldsymbol{y}_k),$$

while the solution of this kind of system is a sequence $\{\boldsymbol{y}_k\}_{k=0}^{\infty}$ starting at the initial state $\boldsymbol{y}_0$. The mechanical systems generally have a continuous-time description, but, as will be explained in Section 2.2.5, the analysis of the solutions of this kind of problem can profitably be performed using a discrete - time approach via the Poincaré maps, see [74].

2.2 Non-smooth dynamical systems

2.2.1 Some philosophical notes

During the last decades, the interest in non-smooth dynamical systems has grown significantly in different fields of Physics and Engineering. With the application of discontinuous mathematical models, a great number of different physical phenomena can be studied and interpreted, and the behaviour of real discontinuous systems becomes predictable. Classical mechanical examples that can be associated with non-smooth equations of motion are impact phenomena, e.g. the motion of a bouncing ball or a bell, as well as systems with the presence of unilateral constraints or dry friction. The discontinuous nature of this physical phenomena can be modelled using ODEs similar to (2.1), but with a discontinuous right-hand-side described by a non-smooth vector field $\boldsymbol{f}(t, \boldsymbol{y}(t))$.

In the scientific community, the most interesting objections against the use of non-smooth models for the analysis of real systems can essentially be reduced to these two questions:

1) *why should I use a complex non-smooth dynamical model, if I can easily approximate it with a smooth one?*

2) *why should I use a complex discontinuous dynamical model, if any physical structure can always be considered as a continuous object (at least for a scale greater than the atomic one)?*

The first point deals with the practical analysis of a dynamical system with a discontinuous right-hand-side and it is the easiest to debate, since it has been proved that non-smooth dynamical models show a great number of different possible behaviours, greater than smooth models, and some of them can be obtained only considering discontinuous ODEs. In fact, as reported in [57, 79], possible stability behaviours of a mechanical structure are lost when the discontinuous dynamical model is smoothed out and when the computation of the solution is performed using these approximated equations of motion. Hence, the richer dynamical behaviour of non-smooth systems can be appreciated only if also the model used for the analysis is non-smooth.

The second is a philosophical question and the answer is not so easy, since it is strictly related to the possible ways that a scientist can follow in

the passage from a physical model to a mathematical model of the analysed phenomenon, which is maybe one of the most difficult topics in Science and Engineering.

For a scale greater than the atomic one, a mechanical system can certainly be described by a continuous model, so the presence of discontinuities in the mathematical model may seem something that should be avoided, since when a change in the configuration occurs, the real passage from a status to another one can be seen as a continuous transition, see [57].

Actually, the real difference between the application of a smooth or a non-smooth dynamical model is the time scale. In fact, if the considered time scale is close to the time interval in which the transition between the configurations occurs, then the correct model is obviously a continuous one, since in this case, it is possible to appreciate the continuous dynamics of the structure. On the contrary, when the time scale is far greater than the time interval in which the transition occurs, then the change in the status can be modelled as a single infinitesimal event in a more complex evolution of the motion of the system, so a discontinuous model is more suitable. Therefore, the correct model for a real physical system cannot be decided *a priori*, but it depends on the purpose of the analysis and, in particular, on the features of the real phenomenon that one wants to underline.

This answer, sketched maybe in a simplistic and conceptual way, highlights the main reason that justifies the use of non-smooth models for the analysis of discontinuous mechanical systems, however, it raises new and more interesting and difficult questions. For instance, what is the range in which the continuous or discontinuous models are valid? And when different behaviours are predicted by the continuous and discontinuous models, which is the real one that occurs in the physical system? In the following Chapters, a mechanical structure is studied, for which an unstable behaviour can be detected when the constraint is considered discontinuous, on the contrary, this instability disappears when a smooth constraint

is supposed to be present in the structure [2]. Which is the real behaviour of the system? Is it the one predicted by the discontinuous model that describes the macroscopic jump in the geometrical properties of the constraint, or maybe the continuous one that seems to be more realistic, since, at a small scale, all the mechanical systems can be considered smooth?

The answer to these questions has partially been given above, in the discussion on what is the time scale which we are interested in. We can try to give an explanation to these philosophical doubts, proposing a first hypothesis on what could be the reason for these possible discordant behaviours. In particular, some conceptual reflections can be performed, dealing with the concept of stability, whose definition can be interpreted as the source of this paradoxical behaviour.

One must note that the Liapunov definition of stability of a fixed point is essentially a local notion since it refers to a small neighbourhood of the initial conditions, namely a small ball in the phase space with the centre in the equilibrium point. Furthermore, the stability is essentially determined through a linearisation of the equations of motion near a given solution, hence the orbits of the nonlinear and linearised system are very close only when the perturbation is small, so inside a small neighbourhood of the considered solution.

This means that also the validity of the stability analysis is located in the vicinity of the considered reference solution, while outside the Liapunov ball (i.e. for ε and $\delta(\varepsilon)$ not sufficiently small), the system generally shows a behaviour that cannot be predicted by the Liapunov definition of stability.

For this reason, a smooth model for a mechanical system may predict a stable configuration in a very small neighbourhood of the fixed point. On the contrary, outside this Liapunov ball, but actually not so far from the fixed point, the real nonlinear system may evolve following unstable

[2] I am indebted to my colleagues and friends Giovanni and Alessandro for their help in the possible solution of what we used to call, during our fruitful discussions, the Gnome Paradox: *"let's suppose that there exists a perfectly smooth mechanical system and that a small gnome files away just a single atom from this perfect structure, transforming it into a non-smooth mechanical system. Do these two very similar structures need such a completely different model? Why should I have a completely different behaviour, since the non-smooth models have a richer set of possible solutions that cannot be predicted by a smooth model? What is the suitable model for the best interpretation of the real behaviour of the system?"*

orbits, which can be correctly caught by the non-smooth model, predicting an unstable behaviour for the system.

The difference in the predictions of the continuous or discontinuous models can then be interpreted as a sort of discrepancy between the Liapunov balls associated with the smooth and non-smooth representations. Since the models are different from a mathematical point of view, also the neighbourhoods, in which the stability analysis has a precise theoretical and practical meaning, can be different.

Let's finally note that the difference in the Liapunov balls is not surprising, since a hard change in the mathematical model occurs, leading to a completely different theoretical framework. This happens in other fields of Mechanics, for example in the realm of homogenization problems in Solid Mechanics, when the microstructure is considered as a discrete model and the effective homogenized body is modelled as a continuum.

From the two scenarios presented above, it is clear that actually the prediction of the two models are not in contrast and can be associated with a precise real behaviour. Moreover, each prediction has a particular time scale in which it could be considered valid, hence the "correct real behaviour" is something that cannot be precisely defined if the time scale is not specified.

These philosophical topics have briefly been introduced in order to show the difficulties in the treatment of this kind of discontinuous phenomenon. In the following Chapter, only the non-smooth model will be considered, with all the implications described above, while the connection between the stability of the smooth and non-smooth model have been neglected.

2.2.2 Classification of non-smooth dynamical systems

The relation between smooth and non-smooth models for physical phenomena have been investigated in the previous Section 2.2.1 and some philosophical concepts have been presented, regarding the validity of a smooth as well as non-smooth dynamical models for the interpretation of discontinuous real systems. In this Section, the focus is on the classification of different non-smooth systems and the formalism adopted for the analysis of this kind of problem.

The field of non-smooth dynamics is wide and a general classification

of all the possible discontinuities that can be considered in a mathematical model is not a trivial task. For the purpose of this Thesis, the following common classification of non-smooth mechanical systems, see [46, 57], will be adopted:

- *Non-smooth continuous systems*: the vector field in the right-hand-side of the ODEs is continuous, while the Jacobian matrix is discontinuous (e.g. a system in which the stiffness depends on the state variables [3]);
- *Filippov's systems*: the vector field in the right-hand-side of the ODEs is discontinuous, but they still remain continuous-time dynamical systems (e.g. a system with the presence of dry friction);
- *Hybrid systems*: the vector field is discontinuous and the description of the motion is composed of both continuous-time and discrete-time dynamics (e.g. the motion of bells and all those systems where impacts occur, namely where the configuration suddenly "jumps" onto another point in the phase space);

Although they have been considered distinct in this physically-based classification, the first two points of the list above can actually be treated in a unitary way using the methods introduced by Filippov [32], hence the first class can simply be considered as a special case of the second class, from a mathematical point of view. The third kind of system is much more complex to describe and they are adopted to model the behaviour of simple mechanical systems with impact phenomena. However, this third class of discontinuous systems will not be covered in this Thesis.

This classification will be more clear after the analysis of the mathematical models presented in Section 2.2.3, where discontinuous vector fields and solutions are investigated.

Another common classification of discontinuous systems, see [27], is based on the continuity with respect to time:

[3] Actually, to have a piecewise-smooth dynamical system, the dependency of the stiffness on the switching rule cannot be general. In particular, when the discontinuity involves only the k-th phase variable y_k (possibly after a coordinate transformation), the Jacobian matrix must change only in the k-th column, see [57]. This assumption is commonly adopted in the analysis of invariant cones [16, 46, 57], however in the present Thesis a more general situation is investigated, in which this condition is not fulfilled.

- *Non-smooth flows*: continuous-time dynamical systems with discontinuous vector field;
- *Non-smooth maps*: discrete-time dynamical systems with discontinuous vector field;
- *Hybrid systems*: the vector field is discontinuous and the description of the motion is composed of both continuous-time and discrete-time dynamics;

It's clear that the third class is common for both the classifications presented above, while non-smooth continuous systems and Filippov's systems are special examples of non-smooth flows.

2.2.3 Filippov piecewise-smooth systems

Non-smooth continuous systems and Filippov systems can be studied in a unitary way in the framework defined by the Russian mathematician A.F. Filippov in [32].

The analysis performed by Filippov of non-smooth dynamical systems defined by ODEs with discontinuous right-hand-side is based on the extension of the classical idea of solution of ODEs to the solution of a *differential inclusion*, through a process based on Convex Analysis. Applying the so-called *Filippov's convex method*, the problems of non-smooth dynamics become well-posed, the solution can be found in a rigorous way and these systems can be studied in a well-defined general theoretical framework. The work of Filippov takes into consideration different kinds of possible discontinuities, however, in the following part, only problems with a vector field discontinuous in the phase vector $\boldsymbol{y}$ will be considered (in principle, the right-hand-side could also be continuous in the state variable vector $\boldsymbol{y}$ and discontinuous in the time t). The hybrid systems introduced in Section 2.2.2 cannot be studied directly in Filippov's theoretical framework, however, they will not be considered in the description below, since their analysis is beyond the purposes of this Thesis.

Let's suppose that a n-dimensional domain $\mathcal{V} \subseteq \mathbb{R}^n$, contained in the phase space, can be partitioned into a set of m subdomains $\mathcal{V}_i$, for all $i = 1, 2, \ldots, m$, such that $\mathcal{V} \equiv \bigcup_{i=1}^{m} \mathcal{V}_i$. This definition is obviously suitable also when the complete domain $\mathcal{V}$ is assumed to be the entire phase space $\mathbb{R}^n$.

Two n-dimensional subdomains $\mathcal{V}_i$ and $\mathcal{V}_j$ are assumed to be separated each other by the $(n-1)$-dimensional subspace Σ_{ij}. The subspaces Σ_{ij}, for all $i, j = 1, 2, \ldots, m$, are generally called *switching manifolds* and, in the example treated in this Thesis, they are supposed to be sufficiently regular to be described by smooth equations $h_{ij}(\boldsymbol{y}) = 0$, where $h_{ij} : \mathbb{R}^n \to \mathbb{R}$ and $h_{ij} \in \mathcal{C}^1$.

Definition 21 (see [32, 57])**.** A general vector field $\boldsymbol{g}(\boldsymbol{x}) : \mathbb{R}^p \to \mathbb{R}^q$ is considered to be *defined almost everywhere* in a given domain $\mathcal{D} \subseteq \mathbb{R}^p$, when it is defined everywhere in the domain, with the exception of a set of points of $\mathcal{D}$ with zero measure.

Definition 22 (see [32])**.** A vector field $\boldsymbol{f}(\boldsymbol{y})$ is called *continuous up to the boundary* if it tends to a finite limit for $\boldsymbol{y}$ approaching each point of the boundary Σ_{ij} of the domain $\mathcal{V}_i$, in which the vector field is defined.

Definition 23 (see [32, 57])**.** A vector field $\boldsymbol{f}(\boldsymbol{y})$ is called *piecewise continuous* in the domain $\mathcal{V}$ if the latter can be partitioned into the subdomains $\mathcal{V}_i$, separated by the switching manifolds Σ_{ij} as presented above, and if, in each part of the domain $\mathcal{V}_i$, the function $\boldsymbol{f}$ is continuous in the phase vector $\boldsymbol{y}$ up to the boundary.

In this Chapter, only piecewise continuous vector fields are considered for the description of a non-smooth mechanical system and, according to the previous definitions, they can be interpreted as a set of vector fields $\boldsymbol{f}_i(\boldsymbol{y})$ defined in each $\mathcal{V}_i$, for all $i = 1, 2, \ldots, m$. Hence, each $\boldsymbol{f}_i$ is continuous and has a finite limit approaching the switching manifolds.

Definition 24 (see [27, 32, 57])**.** The evolution in time of a continuous-time autonomous *piecewise-smooth dynamical system* can be described by a set of ordinary differential equations

$$\dot{\boldsymbol{y}}(t) = \begin{cases} \boldsymbol{f}_1(\boldsymbol{y}(t)) & \boldsymbol{y} \in \mathcal{V}_1 \\ \boldsymbol{f}_2(\boldsymbol{y}(t)) & \boldsymbol{y} \in \mathcal{V}_2 \\ \cdots & \cdots \\ \boldsymbol{f}_m(\boldsymbol{y}(t)) & \boldsymbol{y} \in \mathcal{V}_m \end{cases}, \tag{2.11}$$

together with the initial conditions $\boldsymbol{y}(0) = \boldsymbol{y}_0$.

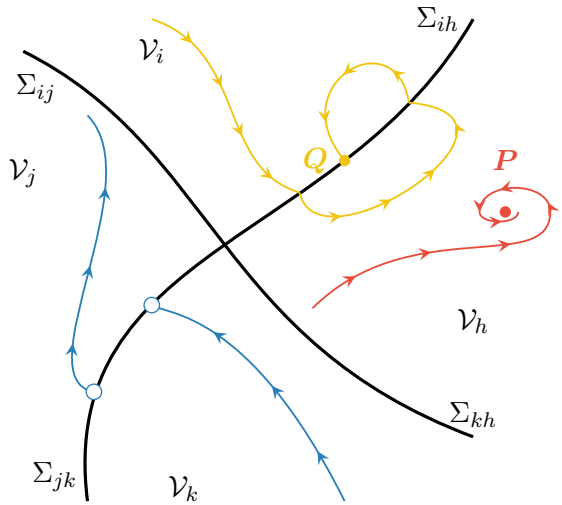

Figure 2.5: Partition of the phase space into four subdomains $\mathcal{V}_p$ ($p = i, j, k, h$) separated by the switching manifold Σ_{pq}. If the evolution of an orbit is contained in a single subdomain (red trajectory), the system behaves like a smooth dynamical one and equilibrium configurations may be present (e.g. point $\boldsymbol{P}$), which are analogous to common fixed points. A boundary equilibrium configuration may also be present in the phase portrait (point $\boldsymbol{Q}$), such that it is approached by an orbit (yellow trajectory) that passes from a subdomain to the other, converging to the fixed point. When an orbit crosses a switching manifold (blue trajectory), the vector field is continuous up to the boundary if the limit for the solution approaching the switching manifold exists (however this limit can possibly be discontinuous).

Let's observe that according to this formulation, no information about the behaviour of the dynamical system on the switching manifolds Σ_{ij} has been given and this ambiguity is the primary source of all the troubles in the solution of these kinds of differential problems. For example, when an orbit passes from one subdomain $\mathcal{V}_i$ to another one $\mathcal{V}_j$, crossing in a well-defined direction the switching manifold Σ_{ij} and remaining continuous in this change of the subdomain, the solution $\boldsymbol{y}(t)$ of the system (2.11) could in principle be considered defined almost everywhere.

On the contrary, a more suitable definition of solution must be found, when the limit of the solution $\boldsymbol{y}(t)$ is finite but tends to different values

when Σ_{ij} is approached from distinct subdomains, or when a clear direction of intersection cannot be defined (since, for example, there exists a sliding orbit on the switching manifold).

For the sake of clarity and without loss of generality, let's restrict the case to non-smooth dynamical systems whose domain can be decomposed into only two subdomains, $\mathcal{V}^-$ and $\mathcal{V}^+$, separated by the switching manifold Σ. The equation (2.11) becomes

$$\dot{\boldsymbol{y}}(t) = \begin{cases} \boldsymbol{f}^-(\boldsymbol{y}) & \boldsymbol{y} \in \mathcal{V}^- \\ \boldsymbol{f}^+(\boldsymbol{y}) & \boldsymbol{y} \in \mathcal{V}^+ \end{cases}, \tag{2.12}$$

where $\boldsymbol{f}^-$ and $\boldsymbol{f}^+$ are the vector fields respectively for the negative and positive subdomains. This assumption has been made only for a better comprehension of the system, but the generalisation of the following results to the case of m subspaces is trivial. However the mechanical systems studied in the following Chapters have exactly this form.

The idea behind Filippov's convex method is the extension of differential systems like (2.11) to the so-called *differential inclusions*, using the tools provided by Convex Analysis that will be briefly exposed below.

Definition 25 (see [57])**.** A given set $\mathcal{S} \subset \mathbb{R}^n$ is called a *convex set* if for any $\boldsymbol{x}, \boldsymbol{z} \in \mathcal{S}$, also $(1-q)\boldsymbol{x} + q\boldsymbol{z} \in \mathcal{S}$, for all $q \in [0,1]$.

In simple terms, a set is convex when it contains the line segments between any of its elements.

Definition 26 (see [57])**.** The smallest closed and convex set that contains two elements $\boldsymbol{x}, \boldsymbol{z} \in \mathbb{R}^n$ is called *convex hull* and it can be defined in symbols as

$$\overline{\text{co}}\,\{\boldsymbol{x}, \boldsymbol{z}\} = \{(1-q)\boldsymbol{x} + q\boldsymbol{z}, \forall q \in [0,1]\}\,.$$

Definition 27 (see [57])**.** The scalar function $F(x)$, $x \in \mathbb{R}$ is called a *set-valued function* if it is a function almost everywhere, except at a finite set of zero measure of the domain, in which $F(x)$ is a subset of $\mathbb{R}$.

On the basis of the definition above, the smooth functions in Classical Analysis can be defined as *single-valued functions*. The definition has been given for a scalar function defined on a one-dimensional domain, but the extension to vector fields defined over multi-dimensional domains is trivial and will be omitted here.

Definition 28 (see [57]). A set-valued vector field $\boldsymbol{F}(\boldsymbol{x})$ is called *upper - semicontinuous* in the point $\boldsymbol{x}$ if for all $\varepsilon > 0$ there exists a $\delta > 0$, such that if $||\boldsymbol{x} - \boldsymbol{z}|| < \delta$, then $\boldsymbol{F}(\boldsymbol{z}) \subset \boldsymbol{F}(\boldsymbol{x}) + B_\varepsilon$, where B_ε is the n-dimensional open ball with radius ε and centred in the origin.

For a set-valued function, a new definition of derivative must be introduced, to deal with the case in which the value of the function is not unique and different limits can be present.

Definition 29 (see [23, 32, 57]). Let's consider a scalar piecewise continuous function $f(x)$ and suppose that in any point $x \in \mathbb{R}$ the derivative of the function has two finite left and right limit $f'_-(x)$ and $f'_+(x)$, possibly different in the points where the function is non-smooth. Then the *generalised derivative of Clarke* is defined as any possible derivative included between $f'_-(x)$ and $f'_+(x)$, i.e.

$$f'_q(x) = (1-q)f'_-(x) + qf'_+(x), \quad \text{for a fixed } q \in [0,1].$$

Definition 30 (see [23, 32, 57]). The set of all possible generalised derivatives is called *generalised differential* and it is the convex hull of the elements $f'_-(x)$ and $f'_+(x)$, i.e.

$$\partial f = \overline{\text{co}}\left\{f'_-(x), f'_+(x)\right\} = \left\{(1-q)f'_-(x) + qf'_+(x), \forall q \in [0,1]\right\}.$$

The definition of generalised derivative and generalised differential can be extended to both scalar and vector field, observing that for a multi-dimensional domain $\boldsymbol{x} \in \mathbb{R}^n$, there are more than two directions in which the limit can be calculated, approaching the discontinuity. This extension to scalar and vectorial fields will not be covered below, since a complete definition of all mathematical tools provided by Convex Analysis is beyond the scope of this Thesis. However, only a conceptual view on this topic is necessary to understand the ideas behind the solution of this kind of dynamical system and for all the mathematical details see [23, 32].

Definition 31 (see [32, 57]). A *differential inclusion* is a particular kind of piecewise differential equation, in the form

$$\dot{\boldsymbol{y}}(t) \in \boldsymbol{F}(\boldsymbol{y}(t)),$$

where $\boldsymbol{F}(\boldsymbol{y})$ is a set-valued vector field. The function $\boldsymbol{y}$ that fulfils the previous relation is called a *solution* of the differential inclusion.

According to Filippov, the ODEs with discontinuous right-hand-side can be associated with a differential inclusion. In particular, when $\boldsymbol{y} \in \mathcal{V}_i$ the set-valued vector field $\boldsymbol{F}(\boldsymbol{y})$ is simply equal to $\boldsymbol{f}_i(\boldsymbol{y})$ (interpreted as a set containing only one element equal to $\boldsymbol{f}_i$). On the contrary, when $\boldsymbol{y} \in \Sigma_{ij}$, the set-valued vector field $\boldsymbol{F}(\boldsymbol{y})$ is assumed to be equal to the convex hull of all the limit values of the function $\boldsymbol{f}_i(\boldsymbol{y})$ on the switching manifold Σ_{ij} (and these limits always exist, due to the fact that we have assumed a piecewise continuous vector field). For the considered case (2.12), the convex extension for $\boldsymbol{y} \in \Sigma$ becomes

$$\boldsymbol{F}(\boldsymbol{y}) = \overline{\text{co}}\left\{\boldsymbol{f}^-(\boldsymbol{y}), \boldsymbol{f}^+(\boldsymbol{y})\right\} = \left\{(1-q)\boldsymbol{f}^-(\boldsymbol{y}) + q\boldsymbol{f}^+(\boldsymbol{y}), \forall q \in [0,1]\right\},$$

see, [57], hence the differential inclusion that must be solved is

$$\dot{\boldsymbol{y}}(t) \in \boldsymbol{F}(\boldsymbol{y}) = \begin{cases} \boldsymbol{f}^-(\boldsymbol{y}) & \boldsymbol{y} \in \mathcal{V}^- \\ \overline{\text{co}}\left\{\boldsymbol{f}^-(\boldsymbol{y}), \boldsymbol{f}^+(\boldsymbol{y})\right\} & \boldsymbol{y} \in \Sigma \\ \boldsymbol{f}^+(\boldsymbol{y}) & \boldsymbol{y} \in \mathcal{V}^+ \end{cases}, \tag{2.13}$$

In simple terms, the concept of ODEs has been extended using differential inclusion, where the right-hand side is in general a set. In particular, for the standard case inside each subdomain $\mathcal{V}^{\pm}$, the set is composed only of a single element, otherwise the convex hull is considered. In general, the solution of a classical ODE is a particular function, whose derivative in time is always equal to the given vector field $\boldsymbol{f}$. In this case, the solution of a differential inclusion is the special function $\boldsymbol{y}(t)$, whose first derivative in time is contained in the sets defined by the set-valued function $\boldsymbol{F}(\boldsymbol{y})$. From an intuitive point of view, the conditions that the solution must fulfil are well-defined also for differential inclusions, however, in simple words, there is more freedom in this case since the derivative of the solution in time must belong to a given set and not be exactly equal to a single and specific value.

Finally, the solutions of differential inclusions have been studied and many theorems have been found, that help the definition of a solution also for the non-smooth ODEs with discontinuous right-hand-side.

Theorem 3 (see [32, 57]). *Let's considered a set-valued vector field $\boldsymbol{F}(\boldsymbol{y})$ which is assumed to be nonempty, bounded, closed, convex, and upper-semicontinuous.*

Then, for all initial condition $\boldsymbol{y}_0 \in \mathbb{R}^n$ there exists an absolutely continuous function $\boldsymbol{y}(t)$ which is a solution of the initial value problem

$$\dot{\boldsymbol{y}} \in \boldsymbol{F}(\boldsymbol{y}), \qquad \boldsymbol{y}(0) = \boldsymbol{y}_0.$$

Definition 32 (see [32, 57])**.** A continuous function $\boldsymbol{y}(t)$ is considered a solution in the sense of Filippov of the piecewise-smooth dynamical system described by the discontinuous ODEs (2.11) if for almost all t the function fulfils

$$\dot{\boldsymbol{y}} \in \boldsymbol{F}(\boldsymbol{y}),$$

where $\boldsymbol{F}(\boldsymbol{y})$ is the convex hull of all the limits of $\boldsymbol{f}_i(\boldsymbol{y})$.

The previous Theorem 3 and Definition 32 provide a rigorous mathematical basis for the analysis of piecewise-smooth problems, since they define the hypotheses for the existence of a solution of a differential inclusion and the extension to the concept of solution from discontinuous systems to differential inclusions. The problem that will be analysed is a particular case of those studied above, but after this explanation from a more general perspective, its collocation in the framework of the analysis of discontinuous dynamical system should be more clear.

A final example, depicted in Figure 2.6 and regarding the possible situations that can be encountered in the analysis of systems in the form (2.12), may now clarify the analysis of a Filippov system, see [32, 46, 51, 57]. The dynamical system is described by the two subspaces $\mathcal{V}^{\pm}$

$$\mathcal{V}^{-} = \{\boldsymbol{y} \in \mathbb{R}^n : h(\boldsymbol{y}) < 0\},$$
$$\mathcal{V}^{+} = \{\boldsymbol{y} \in \mathbb{R}^n : h(\boldsymbol{y}) > 0\},$$

while the switching manifold is identified by the function $h(\boldsymbol{y})$, so that

$$\Sigma = \{\boldsymbol{y} \in \mathbb{R}^n : h(\boldsymbol{y}) = 0\}.$$

The switching manifold is always supposed to be sufficiently smooth to be able to define a local unit normal vector, such that

$$\boldsymbol{n}(\boldsymbol{y}) = \frac{\nabla h((\boldsymbol{y}))}{||\nabla h((\boldsymbol{y}))||}.$$

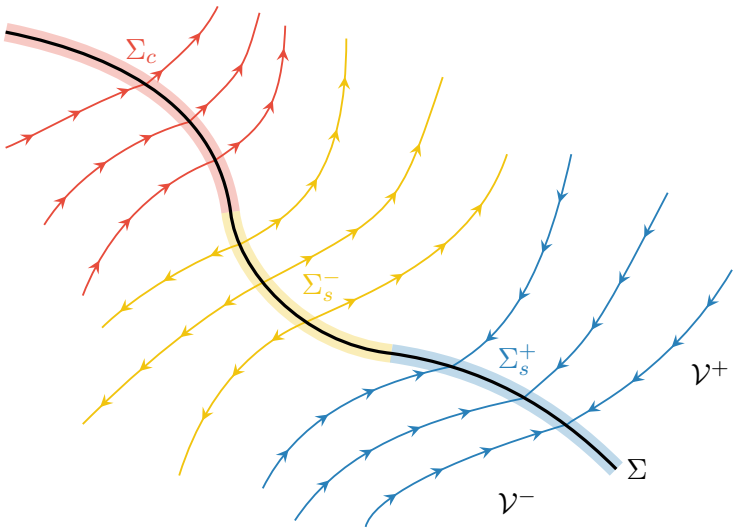

Figure 2.6: Partition of the switching manifold Σ in different parts, on the basis of the crossing or sliding properties. The orbits approaching the subspace Σ_c (red) cross the manifold, since the signs of the projections onto the normal to switching surface of the orbital velocity calculated in the discontinuity are the same, both for the negative and positive system. The orbits approaching Σ_s^+ (blue) produce an attractive sliding, since all the trajectories are directed towards the manifold. On the contrary, the orbits approaching Σ_s^- (yellow) tends to evolve far from the switching manifold, in opposite directions, so this subspace is repulsive.

The behaviour of the dynamical system on the switching manifold is described by the quantity

$$b(\boldsymbol{y}) = \left(\boldsymbol{n}(\boldsymbol{y}) \cdot \boldsymbol{f}^-(\boldsymbol{y})\right)\left(\boldsymbol{n}(\boldsymbol{y}) \cdot \boldsymbol{f}^+(\boldsymbol{y})\right) = \left(\boldsymbol{n}^{\mathrm{T}}\boldsymbol{f}^-\right)\left(\boldsymbol{n}^{\mathrm{T}}\boldsymbol{f}^+\right),$$

and in particular the following classification of the points of the switching manifold can be performed:

i) *crossing*: this subspace Σ_c is composed of all the points of the switching manifold for which the orbit that approaches these points simply

crosses the hypersurface describing the discontinuity, i.e.

$$\Sigma_c = \left\{ \boldsymbol{y} \in \Sigma : b(\boldsymbol{y}) = \left(\boldsymbol{n}^{\mathrm{T}} \boldsymbol{f}^{-} \right) \left(\boldsymbol{n}^{\mathrm{T}} \boldsymbol{f}^{+} \right) > 0 \right\};$$

ii) *sliding*: this subspace Σ_s is composed of all the points of the switching manifold for which the orbit "slides" on hypersurface describing the discontinuity, i.e.

$$\Sigma_s = \left\{ \boldsymbol{y} \in \Sigma : b(\boldsymbol{y}) = \left(\boldsymbol{n}^{\mathrm{T}} \boldsymbol{f}^{-} \right) \left(\boldsymbol{n}^{\mathrm{T}} \boldsymbol{f}^{+} \right) < 0 \right\};$$

This case can be further classified on the basis of the sign of $\boldsymbol{n}^{\mathrm{T}} \boldsymbol{f}^{-}$ (or $\boldsymbol{n}^{\mathrm{T}} \boldsymbol{f}^{+}$) as

$$\Sigma_s^{-} = \left\{ \boldsymbol{y} \in \Sigma_s : \boldsymbol{n}^{\mathrm{T}} \boldsymbol{f}^{-} < 0 \right\}$$
$$\Sigma_s^{+} = \left\{ \boldsymbol{y} \in \Sigma_s : \boldsymbol{n}^{\mathrm{T}} \boldsymbol{f}^{-} > 0 \right\}$$

and, in particular, for the points belonging to Σ_s^{-} (Σ_s^{+}), the sliding motion is called *repulsive* (*attractive*). In fact, the orbits near the points of Σ_s^{+} are directed toward the switching manifold, so they are "trapped" and forced to remain on the discontinuity until they possibly reach a point of the switching manifold in which the orbits can leave Σ (e.g. the crossing points of Σ_c). On the contrary, as for the orbits that approach the points of Σ_s^{-}, they are directed away from the hypersurface Σ and tend to evolve far from the discontinuity, so this part of the switching manifold is repulsive.

Let's note that, in case of sliding, the flow in Σ_s is described by a differential equation $\dot{\boldsymbol{y}} = \boldsymbol{f}^0(\boldsymbol{y})$, whose vector field $\boldsymbol{f}^0$ can be determined by the so-called Filippov's extension. First of all, the differential inclusion (2.13) is fulfilled in the points of the switching manifold, hence in Σ_s the set-valued function $\boldsymbol{F}(\boldsymbol{y})$ is assumed to be equal to the convex hull $\overline{\mathrm{co}} \left\{ \boldsymbol{f}^{-}(\boldsymbol{y}), \boldsymbol{f}^{+}(\boldsymbol{y}) \right\}$. The vector field $\boldsymbol{f}^0$ is an element of the convex hull

$$\boldsymbol{f}^0(\boldsymbol{y}) = (1-q)\boldsymbol{f}^{-} + q\boldsymbol{f}^{+},$$

for a *specific* value of the parameter $q \in [0, 1]$. This special value can be computed, observing that the evolution on the switching manifold must

be tangent to the discontinuity hypersurface, thus the vector field must be orthogonal to the unit vector normal to the switching manifold, so that

$$\boldsymbol{f}^0(\boldsymbol{y}) \cdot \boldsymbol{n}(\boldsymbol{y}) = 0.$$

The value of the parameter q can now be calculated as

$$\boldsymbol{f}^0(\boldsymbol{y}) \cdot \boldsymbol{n}(\boldsymbol{y}) = (1-q)\boldsymbol{f}^- \cdot \boldsymbol{n} + q\boldsymbol{f}^+ \cdot \boldsymbol{n} = 0,$$

leading to

$$q = -\frac{\boldsymbol{f}^- \cdot \boldsymbol{n}}{(\boldsymbol{f}^+ - \boldsymbol{f}^-) \cdot \boldsymbol{n}}. \tag{2.14}$$

Finally, see [32, 52, 57], the equations of motion can be deduced substituting the value of q in (2.14) into the expression of $\boldsymbol{f}^0$, leading to the differential equation

$$\dot{\boldsymbol{y}} = \frac{(\boldsymbol{f}^+ \cdot \boldsymbol{n})\boldsymbol{f}^- - (\boldsymbol{f}^- \cdot \boldsymbol{n})\boldsymbol{f}^+}{(\boldsymbol{f}^+ - \boldsymbol{f}^-) \cdot \boldsymbol{n}}. \tag{2.15}$$

For a generic non-smooth problem, the switching manifold Σ can be decomposed in its crossing and sliding parts, Σ_c and Σ_s respectively, so the definition of the vector field $\boldsymbol{f}^{\pm}$ allows the explicit determination of the switching properties of the discontinuity.

Particular solutions of non-smooth dynamical systems like (2.11) are equilibrium points, that can be located in different parts of the phase space, namely inside the subspaces $\mathcal{V}_i$ or exactly on the switching manifolds Σ_{ij}.

In the literature dealing with non-smooth dynamics, many examples have been provided concerning internal and boundary equilibria and all the implications and different behaviours that this kind of system shows in the evolution of the motion, see [33, 62, 63, 80]. Moreover, an interesting part of the analysis of these discontinuous systems is the determination of bifurcation points, leading to a wide range of different possible behaviours. The classification of all possible bifurcations and equilibrium configuration is beyond the scope of this Thesis and will be neglected, since the theoretical concepts introduced above are only functional to the analysis of a specific mechanical problem that will be introduced in the next Chapter 3.

As a final remark, the theoretical aspects treated in this Section are useful to understand the analysis that will be performed in the next Chapters. The topic of this Thesis is only a simplified version of a Filippov dynamical system, since we will demonstrate that, for the problem analysed below, only crossing conditions can be present, so all the complicated features of the Filippov system involving differential inclusions could in principle be discarded. However, the explanation given above shows the theoretical background and the complete framework in which this problem can be considered.

2.2.4 The reference mechanical system and the presence of invariant sets

The aim of this Thesis is the definition of an instability criterion for piecewise-smooth mechanical systems that can be written in the form

$$\dot{\boldsymbol{y}}(t) = \begin{cases} \boldsymbol{f}^{-}(\boldsymbol{y}) & \boldsymbol{y} \in \mathcal{V}^{-} \\ \boldsymbol{f}^{+}(\boldsymbol{y}) & \boldsymbol{y} \in \mathcal{V}^{+} \end{cases}. \tag{2.16}$$

No well-known criteria can be adopted for non-smooth structures, so the only way to understand the behaviour of a discontinuous system is through the investigation of the presence of particular invariant sets in the phase space. If an invariant set with given instability properties is successfully detected for a given combination of design parameters, then the behaviour of the system (at least near the invariant manifold) is known and some qualitative results for the entire system can be extracted.

The analysis of the mechanical structure that will be presented in Chapter 3 is based on the identification of a particular kind of invariant set, called *invariant cone*, see [14, 16, 51, 52, 86]. The mathematical description of an invariant cone will be investigated extensively in Chapter 4, however, a conceptual and intuitive interpretation of this invariant manifold will be given now, to better understand the notions of Poincaré maps and attractivity that will be analysed in the Sections below.

An invariant cone is a non-smooth $\mathbb{R}^{n-1}$ manifold embedded in the $\mathbb{R}^n$ phase space. The tip of this multidimensional cone is located in the origin, which is also the equilibrium point, exactly on the discontinuity between the subspaces $\mathcal{V}^{\pm}$ in which the phase space can be partitioned, hence the analysed invariant cone is composed by two different parts.

If an asymptotically stable invariant cone exists, then the orbits laying on it may present three different configurations, see Figure 2.7:

- the trajectories on the invariant manifold evolve in time proceeding toward the tip of the cone in a sort of spiralling path;
- the trajectories on the invariant manifold evolve in time proceeding far from the tip of the cone in a sort of spiralling path, thus the origin can be considered an unstable fixed point;
- the trajectories are periodic and the orbits on the cone are closed;

The investigation on the stability of the equilibrium point located on the tip of the invariant cone is then reduced to the analysis of the presence of this kind of invariant manifold and on its attractivity.

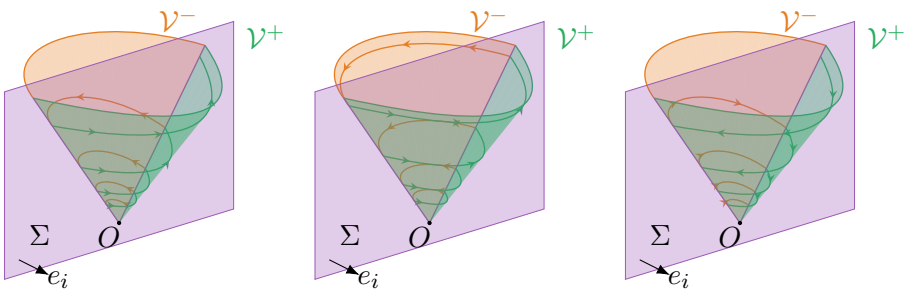

(a) *unstable invariant cone* **(b)** *periodic orbits* **(c)** *stable invariant cone*

Figure 2.7: Conceptual sketch of piecewise invariant cones in a 3D phase space. The cone is composed of two parts, each of them embedded in the positive and negative subdomain $\mathcal{V}^{\pm}$, divided by the switching manifold Σ. The family of the orbits belonging to the invariant cone may i) spiral out from the tip of the cone (Fig. 2.7a), ii) spiral in toward the vertex (Fig. 2.7c) or iii) be composed of periodic orbits (Fig. 2.7b). These different cases reveal a precise stability behaviour of the equilibrium configuration, which is located at the tip of the cone.

For this purpose, some theoretical tools must be introduced for the analysis of solutions more complicated than fixed points, for instance, periodic orbits. The investigation on the attractivity of a smooth or non-

smooth invariant set can be performed considering the behaviour of perturbed solutions near a particular reference one that belongs to the given invariant manifold. This kind of analysis can essentially be carried out in two ways:

- the *continuous-time approach*, where a linearisation of the differential equations (2.3) near a given solution of the autonomous system is performed, introducing a perturbation in the initial conditions, see [57];
- the *discrete-time approach*, where a Poincaré map is introduced, see Section 2.2.5, and in particular the Jacobian matrix of the Poincaré map is analysed, to understand the influence of a small perturbation in the initial conditions, see [51, 86];

Both strategies can successfully be used to define the attractivity of a cone, however, in Chapter 4, the first approach has been adopted, since easier computations can be performed, with respect to the second method.

2.2.5 Poincaré maps for the identification of invariant sets

A Poincaré map is a useful theoretical tool for the analysis of solutions of autonomous dynamical systems which are more complex than fixed points. It will be defined for a smooth system, see[54, 74, 88], and then this idea will be extended for the analysis of non-smooth ones.

Let's consider the autonomous dynamical system (2.3) and let's suppose that there exists a limit cycle $\mathscr{L}$ in the $\mathbb{R}^n$ phase space, passing through a given point $\boldsymbol{y}^*$. Let's consider a $(n-1)$-dimensional hyperplane Σ, called *Poincaré section*, which is transversal to the limit cycle in the point $\boldsymbol{y}^*$. The orbit of the cycle $\mathscr{L}$, emanating from $\boldsymbol{y}^*$, "hits" the cross-section Σ in the point $\boldsymbol{y}^*$, after one period T.

Due to the continuity of the solution $\boldsymbol{\varphi}_t(\boldsymbol{y})$ with respect to the initial conditions, there exists a sufficiently small neighbourhood $U \subset \Sigma$ of $\boldsymbol{y}^*$, for which the orbits with initial conditions $\boldsymbol{y} \in U$ hit the cross-section in another neighbourhood $V \subset \Sigma$, in approximately one period T. Hence, the flow $\boldsymbol{\varphi}_t(\boldsymbol{y})$ and the hyperplane Σ define a map $\boldsymbol{P}$ from a neighbourhood of $\boldsymbol{y}^*$ to another neighbourhood of $\boldsymbol{y}^*$.

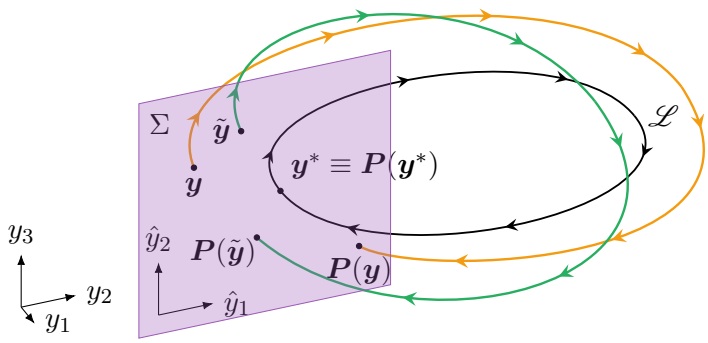

Figure 2.8: Sketch of a Poincaré map in a 3D phase space. The black closed orbit $\mathscr{L}$ intersects the Poincaré section Σ in a single point $\boldsymbol{y}^*$. The generic points $\boldsymbol{y}, \tilde{\boldsymbol{y}} \in \Sigma$ are mapped to the plane itself through orbits obtained as perturbations from the reference periodic solution $\mathscr{L}$. The points of the Poincaré map $\boldsymbol{P}$ can be defined in a global reference frame $Oy_1y_2y_3$, as well as in a local one defined on the section Σ, namely $O\hat{y}_1\hat{y}_2$.

Definition 33 (see [54])**.** The map $\boldsymbol{P} : \Sigma \to \Sigma$ that maps the points of the hyperplane onto itself, following the flow $\boldsymbol{\varphi}_t$, is called the *Poincaré map* associated with the limit cycle $\mathscr{L}$.

Due to the definition of Poincaré section, the continuous-time dynamical system described by the flow $\boldsymbol{\varphi}_t$ is transformed into a discrete-time dynamical system through the map

$$\boldsymbol{P} : \Sigma \to \Sigma, \qquad \boldsymbol{y}_{k+1} = \boldsymbol{P}(\boldsymbol{y}_k), \quad \boldsymbol{y}_k \in \Sigma,$$

so that the motion is fully described by the sequence of points $\{\boldsymbol{y}_k\}_{k=1}^{\infty}$ belonging to the cross-section Σ. In this approach the time variable t becomes unnecessary and it can be substituted in the flow $\boldsymbol{\varphi}_t$ by the crossing time $t_k = t(\boldsymbol{y}_k)$, which is assumed as a function of the initial point of the Poincaré map.

Although the Poincaré map is uniquely defined from a theoretical point of view, the mathematical description of the map can be given in different ways. In fact, the mapped points can be thought as n-dimensional points that belong to a particular $(n-1)$-dimensional subset Σ of the en-

tire phase space, or equivalently as $(n-1)$-dimensional points defined in a local description of the Poincaré section, namely,

$$\hat{\boldsymbol{y}} \mapsto \boldsymbol{P}(\hat{\boldsymbol{y}}),$$

where the vector $\hat{\boldsymbol{y}} \in \Sigma \subset \mathbb{R}^{n-1}$ has been introduced as the restriction of $\boldsymbol{y}$ onto the Poincaré section, see [57]. In the following Chapters, with abuse of notation, when the concept of Poincaré map will be used from a theoretical perspective, in both cases the Poincaré maps will be denoted by $\boldsymbol{P}$, since the concept of Poincaré map is general and valid for any local description of the $(n-1)$-manifold of the Poincaré section. However, when the distinction between the two mathematical representations is necessary to fully understand the implementation of this theoretical tool and all the computations, a superimposed hat $\hat{\boldsymbol{P}}$ is used to represent a generic point in the local $(n-1)-$dimensional reference frame on Σ.

Moreover, one must note that the Poincaré map is locally defined, near the point $\boldsymbol{y}^*$ of the limit cycle $\mathscr{L}$. Thus, the well-definiteness of the map from any point of Σ is not guaranteed *a priori*, since the flow $\boldsymbol{\varphi}_t(\boldsymbol{y}_0)$, in principle, could not intersect the Poincaré section. The above definition of Poincaré map can be particularised in order to investigate the cases in which the cross-section Σ is defined in a Euclidean space, where the closed orbit $\mathscr{L}$ emanating from $\boldsymbol{y}^*$ could in principle intersect the Poincaré section more than once. The cross-section divides the Euclidean phase space into two different subspaces and the Poincaré maps for the two subspaces are called $\boldsymbol{P}'$ and $\boldsymbol{P}''$, respectively.

If k intersections [4] can be found between the reference limit cycle and the Poincaré section in a period T, then the Poincaré map after k intersections can be computed as

$$\boldsymbol{P} = \underbrace{\tilde{\boldsymbol{P}} \circ \cdots \circ \tilde{\boldsymbol{P}}}_{k/2 \quad times},$$

where the operator '$\circ$' is intended as the composition of functions and $\tilde{\boldsymbol{P}} = \boldsymbol{P}'' \circ \boldsymbol{P}'$, assuming, without loss of generality, that the Poincaré map

[4] in this representation, k is always considered as an even number, since we are referring to all the intersections (between the given orbit and the cross-section) that *follow* the initial point $\boldsymbol{y}^*$ in the evolution of the trajectory within the period T, discarding the initial point $\boldsymbol{y}^*$; the number of intersections k could be odd only when the orbit is tangential to the section in a crossing point, but, for the sake of simplicity, this case is neglected in the considered representation of the composition of Poincaré maps.

of the first system in which the orbit enters is $\boldsymbol{P}'$. This practical considerations will be useful in further calculations, in order to understand the composition of halfmaps for piecewise-smooth dynamical systems.

The Poincaré maps are generally introduced in order to better represent and analyse the solutions of dynamical systems with limit cycles or other invariant sets that are more complicated than fixed points. For instance, a limit cycle for the flow $\boldsymbol{\varphi}_t$ corresponds to a fixed point $\boldsymbol{y}^*$ of the Poincaré map $\boldsymbol{P}$, as we have already seen from the definitions above. Moreover, an higher order invariant set, e.g. an invariant 2-torus (obtained by a 2-periodic solution of the dynamical system) can be described by the intersection of the 2-torus and the $(n-1)$-hyperplane Σ, hence the point of the map lies on a set of 1-dimensional curves on the Poincaré section. In general, a k-dimensional invariant set in the continuous-time flow $\boldsymbol{\varphi}_t$ is described by one or more $(k-1)$-dimensional invariant tori in Σ, by the Poincaré map $\boldsymbol{P}$, see [74].

Regularity properties can be derived for Poincaré maps, e.g. $\boldsymbol{P}$ is continuous and differentiable if the vector field $\boldsymbol{f}$ is transversal to Σ at the points $\boldsymbol{y}$ and $\boldsymbol{P}(\boldsymbol{y})$. However, the benefits of the reduction in the dimension of the invariant sets describing the motion of the dynamical system are often cancelled out by the fact that the explicit definition of the Poincaré map is not trivial and it is not easy to use in practical applications.

The concept of Poincaré map can easily be extended to the case of non-smooth dynamics, see [42, 51, 52, 86, 87], in order to determine the behaviour of discontinuous systems and to detect possible invariant sets. The fundamental assumption that supports the analysis of the piecewise systems like (2.16) is that the Poincaré section is assumed to coincide with the switching manifold Σ, between the two subspaces $\mathcal{V}^-$ and $\mathcal{V}^+$ in which the phase space is partitioned. With this assumption, the Poincaré map simply becomes the composition of a series of *Poincaré halfmaps* valid for each subsystem, $\boldsymbol{P}^-(\hat{\boldsymbol{y}})$ and $\boldsymbol{P}^+(\hat{\boldsymbol{y}})$ for the subspace $(-)$ and $(+)$ respectively, such that

$$\boldsymbol{P} = \cdots \circ \boldsymbol{P}^+ \circ \boldsymbol{P}^- \circ \cdots \circ \boldsymbol{P}^- \circ \boldsymbol{P}^+ \circ \boldsymbol{P}^-, \tag{2.17}$$

where it has been assumed that, without loss of generality, the first halfmap to be applied is the negative one $\boldsymbol{P}^-$. The discrete map (2.17), between the points belonging to the switching manifold, substitutes the in-

vestigation of the continuous-time orbits of the dynamical systems. Moreover, specific invariant sets can be defined only considering the points of the Poincaré map, imposing a particular "rule" for the discrete transition from a point to another one.

For instance, as will be described in details in Chapters 4, the invariant cones introduced in Section 2.2.4 can be defined as particular invariant sets, described by the points $\hat{\boldsymbol{n}} \in \Sigma$, such that $\boldsymbol{P}(\hat{\boldsymbol{n}}) = \mu\hat{\boldsymbol{n}}$, where $\mu \in \mathbb{R}^+$. The definition of an invariant set using a Poincaré map can be generally simpler, since the conditions that must be imposed are restricted only on those points belonging to the Poincaré section, therefore the behaviour of the entire system is condensed in the evolution of specific points of a discrete map.

2.2.6 Attractivity of an invariant set: monodromy matrix and Floquet multipliers

An important feature of an invariant set is the attractivity, the property that allows to predict the behaviour of the system with initial conditions located in the neighbourhood of the considered invariant manifold. The attractivity of a nonsmooth invariant set can be studied extending the concept of monodromy matrix and Poincaré maps that are generally defined for a smooth system, see [57]. In this paragraph, these analytical tools will be described.

Let's consider the first order ODEs (2.3) describing an autonomous dynamical system, together with a reference known solution $\tilde{\boldsymbol{y}}(t)$ of this set of differential equations, with initial condition $\tilde{\boldsymbol{y}}_0$, such that

$$\dot{\tilde{\boldsymbol{y}}}(t) = \boldsymbol{f}(\tilde{\boldsymbol{y}}(t)), \tag{2.18}$$

for all t.

The perturbed solution near the reference orbit, depicted in Figure 2.9, can be expressed by $\tilde{\boldsymbol{y}}(t) + \delta\boldsymbol{y}(t)$, and it also fulfils the same differential equation (2.3), hence

$$(\tilde{\boldsymbol{y}}(t) + \delta\boldsymbol{y}(t))^{\cdot} = \boldsymbol{f}(\tilde{\boldsymbol{y}}(t) + \delta\boldsymbol{y}(t)), \tag{2.19}$$

with the perturbed initial conditions $\tilde{\boldsymbol{y}}_0 + \delta\boldsymbol{y}_0$. The right-hand-side of equa-

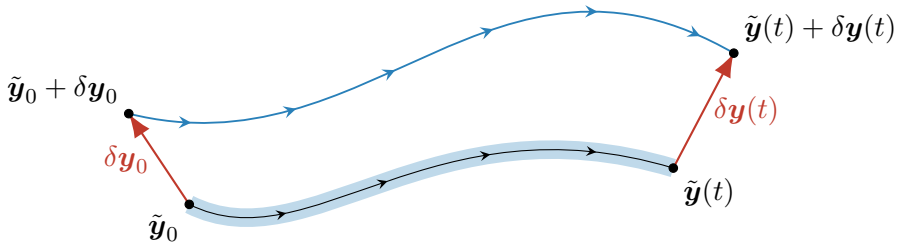

Figure 2.9: Perturbation of a general solution of a smooth dynamical system. A small perturbation $\delta\boldsymbol{y}_0$ is given to the initial conditions of the reference solution $\tilde{\boldsymbol{y}}(t)$, defining a perturbed one $\tilde{\boldsymbol{y}}(t) + \delta\boldsymbol{y}(t)$, that evolves in time. The perturbation from the reference orbit at a given time t is described by the vector $\delta\boldsymbol{y}(t)$.

tion (2.19) can be expanded in Taylor series as

$$(\tilde{\boldsymbol{y}}(t) + \delta\boldsymbol{y}(t))^{\cdot} = \dot{\tilde{\boldsymbol{y}}} + \dot{\delta\boldsymbol{y}} = \boldsymbol{f}(\tilde{\boldsymbol{y}}(t) + \delta\boldsymbol{y}(t)) = \boldsymbol{f}(\tilde{\boldsymbol{y}}) + \frac{\partial \boldsymbol{f}}{\partial \boldsymbol{y}}(\tilde{\boldsymbol{y}})\delta\boldsymbol{y} + H.O.T.$$

which can be rewritten, using equation (2.18) and neglecting the higher order terms, as a linear relation in the perturbation, namely

$$\dot{\delta\boldsymbol{y}}(t) = \frac{\partial \boldsymbol{f}}{\partial \boldsymbol{y}}(\tilde{\boldsymbol{y}})\, \delta\boldsymbol{y}(t),$$

together with the incremental initial conditions $\delta\boldsymbol{y}(t_0) = \delta\boldsymbol{y}_0$. This differential equation in the increment $\delta\boldsymbol{y}$ can generally be solved as a function of the incremental initial conditions, obtaining

$$\delta\boldsymbol{y}(t) = \boldsymbol{\Phi}(t, t_0, \tilde{\boldsymbol{y}}_0)\delta\boldsymbol{y}_0,$$

where $\boldsymbol{\Phi}(t, t_0, \tilde{\boldsymbol{y}_0})$ is called *fundamental solution matrix* and describes the evolution in time of the perturbation of a given reference solution. Let's note that for autonomous systems the fundamental solution matrix does not depends on the initial time t_0. For a linear autonomous system $\boldsymbol{f}(\boldsymbol{y}) = \boldsymbol{A}\boldsymbol{y}$ the form of the fundamental solution matrix is well-known and it can be computed as

$$\boldsymbol{\Phi}(t, \tilde{\boldsymbol{y}}_0) = e^{\boldsymbol{A}t},$$

since the perturbation and the solution of a linear system fulfil the same linear relation.

Definition 34 (see [57])**.** For a T-periodic reference solution of an autonomous system, the fundamental solution matrix calculated at time T, namely,

$$\mathbf{\Phi}_T = \mathbf{\Phi}(T, \tilde{\boldsymbol{y}}_0),$$

is called *monodromy matrix*.

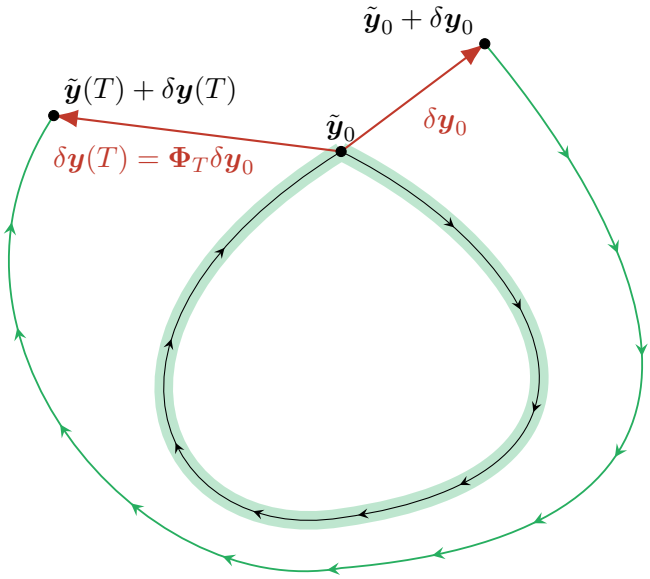

Figure 2.10: Perturbation of a periodic orbit. A small perturbation $\delta\boldsymbol{y}_0$ is given to the initial conditions $\tilde{\boldsymbol{y}}_0$, from which a periodic solution originates. The monodromy matrix $\mathbf{\Phi}_T$ applied to the initial perturbation allows the computation of the perturbed solution after a period T.

The monodromy matrix plays an important role in the description of a periodic system, since the evolution of the perturbations in the neighbourhood of the given reference periodic solution after the k-th cycle can

be expressed by the composition of k monodromy matrices

$$\delta \boldsymbol{y}(kT) = \underbrace{\boldsymbol{\Phi}_T \boldsymbol{\Phi}_T \boldsymbol{\Phi}_T \cdots \boldsymbol{\Phi}_T}_{k-times} \delta \boldsymbol{y}_0 = \boldsymbol{\Phi}_T^k \delta \boldsymbol{y}_0. \tag{2.20}$$

Moreover, the monodromy matrix can also be diagonalized as $\boldsymbol{\Phi}_T = \boldsymbol{U}\boldsymbol{\Lambda}\boldsymbol{U}^{-1}$, so the evolution of the perturbations as functions of time is described by

$$\delta \boldsymbol{y}(kT) = \boldsymbol{U}\boldsymbol{\Lambda}^k\boldsymbol{U}^{-1} \delta \boldsymbol{y}_0. \tag{2.21}$$

Definition 35 (see [57])**.** The eigenvalues of the monodromy matrix $\boldsymbol{\Phi}_T$ are called *Floquet multipliers*.

If the modulus of all the Floquet multipliers is lower than 1, the perturbation decays when $t \to +\infty$, i.e. the reference periodic solution is *asymptotically stable* and the perturbed solution approaches the reference one (the orbit is attractive). On the contrary, when at least one eigenvalue of the monodromy matrix has a modulus greater than 1, the perturbation grows up and the reference periodic solution is *unstable*.

One must note that for an autonomous system (actually the definitions above are more general and hold true also for non autonomous one), the vector field $\boldsymbol{f}(\tilde{\boldsymbol{y}}_0)$ calculated at the initial time is always an eigenvector of the monodromy matrix and the associated eigenvalue is equal to 1. This result comes from the fact that, when an initial perturbation is chosen exactly as the vector field $\boldsymbol{f}_0$, the initial condition still remains on the reference solution, since the initial point is simply shifted along the reference orbit in a point different from $\tilde{\boldsymbol{y}}_0$. This choice of initial conditions leads to the equivalence of perturbed and reference solution, in case of autonomous system. Moreover, due to the periodicity of the reference solution, the perturbation after one period must be the same, hence $\boldsymbol{f}_0 = \boldsymbol{\Phi}_T \boldsymbol{f}_0$, which implies that $\boldsymbol{f}_0$ is an eigenvector of $\boldsymbol{\Phi}_T$, with the associated eigenvalue equal to 1. Furthermore, since one of the eigenvalues is always equal to 1, for an autonomous dynamical system the stability properties are defined by the other $n-1$ Floquet multipliers.

The concept of monodromy matrix and Floquet multipliers can be generalised and extended to the case of piecewise-smooth systems, like (2.16). The linearisation of the right-hand side of the equations of motion is not a problem for a smooth system, however, the presence of the switching manifold for piecewise systems introduces some difficulties in the definition

of the perturbed solution, that must carefully be understood and considered.

Due to the presence of the discontinuity, there could be in principle a finite time interval δt_p in which the reference solution and the perturbed one may belong to a different subspace $\mathcal{V}^{\pm}$. This fact would lead to an incorrect definition of the evolution in time of the perturbation $\delta \boldsymbol{y}(t)$, since essentially the linearisation of the vector field $\boldsymbol{f}^{\pm}$ would be performed in the wrong subspace.

This problem is overcome with the introduction of the so-called *saltation matrix* $\boldsymbol{S}$, which essentially describes how the perturbation of the given solution evolves in the infinitesimal time interval when the orbit crosses the switching manifold.

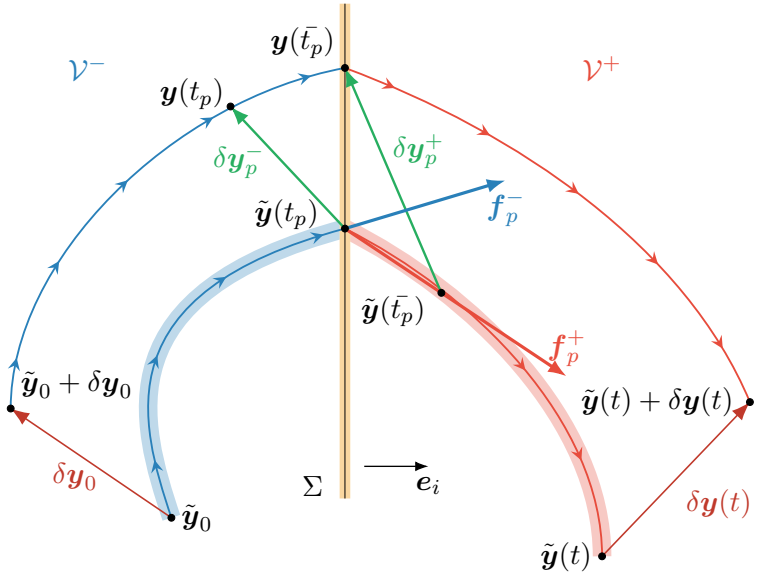

Figure 2.11: Evolution of the reference solution $\tilde{\boldsymbol{y}}(t)$ and of a perturbed one $\tilde{\boldsymbol{y}}(t) + \delta \boldsymbol{y}(t)$, for autonomous piecewise systems described by two subdomains $\mathcal{V}^{\pm}$. Due to the time delay $\bar{t_p} - t_p$ between the intersections of the two solutions with the switching manifold, a saltation matrix $\boldsymbol{S}^{\pm}$ must be introduced, for the correct computation of the evolution of the perturbation in time.

As can be seen in Figure 2.11, let's suppose, without loss of generality,

that the reference solution $\tilde{\boldsymbol{y}}(t)$, with initial conditions $\tilde{\boldsymbol{y}}(0) = \tilde{\boldsymbol{y}}_0$ located in the negative subspace $\mathcal{V}^-$, crosses the switching manifold at time t_p, while a perturbed solution $\boldsymbol{y}(t)$, with initial conditions $\boldsymbol{y}(0) = \tilde{\boldsymbol{y}}_0 + \delta\boldsymbol{y}_0$ still in the negative subspace, crosses the manifold Σ at time $\bar{t}_p$. The time interval δt_p is the time delay in which the two orbits are in two different subspaces.

Let's now define the perturbations $\delta\boldsymbol{y}_p^-$ and $\delta\boldsymbol{y}_p^+$ as

$$\delta\boldsymbol{y}_p^- = \boldsymbol{y}(t_p) - \tilde{\boldsymbol{y}}(t_p) \qquad\qquad \delta\boldsymbol{y}_p^+ = \boldsymbol{y}(\bar{t}_p) - \tilde{\boldsymbol{y}}(\bar{t}_p), \tag{2.22}$$

which are the perturbation vectors from the reference solution, calculated at t_p and $\bar{t}_p$, respectively. The main purpose is now the definition of the relation between the perturbations $\delta\boldsymbol{y}_p^-$ and $\delta\boldsymbol{y}_p^+$.

The reference solution at time $\bar{t}_p = t_p + \delta t_p$ can be written in Taylor expansion, truncated to the first order terms, as

$$\tilde{\boldsymbol{y}}(\bar{t}_p) = \tilde{\boldsymbol{y}}(t_p + \delta t_p) \approx \tilde{\boldsymbol{y}}(t_p) + \dot{\tilde{\boldsymbol{y}}}(t_p)\delta t_p = \tilde{\boldsymbol{y}}(t_p) + \boldsymbol{f}_p^+\delta t_p, \tag{2.23}$$

where $\dot{\tilde{\boldsymbol{y}}}(t_p) = \boldsymbol{f}^+(t_p) = \boldsymbol{f}_p^+$, because the reference solution is assumed to enter in the positive subspace $\mathcal{V}^+$. Analogously, the perturbed solution can be expanded as

$$\boldsymbol{y}(\bar{t}_p) = \boldsymbol{y}(t_p + \delta t_p) \approx \boldsymbol{y}(t_p) + \dot{\boldsymbol{y}}(t_p)\delta t_p = \boldsymbol{y}(t_p) + \boldsymbol{f}_p^-\delta t_p, \tag{2.24}$$

where $\dot{\boldsymbol{y}}(t_p) = \boldsymbol{f}^-(t_p) = \boldsymbol{f}_p^-$, since the perturbed solution is still in the negative subsystem $\mathcal{V}^-$ at time t_p. Substituting the first definition of (2.22) into (2.24), the latter becomes

$$\boldsymbol{y}(\bar{t}_p) \approx \tilde{\boldsymbol{y}}(t_p) + \delta\boldsymbol{y}_p^- + \boldsymbol{f}_p^-\delta t_p. \tag{2.25}$$

The link between the perturbations can now be written, according to (2.22), (2.23), and (2.25), as

$$\delta\boldsymbol{y}_p^+ = \delta\boldsymbol{y}_p^- + (\boldsymbol{f}_p^- - \boldsymbol{f}_p^+)\delta t_p, \tag{2.26}$$

where the time delay δt_p can be calculated from the switching condition. Let's suppose that the switching manifold can be described by a condition in the form

$$\boldsymbol{y}(t) \in \Sigma \quad \Longleftrightarrow \quad h(\boldsymbol{y}(t)) = 0, \tag{2.27}$$

where a smooth function $h : \mathbb{R}^n \to \mathbb{R}$ has been introduced. This definition of the constraint implies that $h(\boldsymbol{y}(\bar{t}_p)) = 0$ is fulfilled, while its left-hand-side can be approximated, according to (2.25), with a Taylor expansion as

$$h(\boldsymbol{y}(\bar{t}_p)) = h(\tilde{\boldsymbol{y}}(t_p)+\delta\boldsymbol{y}_p^- + \boldsymbol{f}_p^-\delta t_p) \approx h(\tilde{\boldsymbol{y}}(t_p))+\frac{\partial h}{\partial \boldsymbol{y}}(\boldsymbol{y}(t_p))\cdot(\delta\boldsymbol{y}_p^- + \boldsymbol{f}_p^-\delta t_p),$$

where $\frac{\partial h}{\partial \boldsymbol{y}}(\boldsymbol{y}(t_p)) = \boldsymbol{n}(\boldsymbol{y}(t_p))$ is the gradient of the switching condition, which is the normal vector to the surface, when the switching manifold is an hyperplane. Moreover, recalling that also $h(\tilde{\boldsymbol{y}}(t_p)) = 0$, the following relation holds

$$h(\boldsymbol{y}(\bar{t}_p)) \approx \boldsymbol{n}^{\mathrm{T}}(\delta\boldsymbol{y}_p^- + \boldsymbol{f}_p^-\delta t_p) = 0,$$

thus the time delay can be calculated as

$$\delta t_p = -\frac{\boldsymbol{n}^{\mathrm{T}}\delta\boldsymbol{y}_p^-}{\boldsymbol{n}^{\mathrm{T}}\boldsymbol{f}_p^-}, \tag{2.28}$$

where the scalar product has been substituted by the equivalent operation of the product between two vectors, with the introduction of the transposition.

The relation between the perturbations can now be written, substituting (2.28) into (2.26), as

$$\delta\boldsymbol{y}_p^+ = \delta\boldsymbol{y}_p^- + \frac{\boldsymbol{f}_p^+ - \boldsymbol{f}_p^-}{\boldsymbol{n}^{\mathrm{T}}\boldsymbol{f}_p^-}\boldsymbol{n}^{\mathrm{T}}\delta\boldsymbol{y}_p^- = \left[\boldsymbol{I} + \frac{(\boldsymbol{f}_p^+ - \boldsymbol{f}_p^-)\boldsymbol{n}^{\mathrm{T}}}{\boldsymbol{n}^{\mathrm{T}}\boldsymbol{f}_p^-}\right]\delta\boldsymbol{y}_p^- = \boldsymbol{S}^-\delta\boldsymbol{y}_p^-,$$

where $\boldsymbol{I}$ is the identity matrix, while the saltation matrix

$$\boldsymbol{S}^- = \boldsymbol{I} + \frac{(\boldsymbol{f}_p^+ - \boldsymbol{f}_p^-)\boldsymbol{n}^{\mathrm{T}}}{\boldsymbol{n}^{\mathrm{T}}\boldsymbol{f}_p^-} \tag{2.29}$$

has been finally introduced, linking the perturbations at the switching time t_p. Let's note that the saltation matrix (2.29) allows the definition of the perturbation in the new subsystem $\mathcal{V}^+$, given the perturbation expressed in the old subspace $\mathcal{V}^-$, thus it defines the new perturbation after the crossing of the fundamental orbit. The opposite relation is obviously defined by the inverse of the saltation matrix, which can be calculated as

$$(\boldsymbol{S}^-)^{-1} = \boldsymbol{I} + \frac{(\boldsymbol{f}_p^- - \boldsymbol{f}_p^+)\boldsymbol{n}^{\mathrm{T}}}{\boldsymbol{n}^{\mathrm{T}}\boldsymbol{f}_p^+}.$$

The complete evolution of the perturbed solution can now be calculated in three steps:

- for $t \in [t_0, t_p]$, the reference and perturbed solutions both live in the same subsystem $\mathcal{V}^-$, so the perturbation can be computed as

$$\delta \boldsymbol{y}(t) = \boldsymbol{\Phi}(t, t_0, \tilde{\boldsymbol{y}}_0)\delta \boldsymbol{y}_0;$$

- for $t \in (t_p, t_p^+]$, the crossing of the reference orbit from $\mathcal{V}^-$ to $\mathcal{V}^+$ occurs, in an infinitesimal time interval, hence the reference and perturbed solutions are in different subspaces; the perturbation just after the crossing at time t_p^+ can be calculated using the above definition of saltation matrix, assuming that $\bar{t}_p \to t_p^+$ for a small perturbation, hence

$$\delta \boldsymbol{y}(t_p^+) = \boldsymbol{S}^- \delta \boldsymbol{y}(t_p) = \boldsymbol{S}^- \boldsymbol{\Phi}(t_p, t_0, \tilde{\boldsymbol{y}}_0)\delta \boldsymbol{y}_0;$$

- for $t \in (t_p^+, t_q]$, where t_q is the time in which a new crossing appears in the solution, the reference and perturbed solution both live in the same subsystem $\mathcal{V}^+$, so the perturbation can be computed as

$$\delta \boldsymbol{y}(t) = \boldsymbol{\Phi}(t, t_p^+, \boldsymbol{y}(t_p^+))\delta \boldsymbol{y}(t_p^+) = \boldsymbol{\Phi}(t, t_p^+, \boldsymbol{y}(t_p^+))\boldsymbol{S}^- \boldsymbol{\Phi}(t_p, t_0, \tilde{\boldsymbol{y}}_0)\delta \boldsymbol{y}_0.$$

This three-step process can then be replicated for further intersections of the fundamental orbit with the switching manifold, so the perturbation of the reference solution is obtained by the composition of the proper fundamental solution matrices and saltation matrices.

The hypothesis on the location of the initial condition $\tilde{\boldsymbol{y}}_0$ in the negative subspace is obviously not important in the above calculations, and when the trajectories passes from $\mathcal{V}^+$ to $\mathcal{V}^-$, the inverted link $\delta \boldsymbol{y}_p^- = \boldsymbol{S}^+ \delta \boldsymbol{y}_p^+$ can be obtained, with the new saltation matrix

$$\boldsymbol{S}^+ = \boldsymbol{I} + \frac{(\boldsymbol{f}_p^- - \boldsymbol{f}_p^+)\boldsymbol{n}^{\mathrm{T}}}{\boldsymbol{n}^{\mathrm{T}} \boldsymbol{f}_p^+}, \tag{2.30}$$

which is equal to the inverse $(S^-)^{-1}$.

The concept of monodromy matrix can then be extended for a non-smooth mechanical system, when the solution is periodic. It can be computed from the fundamental solution matrices, analysing all the intersections of the reference orbit with the switching manifold from the initial condition to the final time T (when the orbit becomes periodic), yielding to

$$\boldsymbol{\Phi}_T = \boldsymbol{\Phi}(T - t_k, t_k, \boldsymbol{y}(t_k))\boldsymbol{S}^{(k)}\boldsymbol{\Phi}(t_k - t_{k-1}, t_{k-1}, \boldsymbol{y}(t_{k-1}))\boldsymbol{S}^{(k-1)} \cdots \\ \cdots \boldsymbol{S}^{(1)}\boldsymbol{\Phi}(t_1 - t_0, t_0, \boldsymbol{y}(t_0), \quad (2.31)$$

where it has been assumed that the system shows k intersections in the time interval $t \in [t_0, T]$ at times $\{t_1, t_2, \ldots, t_k\}$, with the associated saltation matrices $\boldsymbol{S}^{(1)}, \boldsymbol{S}^{(2)}, \ldots, \boldsymbol{S}^{(k)}$.

Analogously to the smooth case, the evolution of the perturbation of a periodic non-smooth dynamical system can be described by (2.20) and diagonalised as in (2.21), so the same assertions on the Floquet multipliers can be performed and a non-smooth orbit can be considered asymptotically stable if the modulus of all the eigenvalues of the monodromy matrix is lower than 1, otherwise, the non-smooth solution is considered unstable.

2.2.7 Attractivity of an invariant set: Jacobian matrix of the Poincaré maps

In Section 2.2.5 the concept of Poincaré map has been introduced, in order to detect an invariant set in the phase space, thus a family of fundamental reference solutions, whose stability and attractivity can be define on the basis of the techniques described in Section 2.2.6.

However, the Poincaré maps can also be adopted to study the attractivity of the solutions and, in particular, the analysis reduces to the computation of the eigenvalues of the Jacobian matrix of the Poincaré map, that are strictly connected to the Floquet multipliers. In Chapters 4, the Floquet multiplier approach will be adopted in the analysis of the attractivity of the invariant cones, however, the present Section must be considered as a possible alternative and a conceptual sketch through which the link between the continuous-time system and the related Poincaré map can be specified, see [51, 57, 74, 87].

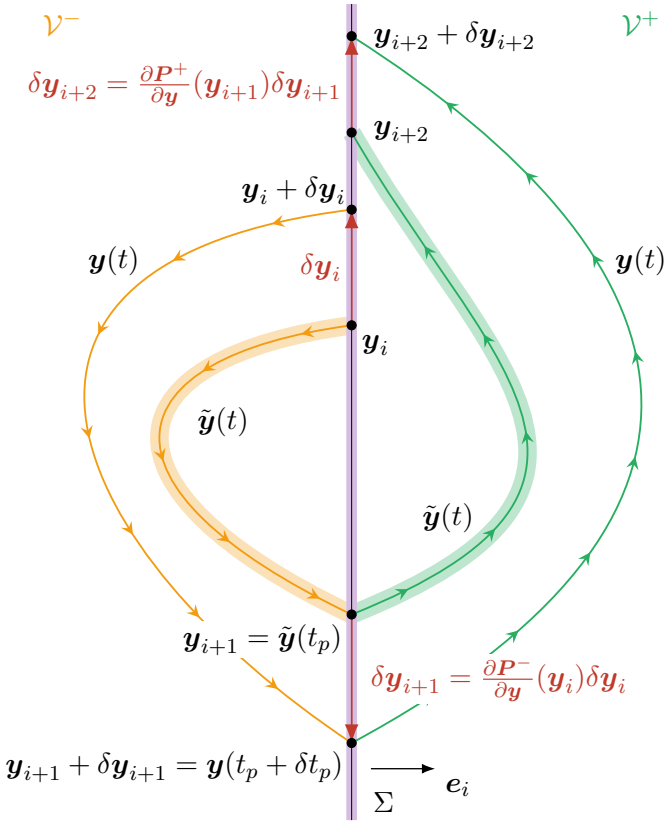

Figure 2.12: Evolution of the reference solution $\tilde{\boldsymbol{y}}(t)$ and of a perturbed one $\boldsymbol{y}(t)$, for autonomous piecewise systems described by two subdomains $\mathcal{V}^{\pm}$. The description of the evolution of the system is obtained by a composition of Poincaré halfmaps $\boldsymbol{P}^{\pm}$, in particular the map $\boldsymbol{y}_i \to \boldsymbol{y}_{i+1} \to \boldsymbol{y}_{i+2} \to \cdots$ for the reference solution and $\boldsymbol{y}_i + \delta\boldsymbol{y}_i \to \boldsymbol{y}_{i+1} + \delta\boldsymbol{y}_{i+1} \to \boldsymbol{y}_{i+2} + \delta\boldsymbol{y}_{i+2} \to \cdots$ for the perturbed one. The behaviour of the perturbations of the Poincaré maps is described by the Jacobian matrix of the Poincaré map.

Before the determination of the Jacobian matrix of the Poincaré map, one must focus on the deep meaning of this discrete map: the continuous flow $\boldsymbol{\varphi}_t(\boldsymbol{y}_0)$ of the dynamical system as (2.3) is transformed into a discrete map $\boldsymbol{y}_{i+1} = \boldsymbol{P}(\boldsymbol{y}_i)$ between points of the phase space that belong to a given manifold Σ. Moreover, in the method studied in Section 2.2.6, the

initial condition of the flow is located in a generic point of the phase space and all the considered perturbations (both the initial one $\delta \boldsymbol{y}_0$ and the $\delta \boldsymbol{y}^{\pm}$ in the crossing points) have generic directions. On the contrary, in the approach presented below, all the perturbations are assumed to be vectors belonging to the Poincaré section Σ. This difference in the perturbation location is the key feature that distinguishes the following method from the one exposed in Section 2.2.6, leading to different final formulas.

Furthermore, the Jacobian matrix is initially derived for the points belonging to the Poincaré section, thought as points of the phase space $\mathbb{R}^n$, because some interesting results, already seen in Section 2.2.6, can be extended and used below. Then, a further restriction to a local reference system of the $(n-1)$-manifold Σ is performed, see [57]. Let's note that the presence of the cross-section Σ, both for smooth and non-smooth systems in the general formulation of a Poincaré map, can yield the same analysis performed in Section 2.2.6 for non-smooth systems. In particular, the time delay due to the switching between the two subspaces analysed in the previous Section is analogous, from the mathematical point of view, to the time delay that will be calculated below between the reference and perturbed map.

Let's consider a given reference solution described by the Poincaré map

$$\boldsymbol{y}_{i+1} = \boldsymbol{P}(\boldsymbol{y}_i), \tag{2.32}$$

defined on the hypersurface Σ described by the condition $h(\boldsymbol{y}) = 0$, where we have introduced a regular parametrisation h describing the Poincaré section, analogously to what have been done in definition (2.27).

When a perturbation of the initial point $\delta \boldsymbol{y}_i$ *belonging to the Poincaré section* Σ is considered, the perturbed point of the discrete Poincaré map can be written as

$$\boldsymbol{y}_{i+1} + \delta \boldsymbol{y}_{i+1} = \boldsymbol{P}(\boldsymbol{y}_i + \delta \boldsymbol{y}_i) = \boldsymbol{P}(\boldsymbol{y}_i) + \frac{\partial \boldsymbol{P}}{\partial \boldsymbol{y}}(\boldsymbol{y}_i)\delta \boldsymbol{y}_i + \text{H.O.T.}$$

where a Taylor expansion of the Poincaré map has been performed. Neglecting the higher order terms and applying the definition (2.32), the perturbation in the mapped point can be expressed as

$$\delta \boldsymbol{y}_{i+1} = \frac{\partial \boldsymbol{P}}{\partial \boldsymbol{y}}(\boldsymbol{y}_i)\delta \boldsymbol{y}_i, \tag{2.33}$$

where $\partial \boldsymbol{P}(\boldsymbol{y}_i)/\partial \boldsymbol{y}$ is the Jacobian matrix of the Poincaré map, calculated in the reference point $\boldsymbol{y}_i$. This Jacobian matrix plays essentially the same role of the fundamental solution matrix, but in this case both the initial $\delta \boldsymbol{y}_i$ and final $\delta \boldsymbol{y}_{i+1}$ increments belong to Σ.

One must note that the Poincaré map is obtained from the continuous flow considering the time parameter as a function of the point itself, i.e. $\boldsymbol{P}(\boldsymbol{y}_i) = \boldsymbol{\varphi}_{t(\boldsymbol{y}_i)}(\boldsymbol{y}_i)$. For this reason, there is a time delay δt_p between time $t_p = t(\boldsymbol{y}_i)$ in which the reference orbit crosses the Poincaré section and time $\bar{t}_p = t(\boldsymbol{y}_i + \delta \boldsymbol{y}_i)$ which is necessary, for the perturbed trajectory, to reach in a new intersection point the manifold Σ. [5]

The perturbation $\delta \boldsymbol{y}_{i+1}$ can be computed as

$$\delta \boldsymbol{y}_{i+1} = \boldsymbol{y}(\bar{t}_p) - \tilde{\boldsymbol{y}}(t_p) = \boldsymbol{y}(t_p + \delta t_p) - \tilde{\boldsymbol{y}}(t_p), \tag{2.34}$$

where in analogy to what have been done in Section 2.2.6, $\tilde{\boldsymbol{y}}(t)$ is the fundamental solution and $\boldsymbol{y}(t)$ is the perturbed one, emanating from the points on the Poincaré section $\boldsymbol{y}_i$ and $\boldsymbol{y}_i + \delta \boldsymbol{y}_i$, respectively.

The right-hand-side of relation (2.34) can be approximated with a Taylor expansion, leading to

$$\delta \boldsymbol{y}_{i+1} = \boldsymbol{y}(t_p) + \dot{\boldsymbol{y}}(t_p)\delta t_p - \tilde{\boldsymbol{y}}(t_p) = \boldsymbol{y}(t_p) - \tilde{\boldsymbol{y}}(t_p) + \boldsymbol{f}_p \delta t_p = \delta \boldsymbol{y}_p^- + \boldsymbol{f}_p \delta t_p, \tag{2.35}$$

where $\delta \boldsymbol{y}_p^- = \boldsymbol{y}(t_p) - \tilde{\boldsymbol{y}}(t_p)$ has been introduced in analogy with the derivation performed in Section 2.2.6, representing the perturbation computed at the crossing time t_p of the reference orbit, while $\boldsymbol{f}_p = \boldsymbol{f}(t_p)$ is the vector field calculated at the time in which the fundamental solution reaches the Poincaré section. Let's note that this calculation is valid both for smooth and non-smooth systems, hence the location of the vector field in the subspace has not been specified with any superscript '$\pm$'.

Since for non-smooth system the Poincaré section coincides with the switching manifold, one may wonder if the vector field $\boldsymbol{f}_p$ at the crossing time is well-defined, and the answer is positive: in non-smooth cases, the Poincaré map is considered as a composition of a given number of Poincaré halfmaps, so the vector field $\boldsymbol{f}_p$ is chosen on the basis of what is the considered halfmap.

[5] The same notation for the time interval of Section 2.2.6 has been adopted, to underline the strict analogy of the two methods.

A saltation matrix has been introduced in Section 2.2.6, to deal with the time delay in which the fundamental and perturbed solutions live in different subspaces. In the Poincaré map approach this is not necessary, because the mapped points of the reference and perturbed orbits are both on the switching manifold and they are obtained by halfmaps that are both defined in the same subdomain $\mathcal{V}^-$ or $\mathcal{V}^+$. However, a time delay is still present, between the reference and perturbed map, which must be considered in the computations.

In particular, the time delay δt_p can be calculated imposing that the constraint $h(\boldsymbol{y}) = 0$ must be fulfilled for the points that belong to the cross-section Σ, see [51], in particular

$$h(\boldsymbol{y}_{i+1} + \delta \boldsymbol{y}_{i+1}) = h(\boldsymbol{y}(t_p + \delta t_p)) = 0,$$

that can be rewritten approximating the function h with a Taylor expansion, considering only the first order terms, as

$$h(\boldsymbol{y}(t_p + \delta t_p)) = h(\boldsymbol{y}(t_p) + \boldsymbol{f}_p \delta t_p) = h(\tilde{\boldsymbol{y}}(t_p) + \delta \boldsymbol{y}_p^- + \boldsymbol{f}_p \delta t_p) =$$
$$h(\tilde{\boldsymbol{y}}(t_p)) + \frac{\partial h}{\partial \boldsymbol{y}}(\tilde{\boldsymbol{y}}(t_p)) \cdot \left(\delta \boldsymbol{y}_p^- + \boldsymbol{f}_p \delta t_p\right) = \boldsymbol{n}(\tilde{\boldsymbol{y}}(t_p))^{\mathrm{T}} \left(\delta \boldsymbol{y}_p^- + \boldsymbol{f}_p \delta t_p\right) = 0,$$

where the gradient $\partial h / \partial \boldsymbol{y}$ of the sufficiently smooth function h coincides to the normal vector to the hypersurface Σ (which is obviously constant if the cross section is a flat plane) and the scalar product has been substituted by the transpose operation.

The time delay δt_p can now be calculated as

$$\delta t_p = -\frac{\boldsymbol{n}^{\mathrm{T}} \delta \boldsymbol{y}_p^-}{\boldsymbol{n}^{\mathrm{T}} \boldsymbol{f}_p},$$

identical to the expression (2.28), and it can be applied in (2.35), leading to

$$\delta \boldsymbol{y}_{i+1} = \delta \boldsymbol{y}_p^- - \frac{\boldsymbol{f}_p \boldsymbol{n}^{\mathrm{T}}}{\boldsymbol{n}^{\mathrm{T}} \boldsymbol{f}_p} \delta \boldsymbol{y}_p^- = \left[\boldsymbol{I} - \frac{\boldsymbol{f}_p \boldsymbol{n}^{\mathrm{T}}}{\boldsymbol{n}^{\mathrm{T}} \boldsymbol{f}_p}\right] \delta \boldsymbol{y}_p^-,$$

where $\boldsymbol{I}$ is the $n \times n$ identity matrix.

Moreover, the increment $\delta \boldsymbol{y}_p^-$ is well-defined from the continuous-time flow, and can be written as a function of the initial perturbation $\delta \boldsymbol{y}_i$ as

$$\delta \boldsymbol{y}_p^- = \boldsymbol{\Phi}(t_p, t_i) \delta \boldsymbol{y}_i,$$

where $\boldsymbol{\Phi}(t_p, t_i)$ is the fundamental solution matrix of the perturbed problem, described in Section 2.2.6. Since the analogy between the monodromy matrix and the Poincaré map approaches is now well understood, the flexible notation denoting some quantities referred to the point $\boldsymbol{y}_{i+1}$ with the subscpript p can now be changed to a more rigorous one, that better highlight the link between the points $\boldsymbol{y}_i$ and $\boldsymbol{y}_{i+1}$ of the Poincaré map.

The perturbation of the Poincaré map can now be written as

$$\delta \boldsymbol{y}_{i+1} = \left[\boldsymbol{I} - \frac{\boldsymbol{f}_{i+1} \boldsymbol{n}_{i+1}^{\mathrm{T}}}{\boldsymbol{n}_{i+1}^{\mathrm{T}} \boldsymbol{f}_{i+1}} \right] \boldsymbol{\Phi}(t_{i+1}, t_i) \delta \boldsymbol{y}_i = \boldsymbol{D}^{(i)} \boldsymbol{\Phi}(t_{i+1}, t_i) \delta \boldsymbol{y}_i, \tag{2.36}$$

where the matrix

$$\boldsymbol{D}^{(i)} = \boldsymbol{I} - \frac{\boldsymbol{f}_{i+1} \boldsymbol{n}_{i+1}^{\mathrm{T}}}{\boldsymbol{n}_{i+1}^{\mathrm{T}} \boldsymbol{f}_{i+1}}$$

has been introduced, that reveals an analogous structure to the saltation matrix. A comparison between (2.33) and (2.36) leads to the final form of the Jacobian matrix of the Poincaré map, see [57, 74],

$$\frac{\partial \boldsymbol{P}(\boldsymbol{y}_i)}{\partial \boldsymbol{y}} = \frac{\partial \boldsymbol{y}_{i+1}}{\partial \boldsymbol{y}} = \left[\boldsymbol{I} - \frac{\boldsymbol{f}_{i+1} \boldsymbol{n}_{i+1}^{\mathrm{T}}}{\boldsymbol{n}_{i+1}^{\mathrm{T}} \boldsymbol{f}_{i+1}} \right] \boldsymbol{\Phi}(t_{i+1}, t_i) = \boldsymbol{D}^{(i)} \boldsymbol{\Phi}(t_{i+1}, t_i). \tag{2.37}$$

When a non-smooth dynamical system composed of two subspaces $\mathcal{V}^-$ and $\mathcal{V}^+$ is considered, the complete Poincaré map can be seen as a composition of Poincaré halfmaps. In particular, if the reference solution is T-periodic after m intersections with the switching manifold, the map can be written as

$$\boldsymbol{y}_m = \boldsymbol{P}(\boldsymbol{y}_0) = \boldsymbol{P}^{(m)} \circ \boldsymbol{P}^{(m-1)} \circ \cdots \circ \boldsymbol{P}^{(1)} \boldsymbol{y}_0,$$

while the evolution of the perturbation after m intersections is described by the composition of the perturbations of all the Poincaré halfmaps, namely

$$\delta \boldsymbol{y}_m = \boldsymbol{D}^{(m)} \boldsymbol{\Phi}(t_m, t_{m-1}) \boldsymbol{D}^{(m-1)} \boldsymbol{\Phi}(t_{m-1}, t_{m-2}) \cdots \\ \cdots \boldsymbol{D}^{(1)} \boldsymbol{\Phi}(t_1, t_0) \delta \boldsymbol{y}_0 = \frac{\partial \boldsymbol{y}_m}{\partial \boldsymbol{y}} \delta \boldsymbol{y}_0.$$

Moreover, the evolution of the perturbed solution after kT periods can be described, using the the Jacobian matrix $\partial \boldsymbol{y}_m / \partial \boldsymbol{y}$ as

$$\delta \boldsymbol{y}(kT) = \left(\frac{\partial \boldsymbol{y}_m}{\partial \boldsymbol{y}} \right)^k \delta \boldsymbol{y}_0,$$

hence the Jacobian matrix $\partial \boldsymbol{y}_m / \partial \boldsymbol{y}$ plays essentially the same role as the monodromy matrix defined in equation (2.31) and it can be diagonalised as performed in (2.21), evidencing the importance of the eigenvalues of the Jacobian matrix of the Poincaré map to determine the stability behaviour of the reference solution.

The Jacobian matrix of the Poincaré map has been derived using a formulation in which the points of the maps are assumed to be vectors of the phase space $\boldsymbol{y}_i \in \mathbb{R}^n$, but the same map can be represented in a local reference frame such that the points are $\hat{\boldsymbol{y}}_i \in \mathbb{R}^{n-1}$. The representation of the Poincaré map in this latter formulation is better from a mathematical point of view, since in this way the Jacobian matrix is not singular.

In order to pass from the global reference frame to the local one, defined on the Poincaré section Σ, a change of coordinates $\hat{\boldsymbol{y}} = \boldsymbol{v}(\boldsymbol{y})$ must be introduced, where the function $\boldsymbol{v} : \mathbb{R}^n \to \mathbb{R}^{n-1}$ is assumed to be, without loss of generality, a linear transformation $\hat{\boldsymbol{y}} = \boldsymbol{V}^{\mathrm{T}} \boldsymbol{y}$, where $\boldsymbol{V}^{\mathrm{T}} \in \mathbb{R}^{(n-1) \times n}$, see [57]. Let's note that this change of coordinates can be applied both on the starting point of the map $\boldsymbol{y}_i$ and on the target point $\boldsymbol{y}_{i+1} = \boldsymbol{P}(\boldsymbol{y}_i)$, because also the latter belongs to the Poincaré section and can be written in the local reference frame, hence the relations $\hat{\boldsymbol{P}}(\boldsymbol{y}) = \boldsymbol{V}^{\mathrm{T}} \boldsymbol{P}(\boldsymbol{y})$ and $\hat{\boldsymbol{P}}(\hat{\boldsymbol{y}}) = \boldsymbol{V}^{\mathrm{T}} \boldsymbol{P}(\hat{\boldsymbol{y}})$ hold.

Applying this change of coordinates together with the chain rule, the Jacobian matrix of the Poincaré map, expressed in the global reference system, can be transformed as follows

$$\frac{\partial \boldsymbol{P}(\boldsymbol{y})}{\partial \boldsymbol{y}} = \frac{\partial \boldsymbol{P}(\boldsymbol{y}(\hat{\boldsymbol{y}}))}{\partial \hat{\boldsymbol{y}}} \frac{\partial \hat{\boldsymbol{y}}}{\partial \boldsymbol{y}} = \frac{\partial \boldsymbol{P}(\hat{\boldsymbol{y}})}{\partial \hat{\boldsymbol{y}}} \boldsymbol{V}^{\mathrm{T}}$$

and, assuming that $\boldsymbol{V}^{\mathrm{T}} \boldsymbol{V}$ is not singular,

$$\begin{aligned} \frac{\partial \boldsymbol{P}(\boldsymbol{y})}{\partial \boldsymbol{y}} = \frac{\partial \boldsymbol{P}(\hat{\boldsymbol{y}})}{\partial \hat{\boldsymbol{y}}} \boldsymbol{V}^{\mathrm{T}} \quad &\to \quad \frac{\partial \boldsymbol{P}(\boldsymbol{y})}{\partial \boldsymbol{y}} \boldsymbol{V} = \frac{\partial \boldsymbol{P}(\hat{\boldsymbol{y}})}{\partial \hat{\boldsymbol{y}}} \boldsymbol{V}^{\mathrm{T}} \boldsymbol{V} \\ &\to \quad \frac{\partial \boldsymbol{P}(\boldsymbol{y})}{\partial \boldsymbol{y}} \boldsymbol{V} \left(\boldsymbol{V}^{\mathrm{T}} \boldsymbol{V} \right)^{-1} = \frac{\partial \boldsymbol{P}(\hat{\boldsymbol{y}})}{\partial \hat{\boldsymbol{y}}}. \end{aligned}$$

The Jacobian of the Poincaré map expressed in the local reference frame can be deduced form the last equation, hence

$$\frac{\partial \hat{\boldsymbol{P}}(\hat{\boldsymbol{y}})}{\partial \hat{\boldsymbol{y}}} = \boldsymbol{V}^{\mathrm{T}} \frac{\partial \boldsymbol{P}(\hat{\boldsymbol{y}})}{\partial \hat{\boldsymbol{y}}} = \boldsymbol{V}^{\mathrm{T}} \frac{\partial \boldsymbol{P}(\boldsymbol{y})}{\partial \boldsymbol{y}} \boldsymbol{V} \left(\boldsymbol{V}^{\mathrm{T}} \boldsymbol{V} \right)^{-1},$$

where $\partial \boldsymbol{P}(\boldsymbol{y})/\partial \boldsymbol{y}$ is known and can be calculated from expression (2.37). Finally, the perturbations of a reference Poincaré map can be computed in the local reference system, analogously to relation (2.33), as

$$\delta \hat{\boldsymbol{y}}_{i+1} = \frac{\partial \hat{\boldsymbol{P}}}{\partial \hat{\boldsymbol{y}}} (\hat{\boldsymbol{y}}_i) \delta \hat{\boldsymbol{y}}_i.$$

As pointed out above, the Jacobian matrix of a Poincaré map for a T-periodic system plays the same role of the monodromy matrix and also in this case a relation analogous to (2.21) can be written, where the Jacobian matrix can be diagonalised, so the eigenvalues of the Jacobian of the Poincaré map are fundamental for the characterisation of the stability behaviour.

Theorem 4 ([41, 57, 74])**.** *Let's consider a T-periodic solution $\tilde{\boldsymbol{y}}(t)$ of an autonomous smooth dynamical system as (2.3). The spectrum of the $(n-1)\times(n-1)$ Jacobian matrix of the Poincaré map $\partial \hat{\boldsymbol{P}}(\hat{\tilde{\boldsymbol{y}}})/\partial \hat{\boldsymbol{y}}$ associated with the periodic solution is $\{\mu_1, \mu_2, \ldots, \mu_{n-2}, \mu_{n-1}\}$, while the spectrum of the $n \times n$ monodromy matrix $\boldsymbol{\Phi}_T$ associated with the same solution is $\{\mu_1, \mu_2, \ldots, \mu_{n-1}, \mu_{n-1}, 1\}$.*

Hence, the difference between the spectra of the two matrices is the presence, for the monodromy matrix, of the unitary eigenvalue $\mu_n = 1$ associated with the eigenvector $\boldsymbol{f}(\boldsymbol{y}_0)$, that can always be found in a periodic solution for any autonomous system.

This result can be extended to the case of a non-smooth dynamical system, so the analysis of the attractivity can be performed using both the method explained in the last two sections.

2.3 Conclusions

In this introductory Chapter, the mathematical framework of Analytical Mechanics has been presented in detail in Section 2.1, where all classical

topics for the mathematical investigation of smooth dynamical systems have been shown. The concepts exposed above will be the basis of the analysis performed in Chapter 3, where the behaviour of a specific reference mechanical structure will be considered.

The same topics are extended in Section 2.2, where some issues on the analysis of discontinuous physical phenomena are introduced in Subsection 2.2.1. In Subsection 2.2.3, the general framework of Filippov theory of ODEs with discontinuous right-hand-side has been investigated, while the approach adopted in the analysis of the main topic of this Thesis is outlined in 2.2.4 and 2.2.5, where the concept of invariant cone is presented. The final Subsections 2.2.6 and 2.2.7 will be very helpful in the analysis of the attractivity of the invariant cones, in particular in Chapter 4.

CHAPTER 3

A reference discontinuous mechanical system

"Everything is more simple than one thinks but at the same time more complex than one can understand"

Johann Wolfgang von Goethe

"The fundamental cause of the trouble is that in the modern world the stupid are cocksure while the intelligent are full of doubts"

Bertrand Russell

A reference example of piecewise-smooth mechanical systems is introduced, which can be modelled by a set of discontinuous ODEs, following the theoretical guidelines exposed in the previous Chapter 2.

The piecewise equations of motion of a special mechanical structure with two degrees of freedom are obtained through the Principle of Virtual Work, see [55]. In this mechanical system, the discontinuity originates from the curvilinear profile that acts as a constraint in the structure, see Figure 3.3, which reveals a jump in the curvature, in the physical point where the equilibrium configuration is located. The case of a doubly circular profile is investigated, the stability behaviour of the equilibrium fixed point is analysed for the single smooth subsystems that compose the entire structure, with the techniques described in [8, 58, 90].

The stability analysis for any 2 d.o.f. mechanical structure (neglecting damping phenomena) is then performed, considering a Hamiltonian formulation of the equation of motion [55].

3.1 Equations of motion of the smooth structure

3.1.1 Kinematic and static description of the structure

Let's consider the structure depicted in Figure 3.1, composed of a rigid bar, of mass density ρ and length l, which is constrained to move, without friction, along a smooth profile γ. In particular, one end of the rigid bar (the point $\boldsymbol{P}$) is constrained to the profile by an elastic hinge with rotational stiffness k_2 and it is linked to a fixed point $\boldsymbol{S}$, with a longitudinal linear spring of stiffness k_1. At the other end (the point $\boldsymbol{L}$), the bar is loaded by a *follower force* $\boldsymbol{F}$, positive when tensile, with a constant modulus.

The main feature of a follower force is that it "follows" the motion of the structure, so the direction of the force changes on the basis of the evolution of the dynamical system. Moreover, a follower force is non-conservative, so it cannot be associated with a scalar potential quantity. In this example, the force $\boldsymbol{F}$ is always parallel to the axis of the rigid bar.

Let's observe that the presence of damping is neglected in this physical model, since the main purpose is now the definition of a simple discontinuous mechanical system that reveals a peculiar behaviour and that can be solved analytically. However, further investigations can be performed and a dissipative source can be considered, leading to a more complex problem from a mathematical point of view.

In order to describe the geometry of the system and to introduce a mathematical model for the evolution in time of the structure, a Cartesian reference frame Oxy is considered, which is defined by a 2-dimensional orthonormal basis composed of the unit vectors $\boldsymbol{e}_1$ and $\boldsymbol{e}_2$.

The structure has two degrees of freedom, hence the evolution in time of this mechanical system can be modelled by two Lagrangian generalised coordinates, which in this example are assumed to be, without loss of generality, the curvilinear coordinate $\xi(t)$ along the profile γ and the angle $\phi(t)$ between the rigid bar and the y-axis, positive if clockwise. The generalised coordinates are assumed to be continuous functions of time, namely, $\xi : \mathbb{R} \to \mathbb{R}$ and $\phi : \mathbb{R} \to \mathbb{R}$.

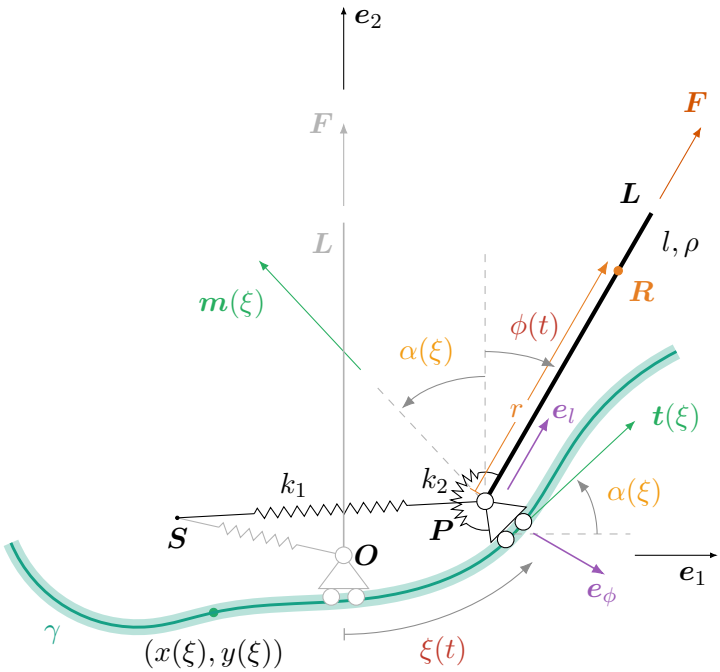

Figure 3.1: A 2 d.o.f. physical model for a mechanical structure composed of a rigid bar of length l and mass density ρ, constrained to move on a curved profile γ and subject to a follower force (positive when tensile). One end of the bar is also constrained with a longitudinal and rotational spring, with stiffness k_1 and k_2, respectively. The generic point on the profile is parametrised by the arc length coordinate ξ, which is also chosen as a Lagrangian generalised coordinate, together with the angle ϕ.

As a notation remark, the number of degrees of freedom is intended here as the number of *generalised coordinates* that describe the motion of the system in the Lagrangian formulation. When the Hamiltonian formulation will be introduced to model the evolution of these systems, they will be referred to as 2 d.o.f. systems anyway, although in this case the phase coordinates that completely define the motion are four.

The rigid profile γ along which the point $\boldsymbol{P}$ is constrained to move can be parametrised by the curvilinear coordinate ξ, so that

$$\gamma := \left\{ \boldsymbol{P} = (x, y) \in \mathbb{R}^2 : x = x(\xi), y = y(\xi), \forall \xi \in \mathbb{R} \right\},$$

and the tangent to the curve $\boldsymbol{P}'(\xi)$, the unit tangent $\boldsymbol{t}(\xi)$, and the unit principal normal $\boldsymbol{n}(\xi)$ at the generic point $\boldsymbol{P}(\xi)$ of the parametric curve can be calculated as

$$\boldsymbol{P}'(\xi) = x'(\xi)\boldsymbol{e}_1 + y'(\xi)\boldsymbol{e}_2, \qquad \boldsymbol{t}(\xi) = \frac{\boldsymbol{P}'(\xi)}{||\boldsymbol{P}'(\xi)||}, \qquad \boldsymbol{n}(\xi) = \frac{\boldsymbol{t}'(\xi)}{||\boldsymbol{t}'(\xi)||}, \tag{3.1}$$

where a dash $'$ denotes differentiation with respect to ξ.

For any given parametrisation of the curve γ, the angle between the tangent $\boldsymbol{P}'$ and the x-axis can easily be calculated as

$$\alpha(\xi) = \arctan\frac{y'(\xi)}{x'(\xi)}, \tag{3.2}$$

furthermore it can be derived with respect to ξ, obtaining

$$\alpha'(\xi) = \frac{x'(\xi)y''(\xi) - x''(\xi)y'(\xi)}{[x'(\xi)]^2 + [y'(\xi)]^2}.$$

The angle α, defined in (3.2), can be used to compute in an explicit form the unit tangent $\boldsymbol{t}$ and the unit normal $\boldsymbol{m}$, so that

$$\boldsymbol{t} = \cos\alpha\,\boldsymbol{e}_1 + \sin\alpha\,\boldsymbol{e}_2, \qquad \boldsymbol{m} = -\sin\alpha\,\boldsymbol{e}_1 + \cos\alpha\,\boldsymbol{e}_2,$$

where in general the unit vector $\boldsymbol{m}$ is different from the principal normal $\boldsymbol{n}$. In fact, $\boldsymbol{m}$ is obtained through an anticlockwise rotation of $\pi/2$ of $\boldsymbol{t}$, so that the unit vectors $\boldsymbol{t}$ and $\boldsymbol{m}$ always define a right-handed reference frame on the parametrised curve, while the direction of $\boldsymbol{n}$ depends on the sign of curvature. On the basis of these definitions, the derivative of the angle can also be expressed as $\alpha' = \boldsymbol{m}\cdot\boldsymbol{t}'$. Moreover, the signed curvature of the profile is defined using the derivative of the aforementioned angle as $\kappa = \alpha'/||\boldsymbol{P}'||$. Note that if ξ is identified with the arc length of the profile then $||\boldsymbol{P}'|| = 1$ and α' coincides with the signed curvature κ.

The kinematic description of the mechanical system has a simpler form if an orthonormal reference frame attached to the rigid bar is introduced, which is defined by the two unit vectors $\boldsymbol{e}_l$ and $\boldsymbol{e}_\phi$, written with respect to the global reference frame as

$$\boldsymbol{e}_l = \sin\phi\,\boldsymbol{e}_1 + \cos\phi\,\boldsymbol{e}_2, \qquad \boldsymbol{e}_\phi = \cos\phi\,\boldsymbol{e}_1 - \sin\phi\,\boldsymbol{e}_2.$$

The time derivative of these vectors can be calculated as

$$\dot{\boldsymbol{e}}_l = \dot{\phi}\,\boldsymbol{e}_\phi, \qquad \dot{\boldsymbol{e}}_\phi = -\dot{\phi}\,\boldsymbol{e}_l,$$

where a superimposed dot denotes the derivative of any function with respect to time.

The positions of the end points $\boldsymbol{P}$ and $\boldsymbol{L}$ of the rigid bar, as well as the location of a generic point $\boldsymbol{R}$ on the bar at distance r from $\boldsymbol{P}$, can be defined as

$$\boldsymbol{P} = x(\xi)\,\boldsymbol{e}_1 + y(\xi)\,\boldsymbol{e}_2 + \boldsymbol{O}, \qquad \boldsymbol{L} = l\boldsymbol{e}_l + \boldsymbol{P}, \qquad \boldsymbol{R} = r\,\boldsymbol{e}_l + \boldsymbol{P},$$

where $\boldsymbol{R}(r=0) = \boldsymbol{P}$ and $\boldsymbol{R}(r=l) = \boldsymbol{L}$. The velocities of the points $\boldsymbol{P}$, $\boldsymbol{L}$ and $\boldsymbol{R}$ are

$$\dot{\boldsymbol{P}} = \dot{\xi}\boldsymbol{P}', \qquad \dot{\boldsymbol{L}} = l\dot{\phi}\,\boldsymbol{e}_\phi + \dot{\boldsymbol{P}}, \qquad \dot{\boldsymbol{R}} = r\dot{\phi}\,\boldsymbol{e}_\phi + \dot{\boldsymbol{P}}, \tag{3.3}$$

where $\boldsymbol{P}'$ is the tangent to the rigid profile at $\boldsymbol{P}$, see definition $(3.1)_1$. The accelerations of the same points can be calculated as

$$\ddot{\boldsymbol{P}} = \ddot{\xi}\boldsymbol{P}' + \dot{\xi}^2\boldsymbol{P}'', \quad \ddot{\boldsymbol{L}} = l\ddot{\phi}\boldsymbol{e}_\phi - l\dot{\phi}^2\boldsymbol{e}_l + \ddot{\boldsymbol{P}}, \quad \ddot{\boldsymbol{R}} = r\,\ddot{\phi}\boldsymbol{e}_\phi - r\,\dot{\phi}^2\boldsymbol{e}_l + \ddot{\boldsymbol{P}}.$$

All these quantities are used in the description of the kinematics for the definition of the equations of motion.

As for the mathematical description of the load, the follower force has a constant modulus F and it is always parallel to the rigid bar, hence

$$\boldsymbol{F} = F\,\boldsymbol{e}_l.$$

The longitudinal spring with stiffness k_1 produces an elastic force $\boldsymbol{F}_s$ proportional to the vector $\boldsymbol{S} - \boldsymbol{P}$, so that

$$\boldsymbol{F}_s = k_1(\boldsymbol{S} - \boldsymbol{P}),$$

where $\boldsymbol{S} = (x_s, y_s)$ is considered a fixed point. The moment applied to the rigid bar at point $\boldsymbol{P}$ due to the rotational spring with stiffness k_2 is given by

$$M = -k_2(\phi + \alpha),$$

where α has been defined in formula (3.2).

3.1.2 The equation of motion through the Principle of Virtual Works

The equations of motion of the analysed structure can be derived using the Principle of Virtual Work, which asserts that a mechanical system is in equilibrium if and only if the total virtual work of all the impressed forces vanishes, for all virtual displacements kinematically admissible by the constraints [55]. The D'Alembert Principle has been used to consider also the dynamics of the system, hence the force of inertia has been introduced in the calculation of the Virtual Work.

For the considered mechanical system, the Principle of Virtual Works can be written as

$$\boldsymbol{F}\cdot\delta\boldsymbol{L}-k_1(\boldsymbol{P}-\boldsymbol{S})\cdot\delta\boldsymbol{P}-k_2(\phi+\alpha)(\delta\phi+\delta\alpha)-\rho\int_0^l\ddot{\boldsymbol{R}}\cdot\delta\boldsymbol{R}\,dr=0, \quad (3.4)$$

for all the admissible virtual displacements. All the forces acting on the system (follower force, elastic force and moment due to the longitudinal and rotational springs, and force of inertia) have been considered in equation 3.4.

The virtual displacements that are kinematically admissible with respect to the geometrical constraints of the structure can be calculated analogously to formulas (3.3), as

$$\delta\boldsymbol{P}=\delta\xi\,\boldsymbol{P}', \qquad \delta\boldsymbol{L}=l\delta\phi\,\boldsymbol{e}_\phi+\delta\boldsymbol{P}, \qquad \delta\boldsymbol{R}=r\delta\phi\,\boldsymbol{e}_\phi+\delta\boldsymbol{P}, \quad (3.5)$$

while the virtual displacement dual to the elastic moment applied to the structure by the rotational spring can be directly written as

$$\delta\phi+\delta\alpha=\delta\phi+\alpha'\delta\xi. \quad (3.6)$$

According to the previous relations (3.5) and (3.6), the virtual displacements have been written as functions of the infinitesimal increments $\delta\xi$ and $\delta\phi$ of the generalised coordinates, so the arbitrariness of the virtual displacements required by the Principle of Virtual Work is equivalent to the arbitrariness of $\delta\xi$ and $\delta\phi$.

Moreover, the external work due to the follower force is

$$\boldsymbol{F}\cdot\delta\boldsymbol{L}=F\boldsymbol{e}_l\cdot\delta\boldsymbol{P},$$

while the inertial term of the virtual work becomes

$$\int_0^l \ddot{\boldsymbol{R}} \cdot \delta \boldsymbol{R}\, dr = \frac{l^2}{2}\left(\frac{2l}{3}\ddot{\phi} + \ddot{\boldsymbol{P}} \cdot \boldsymbol{e}_\phi\right)\delta\phi + l\left(\frac{l}{2}\ddot{\phi}\boldsymbol{e}_\phi - \frac{l}{2}\dot{\phi}^2\boldsymbol{e}_l + \ddot{\boldsymbol{P}}\right)\cdot \delta \boldsymbol{P}.$$

The virtual work equation (3.4) can now be rewritten as

$$\begin{aligned}\left[\left(F + \rho\frac{l^2}{2}\dot{\phi}^2\right)\boldsymbol{e}_l - \rho\frac{l^2}{2}\ddot{\phi}\boldsymbol{e}_\phi - k_1(\boldsymbol{P}-\boldsymbol{S}) - \rho l\ddot{\boldsymbol{P}}\right]\cdot \boldsymbol{P}'\delta\xi - k_2(\phi+\alpha)\alpha'\delta\xi \\ - \left[k_2(\phi+\alpha) + \rho\frac{l^2}{2}\left(\frac{2l}{3}\ddot{\phi} + \ddot{\boldsymbol{P}}\cdot\boldsymbol{e}_\phi\right)\right]\delta\phi = 0, \quad \forall \delta\xi, \delta\phi\end{aligned}$$

and, due to the arbitrariness of $\delta\xi$ and $\delta\phi$, the two equations (in the Lagrangian formalism) governing the dynamics of the structure are derived as

$$\begin{cases}\left(F + \rho\frac{l^2}{2}\dot{\phi}^2\right)\left(x'\sin\phi + y'\cos\phi\right) - \rho\frac{l^2}{2}\ddot{\phi}\left(x'\cos\phi - y'\sin\phi\right) \\ - k_1\left[x'(x-x_s) + y'(y-y_s)\right] \\ - \rho l\left[\ddot{\xi}\left(x'^2 + y'^2\right) + \dot{\xi}^2\left(x'x'' + y'y''\right)\right] - k_2(\phi+\alpha)\alpha' = 0, \\ \\ k_2(\phi+\alpha) + \rho\frac{l^3}{3}\ddot{\phi} + \rho\frac{l^2}{2}\left[\ddot{\xi}\left(x'\cos\phi - y'\sin\phi\right)\right. \\ \left. + \dot{\xi}^2\left(x''\cos\phi - y''\sin\phi\right)\right] = 0,\end{cases} \tag{3.7}$$

which are two second order ordinary differential equations in the generalised coordinates $\xi(t)$ and $\phi(t)$. The set of ODEs (3.7) has been obtained without any simplification of the geometry of the system, so they are *nonlinear* equations of motion, that are in general hard to be solved analytically. On the contrary, they will be solved numerically in Chapter 6, for given combinations of parameters.

3.1.3 Linearised dynamics of the smooth structure

Since a nonlinear set of ODEs cannot generally be solved analytically, a possible strategy to understand the behaviour of the system from a theoretical point of view is the linearisation of the equations of motion.

As we have seen in Section 2.1.2, a solution of linear ODEs can be found in the well-known exponential form. In Section 2.2.6, a reference solution of the equations of motion has been perturbed, revealing that all the other solutions obtained by a sufficiently small perturbation of the initial conditions fulfil a linear set of ODEs described by the Jacobian matrix of the original vector field $\boldsymbol{f}(\boldsymbol{y})$. However, the linearisation of a nonlinear system is an approximation, hence only the local behaviour of the system can be caught, near the fundamental configuration about which the linearisation has been computed.

In the treated example, the reference solution about which the linearisation is performed is assumed to be the point $(\xi(t), \phi(t)) = (0, 0)$, namely the origin of the configuration space. This point is also assumed to be an equilibrium of the mechanical system, hence some hypotheses and restrictions on the free geometrical parameters must be introduced, in order to assure that the origin of the configuration space is a fixed point [1] . The nonlinear differential ODEs (3.7) can be linearised near the configuration $(\xi, \phi) = (0, 0)$, leading to the linear ODEs in the generalised coordinates $\xi(t)$ and $\phi(t)$,

$$\begin{cases} \rho\dfrac{l^2}{2}\ddot{\phi}x'(0) + \left[k_2\alpha' - Fx'\right]_{\xi=0}\phi + \rho l\ddot{\xi}\left[x'^2 + y'^2\right]_{\xi=0} \\ + \left[k_1\left(x''(x-x_s) + x'^2 + y''(y-y_s) + y'^2\right) - Fy'' + k_2\left(\alpha'^2 + \alpha\alpha''\right)\right]_{\xi=0}\xi \\ + \left[k_1\left(x'(x-x_s) + y'(y-y_s)\right) - Fy' + k_2\alpha'\alpha\right]_{\xi=0} = 0, \\ \\ \rho\dfrac{l^3}{3}\ddot{\phi} + k_2\phi + \rho\dfrac{l^2}{2}x'(0)\ddot{\xi} + k_2\alpha'(0)\xi + k_2\alpha(0) = 0, \end{cases} \tag{3.8}$$

which well approximate the nonlinear system for small $\xi(t)$ and $\phi(t)$.

With the introduction of the vector of Lagrangian generalised coor-

[1] One must note that the classical workflow followed in the analysis of dynamical systems is now inverted in the present work. Usually, the geometrical and mechanical parameters are known, hence first of all the equilibria of the system are detected and then a linearisation is performed near these fixed points. On the contrary, in this case, a given equilibrium configuration is assumed *a priori*, since only the specific equilibria located on the switching manifold are investigated in this work. This choice leads at first to the definition of the linearised approximation near the considered boundary configuration. Then, the properties that geometrical and mechanical parameters must fulfil are obtained *a posteriori*, in order to assure that the selected configuration is a fixed point.

dinates $\boldsymbol{q}(t) = [\xi(t), \phi(t)]^{\mathrm{T}}$, the equations (3.8) governing the linearised dynamics of the structure can be written in a compact matrix form, as

$$\boldsymbol{M}\ddot{\boldsymbol{q}}(t) + \boldsymbol{K}\boldsymbol{q}(t) = \boldsymbol{f}(t), \tag{3.9}$$

where $\boldsymbol{M}$ is the mass matrix, $\boldsymbol{K}$ the stiffness matrix and $\boldsymbol{f}$ the vector of generalized forces, respectively

$$\boldsymbol{M} = \rho l \begin{bmatrix} x'^2 + y'^2 & \dfrac{l}{2}x' \\ \dfrac{l}{2}x' & \dfrac{l^2}{3} \end{bmatrix}_{\xi=0}, \tag{3.10}$$

$$\boldsymbol{K} = \begin{bmatrix} k_1\left(x''(x-x_s) + x'^2 + y''(y-y_s) + y'^2\right) - Fy'' + k_2\left(\alpha'^2 + \alpha\alpha''\right) & k_2\alpha' - Fx' \\ k_2\alpha' & k_2 \end{bmatrix}_{\xi=0}, \tag{3.11}$$

and

$$\boldsymbol{f} = \begin{bmatrix} Fy' - k_1\left(x'(x-x_s) + y'(y-y_s)\right) - k_2\alpha'\alpha \\ -k_2\alpha \end{bmatrix}_{\xi=0}.$$

Finally, the solution $(\xi, \phi) = (0, 0)$ can be considered an equilibrium point if and only if the following conditions on the geometry are fulfilled

$$y'(0) = 0, \qquad x(0) = x_s, \tag{3.12}$$

which physically mean that the constraint profile must be horizontal at $\xi = 0$ (and therefore also $\alpha(0) = 0$) and the fixed point $\boldsymbol{S}$ of the linear spring must be aligned vertically with the point of the curve at $\xi = 0$. These conditions can be found imposing that the nonlinear equations (3.7) hold true for vanishing ξ and ϕ or assuming that $\boldsymbol{f} = 0$ in the linearised version (3.9) of the equation of motions .

3.2 Equations of motion of the piecewise-smooth structure

3.2.1 From smooth to non-smooth mechanical systems

The profile on which the rigid bar is constrained to move has been supposed smooth, so the parametrisation of the curve γ is sufficiently regular

to be continuous and differentiable for each value of ξ, in other words, $\boldsymbol{P}(\xi) \in \mathcal{C}^1$. This hypothesis on the parametrisation must now be relaxed to deal with discontinuous mechanical systems.

In particular, the non-smooth dynamical systems analysed in this Thesis can be considered as a composition of several smooth dynamical systems, described by ODEs as equations (3.7). These subsystems are linked together by some *switching rules* that determine the region of the configuration space in which each set of smooth differential equations of motion is valid, as was presented in Section 2.2.3 from a more theoretical point of view.

As for the mechanical structure considered in this Chapter, when the rigid constraint can be modelled by a set of continuous curves with different parametrisations, the same formalism described in Section 2.2.3 can be adopted (here from a Lagrangian point of view). The equations of motion of the non-smooth mechanical structure simply become a set of different ODEs of the form of (3.7) (or their linearised version (3.9)), together with the proper set of switching rules that identifies which is the valid equation, given the values of the generalised coordinates ξ and ϕ.

Let's now consider the mechanical system described above and suppose that the rigid constraint γ is discontinuous [2] in $\xi = 0$, so that two different parametrisations for the curve can be written, namely, γ^- for $\xi < 0$ and γ^+ for $\xi > 0$. If $\xi = 0$, exactly on the discontinuity, the curve is supposed to be continuous, but the derivatives of the parametrisations at this point could possibly be discontinuous. These two different parametrisations for the curved constraint lead to the definition of two different mechanical subsystems, identified by the symbols $(-)$ and $(+)$, for $\xi < 0$ and $\xi > 0$, respectively. Each subsystem is described by a nonlinear second order ODE (3.7), so that the nonlinear equations of motion of the complete structure is

$$\begin{cases} \ddot{\boldsymbol{q}}(t) = \boldsymbol{g}^-(\boldsymbol{q}(t), \dot{\boldsymbol{q}}(t)), & \xi < 0 \\ \ddot{\boldsymbol{q}}(t) = \boldsymbol{g}^+(\boldsymbol{q}(t), \dot{\boldsymbol{q}}(t)), & \xi > 0 \end{cases} \tag{3.13}$$

[2] Let's note that, for the sake of brevity, the term *discontinuous system* will sometimes be employed in the text as a synonymous for piecewise-smooth system. Hence, the term "discontinuous" must not be related to a discontinuity in the curve that describes the constraint, since, in the examples treated in this Thesis, the discontinuity in the curved profile is only a jump in the curvature.

where, for brevity, the structure of equations (3.7) have been rewritten as $\ddot{\boldsymbol{q}} = \boldsymbol{g}^{\pm}(\boldsymbol{q})$, introducing a nonlinear vector field $\boldsymbol{g} : \mathbb{R}^2 \to \mathbb{R}^2$. Moreover, let's assume that the configuration $(\xi, \phi) = (0, 0)$ is an equilibrium, so that the conditions (3.12) are supposed to be fulfilled. Note that the fixed point in which we are interested in is located exactly on the discontinuity between the two subsystems.

Since we are interested in the analysis of stability of the equilibrium point $(\xi, \phi) = (0, 0)$, a linearisation of the system (3.13) can be performed near the fixed point, leading to the piecewise-linear equations of motion

$$\begin{cases} \boldsymbol{M}^{-}\ddot{\boldsymbol{q}}(t) + \boldsymbol{K}^{-}\boldsymbol{q}(t) = \boldsymbol{0}, & \xi < 0 \\ \boldsymbol{M}^{+}\ddot{\boldsymbol{q}}(t) + \boldsymbol{K}^{+}\boldsymbol{q}(t) = \boldsymbol{0}, & \xi > 0 \end{cases} \tag{3.14}$$

Let's observe now that both (3.13) and (3.14) are actually nonlinear equations of motion, because of the discontinuity and the presence of the switching rules. Thus, while for a smooth structure the linearisation of the equations of motion allows the direct analytical determination of some interesting features of the dynamical system (at least near a given solution), in this case, the linearisation still produces a nonlinear problem, that cannot easily be solved. This is the reason why the stability analysis of this kind of problem is not trivial and straightforward stability criteria are not present for non-smooth mechanical systems. However, the behaviour of a piecewise-linear dynamical system in the form (3.14) can be understood in a simpler way, with respect to a nonlinear piecewise-smooth one, since at least in each single subsystem the solution can be written in the well-known exponential form.

Finally, one may note that in equations (3.13) and (3.14), the problem is not well-defined for $\xi = 0$, since a discontinuity is present and a jump occurs in the value of the vector field of the ODEs. The aim of the Filippov's theory introduced in Section 2.2.3 is exactly the definition of the solutions of a dynamical system revealing this kind of discontinuity and, according to the convex method adopted by Filippov, the differential equations (3.13) and (3.14) are generally transformed into differential inclusions. However, in Chapter 4, the orbits of this kind of mechanical problem will be described in depth and, in particular, the absence of sliding regions in the switching manifold will be proved in Section 4.2.

For this reason, the solutions of the mechanical system (3.14) are con-

tinuous and each orbit always crosses the discontinuity in a well-defined direction, unless in a set of zero measure in which the orbital velocities are tangent to the switching manifold [3] (i.e. when $\xi = 0$ and also $\dot{\xi} = 0$). Hence, the behaviour of the system for initial conditions on the switching manifold is well-defined and the application of Filippov convex method can be avoided. In fact, from a practical point of view and despite in the aforementioned set of pathological cases, the condition $\xi = 0$ can be associated with both subsystems, leading to the same final solution, for any choice of the positive or negative ODEs, with initial conditions in the form $\boldsymbol{q}(0) = [0, \phi_0]^{\mathrm{T}}$ and $\dot{\boldsymbol{q}}(0) = [0, \dot{\phi}_0]^{\mathrm{T}}$, for all $\phi_0, \dot{\phi}_0 \in \mathbb{R}$.

3.2.2 The piecewise-linear structure: doubly circular profile

In the previous paragraph, we defined the passage from a smooth structure to a non-smooth one, with a discontinuity in the point $(\xi, \phi) = (0, 0)$, which divides the smooth constraint into two different parts, $(-)$ and $(+)$, respectively. Now, a specific parametrisation of the curves for the two subsystems can be assigned, as a function of the arc length ξ. The linearised equations of motion are considered at first in this paragraph, which are the fundamental equations that will be used in the solution of the problem in the next Chapters, while the nonlinear equations of motion will be presented in the next Section 3.2.3.

Let's assume that the two parts in which the non-smooth constraint is divided are two circular profiles with a positive and negative curvature, as depicted in Figure 3.2, so that the curves of the two subsystems are described by the parametrisations

$$x(\xi) = R_{\pm} \sin \frac{\xi}{R_{\pm}}, \qquad y(\xi) = \pm R_{\pm} \left(1 - \cos \frac{\xi}{R_{\pm}} \right), \tag{3.15}$$

where R_{-} (R_{+}) refers to the negative (positive) subsystem with $\xi < 0$ ($\xi > 0$). The parametrisation above is written in such a way the radius of curvature $R_{\pm} > 0$ is supposed to always assume a positive value.

The linearised equations of motion (3.8) (and the expressions of the stiffness and mass matrix, (3.11) and (3.10), respectively) contain the val-

[3] This pathological cases are treated in Section 4.2 and are generally neglected in the present analysis, since the investigations concerning the invariant cones performed in the next Chapter 4 cannot be adopted for these specific conditions.

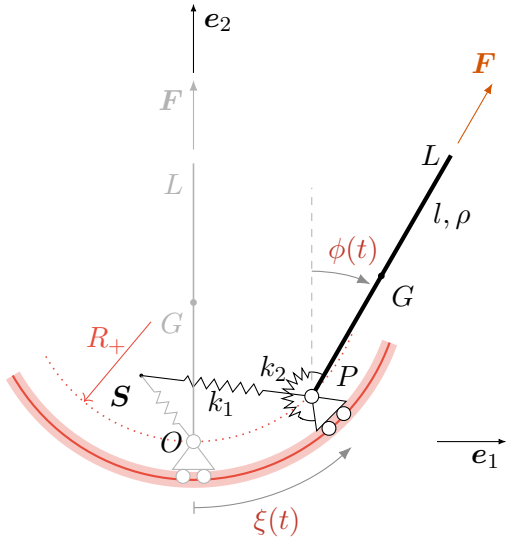

(a) *positive curvature*

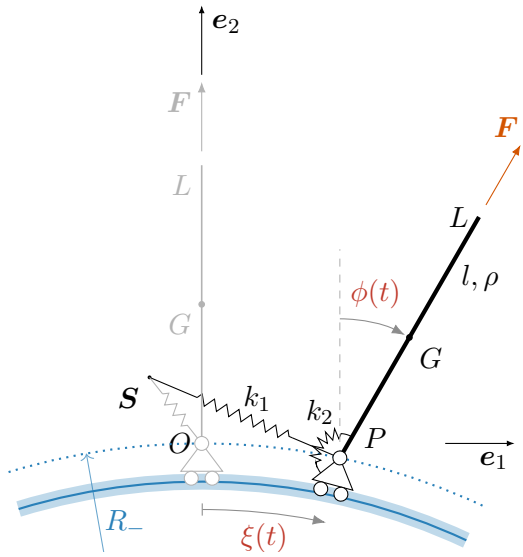

(b) *negative curvature*

Figure 3.2: Two examples of 2 d.o.f. *smooth* mechanical systems with different parametrisations for the curved profile γ. The opposite sign in the curvature yields to different behaviours, concerning in particular flutter and divergence critical loads, as shown in Section 3.4.

ues of the coordinates of the parametrisation and their derivatives, computed in the equilibrium configuration $(\xi, \phi) = (0, 0)$. A trivial calculation from (3.15) leads to the following expressions,

$$\begin{aligned} &x(0) = 0, && y(0) = 0, && x'(0) = 1, \\ &y'(0) = 0, && x''(0) = 0, && y''(0) = \pm 1/R_{\pm}. \end{aligned}$$

Moreover, conditions (3.12) must be fulfilled, in order to guarantee that the point $(\xi, \phi) = (0, 0)$ is a real equilibrium: the first condition $(3.12)_1$ holds true *a priori* (from the choice of the parametrisation), while $(3.12)_2$ is fulfilled if $x_s = x(0) = 0$. Furthermore, from the observations above, also $\alpha(0) = 0$ holds.

After the substitution of all the properties above into (3.11) and (3.10), the mass and stiffness matrices become

$$\boldsymbol{M} = \rho l \begin{bmatrix} 1 & l/2 \\ l/2 & l^2/3 \end{bmatrix}, \qquad \boldsymbol{K}^{\pm} = \begin{bmatrix} k_1 + \dfrac{k_2}{R_{\pm}^2} \mp \dfrac{k_1 y_s}{R_{\pm}} \mp \dfrac{F}{R_{\pm}} & \pm \dfrac{k_2}{R_{\pm}} - F \\ \pm \dfrac{k_2}{R_{\pm}} & k_2 \end{bmatrix}, \tag{3.16}$$

observing that the mass matrix is the same for both negative and positive systems.

Therefore, the piecewise-linear dynamical system with a doubly circular profile, composed of the $(-)$ and $(+)$ subsystems described above is depicted in Figure 3.3, while the equations of motion can now be written as

$$\begin{cases} \boldsymbol{M}\ddot{\boldsymbol{q}}(t) + \boldsymbol{K}^{-}\boldsymbol{q}(t) = \boldsymbol{0}, & \xi < 0 \\ \boldsymbol{M}\ddot{\boldsymbol{q}}(t) + \boldsymbol{K}^{+}\boldsymbol{q}(t) = \boldsymbol{0}, & \xi > 0 \end{cases}. \tag{3.17}$$

Let's remark that these equations of motion are still nonlinear, due to the presence of the switching rules. The mechanical system described by (3.17) is the reference structure that will be considered in this Thesis and the main purpose of the present work is the determination of its behaviour near the equilibrium point $(\xi, \phi) = (0, 0)$. As discussed in Section 2.2.4, due to the presence of the discontinuity and the follower non-conservative force, no instability criteria can be found.

In the next Chapters, this reference structure is studied and generalised, and a particular and counterintuitive behaviour is detected: the

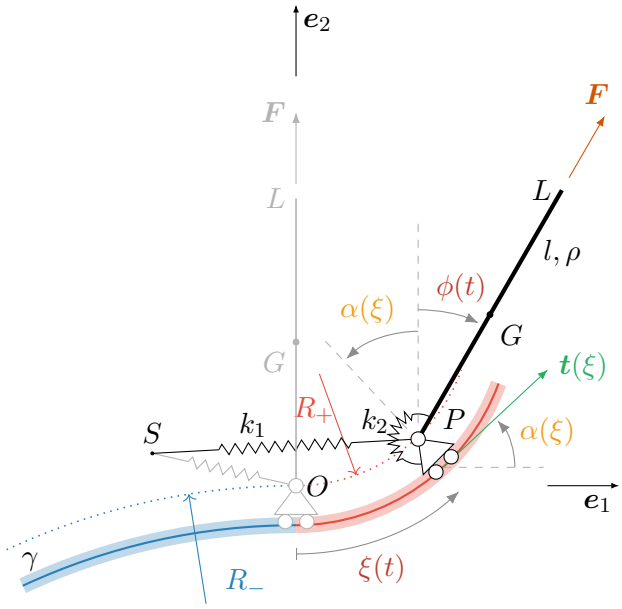

Figure 3.3: A discontinuous structure that can be modelled as a 2 d.o.f. piecewise-smooth dynamical system. The curved profile can be seen as the composition of the two structures presented in Figure 3.2, the junction between two circular profiles with positive and negative structure. In the point at $\xi = 0$, the doubly circular profile is continuous, as well as the tangent vector, while a jump in the curvature is present, determining the unexpected behaviour described in the next Chapter 4.

combined structure may present an unstable behaviour, although each single subsystem is stable, as predicted from a purely mathematical point of view by Carmona *et al.* [16]. This particular phenomenon is investigated from a mechanical perspective in Chapters 4, 5, and 6.

A non-dimensional analysis is generally an interesting technique for the generalisation of the results obtained in structural analysis, especially when the theoretical description of the possible behaviours of a structure is more important than the physical interpretation of the evolution of a real and specific mechanical system.

For this reason, the following non-dimensional parameters are intro-

duced,

$$\zeta_{\pm} = \frac{R_{\pm}}{l} \qquad k = \frac{k_1 l^2}{k_2} \qquad \gamma = \frac{Fl}{k_2} \qquad \sigma = \frac{y_s}{l}, \tag{3.18}$$

which are the fundamental physical quantities that summarise the informations of all the mechanical and geometrical parameters describing the structure. After the substitution of (3.18) into (3.16), the equations of motion of the two subsystems of the discontinuous structure become

$$\Theta \begin{bmatrix} 1 & \frac{1}{2} \\ \frac{1}{2} & \frac{1}{3} \end{bmatrix} \begin{bmatrix} \ddot{\overline{\xi}}(\tau) \\ \ddot{\overline{\phi}}(\tau) \end{bmatrix} + \begin{bmatrix} \frac{k}{\zeta_{\pm}}(\zeta_{\pm} \mp \sigma) + \frac{1 \mp \gamma\zeta_{\pm}}{\zeta_{\pm}^2} & \frac{-\gamma\zeta_{\pm} \pm 1}{\zeta_{\pm}} \\ \pm\frac{1}{\zeta_{\pm}} & 1 \end{bmatrix} \begin{bmatrix} \overline{\xi}(\tau) \\ \overline{\phi}(\tau) \end{bmatrix} = \mathbf{0}, \tag{3.19}$$

where a reference time T and the non-dimensional time $\tau = t/T$ have been introduced, together with the non-dimensional generalised coordinates $\overline{\xi}(\tau) = \xi(t)/l$ and $\overline{\phi}(\tau) = \phi(t)$, and the other non-dimensional parameter

$$\Theta = \frac{\rho l^3}{T^2 k_2}. \tag{3.20}$$

The superimposed dot over a non-dimensional generalised coordinate $\overline{\xi}(\tau)$ or $\overline{\phi}(\tau)$ means derivation with respect to the non-dimensional time τ. This abuse of notation is useful to avoid the presence of too many symbols in the formulas, while this formalism intuitive from a physical point of view, since a superimposed dot always means a time derivative (both for dimensional and non-dimensional variables).

Finally, the non-dimensional parameter

$$\chi = \frac{\zeta_-}{\zeta_+} = \frac{R_-}{R_+}$$

can be introduced, in order to denote the ratio between the two radii of the circular constraints.

As a final remark, this non-dimensional formulation of the problem will be extensively used for the numerical results, while it will not be used for the derivation of the instability criteria in the Chapters 4, to avoid a heavy notation. However, the results of Chapters 4 are obviously valid both for the dimensional and the non-dimensional formulation.

3.2.3 The nonlinear piecewise-smooth structure: doubly circular profile

In the previous Section 3.2.2, the linearised equations of motion of the reference mechanical structure with a doubly circular profile have been obtained. These linearised equations (3.17) or (3.19) are crucial to define the behaviour of the system near the equilibrium point $(\xi, \phi) = (0, 0)$. Since, from a theoretical point of view, they are the only relations from which analytical results can be obtained, they have been derived at first.

Actually, the complete time evolution of the mechanical structure is described by the nonlinear equations of motion

$$\begin{cases} \left(F + \dfrac{\rho l^2}{2}\dot{\phi}^2\right)\sin\left(\phi \pm \dfrac{\xi}{R_\pm}\right) - \dfrac{\rho l^2}{2}\ddot{\phi}\cos\left(\phi \pm \dfrac{\xi}{R_\pm}\right) \\ + k_1(\pm y_s - R_\pm)\sin\left(\dfrac{\xi}{R_\pm}\right) \mp \dfrac{k_2}{R_\pm}\left(\phi \pm \dfrac{\xi}{R_\pm}\right) - \rho l\ddot{\xi} = 0, \\ \\ k_2\left(\phi \pm \dfrac{\xi}{R_\pm}\right) + \dfrac{\rho l^3}{3}\ddot{\phi} + \dfrac{\rho l^2}{2}\ddot{\xi}\cos\left(\phi \pm \dfrac{\xi}{R_\pm}\right) - \dfrac{\rho l^2}{2R_\pm}\dot{\xi}^2\sin\left(\dfrac{\xi}{R_\pm} \pm \phi\right) = 0, \end{cases} \tag{3.21}$$

which is obtained by substituting into equations (3.8) all the results that can be obtained from the parametrisation (3.15).

Rearranging equations (3.21), using the non-dimensional parameters defined in (3.18) and (3.20), the following non-dimensional nonlinear ODEs can also be written

$$\begin{cases} \left(\gamma + \dfrac{\Theta}{2}\dot{\overline{\phi}}^2\right)\sin\left(\overline{\phi} \pm \dfrac{\overline{\xi}}{\zeta_\pm}\right) - \dfrac{\Theta}{2}\ddot{\overline{\phi}}\cos\left(\overline{\phi} \pm \dfrac{\overline{\xi}}{\zeta_\pm}\right) - \Theta\ddot{\overline{\xi}}, \\ + k\left(\pm\sigma - \zeta_\pm\right)\sin\left(\dfrac{\overline{\xi}}{\zeta_\pm}\right) \mp \dfrac{1}{\zeta_\pm}\left(\overline{\phi} \pm \dfrac{\overline{\xi}}{\zeta_\pm}\right) = 0 \\ \\ \left(\overline{\phi} \pm \dfrac{\overline{\xi}}{\zeta_\pm}\right) + \dfrac{\Theta}{3}\ddot{\overline{\phi}} + \dfrac{\Theta}{2}\ddot{\overline{\xi}}\left(\overline{\phi} \pm \dfrac{\overline{\xi}}{\zeta_\pm}\right) \mp \dfrac{\Theta}{\zeta_\pm}\dot{\overline{\xi}}^2\sin\left(\overline{\phi} \pm \dfrac{\overline{\xi}}{\zeta_\pm}\right) = 0, \end{cases} \tag{3.22}$$

where again the superimposed dots means derivation with respect to the non-dimensional time τ. These nonlinear equations will be solved in the Chapter 6 through a numerical approach, in order to understand the real

behaviour of the structure with generic initial conditions near the equilibrium point.

3.3 Stability of equilibra for a smooth 2 d.o.f. mechanical system

In the previous paragraphs, the mathematical model of the mechanical structure under analysis has been presented and the equations of motion have been obtained. Moreover, the linearised equations in the vicinity of the reference equilibrium point $(\xi, \phi) = (0, 0)$ have been derived.

The next step for the comprehension of the behaviour of this system is the stability analysis of the equilibrium configuration. The starting point is the investigation of the stability of each single smooth subsystem, which can be performed with classical techniques presented in this Section. On the contrary, the stability analysis of the piecewise-smooth complete structure requires more sophisticated tools, so this topic will be treated extensively in Chapter 4.

3.3.1 Solution of linearised equations of motion

In the vicinity of the equilibrium configuration $(\xi, \phi) = (0, 0)$ the vibrations of the piecewise system are governed by equation (3.17). The analysis of the complete system starts from the investigation of the solution of each single subsystem that compose the entire piecewise-smooth structure.

Solution in the Lagrangian formulation Let's now analyse the behaviour of a generic smooth mechanical system with two degrees of freedom in the Lagrangian formulation, that can be described by a general set of ODEs in the form

$$\boldsymbol{M}\ddot{\boldsymbol{q}}(t) + \boldsymbol{K}\boldsymbol{q}(t) = \boldsymbol{0}, \tag{3.23}$$

and by the initial conditions on the position $\boldsymbol{q}(0) = \boldsymbol{q}_0$ and on the velocity $\dot{\boldsymbol{q}}(0) = \dot{\boldsymbol{q}}_0$ at the initial time $t = 0$. This description is general and is suitable for all linearised 2 d.o.f. mechanical systems (when damping is neglected), presenting an equilibrium point in the origin of the configuration space $(q_1, q_2) = (0, 0)$.

The solution to equation (3.23) can be found through exponential functions as explained in Section 2.1.2. The vector of generalised coordinate is assumed to be written in the form

$$\boldsymbol{q}(t) = \boldsymbol{\psi}^{(j)} e^{\lambda_j t}, \tag{3.24}$$

where in this case $\boldsymbol{\psi}^{(j)} \in \mathbb{C}^2$ is a 2-dimensional complex vector and $\lambda \in \mathbb{C}$ is a scalar, which can be determined from the eigenvalue problem

$$\left(\lambda_j^2 \boldsymbol{M} + \boldsymbol{K}\right) \boldsymbol{\psi}^{(j)} = \boldsymbol{0}, \tag{3.25}$$

obtained substituting the ansatz (3.24) into the equation of motion (3.23).

An analogous formulation, similar to (3.24) and more common in the field of Structural Mechanics, takes into consideration the ansatz

$$\boldsymbol{q}(t) = \boldsymbol{\psi}^{(j)} e^{i\omega_j t},$$

leading to the eigenvalue problem

$$(-\omega_j^2 \boldsymbol{M} + \boldsymbol{K})\boldsymbol{\psi}^{(j)} = \boldsymbol{0},$$

analogous to (3.25). The scalar quantities ω_j are generally called *natural frequencies* of the mechanical system, while the associated eigenvectors are called *eigenmodes*. These two formulations are analogous, however the former will be adopted, since it can be extended easily in case of Hamiltonian formulation, leading directly to the results presented in Section 2.1.3.

It is clear from (3.25) that two possible solutions for λ_j^2 exist, namely λ_1^2 and λ_2^2, leading to four possible values $\pm\lambda_1$ and $\pm\lambda_2$ for the coefficient of the solution (3.24). Therefore, the generalised coordinate vector $\boldsymbol{q}(t)$ can be written as the linear combination of four exponential terms as

$$\boldsymbol{q}(t) = \sum_{j=1}^{2} \boldsymbol{\psi}^{(j)} \left(A_j e^{\lambda_j t} + B_j e^{-\lambda_j t} \right).$$

The four arbitrary constants A_j and B_j can be determined from initial conditions $\boldsymbol{q}_0$ and $\dot{\boldsymbol{q}}_0$ as

$$\begin{bmatrix} A_1 \\ A_2 \\ B_1 \\ B_2 \end{bmatrix} = \begin{bmatrix} \boldsymbol{\Psi}^{-1} & \boldsymbol{\Psi}^{-1}\boldsymbol{\Omega}^{-1} \\ \boldsymbol{\Psi}^{-1} & \boldsymbol{\Psi}^{-1}\boldsymbol{\Omega}^{-1} \end{bmatrix} \begin{bmatrix} q_{01} \\ q_{02} \\ \dot{q}_{01} \\ \dot{q}_{02} \end{bmatrix},$$

where the following matrices have been introduced,

$$\boldsymbol{\Psi} = \begin{bmatrix} \psi_1^{(1)} & \psi_1^{(2)} \\ \psi_2^{(1)} & \psi_2^{(2)} \end{bmatrix}, \qquad \boldsymbol{\Omega} = \begin{bmatrix} \lambda_1 & 0 \\ 0 & \lambda_2 \end{bmatrix}.$$

Solution in the Hamiltonian formulation The approach introduced above for the description of the solution of a dynamical system is a common procedure in Structural Mechanics, however, for our purpose, the Hamiltonian description is more convenient and will be introduced for the stability analysis. The passage from a Lagrangian to a Hamiltonian formulation of Dynamics has been pointed out in Section 2.1.6, while the stability criteria for fixed points in the Hamiltonian description, can be found in Section 2.1.3.

The linearised equations of motion (3.23) can be rewritten in the Hamiltonian formulation as an autonomous system defined by a set of *first order* ordinary differential equations

$$\dot{\boldsymbol{y}}(t) = \boldsymbol{A}\,\boldsymbol{y}(t), \tag{3.26}$$

where the state vector $\boldsymbol{y}(t) = [\boldsymbol{q}(t), \dot{\boldsymbol{q}}(t)]^{\mathrm{T}}$ has been introduced, which contains the vector of the generalised coordinates and its first derivative in time. The ODEs (3.26) are analogous to those analysed in Section 2.1.2.

For a *mechanical* system, whose linearised dynamic is described by the mass matrix $\boldsymbol{M}$ and stiffness matrix $\boldsymbol{K}$, the Jacobian matrix of the equations of motion, calculated in the equilibrium configuration, can be written as

$$\boldsymbol{A} = \begin{bmatrix} \mathbf{0} & \boldsymbol{I} \\ -\boldsymbol{M}^{-1}\boldsymbol{K} & \mathbf{0} \end{bmatrix} = \begin{bmatrix} \mathbf{0} & \boldsymbol{I} \\ \boldsymbol{\Gamma} & \mathbf{0} \end{bmatrix} \tag{3.27}$$

where $\boldsymbol{I}$ is the 2×2 identity matrix and the matrix $\boldsymbol{\Gamma} = -\boldsymbol{M}^{-1}\boldsymbol{K}$ has been introduced. A general mechanical system, previously defined by two generalised coordinates in the Lagrangian formulation, is now described by four phases in the Hamiltonian formulation, so the number of unknowns doubles, but the order of the ODEs decreases, from second to first order.

As presented in section 2.1.2, the linearised equations of motion (3.26) can be solved using an exponential ansatz $\boldsymbol{y}(t) = \boldsymbol{v}^{(j)} e^{\lambda_j t}$, where now

$\boldsymbol{v}^{(j)} \in \mathbb{C}^4$ is assumed to be a 4-dimensional complex vector, leading to the eigenvalue problem

$$\boldsymbol{A}\,\boldsymbol{v}^{(j)} = \lambda_j \boldsymbol{v}^{(j)}. \tag{3.28}$$

The solution in the Lagrangian and Hamiltonian formulation must obviously be linked and it is instructive to underline this connection. Considering the structure of the matrix $\boldsymbol{A}$, the eigenvalue problem (3.28) can be solved computing the λ_j from equation

$$\begin{vmatrix} -\lambda_j \boldsymbol{I} & \boldsymbol{I} \\ -\boldsymbol{M}^{-1}\boldsymbol{K} & -\lambda_j \boldsymbol{I} \end{vmatrix} = \det[-\lambda_j \boldsymbol{I}]\det[-\lambda_j \boldsymbol{I} - \boldsymbol{I}(\lambda_j \boldsymbol{I})^{-1}\boldsymbol{M}^{-1}\boldsymbol{K}] =$$
$$\lambda_j^2 \det\left[-\frac{1}{\lambda_j}\left(\lambda_j^2 \boldsymbol{I} + \boldsymbol{M}^{-1}\boldsymbol{K}\right)\right] = \det\left[\boldsymbol{M}^{-1}\left(\lambda_j^2 \boldsymbol{M} + \boldsymbol{K}\right)\right] =$$
$$\frac{1}{\det \boldsymbol{M}} \det\left[\lambda_j^2 \boldsymbol{M} + \boldsymbol{K}\right] = 0, \tag{3.29}$$

where the formula for the determinant of a block matrix has been adopted [76]. The final result is exactly the same condition that must be imposed to solve the eigenvalue problem (3.25), hence the eigenvalues λ_j in problem (3.25) and (3.28) are exactly the same. As for the eigenvectors, the $\boldsymbol{v}^{(j)}$ can be written as

$$\begin{aligned} \boldsymbol{v}^{(1,2)} &= [\psi_1^{(1)},\ \psi_2^{(1)},\ \pm\lambda_1\psi_1^{(1)},\ \pm\lambda_1\psi_2^{(1)}]^{\mathrm{T}}, \\ \boldsymbol{v}^{(3,4)} &= [\psi_1^{(2)},\ \psi_2^{(2)},\ \pm\lambda_2\psi_1^{(2)},\ \pm\lambda_2\psi_2^{(2)}]^{\mathrm{T}}, \end{aligned} \tag{3.30}$$

where the components $\psi_k^{(j)}$ of the eigenvectors of the problem (3.25) has been used.

As defined in Section 2.1.2, the solution of the first order ODEs (3.26) with assigned initial condition $\boldsymbol{y}(0) = \boldsymbol{y}_0$ is unique and can be written through the *fundamental solution matrix* as

$$\boldsymbol{y}(t) = e^{\boldsymbol{A}t}\,\boldsymbol{y}_0. \tag{3.31}$$

For the sake of clarity, for the mechanical structure described in Section 3.1.1, which is the reference dynamical system in this Thesis, the solution

in the expanded form is

$$\begin{bmatrix} \xi(t) \\ \phi(t) \\ \dot{\xi}(t) \\ \dot{\phi}(t) \end{bmatrix} = e^{\boldsymbol{A}t} \begin{bmatrix} \xi(0) \\ \phi(0) \\ \dot{\xi}(0) \\ \dot{\phi}(0) \end{bmatrix},$$

where the generalised coordinates ξ, ϕ and their first derivatives $\dot{\xi}$ and $\dot{\phi}$ have been explicitly written in the formulation.

3.3.2 Stability analysis of a linearised 2-d.o.f. dynamical system

In Section 2.1.3, some criteria for the stability analysis of a fixed point has been outlined. For a smooth mechanical system described by first order ODEs, the Liapunov Theorem 2 can be adopted in order to understand the behaviour of the solution. The Liapunov criteria of linear stability are based on the nature of the eigenvalues λ_j of the Jacobian matrix $\boldsymbol{A}$ and in particular on the sign of the real part of the eigenvalues.

For a 2 d.o.f. mechanical system, the eigenvalue problem (3.28) can be solved with the same procedure exposed in (3.29), in particular the determinant can be rewritten as

$$\begin{vmatrix} -\lambda_j \boldsymbol{I} & \boldsymbol{I} \\ \boldsymbol{\Gamma} & -\lambda_j \boldsymbol{I} \end{vmatrix} = \det\left[\boldsymbol{\Gamma} - \lambda_j^2 \boldsymbol{I}\right], \tag{3.32}$$

hence the eigenvalues of $\boldsymbol{A}$ are exactly the square roots of the eigenvalues of the matrix $\boldsymbol{\Gamma}$. The characteristic polynomial obtained from (3.32) is

$$\mathcal{P}(\lambda_j) = \lambda_j^4 - \mathrm{tr}(\boldsymbol{\Gamma})\lambda_j^2 + \det(\boldsymbol{\Gamma}) = 0,$$

hence, for a 2 d.o.f. mechanical system with a 4 - dimensional phase space, the eigenvalues of $\boldsymbol{A}$ can be explicitly written as

$$\lambda_j = \pm\sqrt{\frac{I_1 \pm \sqrt{I_1^2 - 4I_2}}{2}}, \tag{3.33}$$

where $I_1 = \mathrm{tr}\,\boldsymbol{\Gamma}$ and $I_2 = \det\boldsymbol{\Gamma}$ are the first and second invariants of the matrix $\boldsymbol{\Gamma}$.

The Liapunov Theorem 2 states that the equilibrium configuration of a linear system is stable when the real parts of all eigenvalues are non-positive, otherwise the equilibrium is unstable. It is evident from (3.33) that symmetry with respect to the origin of the complex plane is present, due to the '$\pm$' before the external square root. This implies that, when an eigenvalue with a negative real part is detected, a symmetric eigenvalue with a positive real part is also present in the spectrum, hence a stable linear system can only be associated with four eigenvalues with vanishing real parts.

For these smooth mechanical systems with 2 d.o.f. described by the Jacobian matrix (3.27), only four cases can be distinguished:

- *stability*: the four eigenvalues are all purely imaginary, $\lambda_j \in i\mathbb{R}$, so that $\lambda_{1,2} = \pm i\beta_1$ and $\lambda_{3,4} = \pm i\beta_2$, with $\beta_k \in \mathbb{R}$. In particular, this is a *critical case* of stability, in fact the linearised system can be considered stable (the imaginary eigenvalues lead to periodic orbits near the equilibrium configuration), while the stability of the nonlinear system, from which the linearisation is obtained, cannot be defined, due to the vanishing real parts of the λ_j. This kind of equilibrium point are also called *marginally stable*.

- *saddle-node instability*: two eigenvalues are real and the other two are purely imaginary, i.e. $\lambda_{1,2} = \pm\alpha_1$, while $\lambda_{3,4} = \pm i\beta_2$, with $\alpha_k, \beta_k \in \mathbb{R}$. Along the eigenvectors associated with the imaginary eigenvalues and the real eigenvalue with negative real part, the solution is stable for $t \in [0, +\infty)$, but along the remaining eigenvectors an exponential growth of the solution is expected.

- *divergence instability*: all the eigenvalues are real numbers, i.e. $\lambda_{1,2} = \pm\alpha_1$ and $\lambda_{3,4} = \pm\alpha_2$, with $\alpha_k \in \mathbb{R}$. Along the two eigenvectors associated with the real eigenvalues with positive real part, the solution reveals an exponential growth.

- *flutter instability*: all the eigenvalues λ_j are complex conjugate pair, so that $\lambda_{1,2,3,4} = \pm(\alpha \pm i\beta)$, with $\alpha, \beta \in \mathbb{R}$, and $\alpha \neq 0$. The behaviour is unstable since there are eigenvalues with positive real part, however the presence of a not vanishing imaginary part produces oscillations in the solution.

Actually, the distinction between divergence and saddle-node instability is not really essential, since in both cases the unstable behaviour is governed by a solution proportional to $e^{\lambda t}$, $\lambda \in \mathbb{R}^+$, which produces an exponential growth for $t \in [0, +\infty)$.

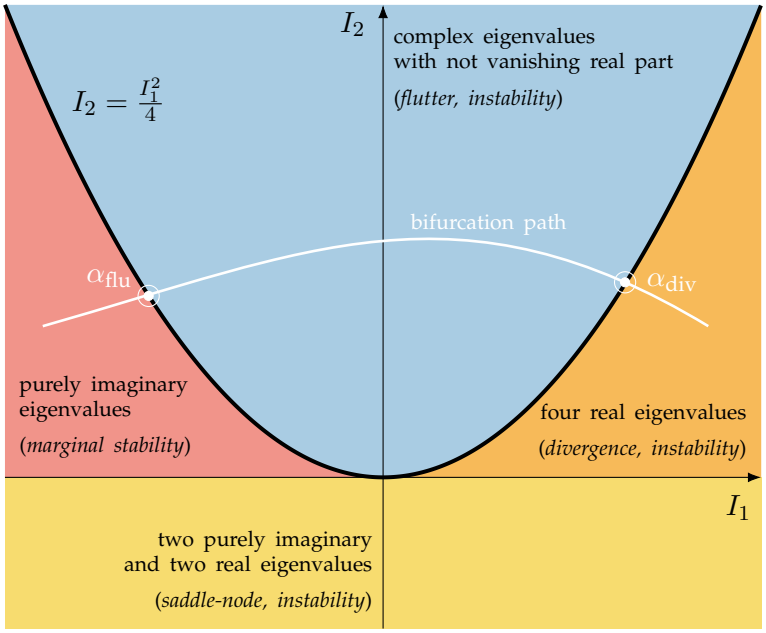

Figure 3.4: Diagram in the I_1-I_2 plane of the invariants, describing the possible different behaviours of a generic 2 d.o.f. mechanical system. On the basis of the invariants I_1 and I_2 of the matrix $\mathbf{\Gamma} = -\boldsymbol{M}^{-1}\boldsymbol{K}$, four regions can be identified: stability (red), divergence instability (orange), saddle-node instability (yellow), and flutter instability (light blue). When a bifurcation analysis is performed with respect to a bifurcation parameter α, a parametric path can be drawn in the I_1-I_2 plane (the white curve) as a function of α , while the intersections of this path with the boundaries of the various regions determine the critical values of the considered bifurcation parameter.

The above conditions on the nature of the eigenvalues can be associated with the values of the first and second invariants I_1 and I_2, as depicted in Figure 3.4, where the 2-D plane $I_1 - I_2$ is divided into four different areas and each one reveals a particular behaviour. From the structure

of the eigenvalues in formula (3.33), it is evident that a first subdivision of the plane $I_1 - I_2$ can be performed:

- $I_1^2 - 4I_2 > 0$ (i.e. $I_2 < I_1^2/4$): in this case the internal square root of (3.33) is a real number since the argument is positive. Moreover, the argument $I_1 \pm \sqrt{I_1^2 - 4I_2}$ must a real number, since the invariants are real, so the eigenvalues are $\lambda_j \in \mathbb{R}$ or $\lambda_j \in i\mathbb{R}$.

- $I_1^2 - 4I_2 < 0$ (i.e. $I_2 > I_1^2/4$): in this case the internal square root of (3.33) is a purely imaginary number since the argument is negative. Then, the arguments of the external square root are complex conjugate numbers, hence the eigenvalues are of the form $\lambda_{1,2,3,4} = \pm(\alpha \pm i\beta)$.

Therefore, in the plane $I_1 - I_2$, a parabola

$$I_2 = \frac{I_1^2}{4}$$

may be identified. In the area above this curve, the points are related to a mechanical system that show a flutter instability, otherwise, for $I_2 < I_1^2/4$, flutter is forbidden. As for the configurations below the parabola, the following further subdivision can be performed:

- $I_2 < 0$: if I_2 is negative, then the term $-4I_2$ is positive and the following relation holds, $\sqrt{I_1^2 - 4I_2} > |I_1|$. Since the point is below the parabola, then $\sqrt{I_1^2 - 4I_2} \in \mathbb{R}$. Hence, the terms $I_1 \pm \sqrt{I_1^2 - 4I_2}$ are positive in one case and negative in the other (on the basis of the sign of I_2), so two eigenvalues are purely imaginary and two are real numbers. In this case, a saddle-node instability is present.

- $I_2 > 0$: if I_2 is positive, then the term $-4I_2$ is negative and the following relation holds, $\sqrt{I_1^2 - 4I_2} < |I_1|$. Since the point is below the parabola, then $\sqrt{I_1^2 - 4I_2} \in \mathbb{R}$. Therefore, if $I_1 > 0$, then the terms $I_1 \pm \sqrt{I_1^2 - 4I_2}$ are both positive and the eigenvalues are all real numbers (divergence instability), otherwise, if $I_1 < 0$, the argument $I_1 \pm \sqrt{I_1^2 - 4I_2}$ are both negative and the eigenvalues are purely imaginary (stability).

The identification of a special 2 d.o.f. dynamical system with a specific point of the $I_1 - I_2$ plane can be useful for the comprehension of the behaviour of the structure. Moreover, a bifurcation analysis can be performed easily, in fact, the change of the considered bifurcation parameter can be associated with a parametric path in the plane of invariants, which is parametrised by the bifurcation parameter itself. The intersection points between this path and the boundaries of the four areas described above represent the critical points in which the system loses its structural stability and a bifurcation of the equilibrium can be observed.

3.3.3 Explicit calculation of the matrix exponential for the stable 2 d.o.f. smooth system

In Section 2.1.2, the computation of the matrix exponential for a generic dynamical system has been performed. These results can now be applied, with the restriction that the present analysis deals with a 2 d.o.f. *mechanical* system, so that the structure of the Jacobian matrix $\boldsymbol{A}$ is described by expression (3.27). Moreover, a further assumption is also that the smooth dynamical system is stable in the vicinity of the equilibrium configuration, since we are interested in the analysis of a possible unstable behaviour of the entire structure, when the subsystems are both stable (obtaining for a mechanical system the theoretical results exposed in [16], as will be treated in the next Chapter 4).

As presented in Section 2.1.2, for a generic matrix $\boldsymbol{A}$, the matrix exponential fulfils the relation

$$e^{\boldsymbol{A}} = \boldsymbol{U} e^{\overline{\boldsymbol{A}}} \boldsymbol{U}^{-1}, \tag{3.34}$$

where $\overline{\boldsymbol{A}}$ and $\boldsymbol{U}$ describe the Jordan canonical form of the Jacobian matrix $\boldsymbol{A}$, i.e. $\boldsymbol{A} = \boldsymbol{U}\overline{\boldsymbol{A}}\boldsymbol{U}^{-1}$, and, furthermore, $\overline{\boldsymbol{A}}$ is composed of Jordan blocks, whose dimensions depend on the algebraic and geometric multiplicities of the eigenvalues of $\boldsymbol{A}$.

In case of a *stable* smooth configuration, the matrix $\boldsymbol{A}$ can be diagonalised (a particular case of Jordan form, with only 1×1 Jordan blocks) and its purely imaginary eigenvalues are assumed to be equal to $\lambda_{1,2} = \pm i\beta_1$ and $\lambda_{3,4} = \pm i\beta_2$. One must note that in this analysis we also assume that $\beta_1 \neq \beta_2$, since this particular condition denotes grazing of an unstable

boundary (i.e. the configuration is exactly on the parabola $I_2 = I_1^2/4$, see Figure 3.4), an occurrence which is excluded here.

According to all these assumptions, the Jacobian matrix in the canonical Jordan form can be written as

$$\overline{\boldsymbol{A}} = \begin{bmatrix} i\beta_1 & 0 & 0 & 0 \\ 0 & -i\beta_1 & 0 & 0 \\ 0 & 0 & i\beta_2 & 0 \\ 0 & 0 & 0 & -i\beta_2 \end{bmatrix}, \tag{3.35}$$

while $\boldsymbol{U}$, which is orthogonal in this specific case, is defined as the matrix having the eigenvectors (3.30) gathered in columns, so that

$$\boldsymbol{U} = \left[\boldsymbol{v}^{(1)}, \boldsymbol{v}^{(2)}, \boldsymbol{v}^{(3)}, \boldsymbol{v}^{(4)}\right] = \begin{bmatrix} \psi_1^{(1)} & \psi_1^{(1)} & \psi_1^{(2)} & \psi_1^{(2)} \\ \psi_2^{(1)} & \psi_2^{(1)} & \psi_2^{(2)} & \psi_2^{(2)} \\ i\beta_1\psi_1^{(1)} & -i\beta_1\psi_1^{(1)} & i\beta_2\psi_1^{(2)} & -i\beta_2\psi_1^{(2)} \\ i\beta_1\psi_2^{(1)} & -i\beta_1\psi_2^{(1)} & i\beta_2\psi_2^{(2)} & -i\beta_2\psi_2^{(2)} \end{bmatrix}, \tag{3.36}$$

and the inverse of $\boldsymbol{U}$ is given by

$$\boldsymbol{U}^{-1} = \frac{1}{2(\psi_1^{(1)}\psi_2^{(2)} - \psi_2^{(1)}\psi_1^{(2)})} \begin{bmatrix} \psi_2^{(2)} & -\psi_1^{(2)} & -i\psi_2^{(2)}/\beta_1 & i\psi_1^{(2)}/\beta_1 \\ \psi_2^{(2)} & -\psi_1^{(2)} & i\psi_2^{(2)}/\beta_1 & -i\psi_1^{(2)}/\beta_1 \\ -\psi_2^{(1)} & \psi_1^{(1)} & i\psi_2^{(1)}/\beta_2 & -i\psi_1^{(1)}/\beta_2 \\ -\psi_2^{(1)} & \psi_1^{(1)} & -i\psi_2^{(1)}/\beta_2 & i\psi_1^{(1)}/\beta_2 \end{bmatrix}. \tag{3.37}$$

Moreover, the matrix exponential of a diagonal matrix $\overline{\boldsymbol{A}}$ can easily be computed according to what have been presented in Section 2.1.2, as

$$e^{\overline{\boldsymbol{A}}t} = \begin{bmatrix} \cos\beta_1 t + i\sin\beta_1 t & 0 & 0 & 0 \\ 0 & \cos\beta_1 t - i\sin\beta_1 t & 0 & 0 \\ 0 & 0 & \cos\beta_2 t + i\sin\beta_2 t & 0 \\ 0 & 0 & 0 & \cos\beta_2 t - i\sin\beta_2 t \end{bmatrix}.$$

Finally, formulas (3.35), (3.36), and (3.37) can be substituted into (3.34), obtaining the matrix exponential which describes the solution of the lin-

earised smooth *mechanical* system

$$e^{\boldsymbol{A}t} = \begin{bmatrix} \frac{a_1\cos\beta_1 t - a_2\cos\beta_2 t}{a_1-a_2} & \frac{a_1a_2(\cos\beta_2 t-\cos\beta_1 t)}{a_1-a_2} & \frac{a_1\beta_2\sin\beta_1 t - a_2\beta_1\sin\beta_2 t}{a_1\beta_1\beta_2-a_2\beta_1\beta_2} & \frac{a_1a_2(\beta_1\sin\beta_2 t-\beta_2\sin\beta_1 t)}{a_1\beta_1\beta_2-a_2\beta_1\beta_2} \\ \frac{\cos\beta_1 t-\cos\beta_2 t}{a_1-a_2} & \frac{a_1\cos\beta_2 t-a_2\cos\beta_1 t}{a_1-a_2} & \frac{\beta_2\sin\beta_1 t-\beta_1\sin\beta_2 t}{a_1\beta_1\beta_2-a_2\beta_1\beta_2} & \frac{a_1\beta_1\sin\beta_2 t-a_2\beta_2\sin\beta_1 t}{a_1\beta_1\beta_2-a_2\beta_1\beta_2} \\ \frac{a_2\beta_2\sin\beta_2 t-a_1\beta_1\sin\beta_1 t}{a_1-a_2} & \frac{a_1a_2(\beta_1\sin\beta_1 t-\beta_2\sin\beta_2 t)}{a_1-a_2} & \frac{a_1\cos\beta_1 t-a_2\cos\beta_2 t}{a_1-a_2} & \frac{a_1a_2(\cos\beta_2 t-\cos\beta_1 t)}{a_1-a_2} \\ \frac{\beta_2\sin\beta_2 t-\beta_1\sin\beta_1 t}{a_1-a_2} & \frac{a_2\beta_1\sin\beta_1 t-a_1\beta_2\sin\beta_2 t}{a_1-a_2} & \frac{\cos\beta_1 t-\cos\beta_2 t}{a_1-a_2} & \frac{a_1\cos\beta_2 t-a_2\cos\beta_1 t}{a_1-a_2} \end{bmatrix}, \tag{3.38}$$

where the scalars $a_1, a_2 \in \mathbb{R}$ have been introduced, such that

$$a_1 = \frac{\psi_1^{(1)}}{\psi_2^{(1)}} = -\frac{\beta_1^2+\Gamma_{22}}{\Gamma_{21}}, \qquad a_2 = \frac{\psi_1^{(2)}}{\psi_2^{(2)}} = -\frac{\beta_2^2+\Gamma_{22}}{\Gamma_{21}},$$

and where Γ_{hk} are the elements of the matrix $\boldsymbol{\Gamma}$.

As a final remark, using the following property

$$\boldsymbol{AB} = \boldsymbol{BA} \Longrightarrow e^{\boldsymbol{A}}e^{\boldsymbol{B}} = e^{\boldsymbol{A}+\boldsymbol{B}},$$

and assuming $\boldsymbol{B} = -\boldsymbol{A}$, the inverse of the matrix exponential (3.38) can be computed with a simple change in the sign of t, namely

$$(e^{\boldsymbol{A}t})^{-1} = e^{-\boldsymbol{A}t}.$$

3.4 Flutter and divergence instability in the smooth structure

The stability of a piecewise-smooth system is a cumbersome problem and it will be described in Chapter 4. On the contrary, for a smooth dynamical system, an explicit calculation of the natural frequencies of the system leads to a complete characterisation of the behaviour of the structure. In particular, the linearised dynamics near an equilibrium point is considered and the nature of the frequencies allows the determination of the ranges of the load parameter F, for which the system reveals stability, flutter, or divergence.

3.4.1 Flutter and divergence loads for a smooth structure

As an introductory example, let's consider a smooth profile modelled by the general curve $y = g(x)$ in the Cartesian reference frame, such that $g \in \mathcal{C}^2$, the curve passes through the origin, i.e. $g(0) = 0$, and the first and second derivatives calculated in $x = 0$ vanish, i.e. $g'(0) = g''(0) = 0$.

This curve may represent a profile which is analogous to that described in Section 3.2 for the considered reference structure, however, it is *smooth*, since in this case the second derivative is continuous in the origin (i.e. in the origin there is not a jump in the curvature). This analogy is useful to highlight the role of the discontinuity in the stability behaviour of the smooth and non-smooth system, which leads to the paradoxical behaviour exposed in Section 2.2.1.

The parametric description of the considered curve $y = g(x)$ with respect to the curvilinear coordinate ξ is

$$\begin{cases} x(\xi) = \xi \\ y(\xi) = g(\xi) \end{cases}$$

hence the following conditions hold

$$\begin{array}{llll} x(0) = 0, & x'(0) = 1, & x''(0) = 0, & \alpha(0) = 0, \\ y(0) = 0, & y'(0) = g'(0) = 0, & y''(0) = g''(0) = 0, & \alpha'(0) = 0. \end{array} \tag{3.39}$$

The mass and stiffness matrix representing the linearised equations of motion near the equilibrium configuration $(\xi, \phi) = (0, 0)$ are computed imposing relations (3.39) into (3.10) and (3.11), so that

$$\boldsymbol{M} = \begin{bmatrix} 1 & \frac{l}{2} \\ \frac{l}{2} & \frac{l^2}{3} \end{bmatrix} \qquad \boldsymbol{K} = \begin{bmatrix} k_1 & -F \\ 0 & k_2 \end{bmatrix}.$$

One must observe that, for any $g(x)$ that fulfils the hypotheses given above (i.e. $g \in \mathcal{C}^2$ passes through the origin with horizontal tangent and vanishing curvature), the stiffness and mass matrices are always the same, thus the following results hold for all the possible parametrisations g describing a smooth profile.

The Jacobian matrix $\boldsymbol{A}$ of the linearised dynamical system, according to the Hamiltonian formulation, see Section 3.3, can be computed

adopting the previous definitions of stiffness and mass matrix into relation (3.27), obtaining

$$\boldsymbol{\Gamma} = -\boldsymbol{M}^{-1}\boldsymbol{K} = \begin{bmatrix} -4k_1 & 4F + \frac{6k_2}{l} \\ \frac{6k_1}{l} & -\frac{12k_2}{l^2} - \frac{6F}{l} \end{bmatrix}$$

and

$$\boldsymbol{A} = \begin{bmatrix} 0 & 0 & 1 & 0 \\ 0 & 0 & 0 & 1 \\ -4k_1 & 4F + \frac{6k_2}{l} & 0 & 0 \\ \frac{6k_1}{l} & -\frac{12k_2}{l^2} - \frac{6F}{l} & 0 & 0 \end{bmatrix}.$$

The four eigenvalues of the Jacobian matrix $\boldsymbol{A}$ are

$$\lambda_j = \pm\frac{1}{l^2}\sqrt{-(3Fl^3 + 2k_1l^4 + 6k_2l^2) \pm l^2\sqrt{(3Fl + 2k_1l^2 + 6k_2)^2 - 12k_1k_2l^2}},$$

while the critical load can be calculated from the parabola in the invariant plane depicted in Figure 3.4, computing the first and second invariants of $\boldsymbol{\Gamma}$ as

$$I_1 = \operatorname{tr}\boldsymbol{\Gamma} = -\frac{4k_1l^2 + 12k_2 + 6Fl}{l^2} \qquad I_2 = \det\boldsymbol{\Gamma} = \frac{12k_1k_2}{l^2}.$$

As explained in Section 3.3.2, in the $I_1 - I_2$ plane, each possible structure can be identified by a specific point, whose location in the plane is associated with a given possible behaviour. When a parameter is changed, e.g. as in bifurcation analyses, a path in this $I_1 - I_2$ plane can be drawn, as a function of the bifurcation parameter. The critical values of this parameter are located where the qualitative behaviour of the system dramatically changes, hence at the crossing points between the path and the boundaries of the four areas.

In the case presented above, the determinant of $\boldsymbol{\Gamma}$ is always positive, so all the possible configurations of the system will be in the positive half-space $I_2 > 0$. Moreover, assuming the load as the bifurcation parameter, the path described when F is changed is simply an horizontal line, since I_2

does not depend on F. Therefore, the flutter and divergence critical loads are located at the intersection points between the horizontal line and the parabola $I_2 = I_1^2/4$, hence

$$I_2 = \frac{I_1^2}{4} \quad \longrightarrow \quad \frac{12k_1k_2}{l^2} - \frac{1}{4}\left(\frac{4k_1l^2 + 12k_2 + 6Fl}{l^2}\right)^2 = 0,$$

that can be solved in F, obtaining the critical values

$$F_{\text{flu}} = -\frac{2}{3l}(k_1l^2 + 3k_2 - l\sqrt{3k_1k_2}), \quad F_{\text{div}} = -\frac{2}{3l}(k_1l^2 + 3k_2 + l\sqrt{3k_1k_2}), \tag{3.40}$$

which are always negative, so compressive loads, while absolute value of the divergence critical load is greater than the absolute value of the flutter one.

As a conclusion, every structure with a smooth and continuous profile, whose curvature smoothly and continuously changes its sign in the origin, has flutter and divergence critical loads equal to (3.40). Furthermore, also the curve $g(x) = 0$ fulfils these hypotheses, so we can state that the analysis of the linearised behaviour of the smooth mechanical system described above is analogous to the investigation of a profile defined by a straight line. When a jump in the curvature is not present, all the possible profiles have the same compressive flutter and divergence load, so flutter in tension is forbidden. This condition is not true for piecewise-smooth systems with a jump in the curvature, as will be described in Chapter 4.

3.4.2 Flutter and divergence loads for circular profiles

Let's now define the critical loads for the subsystems that compose the reference structure depicted in Figure 3.3, showing a doubly circular profile. One must observe that the subsystems do not fulfil the hypotheses on the function $g(x)$ introduced in Section 3.4.1, however, the determination of the range of values of the load F in which the subsystems $(-)$ and $(+)$ are stable is crucial and the same procedure exposed in the previous paragraph can be adopted.

The matrix $\boldsymbol{\Gamma}^{\pm} = -\boldsymbol{M}^{-1}\boldsymbol{K}^{\pm}$ in case of positive or negative subsystem

is equal to

$$\mathbf{\Gamma}^{\pm}=\begin{bmatrix}\frac{\pm 4l^2R_{\pm}(F+k_1(y_s\mp R_{\pm}))-k_2l(4l\mp 6R_{\pm})}{\rho l^3R_{\pm}^2} & \frac{4Fl^2R_{\pm}^2\mp 4k_2l^2R_{\pm}+6k_2R_{\pm}^2l}{\rho l^3R_{\pm}^2}\\ \frac{\mp 6lR_{\pm}(F+k_1(y_s\mp R_{\pm}))+6k_2(l\pm 2R_{\pm})}{\rho l^3R_{\pm}^2} & \frac{-6R_{\pm}(FlR_{\pm}\mp k_2l+2k_2R_{\pm})}{\rho l^3R_{\pm}^2}\end{bmatrix},$$

while its invariants can be written as

$$\begin{aligned}I_1^-&=-\frac{2\left(lR_-(F(2l+3R_-)+2k_1l(R_-+y_s))+2k_2\left(l^2+3lR_-+3R_-^2\right)\right)}{\rho l^3R_-^2},\\ I_2^-&=\frac{12k_1k_2(R_-+y_s)}{\rho^2l^4R_-},\end{aligned}\tag{3.41}$$

for the negative subsystem, and

$$\begin{aligned}I_1^+&=\frac{2\left(lR_+(F(2l-3R_+)-2k_1l(R_+-y_s))-2k_2\left(l^2-3lR_++3R_+^2\right)\right)}{\rho l^3R_+^2},\\ I_2^+&=\frac{12k_1k_2(R_+-y_s)}{\rho^2l^4R_+},\end{aligned}\tag{3.42}$$

for the positive one. Hence, the eigenvalues of the Jacobian matrix $\boldsymbol{A}^{\pm}$ are

$$\begin{aligned}\lambda_j^-=\pm\Bigg\{&\frac{-lR_-\left(F(2l+3R_-)+2k_1l(y_s+R_-)\right)-2k_2(l^2+3lR_-+3R_-^2)}{l^3\rho R_-^2}\\ &\pm\frac{1}{l^3\rho R_-^2}\Bigg[\Big(lR_-(F(2l+3R_-)+2k_1l(y_s+R_-))\\ &+2k_2(l^2+3lR_-+3R_-^2)\Big)^2-12k_1k_2l^2R_-^3(y_s+R_-)\Bigg]^{\frac{1}{2}}\Bigg\}^{\frac{1}{2}}\end{aligned}$$

for the $(-)$ subsystem, and

$$\begin{aligned}\lambda_j^+=\pm\Bigg\{&\frac{lR_+(F(2l-3R_+)+2k_1l(y_s-R_+))-2k_2(l^2-3lR_++3R_+^2)}{l^3\rho R_+^2}\\ &\pm\frac{1}{l^3\rho R_+^2}\Bigg[\Big(lR_+(F(3R_+-2l)+2k_1l(R_+-y_s))\\ &+2k_2(l^2-3lR_++3R_+^2)\Big)^2+12k_1k_2l^2R_+^3(y_s-R_+)\Bigg]^{\frac{1}{2}}\Bigg\}^{\frac{1}{2}}\end{aligned}$$

for the $(+)$ subsystem.

When the load F is assumed to be the bifurcation parameter, the parametric path in the plane $I_1 - I_2$ is a straight line parallel to the axis I_1. Analogously to what has been performed in the previous paragraph for a generic curve, the flutter and divergence critical loads are obtained imposing that $I_2 = I_1^2/4$, in order to identify the intersections between this parabola and the straight path.

Let's note that the determinant of the matrix $\Gamma^{\pm}$ must be positive to have an intersection between the path and the parabola, otherwise, the equilibrium configuration would be unstable for all values of the force F. Moreover, for the negative subsystem, the load F in the term I_1^-, see relation $(3.41)_1$, is multiplied by the coefficient $2l + 3R_-$, which is always a positive quantity. On the contrary, for the positive subsystem, see relation $(3.42)_1$, the same coefficient is $2l - 3R_+$, which can assume a positive or negative value, on the basis of the ratio R_+/l. This means that for the negative system the value of I_1^- increases only for decreasing values of F, while, for the positive system, I_1^+ increases both for increasing or decreasing values of F. Hence, flutter both in tension and in compression is admissible for the subsystem with positive curvature.

For the negative subsystem, the condition on the determinant $I_2^- > 0$ is fulfilled with the restriction $y_s > -R_-$, and the flutter and divergence critical loads are equal to

$$\begin{aligned} F_{\text{flu}}^- &= -\frac{2R_-k_1l^2(R_- + y_s) + 2k_2\left(l^2 + 3lR_- + 3R_-^2\right) - 2lR_-\sqrt{3k_1k_2R_-(R_- + y_s)}}{lR_-(2l + 3R_-)} \\ F_{\text{div}}^- &= -\frac{2R_-k_1l^2(R_- + y_s) + 2k_2\left(l^2 + 3lR_- + 3R_-^2\right) + 2lR_-\sqrt{3k_1k_2R_-(R_- + y_s)}}{lR_-(2l + 3R_-)}. \end{aligned} \tag{3.43}$$

In this case, it is easy to identify which is the flutter and the divergence load, in fact, from (3.41), the value of I_1^- increases when the value of F decreases. Since the divergence critical load is associated with the highest value of I_1^-, the intersection point associated with divergence instability must be the one presenting the highest absolute value between the two critical loads (3.43).

The critical loads are both negative, so flutter and divergence instability may occur only for compressive follower forces. The determination of the negative sign of the divergence critical load is trivial, while the flutter

critical load is negative only if the following condition is fulfilled

$$2R_-k_1l^2(R_-+y_s)+2k_2\left(l^2+3lR_-+3R_-^2\right)>2lR_-\sqrt{3k_1k_2R_-(R_-+y_s)},$$

which yields to the following expression, when the left-hand-side and right-hand-side are squared,

$$\begin{aligned}&\left[R_-k_1l^2(R_-+y_s)\right]^2+\left[k_2\left(l^2+3lR_-+3R_-^2\right)\right]^2\\&\quad+2R_-l^2k_1k_2(R_-+y_s)\left(l^2+3lR_-+3R_-^2\right)>3l^2R_-^3k_1k_2(R_-+y_s),\end{aligned}$$

that can be further rewritten as

$$\begin{aligned}&\left[R_-k_1l^2(R_-+y_s)\right]^2+\left[k_2\left(l^2+3lR_-+3R_-^2\right)\right]^2\\&\qquad+R_-l^2k_1k_2(R_-+y_s)\left(2l^2+6lR_-+3R_-^2\right)>0.\end{aligned}$$

This condition is always fulfilled with the physical assumptions on the mechanical and geometrical parameters, leading to a negative (compressive) flutter load. Since both values of the critical loads are negative, the system is stable for $F=0$, which is realistic from a physical point of view.

For the positive subsystem, the condition on the determinant I_2^+ is fulfilled with the restriction $y_s<R_+$, and the intersections between the path and the parabola are identified by the values

$$\begin{aligned}F_1=\frac{1}{lR_+(2l-3R_+)}&\left[2k_1l^2R_+(R_+-y_s)+2k_2\left(l^2-3lR_++3R_+^2\right)\right.\\&\left.-2\,\mathrm{sign}\left[2l-3R_+\right]lR_+\sqrt{3k_1k_2R_+(R_+-y_s)}\right]\end{aligned}\tag{3.44}$$

and

$$\begin{aligned}F_2=\frac{1}{lR_+(2l-3R_+)}&\left[2k_1l^2R_+(R_+-y_s)+2k_2\left(l^2-3lR_++3R_+^2\right)\right.\\&\left.+2\,\mathrm{sign}\left[2l-3R_+\right]lR_+\sqrt{3k_1k_2R_+(R_+-y_s)}\right].\end{aligned}\tag{3.45}$$

In the previous formulas, a dependency on the sign of the term $2l-3R_+$ appears, therefore the value of I_1^+ can increase both for increasing or decreasing values of F, on the basis of the sign of the aforementioned term $2l-3R_+$. The determination of the flutter and divergence critical load is

less trivial than in the case of negative curvature, but the same ideas can be adopted.

First of all, let's note that the term $l^2 - 3lR_+ + 3R_+^2$ that appears in the intersection values and in I_1^+ is always positive, for all values of the ratio R_+/l, in fact

$$l^2 - 3lR_+ + 3R_+^2 = (l - \sqrt{3}R_+)^2 + (2\sqrt{3} - 3)lR_+ > 0.$$

Then, if $2l - 3R_+ \geq 0$ (i.e. $R_+/l \leq 2/3$) the value of I_1^+ increases for increasing values of F, see (3.42), hence the divergence load must be the one with the highest absolute value, so that

$$\frac{R_+}{l} \leq \frac{2}{3} \quad \Rightarrow \quad F_{\text{flu}} = F_1, \quad F_{\text{div}} = F_2$$

On the contrary, if $2l - 3R_+ < 0$ (i.e. $R_+/l > 2/3$) the value of I_1^+ increases for decreasing values of F, see (3.42), and the divergence load is still the one with the highest absolute value, so that

$$\frac{R_+}{l} > \frac{2}{3} \quad \Rightarrow \quad F_{\text{flu}} = F_2, \quad F_{\text{div}} = F_1.$$

Let's note that in the first case, with $R_+/l \leq 2/3$, both flutter and divergence loads are positive (tensile follower force), while for $R_+/l > 2/3$ the critical loads are both negative (compressive force). The determination of the sign of the divergence critical load is trivial, while for the flutter condition, the following relation must hold

$$2k_1 l^2 R_+(R_+ - y_s) + 2k_2\left(l^2 - 3lR_+ + 3R_+^2\right) - 2lR_+\sqrt{3k_1k_2R_+(R_+ - y_s)} > 0, \tag{3.46}$$

namely, the numerator of the flutter critical load must be positive (so that the correct sign is given by the denominator). The left-hand-side can be rewritten in order to obtain a squared binomial, hence

$$\left[l\sqrt{k_1R_+(R_+ - y_s)} - \sqrt{k_2\left(l^2 - 3lR_+ + 3R_+^2\right)}\right]^2 + l\sqrt{k_1k_2R_+(R_+ - y_s)}\left[2\sqrt{l^2 - 3lR_+ + 3R_+^2} - R_+\sqrt{3}\right] > 0.$$

The first term of the sum is always positive, while the sign of the second one must be investigated. The factor of the second term in the square brackets can be rewritten multiplying and dividing by a positive quantity

$$\left[2\sqrt{l^2-3lR_+ +3R_+^2}-R_+\sqrt{3}\right]\cdot\frac{2\sqrt{l^2-3lR_+ +3R_+^2}+R_+\sqrt{3}}{2\sqrt{l^2-3lR_+ +3R_+^2}+R_+\sqrt{3}}$$

leading to

$$2\sqrt{l^2-3lR_+ +3R_+^2}-R_+\sqrt{3}=\frac{(2l-3R_+)^2}{2\sqrt{l^2-3lR_+ +3R_+^2}+R_+\sqrt{3}}>0$$

which is always positive. The condition (3.46) is fulfilled for all possible physical values of the parameters, so the condition on the sign of the value of the flutter critical load has been proved. Finally, one must observe that the limit of (3.43), (3.44), and (3.45) for $R_\pm \to \infty$ leads to (3.40).

Furthermore, the value of y_s, representing the $y-$coordinate of the point $\boldsymbol{S}$ at which the longitudinal spring is constrained, must be chosen in the correct range, in order to neglect structures that are always unstable. In the case of a doubly circular profile, since we are interested in subsystems that are separately stable, the possible range in which this coordinate must be chosen is $y_s \in [-R_-, R_+]$. Actually, in the numerical example presented in Chapter 6, the point $\boldsymbol{S}$ is considered to be exactly at the origin of the Cartesian reference frame, i.e. $y_s = 0$.

As a final remark, analogous calculations can be performed for the non-dimensional problem exposed in section 3.2.2, leading to the following formulas for the non-dimensional critical loads γ. According to relations (3.18), the critical loads for the negative subsystem $(-)$ are

$$\begin{aligned}\gamma^-_{\text{flu}} &= -\frac{2\zeta_-(3\zeta_-+2)(\zeta_-((k+3)\zeta_-+k\sigma+3)+1)-2\sqrt{3k\zeta_-^5(3\zeta_-+2)^2(\zeta_-+\sigma)}}{\zeta_-^2(3\zeta_-+2)^2},\\ \gamma^-_{\text{div}} &= -\frac{2\zeta_-(3\zeta_-+2)(\zeta_-((k+3)\zeta_-+k\sigma+3)+1)+2\sqrt{3k\zeta_-^5(3\zeta_-+2)^2(\zeta_-+\sigma)}}{\zeta_-^2(3\zeta_-+2)^2},\end{aligned} \tag{3.47}$$

with the assumption on the position of $\boldsymbol{S}$ that becomes $\sigma > \zeta_-$. As for the positive subsystem $(+)$, the intersection points with the parabola in the

plane of the invariants are defined by the non-dimensional critical loads

$$\gamma_1 = \frac{2\zeta_+(2-3\zeta_+)(\zeta_+((k+3)\zeta_+ - k\sigma - 3)+1) - 2\sqrt{3k\zeta_+^5(3\zeta_+-2)^2(\zeta_+-\sigma)}}{\zeta_+^2(2-3\zeta_+)^2},$$
$$\gamma_2 = \frac{2\zeta_+(2-3\zeta_+)(\zeta_+((k+3)\zeta_+ - k\sigma - 3)+1) + 2\sqrt{3k\zeta_+^5(3\zeta_+-2)^2(\zeta_+-\sigma)}}{\zeta_+^2(2-3\zeta_+)^2}, \tag{3.48}$$

and, provided that the condition $\sigma < \zeta_+$ is fulfilled, the flutter and divergence loads are

$$\zeta_+ \leq \frac{2}{3} \quad \Rightarrow \quad \gamma_{\text{flu}} = \gamma_1, \quad \gamma_{\text{div}} = \gamma_2,$$

or

$$\zeta_+ > \frac{2}{3} \quad \Rightarrow \quad \gamma_{\text{flu}} = \gamma_2, \quad \gamma_{\text{div}} = \gamma_1,$$

on the basis of the value of the non-dimensional parameter $\zeta_+ = R_+/l$. As underlined above, the value of the y-coordinate of the point $\boldsymbol{S}$ must be chosen in such a way $\sigma \in [-\zeta_-, \zeta_+]$.

3.5 Conclusions

The reference structure introduced in Section 3.1.1, a rigid bar constrained on a curved profile and subjected to a follower force, has been deeply investigated from a mathematical point of view. In particular, the case in which the profile is parametrised by a smooth circular curve has been analysed, since it represents the basic subsystem composing the doubly circular constraint of a piecewise-smooth mechanical system, which is the final target of this investigation. The equations of motion both in the linear and nonlinear case have been obtained in Section 3.1.2 and 2.32, while flutter and divergence critical loads have been computed in Section 3.4.

This analysis of a specific structure has been extended, to deal with general mechanical systems described in their linearised formulation by a Jacobian matrix defined in expression (3.27). In particular, this structure of the Jacobian matrix can be representative of all 2 d.o.f. mechanical systems, provided that the damping components have been neglected.

A stability analysis of smooth systems has been performed, based on the linearisation of the system near the equilibrium configuration, concerning the investigation of the nature of the eigenvalues of the Jacobian matrix, which actually depend on the first and second invariant of the matrix $\boldsymbol{A}$.

While the stability of equilibrium configurations of smooth structures can be determined following well-known techniques, no general criteria can be found for non-conservative piecewise-smooth systems. Thus, the investigation of these 2 d.o.f. piecewise-smooth structures is the main topic treated in the next Chapter 4.

CHAPTER 4

Invariant cones and piecewise-smooth mechanical systems

"A scientist worthy of his name, about all a mathematician, experiences in his work the same impression as an artist; his pleasure is as great and of the same nature."

Jules Henri Poincaré

"Geometry is not true, it is advantageous"

Jules Henri Poincaré

In the previous Chapter 3, a special 2 d.o.f. piecewise-smooth *mechanical* structure has been introduced, revealing a trivial equilibrium configuration in the origin of the phase space. The stability behaviour of this fixed point, located exactly at the discontinuity, can be investigated considering separately the positive and negative subsystems that compose the entire piecewise structure. However, as shown by Carmona *et al.* [16], the stability of the combined system is not generally guaranteed with the assumption of stable subsystems. In particular, Carmona *et al.* discovered that for a three-dimensional piecewise-linear dynamical system, the matching of two stable systems could be unstable, which, translated into a mechanical perspective, is certainly an unexpected and counterintuitive behaviour.

The main purpose of this Thesis is the definition of a theoretical instability criterion, att least for the subset of 2 d.o.f. mechanical systems, together with the determination of a physical structure that may reveal the behaviour predicted by Carmona in purely mathematical systems.

Unfortunately, the classical theorems of Lagrange-Dirichlet and Liapunov, as well as the Linear Stability approach, see Section 2.1.3 and [49, 58, 90], cannot be adopted, since the examined system is subjected to a non-conservative follower force and the equilibrium configuration is exactly on the discontinuity.

The only way to attempt this issue is to directly act on the solution of the dynamical system, assuming that a given invariant set is present in the phase portrait. If this hypothesis is fulfilled, the behaviour of a family of orbits is completely determined, at least for a given set of initial conditions. Moreover, due to the non-symmetric definition of instability of fixed points given by Liapunov, see Theorem 2, if the existence of a family of trajectories (described by the aforementioned invariant set) can be determined, such that the motion of the system evolves far from the equilibrium point, then an unstable behaviour is revealed by the structure.

As can be found in [14, 51, 52, 86, 87], the birth of the unstable behaviour found by by Carmona *et al.* is associated, from a mathematical perspective, to the presence of a particular invariant set in the phase portrait of the analysed piecewise system, called *invariant cone*.

In the following Sections, the conditions for the existence of an invariant cone will be derived for 2 d.o.f. mechanical systems subjected to non-conservative loads. Furthermore, the problem of the attractivity of the invariant set is investigated and some interesting properties are proved for this specific case of 2 d.o.f. structures. Some theoretical and numerical techniques, useful for the comprehension of the problem and for the analysis presented in this Chapter, can be found in [41, 42, 51, 52, 86, 87].

Finally, let's observe that all the following results are obtained for the piecewise-linear version of the equations of motion of the non-smooth system, i.e. for the simplified case in which every single subsystem has been linearised. The ODEs still remain nonlinear, but for this specific case, some theoretical and analytical outcomes can be found, since the exact solution in each subsystem is known and reveals an exponential form.

4.1 Invariant cones in 2 d.o.f. piecewise-linear mechanical system

4.1.1 General description of a 2 d.o.f. mechanical system

Let's consider a generic piecewise-linear system, described in the Hamiltonian formulation by the first order ODEs

$$\dot{\boldsymbol{y}}(t) = \begin{cases} \boldsymbol{A}^{-}\boldsymbol{y}(t), & y_1 < 0 \\ \\ \boldsymbol{A}^{+}\boldsymbol{y}(t), & y_1 > 0 \end{cases}, \tag{4.1}$$

where $\boldsymbol{y} \in \mathbb{R}^4$ is the phase vector and the matrices $\boldsymbol{A}^{\pm}$ have the structure presented in (3.27), so that (4.1) can be considered a mechanical system. The switching rule describes a hyperplane in the 4-dimensional phase space orthogonal to the y_1-axis. The analysis that will be presented below is sufficiently general to model not only the physical structure presented in Chapter 3, but also other 2 d.o.f. mechanical systems composed of two subsystems separated by an hyperplane. Actually, the switching condition seems to be very specific, however all mechanical systems with a hyperplane as a switching manifold can be reduced to (4.1) through a proper rotation in the phase coordinates.

According to the notation exposed in Chapter 2.2, the two *subdomains* in which the phase space is subdivided are $\mathcal{V}^{-} = \left\{\boldsymbol{y} \in \mathbb{R}^4 : y_1 < 0\right\}$, called the negative $(-)$ subsystem and $\mathcal{V}^{+} = \left\{\boldsymbol{y} \in \mathbb{R}^4 : y_1 > 0\right\}$, called the positive $(+)$ subsystem, while the plane $\Sigma = \left\{\boldsymbol{y} \in \mathbb{R}^4 : y_1 = 0\right\}$ is the *switching manifold*. An equivalent definition of the switching manifold, in which the scalar product with the normal unit vector of the hyperplane appears, is $\Sigma = \left\{\boldsymbol{y} \in \mathbb{R}^4 : \boldsymbol{y} \cdot \boldsymbol{e}_1 = 0\right\}$.

As was pointed out in Section 3.2.1 for the reference mechanical structure, the switching rule in problem (4.1) do not assign the condition $y_1 = 0$ to any subsystem. However, it will be clear in Section 4.2 that for the current hypotheses, the use of Filippov's convex method is not necessary and the condition $y_1 = 0$ can actually be considered correct for any choice of the subsystem, since the orbit always crosses the switching manifold and sliding conditions are forbidden. [1]

[1] As discussed in Section 3.2.1 and 4.2, there exists a zero-measure set of initial conditions, neglected in this analysis, in which the evolution of the system is not well-defined.

The piecewise-linear system (4.1) has a trivial equilibrium configuration in the origin of the phase space, exactly on the switching manifold, and the stability of this equilibrium point will be analysed below. The fact that this fixed point is exactly on the discontinuity leads to the impossibility of the application of classical stability criteria.

Since the complete dynamical system (4.1) is assumed to be piecewise-linear, the evolution in time in each subsystem $\dot{\boldsymbol{y}} = \boldsymbol{A}^{\pm}\boldsymbol{y}$ can be described by a proper matrix exponential, see formula (3.31). However, the matrix exponential that must be used for the description of the solution depends on the considered subdomain $\mathcal{V}^{\pm}$, in which the analysed orbit is supposed to lie. Hence, the solution of (4.1) can be obtained by a composition of matrix exponentials, written for the proper negative or positive subdomains.

When the crossing conditions on the switching manifold are fulfilled, i.e. an orbit that "hits" the switching manifold necessarily crosses the hyperplane and enters in the other subspace, the solution in terms of matrix exponentials can be written in a simpler way, since the sequence of fundamental solution matrix that must be used is well-defined. Moreover, in this case, the intersection points between the orbit and the switching manifold can be used as initial conditions for the following evolution in the subdomain in which the orbit is entering, since sliding on the hyperplane Σ is forbidden.

Let's imagine that a generic orbit in the four-dimensional phase space, as depicted in Figure 4.1, starting at the initial condition $\boldsymbol{y}(t_0) = \boldsymbol{y}_0 \in \mathcal{V}^{-}$, crosses the switching manifold Σ at given intersection times, whose sequence is $\{t_1, t_2, \dots, t_{k-1}, t_k, \dots\}$. Provided that the crossing conditions are fulfilled, the solution of the piecewise-linear system (4.1) can be written in the following way

$$\boldsymbol{y}(t) = \begin{cases} e^{\boldsymbol{A}^{-}(t-t_0)}\boldsymbol{y}_0, & t_0 < t \leq t_1 \\ e^{\boldsymbol{A}^{+}(t-t_1)}e^{\boldsymbol{A}^{-}(t_1-t_0)}\boldsymbol{y}_0, & t_1 < t \leq t_2 \\ e^{\boldsymbol{A}^{-}(t-t_2)}e^{\boldsymbol{A}^{+}(t_2-t_1)}e^{\boldsymbol{A}^{-}(t_1-t_0)}\boldsymbol{y}_0, & t_2 < t \leq t_3 \\ \dots & \dots \\ e^{\boldsymbol{A}^{-}(t-t_{k-2})}e^{\boldsymbol{A}^{+}(t_{k-2}-t_{k-3})}\dots e^{\boldsymbol{A}^{-}(t_1-t_0)}\boldsymbol{y}_0, & t_{k-2} < t \leq t_{k-1} \\ e^{\boldsymbol{A}^{+}(t-t_{k-1})}e^{\boldsymbol{A}^{-}(t_{k-1}-t_{k-2})}\dots e^{\boldsymbol{A}^{-}(t_1-t_0)}\boldsymbol{y}_0, & t_{k-1} < t \leq t_k \\ \dots & \dots \end{cases} \tag{4.2}$$

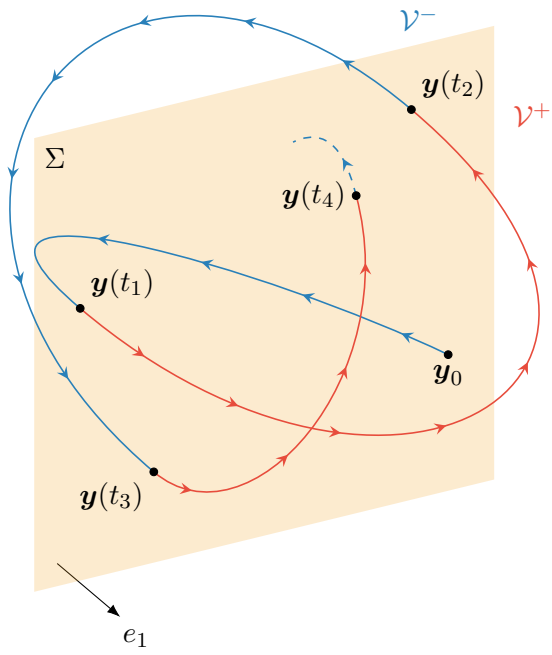

Figure 4.1: A pictorial view of a solution (4.2) of the 4D piecewise-smooth system (4.1), where a reduction to a 3D representation has been performed, for a graphical purpose. When the orbit lying in one of the two subdomains "hits" the switching manifold Σ at time $\{t_1, t_2, t_3, t_4, \dots\}$, the intersection point is assumed to be an initial condition for a new orbit that originates from it and evolves in the other subdomain.

The issue in the analytical treatment of this piecewise solution is that the time sequence is *a priori* unknown, because the intersection times essentially depends on the initial conditions, so they can be calculated only following the evolution of the solution. For this reason, the determination of an invariant set for this kind of problems is a cumbersome task and, in order to simplify it, a good strategy could be the introduction of Poincaré maps, see [41, 42, 51, 52, 86, 87].

As presented in detail in Section 2.2.5, a Poincaré map transforms the continuous-time dynamical system into a discrete-time one, with the introduction of a $(n-1)$-dimensional hyperplane, called Poincaré section, embedded in the n-dimensional phase space. The points of this hyper-

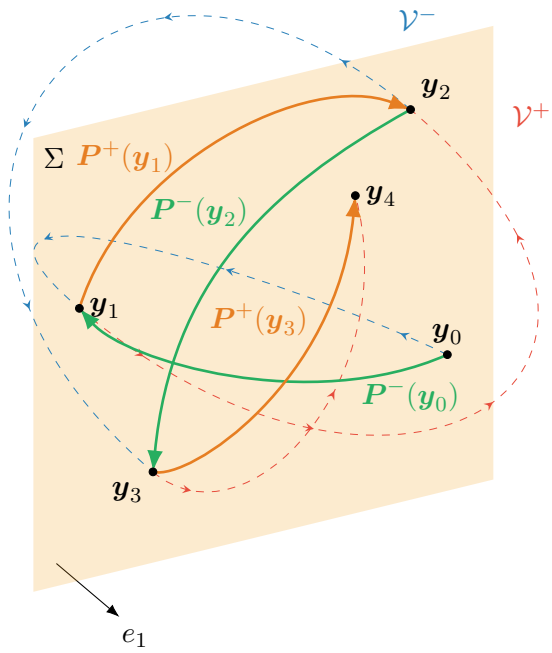

Figure 4.2: The same solution of Figure 4.1 is shown in this pictorial view. However, the continuous-time interpretation of the dynamical system is now substituted by a discrete-time description, which does not directly considered the continuous orbits in the 4D phase space (the blue and red dashed curves). On the contrary, the focus is given to the discrete Poincaré halfmaps between a point $\boldsymbol{y}_k = \boldsymbol{y}(t_k)$ and the following $\boldsymbol{y}_{k+1} = \boldsymbol{y}(t_{k+1})$, depicted as the orange and green arrows.

plane are mapped onto the plane itself through the orbits, so the map $\boldsymbol{P}$ can be introduced, describing a discrete dynamics that contains all the information for the analysis of the continuous-time system. As pointed out also in Section 2.2.5, the concept of Poincaré map is general and refers to a link among the points of a hyperplane in the phase space. On the contrary, the mathematical descriptions of the map can be different, e.g. it can be given in a local $(n-1)$-dimensional reference frame on the hyperplane or in the global reference frame of the $n-$dimensional phase space. The elements defined in the former description will generally be indicated with a hat '$\widehat{\ }$', otherwise they are intended to be expressed in the latter way.

As for the 4-dimensional problem (4.1), a convenient choice for the 3-dimensional Poincaré section is the switching manifold Σ, so that the complete Poincaré map $\boldsymbol{P} : \Sigma \to \Sigma$ can be thought as the composition of two Poincaré halfmaps $\boldsymbol{P}^{\pm} : \Sigma \to \Sigma$, such that

$$\boldsymbol{P} = \boldsymbol{P}^{+} \circ \boldsymbol{P}^{-}, \tag{4.3}$$

where $\boldsymbol{P}^{-}$ ($\boldsymbol{P}^{+}$) is defined in the negative (positive) subsystem. In this description (4.3), the hypothesis that the orbit enters first in the $(-)$ system has been assumed, without loss of generality. One must note that a different choice of the Poincaré section would lead to a more complex description of the Poincaré complete map, since the sequence of intersection times with the switching manifold used above would not be enough for the description of the solution, and also the sequence of intersection time with the Poincaré section would be necessary. Therefore, the identification between the Poincaré section and the switching manifold reduces the complexity of the description.

Let's consider a generic point $\boldsymbol{x} \in \Sigma$, belonging to the switching manifold, and let's suppose, without loss of generality, that the orbit with initial condition equal to $\boldsymbol{x}$ enters in the negative subspace $\mathcal{V}^{-}$. The time evolution in the negative subsystem is described by the first expression in formula (4.2), i.e.

$$\boldsymbol{y}(t) = e^{\boldsymbol{A}^{-}t}\boldsymbol{x},$$

until the orbit reaches the switching manifold at point $\boldsymbol{\xi}$, in a given time interval, namely t^{-}, from the initial time $t = 0$. Then, the orbit crosses [2] the switching manifold and enters in the positive subsystem $\mathcal{V}^{+}$, following the solution described by

$$\boldsymbol{y}(t) = e^{\boldsymbol{A}^{+}(t-t^{-})}e^{\boldsymbol{A}^{-}t^{-}}\boldsymbol{x} = e^{\boldsymbol{A}^{+}(t-t^{-})}\boldsymbol{\xi},$$

where the point $\boldsymbol{\xi}$ can be interpreted as a new initial condition for the second part of the orbit, defined in the positive subdomain. [3] The trajectory

[2] The fact that a generic orbit always crosses the switching manifold will be proved in Section 4.2

[3] The fact that ξ can be considered as an initial condition for the motion in the positive subspace is crucial and it comes from the fact that the considered system is autonomous and the crossing conditions are fulfilled (i.e. sliding is forbidden).

remains inside the $(+)$ subspace until it reaches the point $\boldsymbol{\eta}$ on the switching manifold in a time interval t^+, measured from $t = t^-$. It is evident form the definition of Poincaré map that the negative and positive Poincaré halfmaps consist in the relation among the points $\boldsymbol{x}$, $\boldsymbol{\xi}$ and $\boldsymbol{\eta}$, so that they can be expressed as

$$\boldsymbol{\xi} = \boldsymbol{P}^-(\boldsymbol{x}) = e^{\boldsymbol{A}^- t^-(\boldsymbol{x})}\boldsymbol{x} \qquad \boldsymbol{\eta} = \boldsymbol{P}^+(\boldsymbol{\xi}) = e^{\boldsymbol{A}^+ t^+(\boldsymbol{\xi})}\boldsymbol{\xi}. \tag{4.4}$$

The negative and positive time intervals t^- and t^+ are functions of the initial conditions $\boldsymbol{x}$ and $\boldsymbol{\xi}$, respectively, and they can be defined as

$$\begin{aligned} t^-(\boldsymbol{x}) &= \inf\left\{t > 0 : \boldsymbol{e}_1 \cdot e^{\boldsymbol{A}^- t}\boldsymbol{x} = 0\right\}, \\ t^+(\boldsymbol{\xi}) &= \inf\left\{t > 0 : \boldsymbol{e}_1 \cdot e^{\boldsymbol{A}^+ t}\boldsymbol{\xi} = 0\right\}, \end{aligned} \tag{4.5}$$

where $\boldsymbol{e}_1$ is the unit vector in the phase space along y_1-axis, which also represents the normal to the switching manifold Σ, see [51, 52]. These definitions (4.5) simply represent the fact that all the points $\boldsymbol{x}$, $\boldsymbol{\xi}$, and $\boldsymbol{\eta}$ must be on the switching manifold and that they must be the first intersection between the considered trajectory and the hyperplane Σ.

From a practical point of view, when a Poincaré map is introduced for the analysis of a dynamical system, the time variable present in the continuous-time description of the solution is generally substituted by a function of the initial conditions, since the focus of the discrete-time analysis is on the specific *intersection time* between the Poincaré section and the orbit, for a given initial condition. This mathematical description of the Poincaré maps holds also for the case studied in this Thesis, since the times t^- and t^+ are *a priori* unknown and depends on the initial conditions, as can be seen from (4.5). Due to the fact that the intersection times $t^-(\boldsymbol{x})$ and $t^+(\boldsymbol{\xi})$ are functions of the initial condition, the Poincaré halfmaps are nonlinear relations in the points $\boldsymbol{x}$ and $\boldsymbol{\xi}$.

The Poincaré halfmaps (4.4) defined above have been expressed as 4 - dimensional maps, in fact the points $\boldsymbol{x}$, $\boldsymbol{\xi}$ and $\boldsymbol{\eta}$ are thought as 4 - dimensional points of the phase space belonging to the switching manifold, namely

$$\boldsymbol{x} = [x_1, x_2, x_3, x_4]^{\mathrm{T}}, \quad \boldsymbol{\xi} = [\xi_1, \xi_2, \xi_3, \xi_4]^{\mathrm{T}}, \quad \boldsymbol{\eta} = [\eta_1, \eta_2, \eta_3, \eta_4]^{\mathrm{T}}. \tag{4.6}$$

An analogous 3-dimensional representation of the halfmaps above can be performed, since the aforementioned points can be expressed in a particular local 3-dimensional reference system on the switching manifold. The hyperplane that describes the discontinuity is $y_1 = 0$, hence the first component of the points always vanishes, $x_1 = \xi_1 = \eta_1 = 0$, so that the points can be described in this local reference frame by

$$\hat{\boldsymbol{x}} = [x_2, x_3, x_4]^{\mathrm{T}}, \quad \hat{\boldsymbol{\xi}} = [\xi_2, \xi_3, \xi_4]^{\mathrm{T}}, \quad \hat{\boldsymbol{\eta}} = [\eta_2, \eta_3, \eta_4]^{\mathrm{T}}, \tag{4.7}$$

while the reduced Poincaré halfmaps $\hat{\boldsymbol{\xi}} = \hat{\boldsymbol{P}}^{-}(\hat{\boldsymbol{x}})$ and $\hat{\boldsymbol{\eta}} = \hat{\boldsymbol{P}}^{+}(\hat{\boldsymbol{\xi}})$ are simply described by the 3×3 matrices obtained deleting the first row and column from $e^{\boldsymbol{A}^{-}t^{-}(\boldsymbol{x})}$ and $e^{\boldsymbol{A}^{+}t^{+}(\boldsymbol{\xi})}$.

The complete Poincaré map for the general problem (4.1) is described by $\boldsymbol{P} = \boldsymbol{P}^{+} \circ \boldsymbol{P}^{-}$, while the discrete-time evolution of the solution can be seen as the subsequent composition of the Poincaré halfmaps, so that

$$\begin{aligned} \boldsymbol{\eta}_k &= \boldsymbol{P}_k \circ \boldsymbol{P}_{k-1} \circ \cdots \circ \boldsymbol{P}_2 \circ \boldsymbol{P}_1(\boldsymbol{x}) = \\ &= \boldsymbol{P}_k^{+} \circ \boldsymbol{P}_k^{-} \circ \boldsymbol{P}_{k-1}^{+} \circ \boldsymbol{P}_{k-1}^{-} \circ \cdots \circ \boldsymbol{P}_1^{+} \circ \boldsymbol{P}_1^{-}(\boldsymbol{x}), \end{aligned}$$

where $\boldsymbol{P}_k^{\pm}$ are the Poincaré halfmaps calculated for the time intervals $t_k^{\pm}$. One must note that, the halfmaps $\boldsymbol{P}_k^{\pm}$ are generally different one another, since the time intervals in which the trajectories remains in the same subdomain $\mathcal{V}^{\pm}$ are not constant values. After the introduction of a Poincaré map, the investigation on the presence of a particular invariant set in the phase space reduces to the definition of particular laws that the points of the Poincaré maps must fulfil.

4.1.2 Invariant cones and instability analysis

The Poincaré map introduced in the previous Section is a useful tool for the detection of a particular invariant set in the 4-dimensional phase space described by system (4.1).

As outlined in Section 2.1.4, an invariant set is a particular subset $\mathcal{S}$ of the phase space such that $\boldsymbol{y}(0) \in \mathcal{S}$ implies $\boldsymbol{y}(t) \in \mathcal{S}$, for all t. For a 4-dimensional dynamical system, this subset is a 3-dimensional invariant manifold.

Definition 36 (see [14, 16, 52, 86])**.** An *invariant cone* is a particular invariant set of the phase portrait, such that the Poincaré map describing the evolution of the dynamical system fulfils the condition

$$\boldsymbol{P}(\boldsymbol{n}) = \mu \boldsymbol{n}, \tag{4.8}$$

where $\mu \in \mathbb{R}^+$ is a positive real scalar and $\boldsymbol{n} \in \Sigma$ is a vector of the phase space, belonging to the Poincaré section associated with the Poincaré map $\boldsymbol{P}$.

In the specific case of a piecewise-linear system, the Poincaré map is described by the composition of the halfmaps (4.4), hence an invariant cone exists for the mechanical system (4.1) if and only if there exist a scalar μ and a vector $\boldsymbol{x}$, such that

$$\boldsymbol{\eta} = e^{\boldsymbol{A}^+ t^+(\boldsymbol{\xi}(\boldsymbol{x}))} e^{\boldsymbol{A}^- t^-(\boldsymbol{x})} \boldsymbol{x} = \mu \boldsymbol{x}, \tag{4.9}$$

as also reported in [42, 51, 86].

Let's observe that condition (4.9) is written assuming that the Poincaré halfmaps are expressed in the global reference frame, i.e. the points of the maps are those defined in (4.6). The same condition can equivalently be expressed assuming the relation among the points (4.7), hence

$$\hat{\boldsymbol{\eta}} = \hat{\boldsymbol{P}}^+(\hat{\boldsymbol{\xi}}(\hat{\boldsymbol{x}})) \circ \hat{\boldsymbol{P}}^-(\hat{\boldsymbol{x}}) = \mu \hat{\boldsymbol{x}}$$

where $\hat{\boldsymbol{P}}^{\pm}$ are 3×3 matrices obtained deleting the first row and column of the matrix exponential, as explained above.

The condition (4.9) has the same structure of an eigenvalue problem: the multiplier μ can be seen as a generalised eigenvalue and the vector $\boldsymbol{x}$ as a generalised eigenvector of the matrix $e^{\boldsymbol{A}^+ t^+(\boldsymbol{\xi}(\boldsymbol{x}))} e^{\boldsymbol{A}^- t^-(\boldsymbol{x})}$, which defines the Poincaré map. However, this is a *nonlinear* eigenvalue problem, see [20], since the matrix itself depends on the eigenvector, hence the solution of (4.9) in terms of μ and $\boldsymbol{x}$ is not trivial and classical procedures for linear eigenvalue problems cannot be adopted. Moreover, let's observe that, as in classical eigenvalues problems, the eigenvector $\boldsymbol{x}$ can be scaled with a generic coefficient $\alpha \in \mathbb{R}$, so the eigenvector actually defines a set of points on the straight line described by vector $\alpha \boldsymbol{x}$, for which relation (4.9) is fulfilled.

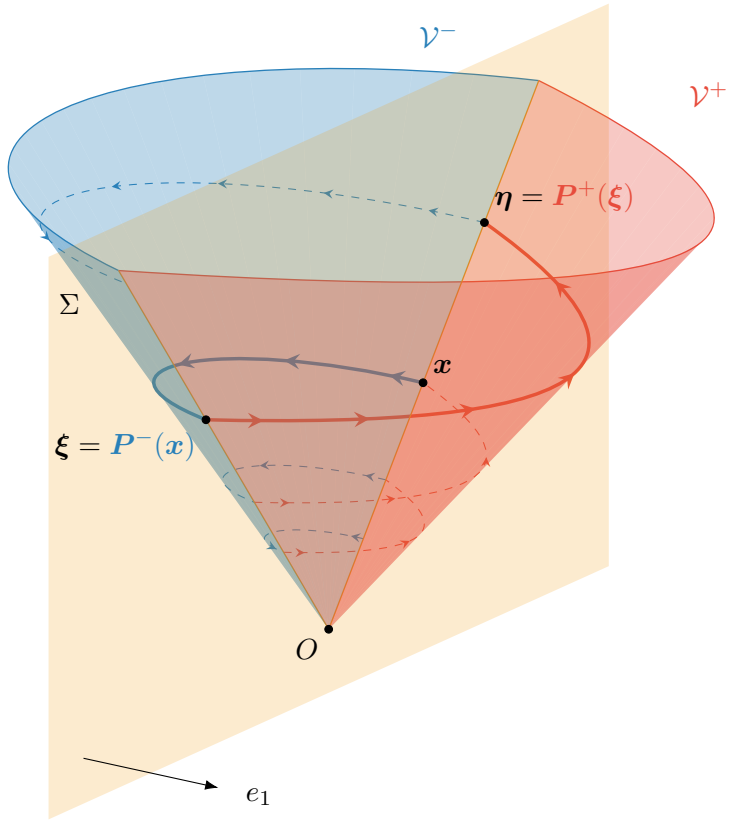

Figure 4.3: A pictorial view of an unstable invariant cone, where the 4D phase space has been reduced to a 3D sketch, for graphical purpose. The hyperplane Σ divides the entire phase space into two subdomains $\mathcal{V}^{\pm}$. The vertex of the invariant cone is the origin of the phase space, which coincides with the analysed equilibrium configuration. The Poincaré map transforms the initial point $\boldsymbol{x}$ to the points $\boldsymbol{\xi} = \boldsymbol{P}^-(\boldsymbol{x})$ and $\boldsymbol{\eta} = \boldsymbol{P}^+(\boldsymbol{P}^-(\boldsymbol{x}))$. The family of orbits belonging to the cone spirals out form the vertex, revealing an unstable equilibrium point.

Furthermore, the two time intervals $t^-(\boldsymbol{x})$ and $t^+(\boldsymbol{\xi}(\boldsymbol{x}))$, nonlinear functions of the initial conditions, fulfil the following conditions

$$t^-(\alpha\boldsymbol{x}) = t^-(\boldsymbol{x}), \qquad t^+(\alpha\boldsymbol{\xi}) = t^+(\boldsymbol{\xi}), \qquad \forall\alpha \in \mathbb{R}, \tag{4.10}$$

as can be seen from the definitions (4.5). These conditions (4.10) are crucial for the analysis of dynamical systems where an invariant cone is present. In fact, when the point $\boldsymbol{\eta} = \mu\boldsymbol{x}$ is considered as a new initial condition in order to observe how the motion of the system evolves after the two initial halfmaps $\boldsymbol{\xi} = \boldsymbol{P}^{-}(\boldsymbol{x})$ and $\boldsymbol{\eta} = \boldsymbol{P}^{+}(\boldsymbol{\xi})$, the new intersection time becomes

$$t^{-}(\boldsymbol{\eta}) = t^{-}(\mu\boldsymbol{x}) = t^{-}(\boldsymbol{x}),$$

and equivalently for the t^{+}. Hence, for the orbits belonging to the invariant cone, the time intervals $t^{\pm}$ are always the same and do not change in the application of further halfmaps. Thus, the property (4.10) also allows the calculation of the coordinates of all the points of the Poincaré map, starting from the initial condition $\boldsymbol{x}^{(0)}$, so that

$$\begin{aligned}
\boldsymbol{x}^{(1)} &= \boldsymbol{\eta}^{(0)} = e^{\boldsymbol{A}^{+}t^{+}} e^{\boldsymbol{A}^{-}t^{-}} \boldsymbol{x}^{(0)}, \\
\boldsymbol{x}^{(2)} &= \boldsymbol{\eta}^{(1)} = e^{\boldsymbol{A}^{+}t^{+}} e^{\boldsymbol{A}^{-}t^{-}} e^{\boldsymbol{A}^{+}t^{+}} e^{\boldsymbol{A}^{-}t^{-}} \boldsymbol{x}^{(0)}, \\
\boldsymbol{x}^{(3)} &= \boldsymbol{\eta}^{(2)} = e^{\boldsymbol{A}^{+}t^{+}} e^{\boldsymbol{A}^{-}t^{-}} e^{\boldsymbol{A}^{+}t^{+}} e^{\boldsymbol{A}^{-}t^{-}} e^{\boldsymbol{A}^{+}t^{+}} e^{\boldsymbol{A}^{-}t^{-}} \boldsymbol{x}^{(0)}, \\
&\dots
\end{aligned}$$

that can clearly be rewritten as

$$\boldsymbol{\eta}^{(k)} = \boldsymbol{x}^{(k+1)} = \mu^{k}\boldsymbol{x}^{(0)}, \tag{4.11}$$

which is an exponential discrete relation. Let's observe that the value of norm of vector $\boldsymbol{\eta}^{(k)}$ increases or decreases, on the basis of the value of the multiplier μ.

It is evident from the considerations presented above on the intersection time intervals that the sum $T = t^{-} + t^{+}$ can be considered as a sort of period for the orbits that belong to an invariant cone, since a trajectory with initial condition $\boldsymbol{x}^{(k)}$ employs exactly a time interval $t^{-} + t^{+}$ to reach the point $\boldsymbol{\eta}^{(k)}$. However, the solution cannot be considered strictly periodic, since after each period the orbit does not return exactly in the same configuration, but the following relation can be written

$$\boldsymbol{y}(kT + \bar{t}) = \mu^{k}\boldsymbol{y}(\bar{t}), \tag{4.12}$$

where $\bar{t}$ is a generic time interval and $\boldsymbol{y}(\bar{t})$ is a generic point belonging to the invariant cone. One must note that (4.12) has the same structure of

condition (4.11), but the former is valid for a generic point lying on the invariant cone.

The geometric interpretation of definition (4.8) is straightforward and it is depicted in Figure 4.3, where a 3D conceptual sketch substitutes the real 4D phase space which is obviously not achievable in a pictorial view. Condition (4.9) imposes that the vectors of initial point $\boldsymbol{x}$ and final point $\boldsymbol{\eta}$ are parallel, lying on the same straight line which passes through the origin and belongs to the switching manifold Σ. The family of orbits that have initial conditions on this straight line, defined by the generalised eigenvector $\boldsymbol{x}$, forms a manifold, which is a 3-dimensional hypercone embedded in a 4-dimensional phase space. The vertex of this cone is at the origin, i.e. at the equilibrium point of the mechanical system. The intersection lines between the invariant cone and the switching manifold Σ are the straight line defined by vectors $\alpha\boldsymbol{x}$ and $\alpha\boldsymbol{\xi}$, $\alpha \in \mathbb{R}$.

According to this geometrical interpretation, the behaviour of a mechanical system can easily be understood in presence of an invariant cone, since the orbits may spiral in or out on the cone, on the basis of the value of μ, evolving towards the vertex or away from it. In particular, the following condition can be determined:

- $\mu > 1$: there exists a family of trajectories, belonging to the invariant cone, that for $t > 0$ spiral out, away from the vertex of the cone, which represents the equilibrium configuration in the phase space. The solution evolves in time far from the fixed point, hence the equilibrium configuration in the origin can be considered *unstable*.

- $\mu < 1$: there exists a family of trajectories, belonging to the invariant cone, that for $t > 0$ spiral in, towards the vertex of the cone. The solution evolves in time approaching the fixed point, hence the orbits belonging to the invariant cone can be considered *stable*. Unfortunately, no condition on the mechanical system can be defined, since other trajectories, different from those on the invariant cone, may be unstable, leading to an unstable mechanical system.

- $\mu = 1$: there exists a family of trajectories, belonging to the invariant cone, which are *periodic*.

For the generic mechanical problem (4.1), the existence of an invariant cone with $\mu > 1$ is a *sufficient condition for instability*, since according to

Definition 8 the presence of a single unstable trajectory is sufficient to consider the whole system unstable. Vice versa, provided that an invariant cone exists, the relation $\mu \leq 1$ is a *necessary condition for stability*.

An important property that must be underlined is that these conditions hold always true, *regardless of the stability behaviour of each single subsystem*. Therefore, an equilibrium configuration of a piecewise-linear mechanical system, which is stable when analysed in each single subsystem that composes the entire structure, can be an unstable fixed point for the entire dynamical system. This kind of structure will be investigated in Chapter 6 and special design parameters will be provided, leading to this unexpected and counterintuitive behaviour.

4.1.3 Physical interpretation of an invariant cone

The unusual unstable behaviour of piecewise-smooth mechanical systems composed of two stable parts can be qualitatively explained from a physical point of view, by the analysis of the mechanical energy of the non-smooth dynamical systems.

Let's consider the linearised equations of motion of the single smooth subsystem (3.23). The stiffness matrix $\boldsymbol{K}$ can be decomposed into the sum of a symmetric and an unsymmetric component,

$$\boldsymbol{K} = \hat{\boldsymbol{K}} + \boldsymbol{G},$$

where $\hat{\boldsymbol{K}}$ collects only the effects of conservative forces (springs and possible dead loads) and $\boldsymbol{G}$ contains only the non-conservative ones (follower force). To be more explicit, for the structure analysed in Chapter 3.2, the stiffness matrix can be decomposed into the following terms

$$\hat{\boldsymbol{K}}^{\pm} = \begin{bmatrix} k_1\left(1 \mp \dfrac{y_s}{R_\pm}\right) + \dfrac{k_2}{R_\pm^2} & \pm\dfrac{k_2}{R_\pm} \\ \pm\dfrac{k_2}{R_\pm} & k_2 \end{bmatrix}, \qquad \boldsymbol{G}^{\pm} = F \begin{bmatrix} \mp\dfrac{1}{R_\pm} & -1 \\ 0 & 0 \end{bmatrix}.$$

For a generic mechanical system, a scalar product of equation (3.23) by $\dot{\boldsymbol{q}}$ and a factorisation of the time derivative lead to the well-known Principle of Conservation of Mechanical Energy, see also [55],

$$\frac{d}{dt}\left(\frac{1}{2}\dot{\boldsymbol{q}} \cdot \boldsymbol{M}\dot{\boldsymbol{q}} + \frac{1}{2}\boldsymbol{q} \cdot \hat{\boldsymbol{K}}\boldsymbol{q}\right) = -\dot{\boldsymbol{q}} \cdot \boldsymbol{G}\boldsymbol{q}, \tag{4.13}$$

where the mechanical energy $\mathcal{H}(t)$ can be introduced, as the sum of the kinetic and total potential energy, i.e.

$$\mathcal{H}(t) = \frac{1}{2}\dot{\boldsymbol{q}} \cdot \boldsymbol{M}\dot{\boldsymbol{q}} + \frac{1}{2}\boldsymbol{q} \cdot \hat{\boldsymbol{K}}\boldsymbol{q}. \tag{4.14}$$

In simple words, the well-known principle of conservation (4.13) states that the variation in time of the mechanical energy is equal to the power of non-conservative forces that act on the system. Expression (4.14) can be rewritten in matrix notation with respect to the phase vector $\boldsymbol{y}(t)$, as

$$\mathcal{H}(t) = \frac{1}{2}\boldsymbol{y}(t) \cdot \boldsymbol{H}\boldsymbol{y}(t), \tag{4.15}$$

introducing the symmetric matrix

$$\boldsymbol{H}^{\pm} = \begin{bmatrix} \hat{\boldsymbol{K}}^{\pm} & \boldsymbol{0} \\ \boldsymbol{0} & \boldsymbol{M} \end{bmatrix}.$$

When only the conservative part $\hat{\boldsymbol{K}}$ of the stiffness matrix is present, in case of a *smooth* mechanical system, the mechanical energy remains constant. On the contrary, when also a non-conservative contribution $\boldsymbol{G}$ can be found, due to the non-conservative loads, the mechanical energy $\mathcal{H}(t)$ varies in time.

The behaviour of the mechanical energy as a function of time, for a specific solution of a smooth system near a *stable* fixed point, can be studied substituting the solution $\boldsymbol{y}(t)$ in terms of the matrix exponential (3.38), which is written for a stable system. Since the elements of the matrix exponential (3.38) are trigonometric functions of time, the mechanical energy is a sum of trigonometric functions, which is generally not periodic, but certainly, it is bounded. Therefore, near a *stable* equilibrium configuration of a smooth dynamical system, the mechanical energy may vary in time if non-conservative forces are present, however the function $\mathcal{H}(t)$ is bounded, revealing a limited growth of the mechanical energy.

On the contrary, something very different may happen for a non-smooth dynamical system: although the energy is bounded for each smooth subsystem forming the entire structure, the switching between these subsystems may be designed in such a way only the intervals in

which the mechanical energy increases are combined. This particular design leads to a global unbounded growth of the energy and the instability of the considered equilibrium configuration.

The mechanical energy at time $t = 0$, for initial conditions $\boldsymbol{y}_0$, can be computed as

$$\mathcal{H}_0 = \mathcal{H}(0) = \frac{1}{2}\boldsymbol{y}_0 \cdot \boldsymbol{H}\boldsymbol{y}_0,$$

where $\boldsymbol{H}$ can be identified with either $\boldsymbol{H}^-$ or $\boldsymbol{H}^+$, since the energy is continuous when a switch in the subsystem is present. Since the solution of a generic piecewise-linear system is represented by expression (4.2), the mechanical energy can be written as a function of time,

$$\mathcal{H}(t) = \begin{cases} \frac{1}{2}e^{\boldsymbol{A}^-(t-t_0)}\boldsymbol{y}_0 \cdot \boldsymbol{H}^- e^{\boldsymbol{A}^-(t-t_0)}\boldsymbol{y}_0, & t_0 < t \leq t_1 \\ \frac{1}{2}e^{\boldsymbol{A}^+(t-t_1)}e^{\boldsymbol{A}^-(t_1-t_0)}\boldsymbol{y}_0 \cdot \boldsymbol{H}^+ e^{\boldsymbol{A}^+(t-t_1)}e^{\boldsymbol{A}^-(t_1-t_0)}\boldsymbol{y}_0, & t_1 < t \leq t_2 \\ \dots & \dots \\ \frac{1}{2}e^{\boldsymbol{A}^-(t-t_k)}\dots\boldsymbol{y}_0 \cdot \boldsymbol{H}^- e^{\boldsymbol{A}^-(t-t_k)}\dots\boldsymbol{y}_0, & t_k < t \leq t_{k+1} \\ \dots & \dots \end{cases} \tag{4.16}$$

where the sequence $\{t_1, t_2, \dots, t_k, t_{k+1}, \dots\}$ represents the intersection times between the considered trajectory and the switching manifold.

Assuming that an invariant cone exists, so that the condition $\boldsymbol{\eta} = \mu\boldsymbol{x}$ holds, the mechanical energy (4.16) for a solution belonging to the invariant cone can be written as

$$\begin{aligned} \mathcal{H}(0) &= \frac{1}{2}\boldsymbol{x} \cdot \boldsymbol{H}\boldsymbol{x}, \\ \mathcal{H}(t^-) &= \frac{1}{2}e^{\boldsymbol{A}^-t^-}\boldsymbol{x} \cdot \boldsymbol{H}e^{\boldsymbol{A}^-t^-}\boldsymbol{x}, \\ \mathcal{H}(t^- + t^+) &= \frac{1}{2}e^{\boldsymbol{A}^+t^+}e^{\boldsymbol{A}^-t^-}\boldsymbol{x} \cdot \boldsymbol{H}e^{\boldsymbol{A}^+t^+}e^{\boldsymbol{A}^-t^-}\boldsymbol{x}, \\ \mathcal{H}(2t^- + t^+) &= \frac{1}{2}e^{\boldsymbol{A}^-t^-}e^{\boldsymbol{A}^+t^+}e^{\boldsymbol{A}^-t^-}\boldsymbol{x} \cdot \boldsymbol{H}e^{\boldsymbol{A}^-t^-}e^{\boldsymbol{A}^+t^+}e^{\boldsymbol{A}^-t^-}\boldsymbol{x}, \\ &\dots \end{aligned}$$

hence the mechanical energy after an integer number of periods $k(t^- + t^+)$,

$k \in \mathbb{N}$, can be computed as

$$\mathcal{H}(k(t^- + t^+)) = \frac{1}{2}\mu^{2k}\boldsymbol{x} \cdot \boldsymbol{H}\boldsymbol{x} = \mu^{2k}\mathcal{H}_0.$$

Therefore, when an unstable invariant cone is detected with a multiplier $\mu > 1$, the mechanical energy suffers an unbounded exponential growth in time, revealing the instability of the system.

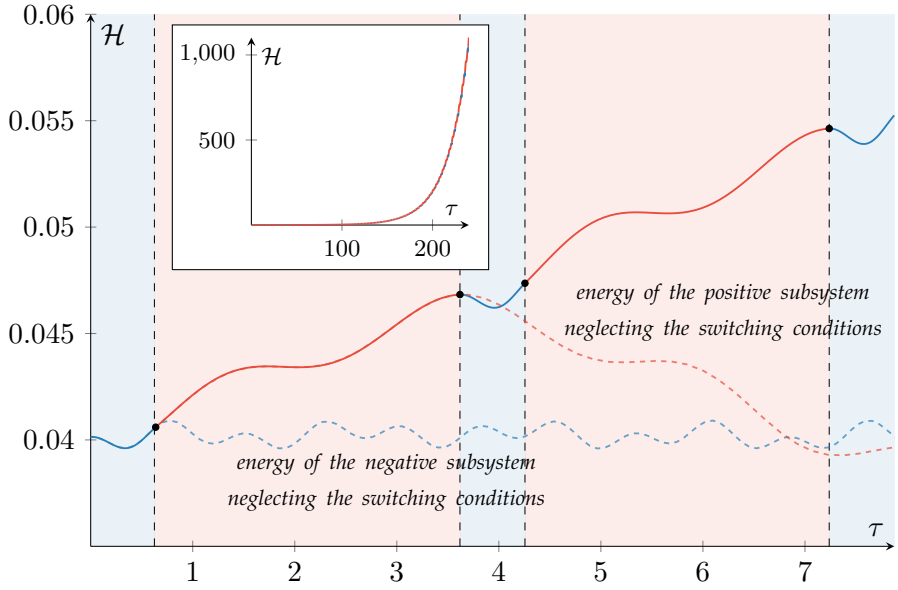

Figure 4.4: Plot of the mechanical energy $\mathcal{H}$ as a function of the non-dimensional time τ (which plays the same role of the time t used in the derivation of formula (4.15)), according to the numerical example treated in Section 6.1.1. The dashed lines represent the evolution of the mechanical energy of the single subsystem, neglecting the switching condition, and they show a bounded behaviour that comes from the stability of each subsystem. On the contrary, the behaviour of the mechanical energy of the entire piecewise-smooth systems, plotted for five time intervals, reveals a growth due to the switching between the subsystems. The exponential growth of the mechanical energy is clearly visible in the detail, revealing a *flutter-like* instability of the combined piecewise system.

This exponential growth is analogous to what happens in smooth dynamical systems subject to follower forces, so the analysed behaviour can be seen as a *flutter-like* instability of a piecewise-linear mechanical system.

Two are the principal outcomes of the analysis performed in this Section 4.1.3 concerning the analysis of the mechanical energy. The first is a qualitative explanation of the physical reason why this kind of piecewise system reveals this particular instability behaviour, i.e. the presence of an unbounded growth of the energy of the complete structure, despite being bounded in each subsystem. The second is the fact that this unstable behaviour may be reached when the mechanical energy of each subsystem is bounded, but only if it oscillates in time inside the considered time interval related to $(-)$ or $(+)$ subdomain. Hence, the presence of a non-conservative source as the follower force is necessary to have this kind of instability that originates from two stable subsystems.

4.2 Analysis of switching conditions

The results obtained in the previous Section 4.1.3 have a hidden hypothesis that will be investigated in depth in this paragraph, namely the fact that the orbits are assumed to intersect the switching manifold and to cross the hypersurface Σ, leaving a subdomain and entering in the other one.

According to the theory of piecewise-smooth dynamical systems presented in Section 2.2.3, two possible scenarios can actually be present for these specific systems: crossing or sliding conditions.

A generic point of the switching manifold Σ is a *crossing point* when the orbit passing through this point crosses the discontinuity surface in a well-defined direction, from $(-)$ to $(+)$ system, or vice versa. Moreover, a continuity condition must also be fulfilled in case of crossing, i.e. the limit points of the trajectories that approach the switching manifold, from $(-)$ and $(+)$ systems, must coincide. As reported at the end of Section 2.2.3, the direction in which the orbit crosses Σ is defined by the orbital velocities calculated in the crossing point, both for $(-)$ and $(+)$ subsystems. Hence, when the projections of these orbital velocities onto the unit normal vector of the switching manifold have the same sign, a crossing point is present. On the contrary, a point of the switching manifold Σ is a *sliding point* when the aforementioned orbital velocities have opposite sign, hence

the solution "slides" on the discontinuity hypersurface Σ.

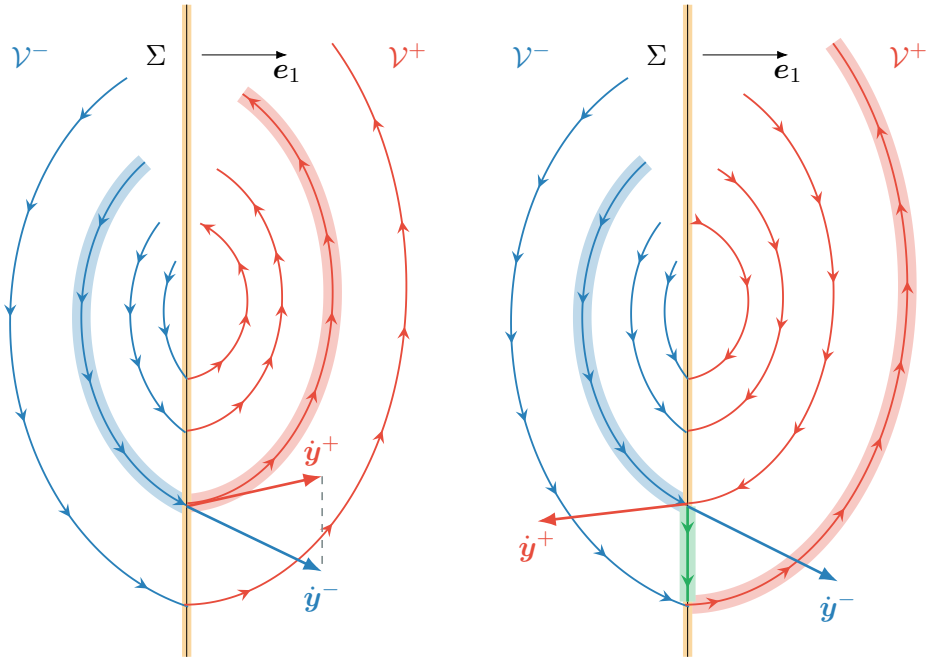

(a) *crossing* **(b)** *sliding*

Figure 4.5: A 2D pictorial view, showing the behaviour of a mechanical system in presence of sliding and crossing conditions, when an orbit approaches the switching manifold Σ, which divides in two subdomains $\mathcal{V}^{\pm}$ the entire phase space. In case of *crossing*, the considered orbit leaves one of the two subsystems and enters in the other, since the orbital velocity, calculated in the crossing point for the two separated system, determine a well-defined direction of the motion. On the contrary, when *sliding* is considered, the orbit can be "trapped" on the switching manifold, since the aforementioned orbital velocities have opposite directions, hence the motion evolves on the plane Σ (green orbit).

In a generic point $\boldsymbol{x} \in \Sigma$, belonging to the switching manifold, the orbital velocity is defined as the first derivative in time of the solution $\boldsymbol{y}(t)$ calculated in the considered point, namely $\dot{\boldsymbol{x}}$. By definition, the orbital velocity coincides with the vector field of equation (4.1) computed in the

given configuration, namely $\dot{\boldsymbol{x}} = \boldsymbol{A}^{\pm}\boldsymbol{x}$. Therefore, the projection of the orbital velocity onto the unit normal vector $\boldsymbol{e}_1$ of the switching manifold can be computed as

$$\dot{\boldsymbol{x}} \cdot \boldsymbol{e}_1 = \boldsymbol{A}^{\pm}\boldsymbol{x} \cdot \boldsymbol{e}_1 = \boldsymbol{x} \cdot \left(\boldsymbol{A}^{\pm}\right)^{\mathrm{T}} \boldsymbol{e}_1 = \boldsymbol{x} \cdot \boldsymbol{e}_3 = x_3,$$

where the property $\left(\boldsymbol{A}^{\pm}\right)^{\mathrm{T}} \boldsymbol{e}_1 = \boldsymbol{e}_3$ comes from the particular structure of the Jacobian matrix $\boldsymbol{A}^{\pm}$, which represents a *mechanical* system.

The fact that the discontinuity is orthogonal to the y_1-axis makes this calculation trivial since it simply confirms that, in the 4-dimensional Hamiltonian formulation of equations of motion, the third component of the phase vector is actually the first derivative of the first component, namely $\dot{x}_1 = x_3$.

Since the orbital velocity is continuous in the first component, i.e. $\dot{x}_1^- = \dot{x}_1^+ = \dot{x}_1$, all the points $\boldsymbol{x}$ of the switching manifold with a non-vanishing third component, $x_3 \neq 0$, are *crossing points*.

As a remark, the same condition exposed above holds true for the second component of the orbital velocity, i.e. $\dot{x}_2 = x_4$, so the continuity is actually assured for the first and second component of the velocity vector. In the literature concerning piecewise-smooth dynamical systems, see [14, 16, 46, 52], a further restriction is often assumed for the matrix $\boldsymbol{A}^{\pm}$, i.e. for a discontinuity in the y_k-axis, the difference between $\boldsymbol{A}^-$ and $\boldsymbol{A}^+$ must be only in the k-th column, while all the other columns must coincide. This continuity hypothesis can actually be written as $\boldsymbol{A}^+ - \boldsymbol{A}^- = (\boldsymbol{A}^+ - \boldsymbol{A}^-)\boldsymbol{e}_1\boldsymbol{e}_i^{\mathrm{T}}$. This assumption leads to orbital velocities that are continuous in all their components, however it is generally violated for mechanical systems (e.g. the structure analysed in Section 3.1.1 clearly does not fulfils this property). [4] In fact, the orbital velocity for the

[4] The condition $\boldsymbol{A}^+ - \boldsymbol{A}^- = (\boldsymbol{A}^+ - \boldsymbol{A}^-)\boldsymbol{e}_1\boldsymbol{e}_i^{\mathrm{T}}$ concerning the continuity of the vector field leads to the classification of the mechanical system as a *non-smooth continuous system*, as reported in Section 2.2.2. This kind of systems is generally simpler to deal with, hence this simplification is often assumed by many authors, see [14, 16, 46, 52]. However, since this condition is not generally fulfilled, the mechanical systems under analysis must be classified as *Filippov's systems*.

2 d.o.f. mechanical system described in this Thesis can be written as

$$\dot{\boldsymbol{x}} = \boldsymbol{A}^{\pm}\boldsymbol{x} = \begin{bmatrix} 0 & 0 & 1 & 0 \\ 0 & 0 & 0 & 1 \\ \Gamma_{11}^{\pm} & \Gamma_{12}^{\pm} & 0 & 0 \\ \Gamma_{21}^{\pm} & \Gamma_{22}^{\pm} & 0 & 0 \end{bmatrix} \begin{bmatrix} 0 \\ x_2 \\ x_3 \\ x_4 \end{bmatrix} = \begin{bmatrix} x_3 \\ x_4 \\ \Gamma_{12}^{\pm} x_2 \\ \Gamma_{22}^{\pm} x_2 \end{bmatrix},$$

hence the orbital velocity would be continuous in all the components, if $\boldsymbol{A}^{-}$ and $\boldsymbol{A}^{+}$ differed only in the first column, namely $\Gamma_{12}^{-} = \Gamma_{12}^{+}$ and $\Gamma_{22}^{-} = \Gamma_{22}^{+}$. In the investigated mechanical systems, from a physical point of view, the discontinuity in the orbital velocity appears in those terms that can be interpreted as accelerations.

In case of a vanishing third component of the vector $\boldsymbol{x}$, namely $x_3 = 0$, the behaviour of the system is not well-defined. In the context of Filippov's theory of non-smooth dynamical systems, it is considered a critical case, for which no prediction can be done on the behaviour of the mechanical system, yielding to a sort of indeterminate situation, see [32]. Moreover, also the Poincaré map in (4.3) and (4.9) is not well-defined, since a correct description of the evolution of the dynamical system can be obtained only when the orbits are not tangent to the Poincaré section, a condition which is not fulfilled in the case of a vanishing third component.

If all the components of the orbital velocity were continuous in these specific undetermined points, then some results for these critical states could be inferred, considering for example the acceleration term $\dot{x}_3$. Unfortunately, this condition is not fulfilled for the mechanical system under analysis, since $\dot{x}_3 = \Gamma_{12}^{\pm} x_2$ is not continuous on the switching manifold. Moreover, these critical cases cannot be considered actual sliding conditions, since, according to Filippov [32], the behaviour in case of sliding is described by equation (2.15), which can be written in this specific case as

$$\dot{\boldsymbol{y}}(t) = \frac{\left(\boldsymbol{e}_1 \cdot \boldsymbol{A}^{-}\boldsymbol{y}(t)\right)\boldsymbol{A}^{+} - \left(\boldsymbol{e}_1 \cdot \boldsymbol{A}^{+}\boldsymbol{y}(t)\right)\boldsymbol{A}^{-}}{\boldsymbol{e}_1 \cdot \left(\boldsymbol{A}^{-} - \boldsymbol{A}^{+}\right)\boldsymbol{y}(t)}\boldsymbol{y}(t), \tag{4.17}$$

but this relation cannot be considered valid, due to the vanishing denominator for $\boldsymbol{y} \in \Sigma$. In [53], during the classification of special 2D Filippov systems from a mathematical perspective, these specific critical cases are called *singular sliding points*. Therefore, they can actually be considered sliding point, nevertheless this definition is not helpful for the concrete

analysis of points with $x_3 = 0$, since the equation (4.17) describing th sliding points is not representative of the problem, as exposed above.

However, one must note that these critical cases originate from a set of initial conditions in the form $\boldsymbol{x} = [0, x_2, 0, x_4]$, for all $x_2, x_4 \in \mathbb{R}$, which is a set of zero measure in the 4-dimensional phase space. Hence, the mathematical model adopted in this Thesis can be considered valid for the interpretation of a mechanical system, despite the presence of a limited set of points in which the solution of the mathematical model is not unique and consequently, predictions on the mechanical behaviour cannot be performed. Therefore, these critical initial conditions are simply neglected and when the presence of an invariant cone is detected, with a vanishing third component in the starting, intermediate or ending point of the Poincaré map, namely $x_3 = 0$, $\xi_3 = 0$, or $\eta_3 = 0$, the cone is simply considered not valid.

The previous demonstration that *almost all* points of the switching manifold reveal a crossing behaviour is crucial, since it is the basis of the mathematical description of the analysed mechanical system, for example in equations (4.3) or (4.9). For the sake of simplicity, the presence of singular sliding have been neglected from the beginning of this analysis, however, it has been proved that this assumption can be considered correct. The existence of only crossing condition also implies that, from a practical point of view, in the numerical computations, the points having $y_1 = 0$ in (4.1) can be assigned both to $(-)$ and $(+)$ subsystem, since the crossing behaviour is well-defined.

Finally, in equation (4.9) defining the condition for the existence of an invariant cone, the application of a negative and positive Poicaré halfmap has been performed *a priori*, to obtain the complete Poincaré map. However, this application can be considered valid if and only the orbital velocity computed in the points $\boldsymbol{x}$, $\boldsymbol{\xi}$, and $\boldsymbol{\eta}$ has a compatible direction with the Poincaré map. Some "feasibility conditions" must be introduced and checked *a posteriori*, to be sure that the defined Poincaré map actually links points that are consistent.

Since the crossing direction is given by the projection onto $\boldsymbol{e}_1$ of the orbital velocity, the following conditions must be fulfilled

$$\begin{aligned} &\dot{x}_1\dot{\xi}_1 = x_3\xi_3 < 0, \quad (\text{or} \quad \dot{\xi}_1\dot{\eta}_1 = \xi_3\eta_3 < 0), \\ &\dot{x}_1\dot{\eta}_1 = x_3\eta_3 > 0, \end{aligned} \tag{4.18}$$

in order to guarantee that the Poincaré map is feasible (the first formula) and that the considered orbit will continue on the invariant cone after the first complete cycle (the second formula). assuming that an invariant cone is present, the relation $\boldsymbol{\eta} = \mu \boldsymbol{x}$ holds from equation (4.9), thus the first condition can be rewritten as

$$x_3 \eta_3 = \mu x_3^2 > 0,$$

which is fulfilled if $\mu > 0$. This is the physical reason behind the choice of a positive multiplier μ in (4.9), together with the geometrical reason concerning the desired shape of the invariant manifold.

4.3 Mathematical properties and attractivity of the invariant cone

4.3.1 The importance of the attractivity

The existence of an invariant cone in the phase space of a dynamical system described by (4.1) is crucial for the definition of an unstable behaviour of the piecewise structure, composed of separately stable subsystems. In fact, according to Liapunov's definition of stability, a single orbit revealing an unstable behaviour of the equilibrium configuration is sufficient for the identification of the fixed point as unstable.

From a physical point of view, the instability definition given by Liapunov is not sufficient to observe an unstable evolution of motion in a practical experiment, because in the real world and in particular in the experimental tests, the uncertainty on the measures plays a fundamental role. In fact, if the set of possible initial conditions that predict an unstable behaviour has zero measure, with respect to the entire set in which it is possible to choose the initial conditions, clearly, the unstable behaviour cannot be reached, from an experimental point of view.

Thus, from an engineering perspective, the existence of an invariant cone is crucial, but it is not enough, since another important feature of the cone is required: the attractivity. If the invariant set is attractive, then also the orbits with initial conditions in the neighbourhood of the cone approach it. Hence, there exists a *region* in the phases space, whose measure

is not zero, in which the initial conditions can be chosen to obtain unstable solutions.

4.3.2 Analysis of a perturbed solution on the invariant cone

Let's suppose that $\{\tilde{\mu}, \tilde{\boldsymbol{x}}\}$ represents a special solution of the nonlinear eigenvalue problem (4.9), so that the following condition is fulfilled

$$e^{\boldsymbol{A}^+ t^+(\tilde{\boldsymbol{x}})} e^{\boldsymbol{A}^- t^-(\tilde{\boldsymbol{x}})} \tilde{\boldsymbol{x}} = \tilde{\mu} \tilde{\boldsymbol{x}}. \tag{4.19}$$

The invariant cone is described by the starting points $\tilde{\boldsymbol{x}}$ and the intermediate and ending points

$$\tilde{\boldsymbol{\xi}} = e^{\boldsymbol{A}^- t^-(\tilde{\boldsymbol{x}})} \tilde{\boldsymbol{x}}, \qquad \tilde{\boldsymbol{\eta}} = e^{\boldsymbol{A}^+ t^+(\tilde{\boldsymbol{x}})} \tilde{\boldsymbol{\xi}}, \tag{4.20}$$

that are located on the Poincaré section Σ, which coincides with the switching manifold.

In Section 2.2.6 and 2.2.7, the analysis of perturbed solutions in the neighbourhood of a reference fundamental one has been pointed out and described in detail for a generic dynamical system of the form $\dot{\boldsymbol{y}} = \boldsymbol{f}(\boldsymbol{y})$. These concepts are now applied to the specific case of a 2 d.o.f. mechanical system described by the discontinuous ODEs (4.1).

First of all, when an invariant cone is detected in the phase portrait of a mechanical system, two constant intersection times $t^-(\tilde{\boldsymbol{x}})$ and $t^+(\tilde{\boldsymbol{x}}) = t^+(\tilde{\boldsymbol{\xi}}(\tilde{\boldsymbol{x}}))$ can be defined, as functions of the initial point $\tilde{\boldsymbol{x}}$ of the invariant cone. In particular, as exposed in Section 4.1.2, a sort of period $T = t^- + t^+$ can be introduced, since after each time interval T the solution reveals a sort of "scaled periodic behaviour" due to the constant scale factor, see relation (4.12).

Two possible strategies have been outlined in Section 2.2.6 and 2.2.7 for the analysis of a perturbed solution: the first considers the continuous-time orbits and introduces the *monodromy matrix* for the analysis of perturbations; the second regards the discrete-time Poincaré map and the linearised perturbations of the points on the section Σ, described by the *Jacobian of the Poincaré map*.

Monodromy matrix As for the first strategy, due to the similarity of the reference solution to a periodic orbit, a monodromy matrix $\boldsymbol{\Phi}_T$ can be introduced for the description of the evolution of the perturbations at each

time kT, for all $k \in \mathbb{Z}$, i.e.

$$\delta \boldsymbol{y}(kT) = \delta \boldsymbol{y}(k(t^- + t^+)) = \boldsymbol{\Phi}_T^k \delta \boldsymbol{y}_0,$$

where the vector $\delta \boldsymbol{y}_0$ is the perturbation of the initial conditions. Let's observe that, due to the underlined periodicity, the monodromy matrix appears in the previous expression with an exponent equal to k. Therefore, although the reference solution is not exactly periodic, its attractivity is governed by the Floquet multipliers of the monodromy matrix. If all the eigenvalues have a modulus lower than 1, then a perturbed trajectory approaches the reference orbit and it can be considered attractive. Moreover, if the reference orbit belongs to the family of solutions described by the invariant cone, then the definition of attractivity can clearly be extended to the invariant set.

For piecewise-linear dynamical systems (4.1), the monodromy matrix can be calculated as

$$\boldsymbol{\Phi}_T = \boldsymbol{S}^+ e^{\boldsymbol{A}^+ t^+(\tilde{\boldsymbol{x}})} \boldsymbol{S}^- e^{\boldsymbol{A}^- t^-(\tilde{\boldsymbol{x}})}, \tag{4.21}$$

where the *saltation matrices* $\boldsymbol{S}^\pm$ have been introduced, see Section 2.2.6, to correctly describe the perturbations when the reference orbit crosses the switching manifold Σ. These saltation matrices are computed according to formulas (2.29) and (2.30). In particular, for the computation of $\boldsymbol{S}^-$, the values of the vector fields at the switching point are

$$\boldsymbol{f}_p^- = \boldsymbol{A}^- \tilde{\boldsymbol{\xi}}, \qquad \boldsymbol{f}_p^+ = \boldsymbol{A}^+ \tilde{\boldsymbol{\xi}},$$

and for $\boldsymbol{S}^+$

$$\boldsymbol{f}_p^- = \boldsymbol{A}^- \tilde{\boldsymbol{\eta}}, \qquad \boldsymbol{f}_p^+ = \boldsymbol{A}^+ \tilde{\boldsymbol{\eta}},$$

while the normal to the switching manifold is simply the 4-dimensional unit vector $\boldsymbol{n} = \boldsymbol{e}_1$. Due to the structure of the Jacobian matrix $\boldsymbol{A}^\pm$, the denominator in expression (2.29) for the saltation matrix $\boldsymbol{S}^-$ is equal to the third component of the point $\tilde{\boldsymbol{\xi}}$, so that

$$\boldsymbol{e}_1 \cdot \boldsymbol{A}^- \tilde{\boldsymbol{\xi}} = \boldsymbol{e}_1 \cdot \boldsymbol{A}^+ \tilde{\boldsymbol{\xi}} = (\boldsymbol{A}^\pm)^{\mathrm{T}} \boldsymbol{e}_1 \cdot \tilde{\boldsymbol{\xi}} = \boldsymbol{e}_3 \cdot \tilde{\boldsymbol{\xi}} = \tilde{\xi}_3,$$

and an analogous relation can be found for $\boldsymbol{S}^+$,. whose denominator is equal to $\tilde{\eta}_3$. Therefore, in the considered 2 d.o.f. mechanical system, the saltation matrices are

$$\boldsymbol{S}^- = \boldsymbol{I} + \frac{1}{\tilde{\xi}_3}(\boldsymbol{A}^+ - \boldsymbol{A}^-)(\tilde{\boldsymbol{\xi}} \otimes \boldsymbol{e}_1), \quad \boldsymbol{S}^+ = \boldsymbol{I} + \frac{1}{\tilde{\eta}_3}(\boldsymbol{A}^- - \boldsymbol{A}^+)(\tilde{\boldsymbol{\eta}} \otimes \boldsymbol{e}_1),$$

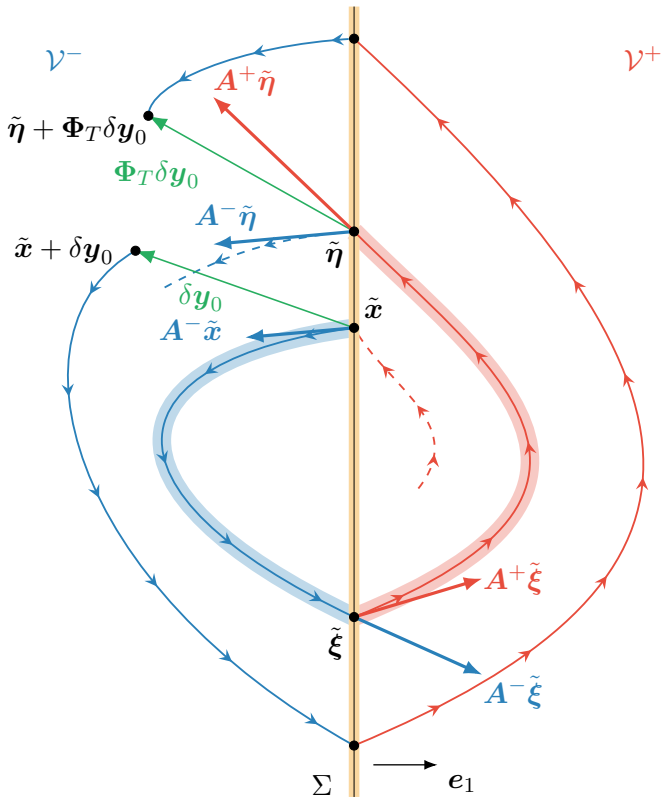

Figure 4.6: Pictorial representation of a reference solution belonging to a given invariant cone (represented by a blue/red thicker line, passing through the initial $\tilde{x}$, intermediate $\tilde{\xi}$, and final $\tilde{\eta}$ points) and a perturbed one, obtained by a small perturbation δy_0 of the initial conditions (the 4D space has been reduced to a 2D sketch for graphical purpose). This picture conceptually describes the presence of an invariant cone for 2 d.o.f. mechanical systems, the orbital velocities at the switching points, and the fundamental role of the monodromy matrix in the description of the perturbed solution.

where $\boldsymbol{I}$ is the 4×4 identity matrix and the symbol '$\otimes$' has been introduced to define the operation $(\boldsymbol{a}\otimes\boldsymbol{b})_{ij} = a_i b_j$, where $\boldsymbol{a}$ and $\boldsymbol{b}$ are two given vectors. The use of the tensor product '$\otimes$' could be considered an abuse of notation, since $\boldsymbol{S}^{\pm}$ have not been considered tensors but only matrices, in the analysis presented this Thesis. However, the compact notation and the easy computational properties of the dyadic product are useful to treat the elements of the monodromy matrix and to derive some mathematical outcomes.

Let's finally observe that the saltation matrices $\boldsymbol{S}^{\pm}$ depend on the values $\tilde{\boldsymbol{\xi}}$ and $\tilde{\boldsymbol{\eta}}$, so they depend on the reference solution, which belongs to the invariant cone.

This strategy, involving the definition of a monodromy matrix, will be used to analyse the attractivity of invariant cones, since it leads to simpler calculations and non-singular matrices.

Jacobian of the Poincaré map The second strategy for the determination of the attractivity of an invariant cone deals with the calculation of the eigenvalues of the Jacobian matrix of the Poincaré map. Since this analysis is more difficult with respect to the first strategy presented above, only a brief exposition of this technique will be shown below, to complete the set of possible approaches in the analysis of this kind of problem.

As reported in Section 2.2.7, the Jacobian matrix of the Poincaré map must be calculated in the local reference frame attached to the switching manifold, to avoid the presence of a vanishing eigenvalue (denoting a singular Jacobian matrix). However, an initial calculation in the global reference frame of the phase space is more convenient and a following coordinate transformation can be performed to obtain the matrix in the local reference frame.

Let's consider a reference solution described by the Poincaré map with initial condition $\tilde{\boldsymbol{x}}$. If a small perturbation $\delta\boldsymbol{x}$ in the initial conditions is applied, the perturbation of the Poincaré map can be written as

$$\delta\boldsymbol{\eta} = \frac{\partial\boldsymbol{P}}{\partial\boldsymbol{x}}(\tilde{\boldsymbol{x}})\delta\boldsymbol{x},$$

where the Jacobian matrix $\partial\boldsymbol{P}/\partial\boldsymbol{x}$ can be calculated applying the chain

rule to expression (4.3), so that

$$\frac{\partial \boldsymbol{P}}{\partial \boldsymbol{x}}(\tilde{\boldsymbol{x}}) = \frac{\partial \boldsymbol{P}^{+}}{\partial \boldsymbol{\xi}}(\tilde{\boldsymbol{\xi}}(\tilde{\boldsymbol{x}}))\frac{\partial \boldsymbol{P}^{-}}{\partial \boldsymbol{x}}(\tilde{\boldsymbol{x}}),$$

where the single Jacobian matrices of the Poincaré halfmaps can be computed from the definitions (4.4) as

$$\begin{aligned}\frac{\partial \boldsymbol{P}^{+}}{\partial \boldsymbol{\xi}}(\boldsymbol{\xi}) &= e^{\boldsymbol{A}^{+}t(\boldsymbol{\xi})}\left[\boldsymbol{I} + \boldsymbol{A}^{+}\frac{\partial t}{\partial \boldsymbol{\xi}}(\boldsymbol{\xi})\right], \\ \frac{\partial \boldsymbol{P}^{-}}{\partial \boldsymbol{x}}(\boldsymbol{x}) &= e^{\boldsymbol{A}^{-}t(\boldsymbol{x})}\left[\boldsymbol{I} + \boldsymbol{A}^{-}\frac{\partial t}{\partial \boldsymbol{x}}(\boldsymbol{x})\right].\end{aligned} \tag{4.22}$$

Let's observe that the Poincaré map transforms the continuous-time dynamic problem to a discrete-time one, so that the time-independent variable becomes a function of the points of the map. Therefore, the Jacobian matrices are nonlinear functions of the coordinates of the points and this dependency must be considered in the differentiation of the map.

The use of the Implicit Function Theorem on the time functions $t(\boldsymbol{x})$ and $t(\boldsymbol{\xi})$, defined in expression (4.5), leads to the following form of the Jacobian matrix (4.22)

$$\frac{\partial \boldsymbol{P}}{\partial \boldsymbol{x}}(\tilde{\boldsymbol{x}}) = \boldsymbol{D}^{+}e^{\boldsymbol{A}^{+}t^{+}(\tilde{\boldsymbol{x}})}\boldsymbol{D}^{-}e^{\boldsymbol{A}^{-}t^{-}(\tilde{\boldsymbol{x}})},$$

where the matrices

$$\boldsymbol{D}^{-} = \boldsymbol{I} - \frac{1}{\tilde{\eta}_3}\boldsymbol{A}^{+}(\tilde{\boldsymbol{\eta}} \otimes \boldsymbol{e}_1), \qquad \boldsymbol{D}^{+} = \boldsymbol{I} - \frac{1}{\tilde{\xi}_3}\boldsymbol{A}^{-}(\tilde{\boldsymbol{\xi}} \otimes \boldsymbol{e}_1),$$

have been introduced.

This 4-dimensional Jacobian matrix is singular, since the Poincaré map is actually defined on an 3-dimensional hypersurface embedded in the phase space. To avoid this singularity, a local reference system must be introduced, whose components are denoted by the superimposed '$\widehat{\ }$'. As figured out in Section 2.2.7, the passage from the global to the local reference frame for the Poincaré map can be performed introducing the matrix $\boldsymbol{V}$, which in this case is equal to

$$\boldsymbol{V}^{\mathrm{T}} = \begin{bmatrix} 0 & 1 & 0 & 0 \\ 0 & 0 & 1 & 0 \\ 0 & 0 & 0 & 1 \end{bmatrix},$$

hence the final Jacobian matrix of the Poincaré map can be computed as

$$\frac{\partial \boldsymbol{P}}{\partial \hat{\boldsymbol{x}}}(\hat{\tilde{\boldsymbol{x}}}) = \boldsymbol{V}^{\mathrm{T}}\boldsymbol{D}^{+}e^{\boldsymbol{A}^{+}t^{+}}\boldsymbol{D}^{-}e^{\boldsymbol{A}^{-}t^{-}}\boldsymbol{V}(\boldsymbol{V}^{\mathrm{T}}\boldsymbol{V})^{-1}. \tag{4.23}$$

Let's observe that in the case under analysis, the calculation of (4.23) is equivalent to extract from $\frac{\partial \boldsymbol{P}}{\partial \boldsymbol{x}}(\tilde{\boldsymbol{x}})$ the submatrix obtained deleting the first row and column.

Due to the periodicity of the solution described above, the perturbations of the Poincaré map after k complete cycles are

$$\delta\hat{\boldsymbol{\eta}}_k = \left(\frac{\partial \boldsymbol{P}}{\partial \hat{\boldsymbol{x}}}(\hat{\tilde{\boldsymbol{x}}})\right)^{k} \delta\hat{\boldsymbol{x}}_0,$$

which is analogous to expression (4.21), revealing the close link between the monodromy matrix and the Jacobian of the Poincaré map.

One must note that the matrices $\boldsymbol{S}^{\pm}$ and $\boldsymbol{D}^{\pm}$ are very similar but not identical, because they describe the evolution of perturbations having different nature. In fact, in the first approach, the perturbation $\delta\boldsymbol{y}_0$ of the initial conditions can be a generic (sufficiently small) vector of the 4-dimensional phase space and the final perturbation after each period, described by the monodromy matrix, is still a generic vector, as can be seen in Figure 4.6. On the contrary, the Poincaré map is defined onto a specific cross-section, hence also the initial and the final perturbations (described by the Jacobian of the Poincaré map) are assumed to belong to the given Poincaré section, as depicted in Figure 2.12 of Section 2.2.7.

4.3.3 Mathematical properties of the invariant cone

In this Section, some theoretical results on the analysis of 2 d.o.f. piecewise mechanical systems will be exposed and demonstrated. Provided that an invariant cone exists in the phase portrait, the outcomes shown below are fundamental tools for the determination of the geometry and attractivity of the considered invariant set. Furthermore, these are new important results that allow a complete description of this 2 d.o.f. mechanical problem.

Let's suppose that an invariant cone has been detected for the considered mechanical system, i.e. there exists a solution $\{\tilde{\mu}, \tilde{\boldsymbol{x}}\}$ of the generalised nonlinear eigenvalue problem (4.9) that fulfils the condition (4.19),

for the sake of simplicity rewritten below

$$e^{\boldsymbol{A}^+ t^+(\tilde{\boldsymbol{x}})} e^{\boldsymbol{A}^- t^-(\tilde{\boldsymbol{x}})} \tilde{\boldsymbol{x}} = \tilde{\mu} \tilde{\boldsymbol{x}}.$$

One must note that an invariant cone is well described only when $\tilde{\boldsymbol{x}}$ is a real vector (the phases are real variables) and $\tilde{\mu}$ is a real number. However, other complex eigenvalues and eigenvectors of the problem (4.19) may exist, that do not represent any physical solution.

In order to simplify the proofs of the following propositions, let's now introduce the matrix

$$\boldsymbol{J} = \begin{bmatrix} \boldsymbol{I}_2 & \boldsymbol{0} \\ \boldsymbol{0} & -\boldsymbol{I}_2 \end{bmatrix},$$

where $\boldsymbol{I}_2$ is the 2×2 identity matrix. When $\boldsymbol{J}$ is applied to a 4-dimensional vector, the sign of the two last components of the vector is changed. Furthermore, the matrix $\boldsymbol{J}$ fulfils the property $\boldsymbol{J}\boldsymbol{J} = \boldsymbol{I}$, where $\boldsymbol{I}$ is the 4×4 identity matrix.

For the given 2 d.o.f. mechanical system under analysis, the inverse of the matrix exponential has a particular structure and can be calculated using the matrix $\boldsymbol{J}$ as

$$(e^{\boldsymbol{A}^\pm t^\pm})^{-1} = \boldsymbol{J} e^{\boldsymbol{A}^\pm t^\pm} \boldsymbol{J},$$

which can also be inverted, so that

$$e^{\boldsymbol{A}^\pm t^\pm} = \boldsymbol{J} (e^{\boldsymbol{A}^\pm t^\pm})^{-1} \boldsymbol{J}.$$

Properties of the invariant cones

Some properties of the solution and other eigenvectors and eigenvalues of (4.9) can now be determined on the basis of the known solution $\{\tilde{\mu}, \tilde{\boldsymbol{x}}\}$ of problem (4.19). In particular, when an invariant cone $\{\tilde{\mu}, \tilde{\boldsymbol{x}}\}$ is detected and the relative intersection times $t^\pm(\tilde{\boldsymbol{x}})$ are computed, the properties of the matrices $e^{\boldsymbol{A}^+ t^+(\tilde{\boldsymbol{x}})}$ and $e^{\boldsymbol{A}^- t^-(\tilde{\boldsymbol{x}})}$ can be investigated and other solutions of the problem (4.9) with the same $t^\pm$ can be determined.

Proposition 1. *If conditions* (4.19) *and* (4.20) *hold, then also* $\{1/\tilde{\mu}, \boldsymbol{J}\tilde{\boldsymbol{\xi}}\}$ *is a solution of the nonlinear eigenvalue problem* (4.19)*, hence*

$$e^{\boldsymbol{A}^+ t^+(\tilde{\boldsymbol{x}})} e^{\boldsymbol{A}^- t^-(\tilde{\boldsymbol{x}})} \boldsymbol{J}\tilde{\boldsymbol{\xi}} = \frac{1}{\tilde{\mu}} \boldsymbol{J}\tilde{\boldsymbol{\xi}}.$$

Proof. The left-hand-side of the expression can be reduced to the right-hand-side in the following way

$$e^{\boldsymbol{A}^+t^+(\tilde{\boldsymbol{x}})}e^{\boldsymbol{A}^-t^-(\tilde{\boldsymbol{x}})}\boldsymbol{J}\tilde{\boldsymbol{\xi}} = \boldsymbol{J}\boldsymbol{J}e^{\boldsymbol{A}^+t^+(\tilde{\boldsymbol{x}})}\boldsymbol{J}\boldsymbol{J}e^{\boldsymbol{A}^-t^-(\tilde{\boldsymbol{x}})}\boldsymbol{J}\tilde{\boldsymbol{\xi}} = \boldsymbol{J}(e^{\boldsymbol{A}^+t^+(\tilde{\boldsymbol{x}})})^{-1}(e^{\boldsymbol{A}^-t^-(\tilde{\boldsymbol{x}})})^{-1}\tilde{\boldsymbol{\xi}} = \boldsymbol{J}(e^{\boldsymbol{A}^+t^+(\tilde{\boldsymbol{x}})})^{-1}\tilde{\boldsymbol{x}} = \frac{1}{\tilde{\mu}}\boldsymbol{J}(e^{\boldsymbol{A}^+t^+(\tilde{\boldsymbol{x}})})^{-1}\tilde{\boldsymbol{\eta}} = \frac{1}{\tilde{\mu}}\boldsymbol{J}\tilde{\boldsymbol{\xi}}.$$

□

This important property implies that when an unstable (i.e. spiralling out) invariant cone is detected, described by $\{\tilde{\mu}, \tilde{\boldsymbol{x}}\}$, with $\tilde{\mu} > 1$, then another stable (i.e. spiralling in) invariant cone $\{1/\tilde{\mu}, \boldsymbol{J}\tilde{\boldsymbol{\xi}}\}$ can be found, for the same mechanical system and with the same intersection time intervals $t^{\pm}(\tilde{\boldsymbol{x}})$. The difference between these two cones is in the attractivity, as can be seen in Proposition 8.

Proposition 2. *If conditions* (4.19) *and* (4.20) *hold, then the nonlinear eigenvalue problem defined by the matrix* $e^{\boldsymbol{A}^-t^-(\tilde{\boldsymbol{x}})}e^{\boldsymbol{A}^+t^+(\tilde{\boldsymbol{x}})}$*, where the first and second terms have been flipped, admits the solutions* $\{\tilde{\mu}, \tilde{\boldsymbol{\xi}}\}$ *and* $\{1/\tilde{\mu}, \boldsymbol{J}\tilde{\boldsymbol{x}}\}$*, hence*

$$e^{\boldsymbol{A}^-t^-(\tilde{\boldsymbol{x}})}e^{\boldsymbol{A}^+t^+(\tilde{\boldsymbol{x}})}\tilde{\boldsymbol{\xi}} = \tilde{\mu}\tilde{\boldsymbol{\xi}}$$
$$e^{\boldsymbol{A}^-t^-(\tilde{\boldsymbol{x}})}e^{\boldsymbol{A}^+t^+(\tilde{\boldsymbol{x}})}\boldsymbol{J}\tilde{\boldsymbol{x}} = \frac{1}{\tilde{\mu}}\boldsymbol{J}\tilde{\boldsymbol{x}}.$$

Proof. The left-hand-side of the first expression can be reduced to the right-hand-side in the following way

$$e^{\boldsymbol{A}^-t^-(\tilde{\boldsymbol{x}})}e^{\boldsymbol{A}^+t^+(\tilde{\boldsymbol{x}})}\tilde{\boldsymbol{\xi}} = e^{\boldsymbol{A}^-t^-(\tilde{\boldsymbol{x}})}\tilde{\boldsymbol{\eta}} = \tilde{\mu}e^{\boldsymbol{A}^-t^-(\tilde{\boldsymbol{x}})}\tilde{\boldsymbol{x}} = \tilde{\mu}\tilde{\boldsymbol{\xi}},$$

while, for the second expression,

$$e^{\boldsymbol{A}^-t^-(\tilde{\boldsymbol{x}})}e^{\boldsymbol{A}^+t^+(\tilde{\boldsymbol{x}})}\boldsymbol{J}\tilde{\boldsymbol{x}} = \boldsymbol{J}\boldsymbol{J}e^{\boldsymbol{A}^-t^-(\tilde{\boldsymbol{x}})}\boldsymbol{J}\boldsymbol{J}e^{\boldsymbol{A}^+t^+(\tilde{\boldsymbol{x}})}\boldsymbol{J}\tilde{\boldsymbol{x}} = \boldsymbol{J}(e^{\boldsymbol{A}^-t^-(\tilde{\boldsymbol{x}})})^{-1}(e^{\boldsymbol{A}^+t^+(\tilde{\boldsymbol{x}})})^{-1}\tilde{\boldsymbol{x}} = \frac{1}{\tilde{\mu}}\boldsymbol{J}(e^{\boldsymbol{A}^-t^-(\tilde{\boldsymbol{x}})})^{-1}(e^{\boldsymbol{A}^+t^+(\tilde{\boldsymbol{x}})})^{-1}\tilde{\boldsymbol{\eta}} = \frac{1}{\tilde{\mu}}\boldsymbol{J}(e^{\boldsymbol{A}^-t^-(\tilde{\boldsymbol{x}})})^{-1}\tilde{\boldsymbol{\xi}} = \frac{1}{\tilde{\mu}}\boldsymbol{J}\tilde{\boldsymbol{x}}.$$

□

The discovery of these new eigenvalues and the relative eigenvectors is a fundamental milestone for the determination of the behaviour of the system and in particular the attractivity of the cone. Let's observe that Propositions 1 and 2 are always valid, however for the specific case $\tilde{\mu} = 1$ further investigation are required, since the two multipliers $\tilde{\mu}$ and $\frac{1}{\tilde{\mu}}$ coalesce. The following Propositions refer exactly to this particular case, which must be analysed in depth.

Proposition 3. *If conditions* (4.19) *and* (4.20) *hold with* $\tilde{\mu} = 1$*, then the algebraic multiplicity of this eigenvalue is not lower than 2.*

Proof. First of all, the matrix $e^{\boldsymbol{A}^- t^-(\tilde{\boldsymbol{x}})} e^{\boldsymbol{A}^+ t^+(\tilde{\boldsymbol{x}})}$ can be rewritten as

$$e^{\boldsymbol{A}^- t^-(\tilde{\boldsymbol{x}})} e^{\boldsymbol{A}^+ t^+(\tilde{\boldsymbol{x}})} = \boldsymbol{J}\boldsymbol{J} e^{\boldsymbol{A}^- t^-(\tilde{\boldsymbol{x}})} \boldsymbol{J}\boldsymbol{J} e^{\boldsymbol{A}^+ t^+(\tilde{\boldsymbol{x}})} \boldsymbol{J}\boldsymbol{J} = \boldsymbol{J} \left(e^{\boldsymbol{A}^- t^-(\tilde{\boldsymbol{x}})} \right)^{-1} \left(e^{\boldsymbol{A}^+ t^+(\tilde{\boldsymbol{x}})} \right)^{-1} \boldsymbol{J} = \boldsymbol{J} \left(e^{\boldsymbol{A}^+ t^+(\tilde{\boldsymbol{x}})} e^{\boldsymbol{A}^- t^-(\tilde{\boldsymbol{x}})} \right)^{-1} \boldsymbol{J}.$$

If the trace operator is applied on both sides of the relation above, the following condition is fulfilled

$$\mathrm{tr}\left[e^{\boldsymbol{A}^- t^-(\tilde{\boldsymbol{x}})} e^{\boldsymbol{A}^+ t^+(\tilde{\boldsymbol{x}})} \right] = \mathrm{tr}\left[\boldsymbol{J} \left(e^{\boldsymbol{A}^+ t^+(\tilde{\boldsymbol{x}})} e^{\boldsymbol{A}^- t^-(\tilde{\boldsymbol{x}})} \right)^{-1} \boldsymbol{J} \right] = \mathrm{tr}\left[\left(e^{\boldsymbol{A}^+ t^+(\tilde{\boldsymbol{x}})} e^{\boldsymbol{A}^- t^-(\tilde{\boldsymbol{x}})} \right)^{-1} \boldsymbol{J}\boldsymbol{J} \right] = \mathrm{tr}\left[\left(e^{\boldsymbol{A}^+ t^+(\tilde{\boldsymbol{x}})} e^{\boldsymbol{A}^- t^-(\tilde{\boldsymbol{x}})} \right)^{-1} \right],$$

where the properties of the trace operator have been applied, see [76]. Thus, since the trace fulfils the properties $\mathrm{tr}(\boldsymbol{A}\boldsymbol{B}) = \mathrm{tr}(\boldsymbol{B}\boldsymbol{A})$, for any matrix $\boldsymbol{A}$ and $\boldsymbol{B}$, this relation can be rewritten

$$\mathrm{tr}\left[e^{\boldsymbol{A}^+ t^+(\tilde{\boldsymbol{x}})} e^{\boldsymbol{A}^- t^-(\tilde{\boldsymbol{x}})} \right] = \mathrm{tr}\left[\left(e^{\boldsymbol{A}^+ t^+(\tilde{\boldsymbol{x}})} e^{\boldsymbol{A}^- t^-(\tilde{\boldsymbol{x}})} \right)^{-1} \right]. \tag{4.24}$$

Moreover, the matrices in the above relation can be properly written in the canonical Jordan form, so the matrices $\boldsymbol{U}$ and $\boldsymbol{\Lambda}$ can be introduced, such that

$$\begin{aligned} e^{\boldsymbol{A}^+ t^+(\tilde{\boldsymbol{x}})} e^{\boldsymbol{A}^- t^-(\tilde{\boldsymbol{x}})} &= \boldsymbol{U}\boldsymbol{\Lambda}\boldsymbol{U}^{-1}, \\ \left(e^{\boldsymbol{A}^+ t^+(\tilde{\boldsymbol{x}})} e^{\boldsymbol{A}^- t^-(\tilde{\boldsymbol{x}})} \right)^{-1} &= \boldsymbol{U}\boldsymbol{\Lambda}^{-1}\boldsymbol{U}^{-1}, \end{aligned} \tag{4.25}$$

where $\boldsymbol{\Lambda}$ contains the Jordan blocks and $\boldsymbol{U}$ the eigenvectors of the matrix $e^{\boldsymbol{A}^+ t^+(\tilde{\boldsymbol{x}})} e^{\boldsymbol{A}^- t^-(\tilde{\boldsymbol{x}})}$. The substitution of (4.25) into expression (4.24) leads to the following condition,

$$\operatorname{tr} \boldsymbol{\Lambda} = \operatorname{tr} \boldsymbol{\Lambda}^{-1}. \tag{4.26}$$

Assuming that the spectrum of the original matrix $e^{\boldsymbol{A}^+ t^+(\tilde{\boldsymbol{x}})} e^{\boldsymbol{A}^- t^-(\tilde{\boldsymbol{x}})}$ contains the four scalars $\{1, \alpha, \beta, \gamma\}$ (since at least one eigenvalue is $\tilde{\mu} = 1$), the left-hand-side and right-hand-side of the equation (4.26) can be computed as

$$\begin{aligned} \operatorname{tr} \Lambda &= 1 + \alpha + \beta + \gamma, \\ \operatorname{tr} \Lambda^{-1} &= 1 + \frac{1}{\alpha} + \frac{1}{\beta} + \frac{1}{\gamma}, \end{aligned}$$

yielding to

$$\alpha + \beta + \gamma = \frac{1}{\alpha} + \frac{1}{\beta} + \frac{1}{\gamma}. \tag{4.27}$$

Moreover, a further condition on the determinant of $e^{\boldsymbol{A}^+ t^+(\tilde{\boldsymbol{x}})} e^{\boldsymbol{A}^- t^-(\tilde{\boldsymbol{x}})}$ must be considered, that allows to fix one of the three undetermined eigenvalues. In fact, the determinant of a matrix exponential related to a mechanical system can be computed as

$$\det e^{\boldsymbol{A}^{\pm} t^{\pm}} = e^{\operatorname{tr}\left(\boldsymbol{A}^{\pm} t^{\pm}\right)} = 1,$$

hence the following relation can be written

$$\det \left[e^{\boldsymbol{A}^+ t^+(\tilde{\boldsymbol{x}})} e^{\boldsymbol{A}^- t^-(\tilde{\boldsymbol{x}})} \right] = \det \left[e^{\boldsymbol{A}^+ t^+(\tilde{\boldsymbol{x}})} \right] \det \left[e^{\boldsymbol{A}^- t^-(\tilde{\boldsymbol{x}})} \right] = 1 = \alpha\beta\gamma.$$

From the above expression we can define one eigenvalue as a function of the others, for instance

$$\gamma = \frac{1}{\alpha\beta},$$

so that the condition (4.27) can be rewritten as

$$(\beta - 1)\left(\beta\alpha^2 - (\beta + 1)\alpha + 1\right) = 0.$$

This equation must then be solved in α and β, obtaining these two cases:

- $\beta = 1, \forall\alpha$, so that the spectrum of the matrix $e^{\boldsymbol{A}^+ t^+(\tilde{\boldsymbol{x}})} e^{\boldsymbol{A}^- t^-(\tilde{\boldsymbol{x}})}$ is $\{1, \alpha, 1, 1/\alpha, \}$;

- $\beta \neq 1$, with two possible values of α, namely

$$\alpha_{1,2} = \frac{(\beta+1) \pm |\beta-1|}{2\beta},$$

so that the spectrum of the matrix $e^{\boldsymbol{A}^+ t^+(\tilde{\boldsymbol{x}})} e^{\boldsymbol{A}^- t^-(\tilde{\boldsymbol{x}})}$ is $\{1, \beta, 1, 1/\beta\}$;

Therefore, if an eigenvalue $\tilde{\mu} = 1$ is found, then the possible spectra must always contain at least two eigenvalues equal to 1, hence the algebraic multiplicity is greater than or equal to 2. □

Proposition 4. *If conditions* (4.19) *and* (4.20) *hold and* $\boldsymbol{x} = \boldsymbol{J\xi}$*, then the associated eigenvalue is* $\tilde{\mu} = 1$*.*

Proof. Assuming that $\tilde{\boldsymbol{x}} = \boldsymbol{J}\tilde{\boldsymbol{\xi}}$, the following relations can be written, starting from (4.19)

$$\tilde{\mu}\tilde{\boldsymbol{x}} = e^{\boldsymbol{A}^+ t^+(\tilde{\boldsymbol{x}})} e^{\boldsymbol{A}^- t^-(\tilde{\boldsymbol{x}})} \tilde{\boldsymbol{x}} = e^{\boldsymbol{A}^+ t^+(\tilde{\boldsymbol{x}})} e^{\boldsymbol{A}^- t^-(\tilde{\boldsymbol{x}})} \boldsymbol{J}\tilde{\boldsymbol{\xi}} = \frac{1}{\tilde{\mu}} \boldsymbol{J}\tilde{\boldsymbol{\xi}} = \frac{1}{\tilde{\mu}} \tilde{\boldsymbol{x}},$$

The comparison between the first and last term of the expression above is clearly valid only if $\tilde{\mu} = 1$. □

Actually, from the numerical examples treated in Chapter 6, also the inverse implication seems to hold true, i.e. if $\tilde{\mu} = 1$, then $\boldsymbol{x} = \boldsymbol{J\xi}$. Although from a physical intuition this condition is reasonable, a proof of this statement has not been found and this will be considered for this reason only a very frequent outcome in the numerical results.

However, the single-directed implication exposed in Proposition 4 is sufficient to state that there may exists, for a certain problem, an invariant cone with $\boldsymbol{x} = \boldsymbol{J\xi}$, having necessarily a multiplier $\tilde{\mu} = 1$. Since some Propositions below are proved assuming that $\boldsymbol{x} \neq \boldsymbol{J\xi}$, the proof may be incorrect if $\tilde{\mu} = 1$, so this case must be further investigated.

Properties on the attractivity of the invariant cones

The attractivity of an invariant cone is described by the Floquet multipliers of the monodromy matrix, according to the theoretical approach exposed in Section 4.3.2, therefore the eigenvalues and eigenvectors of

$$\boldsymbol{\Phi}_T = \boldsymbol{S}^+ e^{\boldsymbol{A}^+ t^+(\tilde{\boldsymbol{x}})} \boldsymbol{S}^- e^{\boldsymbol{A}^- t^-(\tilde{\boldsymbol{x}})}$$

must be determined.

First of all, an interesting feature of the saltation matrix must be observed, i.e. when the saltation matrices are applied to a vector that belongs to the switching manifold (e.g. the vector $\tilde{\boldsymbol{x}}$, $\tilde{\boldsymbol{\xi}}$, or $\tilde{\boldsymbol{\eta}}$), the application of $\boldsymbol{S}^{\pm}$ simply reduce to the application of an identity matrix, for instance

$$\boldsymbol{S}^{-}\tilde{\boldsymbol{x}} = \boldsymbol{I}\tilde{\boldsymbol{x}} + \frac{1}{\tilde{\xi}_3}(\boldsymbol{A}^{+} - \boldsymbol{A}^{-})(\tilde{\boldsymbol{\xi}} \otimes \boldsymbol{e}_1)\tilde{\boldsymbol{x}} = \boldsymbol{I}\tilde{\boldsymbol{x}} + \frac{1}{\tilde{\xi}_3}(\boldsymbol{A}^{+} - \boldsymbol{A}^{-})(\boldsymbol{e}_1 \cdot \tilde{\boldsymbol{x}})\tilde{\boldsymbol{\xi}} = \boldsymbol{I}\tilde{\boldsymbol{x}},$$

since $\boldsymbol{e}_1 \cdot \boldsymbol{a} = 0$, for all vectors $\boldsymbol{a} \in \Sigma$, belonging to the switching manifold.

Proposition 5. *If conditions* (4.19) *and* (4.20) *hold, then $\tilde{\boldsymbol{x}}$ is also an eigenvector of the monodromy matrix $\boldsymbol{\Phi}_T$, corresponding to the Floquet multiplier $\tilde{\mu}$, hence*

$$\boldsymbol{S}^{+}e^{\boldsymbol{A}^{+}t^{+}(\tilde{\boldsymbol{x}})}\boldsymbol{S}^{-}e^{\boldsymbol{A}^{-}t^{-}(\tilde{\boldsymbol{x}})}\tilde{\boldsymbol{x}} = \tilde{\mu}\tilde{\boldsymbol{x}}$$

Proof. The left-hand-side of the expression can be reduced to the right-hand-side in the following way

$$\boldsymbol{S}^{+}e^{\boldsymbol{A}^{+}t^{+}(\tilde{\boldsymbol{x}})}\boldsymbol{S}^{-}e^{\boldsymbol{A}^{-}t^{-}(\tilde{\boldsymbol{x}})}\tilde{\boldsymbol{x}} = \boldsymbol{S}^{+}e^{\boldsymbol{A}^{+}t^{+}(\tilde{\boldsymbol{x}})}\boldsymbol{S}^{-}\tilde{\boldsymbol{\xi}} = \boldsymbol{S}^{+}e^{\boldsymbol{A}^{+}t^{+}(\tilde{\boldsymbol{x}})}\tilde{\boldsymbol{\xi}} = \boldsymbol{S}^{+}\tilde{\boldsymbol{\eta}} = \tilde{\boldsymbol{\eta}} = \tilde{\mu}\tilde{\boldsymbol{x}}.$$

□

Proposition 6. *If conditions* (4.19) *and* (4.20) *hold, then the vector field $\boldsymbol{f}^{-}(\tilde{\boldsymbol{x}}) = \boldsymbol{A}^{-}\tilde{\boldsymbol{x}}$ is an eigenvector of the monodromy matrix $\boldsymbol{\Phi}_T$, corresponding to the Floquet multiplier $\tilde{\mu}$, hence*

$$\boldsymbol{S}^{+}e^{\boldsymbol{A}^{+}t^{+}(\tilde{\boldsymbol{x}})}\boldsymbol{S}^{-}e^{\boldsymbol{A}^{-}t^{-}(\tilde{\boldsymbol{x}})}\boldsymbol{A}^{-}\tilde{\boldsymbol{x}} = \tilde{\mu}\boldsymbol{A}^{-}\tilde{\boldsymbol{x}}.$$

Proof. First of all, let's recall a fundamental property on the commutativity of a matrix and its matrix exponential, i.e. $\boldsymbol{A}^{\pm}e^{\boldsymbol{A}^{\pm}t^{\pm}} = e^{\boldsymbol{A}^{\pm}t^{\pm}}\boldsymbol{A}^{\pm}$. Then, one must note that the vector field $\boldsymbol{f}^{-}(\tilde{\boldsymbol{x}})$, which represents the orbital velocity calculated in the initial condition $\tilde{\boldsymbol{x}}$, fulfils the equation describing the perturbed solution, i.e. when $\boldsymbol{f}^{-}(\tilde{\boldsymbol{x}})$ is taken as the initial perturbation from a reference solution, then the perturbation at the generic time t is exactly the vector field calculated at time t.

This condition is easily proved for a smooth system, but it can be extended to non-smooth dynamical problems. Let's observe that, if the reference orbit crosses the switching manifold from $(-)$ to $(+)$ subdomain in the discontinuity point $\tilde{\boldsymbol{\xi}}$, the application of the saltation matrix $\boldsymbol{S}^-$ to the vector field $\boldsymbol{A}^-\tilde{\boldsymbol{\xi}}$ relative to the halfspace $(-)$ returns the velocity field $\boldsymbol{A}^+\tilde{\boldsymbol{\xi}}$ relative the halfspace $(+)$, in fact

$$\begin{aligned}\boldsymbol{S}^-\boldsymbol{A}^-\tilde{\boldsymbol{\xi}} = \left[\boldsymbol{I} + \frac{1}{\tilde{\xi}_3}(\boldsymbol{A}^+ - \boldsymbol{A}^-)(\tilde{\boldsymbol{\xi}} \otimes \boldsymbol{e}_1)\right]\boldsymbol{A}^-\tilde{\boldsymbol{\xi}} = \\ \boldsymbol{A}^-\tilde{\boldsymbol{\xi}} + \frac{1}{\tilde{\xi}_3}(\boldsymbol{A}^+ - \boldsymbol{A}^-)(\tilde{\boldsymbol{\xi}} \otimes \boldsymbol{e}_1)\boldsymbol{A}^-\tilde{\boldsymbol{\xi}} = \\ \boldsymbol{A}^-\tilde{\boldsymbol{\xi}} + \frac{1}{\tilde{\xi}_3}(\boldsymbol{A}^+ - \boldsymbol{A}^-)(\boldsymbol{A}^-\tilde{\boldsymbol{\xi}} \cdot \boldsymbol{e}_1)\tilde{\boldsymbol{\xi}} = \boldsymbol{A}^-\tilde{\boldsymbol{\xi}} + \boldsymbol{A}^+\tilde{\boldsymbol{\xi}} - \boldsymbol{A}^-\tilde{\boldsymbol{\xi}} = \boldsymbol{A}^+\tilde{\boldsymbol{\xi}},\end{aligned}$$

where clearly $\boldsymbol{A}^-\tilde{\boldsymbol{\xi}} \cdot \boldsymbol{e}_1 = \tilde{\xi}_3$. The same condition holds for the saltation matrix $\boldsymbol{S}^+$, since $\boldsymbol{S}^+\boldsymbol{A}^+\tilde{\boldsymbol{\eta}} = \boldsymbol{A}^-\tilde{\boldsymbol{\eta}}$.

Taking into consideration these properties, the left-hand-side of the original expression can be reduced to the right-hand-side in the following way

$$\begin{aligned}\boldsymbol{S}^+e^{\boldsymbol{A}^+t^+(\tilde{\boldsymbol{x}})}\boldsymbol{S}^-e^{\boldsymbol{A}^-t^-(\tilde{\boldsymbol{x}})}\boldsymbol{A}^-\tilde{\boldsymbol{x}} = \boldsymbol{S}^+e^{\boldsymbol{A}^+t^+(\tilde{\boldsymbol{x}})}\boldsymbol{S}^-\boldsymbol{A}^-e^{\boldsymbol{A}^-t^-(\tilde{\boldsymbol{x}})}\tilde{\boldsymbol{x}} = \\ \boldsymbol{S}^+e^{\boldsymbol{A}^+t^+(\tilde{\boldsymbol{x}})}\boldsymbol{S}^-\boldsymbol{A}^-\tilde{\boldsymbol{\xi}} = \boldsymbol{S}^+e^{\boldsymbol{A}^+t^+(\tilde{\boldsymbol{x}})}\boldsymbol{A}^+\tilde{\boldsymbol{\xi}} = \\ \boldsymbol{S}^+\boldsymbol{A}^+e^{\boldsymbol{A}^+t^+(\tilde{\boldsymbol{x}})}\tilde{\boldsymbol{\xi}} = \boldsymbol{S}^+\boldsymbol{A}^+\tilde{\boldsymbol{\eta}} = \boldsymbol{A}^-\tilde{\boldsymbol{\eta}} = \tilde{\mu}\boldsymbol{A}^-\tilde{\boldsymbol{x}}.\end{aligned}$$

□

Proposition 7. *If conditions* (4.19) *and* (4.20) *hold, then* $\boldsymbol{J}\tilde{\boldsymbol{\xi}}$ *is also an eigenvector of the monodromy matrix* $\boldsymbol{\Phi}_T$*, corresponding to the Floquet multiplier* $1/\tilde{\mu}$*, hence*

$$\boldsymbol{S}^+e^{\boldsymbol{A}^+t^+(\tilde{\boldsymbol{x}})}\boldsymbol{S}^-e^{\boldsymbol{A}^-t^-(\tilde{\boldsymbol{x}})}\boldsymbol{J}\tilde{\boldsymbol{\xi}} = \frac{1}{\tilde{\mu}}\boldsymbol{J}\tilde{\boldsymbol{\xi}}.$$

Proof. From the definition of the matrix $\boldsymbol{J}$, if $\boldsymbol{x}$ is on the Poincaré section Σ then also $\boldsymbol{J}\boldsymbol{x}$ is on the same discontinuity hyperplane. Therfore, since the saltation matrix becomes the identity matrix when applied to a vector that belongs to the switching manifold, the left-hand-side of the expression can

be reduced to the right-hand-side as follows,

$$\boldsymbol{S}^{+}e^{\boldsymbol{A}^{+}t^{+}(\tilde{\boldsymbol{x}})}\boldsymbol{S}^{-}e^{\boldsymbol{A}^{-}t^{-}(\tilde{\boldsymbol{x}})}\boldsymbol{J}\tilde{\boldsymbol{\xi}} = \boldsymbol{S}^{+}e^{\boldsymbol{A}^{+}t^{+}(\tilde{\boldsymbol{x}})}\boldsymbol{S}^{-}\boldsymbol{J}\boldsymbol{J}e^{\boldsymbol{A}^{-}t^{-}(\tilde{\boldsymbol{x}})}\boldsymbol{J}\tilde{\boldsymbol{\xi}} =$$
$$\boldsymbol{S}^{+}e^{\boldsymbol{A}^{+}t^{+}(\tilde{\boldsymbol{x}})}\boldsymbol{S}^{-}\boldsymbol{J}(e^{\boldsymbol{A}^{-}t^{-}(\tilde{\boldsymbol{x}})})^{-1}\tilde{\boldsymbol{\xi}} = \boldsymbol{S}^{+}e^{\boldsymbol{A}^{+}t^{+}(\tilde{\boldsymbol{x}})}\boldsymbol{S}^{-}\boldsymbol{J}\tilde{\boldsymbol{x}} = \boldsymbol{S}^{+}e^{\boldsymbol{A}^{+}t^{+}(\tilde{\boldsymbol{x}})}\boldsymbol{J}\tilde{\boldsymbol{x}} =$$
$$\boldsymbol{S}^{+}\boldsymbol{J}\boldsymbol{J}e^{\boldsymbol{A}^{+}t^{+}(\tilde{\boldsymbol{x}})}\boldsymbol{J}\tilde{\boldsymbol{x}} = \frac{1}{\tilde{\mu}}\boldsymbol{S}^{+}\boldsymbol{J}(e^{\boldsymbol{A}^{+}t^{+}(\tilde{\boldsymbol{x}})})^{-1}\tilde{\boldsymbol{\eta}} = \frac{1}{\tilde{\mu}}\boldsymbol{S}^{+}\boldsymbol{J}\tilde{\boldsymbol{\xi}} = \frac{1}{\tilde{\mu}}\boldsymbol{J}\tilde{\boldsymbol{\xi}}.$$

□

Let's observe that Proposition 5 and 7 are two different conditions if $\boldsymbol{x} \neq \boldsymbol{J}\boldsymbol{\xi}$, otherwise they coincide. Hence, they can be adopted to study the attractivity of the invariant cone only for $\tilde{\mu} \neq 1$, since according to Proposition 4, there may exists a unit multiplier associated with the eigenvector $\boldsymbol{x} = \boldsymbol{J}\boldsymbol{\xi}$. Therefore, this specific case must be studied separately.

Proposition 8. *If conditions* (4.19) *and* (4.20) *hold, together with* $\tilde{\mu} \neq 1$*, then the attractivity is well defined and, in particular, the invariant cone associated with the multiplier* $\tilde{\mu} > 1$ *is always attractive.*

Proof. The attractivity of the invariant cone is determined by the Floquet multipliers. In particular, an orbit that belongs to the cone is attractive if the modulus of all the eigenvalues of the monodromy matrix is lower than 1.

If conditions (4.19) and (4.20) hold, the Floquet multipliers of the monodromy matrix can be written as $\{\tilde{\mu}, \tilde{\mu}, 1/\tilde{\mu}, \lambda\}$, since from Propositions 5, 6, and 7, three eigenvalues are equal to $\tilde{\mu}$, $\tilde{\mu}$, $1/\tilde{\mu}$, with the associated eigenvectors $\tilde{\boldsymbol{x}}$, $\boldsymbol{A}^{-}\tilde{\boldsymbol{x}}$, and $\boldsymbol{J}\tilde{\boldsymbol{\xi}}$, respectively. The fourth unknown eigenvalue λ can be estimated by the determinant of the monodromy matrix, since the condition

$$\lambda \cdot \tilde{\mu} \cdot \tilde{\mu} \cdot \frac{1}{\tilde{\mu}} = \det\left(\boldsymbol{S}^{+}e^{\boldsymbol{A}^{+}t^{+}(\tilde{\boldsymbol{x}})}\boldsymbol{S}^{-}e^{\boldsymbol{A}^{-}t^{-}(\tilde{\boldsymbol{x}})}\right) =$$
$$\det(\boldsymbol{S}^{+}) \cdot \det(e^{\boldsymbol{A}^{+}t^{+}(\tilde{\boldsymbol{x}})}) \cdot \det(\boldsymbol{S}^{-}) \cdot \det(e^{\boldsymbol{A}^{-}t^{-}(\tilde{\boldsymbol{x}})})$$

must be fulfilled. The determinant of an exponential matrix can be calculated as

$$\det\left(e^{\boldsymbol{A}^{\pm}t^{\pm}}\right) = e^{\mathrm{tr}(\boldsymbol{A}^{\pm}t^{\pm})} = 1,$$

which comes from the specific structure of the matrix $\boldsymbol{A}^{\pm}$ for a mechanical system. The determinant of the saltation matrix $\boldsymbol{S}^{-}$ (and also of $\boldsymbol{S}^{+}$, with analogous computations) can be calculated as

$$\det \boldsymbol{S}^{-} = \det\left[\boldsymbol{I} + \frac{1}{\tilde{\xi}_3}(\boldsymbol{A}^{+} - \boldsymbol{A}^{-})(\tilde{\boldsymbol{\xi}} \otimes \boldsymbol{e}_1)\right] = 1 + \frac{1}{\tilde{\xi}_3}\left[(\boldsymbol{A}^{+} - \boldsymbol{A}^{-})\tilde{\boldsymbol{\xi}} \cdot \boldsymbol{e}_1\right] = 1 + \frac{1}{\tilde{\xi}_3}(\boldsymbol{A}^{+}\tilde{\boldsymbol{\xi}} \cdot \boldsymbol{e}_1 - \boldsymbol{A}^{-}\tilde{\boldsymbol{\xi}} \cdot \boldsymbol{e}_1) = 1 + \frac{1}{\tilde{\xi}_3}(\tilde{\xi}_3 - \tilde{\xi}_3) = 1$$

where the property $\boldsymbol{A}^{+}\tilde{\boldsymbol{\xi}} \cdot \boldsymbol{e}_1 = \boldsymbol{A}^{-}\tilde{\boldsymbol{\xi}} \cdot \boldsymbol{e}_1 = \tilde{\xi}_3$ has been used. Therefore, the determinant of the monodromy matrix for a mechanical system is equal to 1, so the remaining multiplier must be $\lambda = 1/\tilde{\mu}$.

In a smooth autonomous system, the multiplier associated with the velocity field of a periodic solution is always equal to 1 and the stability of the periodic solution is obtained by the investigation of the remaining $n-1$ eigenvalues. For a non-smooth system, a solution belonging to an invariant cone can be seen as a sort of generalized periodic solution and, in this case, the eigenvalue associated with the orbital velocity at the initial condition $\tilde{\boldsymbol{x}}$ is equal to $\tilde{\mu}$. This can be explained through the increase (decrease) of the modulus of the orbital velocity when $\tilde{\mu} > 1$ ($\tilde{\mu} < 1$) for a solution that spirals on the cone, since the time intervals t^{-} and t^{+} are constant, despite the modulus of the initial conditions increases (decreases) after each cycle. In accordance with the smooth case, the attractivity depends on the other three multipliers of the monodromy matrix and the direction of the initial orbital velocity is neglected.

Moreover, one of the eigenvectors of the monodromy matrix is the direction of the cone $\tilde{\boldsymbol{x}}$, along which a magnification of the factor $\tilde{\mu}$ in the perturbation is expected, since the reference solution spirals in or out on the invariant cone. For this reason, also this multiplier can be neglected and only the two remaining Floquet multipliers $1/\tilde{\mu}$ and $1/\tilde{\mu}$ really describe the attractivity of the cone. Actually, the eigendirections associated with these eigenvalues are those real perturbations that are "out" of the cone (in fact, if the perturbation is along $\tilde{\boldsymbol{x}}$ or $\boldsymbol{A}^{-}\tilde{\boldsymbol{x}}$, the initial conditions still lie on the cone).

Assuming that an invariant cone with $\tilde{\mu} > 1$ exists, then the Floquet multipliers are lower than 1 and the cone is attractive. On the contrary, if a cone with $\tilde{\mu} < 1$ is found, according to Proposition 1, for the same mechan-

ical system there exist another invariant cone with an eigenvalue equal to $1/\tilde{\mu}$ and with Floquet multipliers lower than 1. Hence, for all mechanical systems for which an invariant cone with $\tilde{\mu} \neq 1$ can be detected, there always exists an attractive cone associated with an unstable equilibrium configuration. □

In order to remark the crucial meaning of Proposition 8, let's now analyse its implications in simple words.

Let's consider an invariant cone described by the solution $\{\tilde{\mu}, \tilde{\boldsymbol{x}}\}$ of condition (4.19) and let's assume that $\tilde{\mu} > 1$. Then, all the orbits with initial conditions on the straight line defined by the direction $\tilde{\boldsymbol{x}}$ spiral out from the equilibrium configuration located in the vertex of the invariant cone, hence the fixed point can be defined unstable.

A given perturbation in the initial condition from a solution belonging to the invariant cone can be decomposed along the eigenvectors of the monodromy matrix. The component of the initial perturbation along the direction $\tilde{\boldsymbol{x}}$ will increase after each period $t^- + t^+$, because the associated Floquet multiplier is $\tilde{\mu} > 1$, but this was already known since the solution spirals out remaining on the cone. The perturbation along $\boldsymbol{A}^- \tilde{\boldsymbol{x}}$, which also belongs to the invariant manifold and in particular is tangent to the cone, will increase because the associated multiplier is $\tilde{\mu}$. However, the explanation is linked to the increase of the orbital velocity of a solution in order to maintain a constant value for the sum of the intersection time intervals $t^- + t^+$.

On the contrary, the other two directions represent perturbations in the initial conditions that do not lie on the hypersurface of the cone. Both the multipliers associated with these directions are lower than 1, so these perturbations tend to decrease after each period $t^- + t^+$, hence the solution tends to the reference one and the cone can be defined as attractive.

Let's now change the initial hypothesis, considering an original invariant manifold described by $\{\tilde{\mu}, \tilde{\boldsymbol{x}}\}$ with an eigenvalue $\tilde{\mu} < 1$, so that the orbits spiral in, towards the stable equilibrium configuration located in the tip of the cone. Analogous considerations can be performed, but now the multipliers associated with the directions of perturbation that do not lie on the invariant cone become greater than 1, leading to a non-attractive cone.

However, according to Proposition 1, *for the same 2 d.o.f. mechanical*

system, there exists another solution of (4.19) with the same time intervals t^- and t^+, thus another invariant cone $\{1/\tilde{\mu}, \boldsymbol{J}\tilde{\boldsymbol{\xi}}\}$, which clearly has an eigenvalue greater that 1. Hence, in the same mechanical system, an attractive cone associated with an unstable equilibrium configuration can be defined.

Hence, when in a 2 d.o.f. mechanical system an invariant cone with $\tilde{\mu} \neq 1$ is found, then two invariant cones are present in the phase portrait: one of them is not attractive and associated with a stable solution spiralling in, towards the vertex of the cone, while the other is attractive and associated with an unstable behaviour of the fixed point in the vertex, with spiralling out orbits. Therefore, when an invariant cone is found with $\tilde{\mu} \neq 1$, the mechanical system is always unstable, and the attractivity enforces this instability, from a physical point of view.

Proposition 9. *If* (4.19) *and* (4.20) *holds with* $\tilde{\mu} = 1$*, then the orbits are periodic and the invariant cone is not attractive.*

Proof. If $\boldsymbol{x} \neq \boldsymbol{J\xi}$ (this hypothesis cannot be excluded since Proposition 4 has been proved only in one direction), then all the four eigenvalues of the monodromy matrix are equal to 1, see Propositions 5, 6, 7, and the first part of the proof of Proposition 8. For this reason, a perturbation of the initial conditions near the invariant cone neither increases nor decreases (it is a sort of stable but non-attractive cone).

On the contrary, if $\boldsymbol{x} = \boldsymbol{J\xi}$, then the vectors $\tilde{\boldsymbol{x}}$ and $\boldsymbol{A}^-\tilde{\boldsymbol{x}}$ still remain eigenvectors of the monodromy matrix $\boldsymbol{\Phi}_T$, with associated eigenvalue $\tilde{\mu} = 1$, see Propositions 5 and 6, while $\boldsymbol{J}\tilde{\boldsymbol{\xi}}$ is not a correct eigenvector, so Proposition 7 cannot be considered. The other two eigenvalues $\mu_{1,2}$ of the spectrum of the monodromy matrix can be calculated through the trace and determinant of $\boldsymbol{\Phi}_T$, hence

$$\begin{aligned} \tilde{\mu} \cdot \tilde{\mu} \cdot \mu_1 \cdot \mu_2 = \det \boldsymbol{\Phi}_T = 1 \quad &\rightarrow \quad \mu_2 = \frac{1}{\mu_1} \\ \tilde{\mu} + \tilde{\mu} + \mu_1 + \mu_2 = \operatorname{tr} \boldsymbol{\Phi}_T \quad &\rightarrow \quad \frac{\mu_1^2 + 1}{\mu_1} = \operatorname{tr} \boldsymbol{\Phi}_T - 2 \end{aligned}$$

The final solution for the two remaining eigenvalues is

$$\mu_{1,2} = \frac{(\operatorname{tr} \boldsymbol{\Phi}_T - 2) \pm \sqrt{\operatorname{tr} \boldsymbol{\Phi}_T (\operatorname{tr} \boldsymbol{\Phi}_T - 4)}}{2},$$

where the trace of the monodromy matrix can be computed as

$$\begin{aligned}\operatorname{tr}\boldsymbol{\Phi}_T = \tilde{\mu} + \operatorname{tr}\left(e^{\boldsymbol{A}^+ t^+(\tilde{\boldsymbol{x}})} e^{\boldsymbol{A}^- t^-(\tilde{\boldsymbol{x}})}\right) + \\ \frac{1}{\tilde{\xi}_3 \tilde{\eta}_3}\left\{\left[e^{\boldsymbol{A}^- t^-(\tilde{\boldsymbol{x}})} \cdot (\boldsymbol{e}_1 \otimes \boldsymbol{A}^+ \tilde{\boldsymbol{\eta}})\right]\left[e^{\boldsymbol{A}^+ t^+(\tilde{\boldsymbol{x}})} \cdot (\boldsymbol{e}_1 \otimes \boldsymbol{A}^- \tilde{\boldsymbol{\xi}})\right] - \right. \\ \left[\boldsymbol{I} \cdot (\boldsymbol{e}_1 \otimes \boldsymbol{A}^- \tilde{\boldsymbol{\xi}})\right]\left[(e^{\boldsymbol{A}^+ t^+(\tilde{\boldsymbol{x}})} e^{\boldsymbol{A}^- t^-(\tilde{\boldsymbol{x}})}) \cdot (\boldsymbol{e}_1 \otimes \boldsymbol{A}^+ \tilde{\boldsymbol{\eta}})\right] - \\ \left.\left[\boldsymbol{I} \cdot (\boldsymbol{e}_1 \otimes \boldsymbol{A}^+ \tilde{\boldsymbol{\eta}})\right]\left[(e^{\boldsymbol{A}^- t^-(\tilde{\boldsymbol{x}})} e^{\boldsymbol{A}^+ t^+(\tilde{\boldsymbol{x}})}) \cdot (\boldsymbol{e}_1 \otimes \boldsymbol{A}^- \tilde{\boldsymbol{\xi}})\right]\right\}.\end{aligned}$$

When the trace of the monodromy matrix is equal to the special values $\operatorname{tr}\boldsymbol{\Phi}_T = 0$ or $\operatorname{tr}\boldsymbol{\Phi}_T = 4$, all the eigenvalues are equal to 1, so the cone is not attractive. Otherwise, there always exists one eigenvalue lower than 1 and the opposite greater than 1, therefore the invariant cone is not attractive. Hence, in all the treated cases when $\tilde{\mu} = 1$, the invariant cone is not attractive and the perturbed orbits with initial condition near the invariant manifold do not approach it for $t \to \infty$. □

4.3.4 Summary of piecewise-smooth system stability

In this Section, the most important outcomes of the previous investigations will be summarised, in order to clarify the behaviour of 2 d.o.f. mechanical piecewise-smooth systems, in presence of invariant cones.

In this analysis, the existence of an invariant cone described by the couple $\{\tilde{\mu}, \tilde{\boldsymbol{x}}\}$, which fulfils the relation (4.19) and (4.20), has been assumed *a priori*. This couple of eigenvalue and eigenvector has been computed solving the original equation (4.9), for example with the numerical method exposed in the next Chapter 5.

First of all, another invariant cone associated with the original solution $\{\tilde{\mu}, \tilde{\boldsymbol{x}}\}$ exists for the same piecewise mechanical system, described by the couple $\{1/\tilde{\mu}, \boldsymbol{J}\tilde{\boldsymbol{\xi}}\}$, see Proposition 1.

Then, according to Proposition 2, other two couples of solutions can be found, namely $\{\tilde{\mu}, \tilde{\boldsymbol{\xi}}\}$ and $\{1/\tilde{\mu}, \boldsymbol{J}\tilde{\boldsymbol{x}}\}$, when the order of application of the two matrix exponentials in (4.9) is inverted, i.e. $e^{\boldsymbol{A}^- t^-(\tilde{\boldsymbol{x}})} e^{\boldsymbol{A}^+ t^+(\tilde{\boldsymbol{x}})}$. Clearly, the latter solutions do not identify further invariant cones, since they simply represent the initial conditions associated with a Poincaré map which at first enter in the positive subdomain (an opposite convention, since in

(4.9) the first map has always been supposed to enter in the negative subdomain), hence the couples represent the same invariant cones defined before.

When a multiplier $\tilde{\mu} \neq 1$ is computed from (4.9), the two cones $\{\tilde{\mu}, \tilde{\boldsymbol{x}}\}$ and $\{1/\tilde{\mu}, \boldsymbol{J}\tilde{\boldsymbol{\xi}}\}$ can be detected. Moreover, the invariant set with an eigenvalue greater than 1 leads to an unstable equilibrium configuration, while the cone is always attractive, see Propositions 5, 6, 7, and 8. The other cone, which is never attractive, leads to a family of orbits that approach the fixed point. Hence, if $\tilde{\mu} \neq 1$ the analysed equilibrium configuration is unstable and the attractivity of the cone determines a "realistic" instability in the system. *The existence of a solution with $\tilde{\mu} \neq 1$ becomes a sufficient condition for instability*, since according to Liapunov's definition, a single unstable solution is sufficient to consider the equilibrium configuration unstable.

If a multiplier $\tilde{\mu} = 1$ is found as a solution of (4.9), which is an eigenvalue with an algebraic multiplicity not lower that 2, then the two couples $\{\tilde{\mu}, \tilde{\boldsymbol{x}}\}$ and $\{1/\tilde{\mu}, \boldsymbol{J}\tilde{\boldsymbol{\xi}}\}$ could possibly coalesce, see Proposition 3. Hence, for $\tilde{\mu} = 1$ a periodic solution is found, which is never attractive, see Proposition 4. However, the existence of a particular solution approaching the fixed point do not necessarily imply that the equilibrium configuration is stable.

4.4 Nonlinear behaviour of 2 d.o.f. piecewise-smooth systems

The presence of an invariant set has been investigated in the previous Sections for 2 d.o.f. piecewise *linear* dynamical systems. However, the mathematical model describing the physical structure introduced in Section 3.2 is fully nonlinear, so one may wonder if the unstable behaviour emerging in the linearised approximation of the nonlinear system is realistic and can be seen in a physical structure.

As presented in Section 2.1.3, a good strategy for the stability analysis of nonlinear smooth dynamical systems is the linearisation of the system in the vicinity of the equilibrium configuration. In particular, the stability analysis of the nonlinear case can be performed, according to Theorem 2 presented in Section 2.1.3, through the characterisation of the nature of the eigenvalues of the linearised system and, excluding the pathological cases

known in Mechanics as *critical cases*, the behaviour of the system near the fixed points can be completely determined.

This strategy is impossible for the piecewise dynamical system considered in this Thesis. In fact, the equilibrium configuration is located exactly on the discontinuity, hence a "smooth linearisation" of the system near the fixed point is unfeasible and the only possible approximation of the nonlinear system is the piecewise-linear one. Hence, the aforementioned Theorem 2 cannot generally be adopted in piecewise systems, since a proper linearised approximation cannot be found.

For the restricted case analysed in this work, i.e. when an invariant cone can be detected in the piecewise-linear approximation of a dynamical system, Weiss *et al.* [86] derived a possible extension of the classical approach exposed above, also in case of non-smooth systems.

Let's consider a piecewise-smooth dynamical system described by the following set of ODEs

$$\dot{\boldsymbol{y}}(t) = \begin{cases} \boldsymbol{f}^{-}(\boldsymbol{y}(t)) = \boldsymbol{A}^{-}\boldsymbol{y}(t) + g^{-}(\boldsymbol{y}(t)), & y_1 \leq 0 \\ \boldsymbol{f}^{+}(\boldsymbol{y}(t)) = \boldsymbol{A}^{+}\boldsymbol{y}(t) + g^{+}(\boldsymbol{y}(t)), & y_1 > 0 \end{cases} \tag{4.28}$$

where, the nonlinear vector fields $\boldsymbol{f}^{\pm}$ have been approximated by a linear part and another sufficiently regular vector field $\boldsymbol{g}^{\pm}$, such that $\boldsymbol{g}^{\pm} \in \mathcal{C}^k$, for a given k and $g^{\pm}(\boldsymbol{y}) = o(||\boldsymbol{y}||)$. For the problems analysed in this Thesis, this approximation of the nonlinear vector field $\boldsymbol{f}^{\pm}$ can always be performed.

Theorem 5 (Weiss, Kupper, Hosham, see [86])**.** *If the piecewise-linear problem associated with the nonlinear system* (4.28) *reveals the presence of an attractive invariant cone, then there exists a sufficiently small neighbourhood of the origin defined by the parameter δ and a regular function $\boldsymbol{w}(u) \in [0, \delta] \subseteq \mathbb{R} \to \Sigma$, $\boldsymbol{w}(0) = \boldsymbol{0}$ and $\frac{\partial \boldsymbol{w}}{\partial u}(0) = \tilde{\boldsymbol{x}}$ such that the manifold*

$$\{\boldsymbol{w}(u) : u \in [0, \delta]\}$$

is locally invariant and attractive for the Poincaré map describing the behaviour of the nonlinear system (4.28)*.*

In simple words, Theorem 5 states that if an invariant and attractive cone for the piecewise-linear case is detected, then a *cone-like* invariant set

can be found near the equilibrium configuration, which is tangent to the invariant cone at the origin and is a sort of "deformed cone", presenting the same properties of the original invariant manifold defined in piecewise-linear systems. Since the hypotheses of Theorem 5 are always fulfilled in case of instability with $\tilde{\mu} > 1$, the piecewise-linear approximation leads to good results for the comprehension of the qualitative behaviour of the system. In particular, the outcomes of the linearised approximation can be extended to the nonlinear original system. Some examples concerning nonlinear structure are presented in Chapter 6, where different cone-like invariant manifolds have been found, revealing unstable behaviours.

4.5 Conclusions

In this Chapter 4, the most important theoretical results for the stability analysis of a 2 d.o.f. mechanical system have been derived. In particular, in Section 4.1.2, the conditions that must be fulfilled for the presence of invariant cones are investigated and a necessary instability criterion for the analysed system has been obtained.

These results are strengthened by the discovery in Section 4.3 that when an invariant cone leads to an unstable behaviour, then the invariant manifold is also attractive, hence the mathematical model is suitable for the description of a physical system showing an unstable behaviour. In the same Section, nine new Propositions have been proved, fundamental properties for the complete characterisation, from a theoretical point of view, of this kind of piecewise dynamical system.

The conditions of crossing are also investigated in Section 4.2, showing that in this case, the sliding motions are forbidden. Moreover, a physical interpretation of this unexpected and counterintuitive behaviour has been given in Section 4.1.3, revealing also that the presence of non-conservative forces is crucial for this kind of instability.

CHAPTER 5

A numerical method for the identification of invariant cones

"I'm convinced mathematics is the most important investigating tool of the legacy of the human enterprise, it being the source of everything"

René Descartes

In the previous Chapter 5, the problem of describing the unusual and counterintuitive behaviour of piecewise mechanical systems has been investigated from a purely theoretical perspective. In particular, the existence of an invariant cone has been assumed as a hypothesis and all the properties of this special invariant manifold have been obtained, especially those regarding its attractivity. In fact, this is a fundamental property that leads to a realistic unstable behaviour of a mechanical system described by the composition of two stable substructures.

The main purpose of the present Chapter is the development of a numerical procedure, through which an invariant cone can be detected when the mechanical parameters of the system are assigned. After a brief introduction on the possible ways for the definition of a numerical algorithms, this procedure will be explained in detail. Moreover, some critical points of the algorithm will be exposed and the possible solutions for these problems will be given. The inspiration for the method developed below comes from a simple 1 d.o.f. example shown in Butenin *et al.* [13].

5.1 Description of the numerical method for cone detection

5.1.1 The two different approaches to the problem

From the point of view of an engineer, the problem of the existence of an invariant cone in a piecewise-linear dynamical system can be analysed from two different perspectives:

i) *check approach*: all the parameters of the mechanical system are well-known and also the loads are fixed, so the only unknown of the problem is the configuration $\boldsymbol{y}(t)$ of the system at each time. This problem can be solved by a classical numerical procedure for the integration of an Initial Value Problem described by first or second order ODEs, e.g. the Newmark's method generally used for dynamical problems or other classical schemes as Runge-Kutta method, see [39, 74, 79]. In case of piecewise-smooth dynamical systems, a change in the set of ODEs that must be solved occurs, on the basis of the switching condition. Therefore, a procedure capable of finding the intersection between the orbits and the switching manifold must be introduced, together with the classical methods of integration of the equations of motion. The outputs of this approach are simply the time evolution of the generalised coordinates and the phase portraits describing the behaviour of the system, both depending on the assigned initial conditions. Hence, following this strategy, the only way to detect an invariant cone is by testing lots of different initial conditions, until a cone appears in the phase portrait.

ii) *design approach*: the purpose of this method is the identification of a specific behaviour of the system without explicit integration of the equations of motion. Hence, *some* mechanical parameters are considered known, while the determination of the values of the remaining ones, for which an invariant cone is present, is the aim of this approach. This procedure is analogous to a bifurcation analysis, in which the free parameters are tuned so that the desired qualitative behaviour of the solution $\boldsymbol{y}(t)$ is determined *a priori*, without any explicit calculation of a particular solution of an Initial Value Problem.

From an engineering perspective, the determination of the solution of a dynamical system is not enough, since the parametric design of the structure plays an essential role in the analysis of mechanical systems and the determination of the structural parameters that yield a certain behaviour is crucial to make the mathematical model a useful tool for real applications.

Therefore, the so-called design approach has been investigated in this Thesis and some new results have been found following this procedure. In fact, most of the papers dealing with this specific topic, especially those with a strong mathematical background, are focused on the *existence* of a special behaviour, while the determination of *how* the wanted performance can be reached is completely neglected. The innovative approach, derived from an engineering perspective, leads to the numerical techniques exposed below. In the following Section 5.1.2, the analysis on the existence of invariant cones in a 2 d.o.f. mechanical system, composed of two stable subsystems, will be performed using the design approach, determining a general procedure that could in principle be extended to study more general mechanical structures with a greater number of degrees of freedom.

5.1.2 Description of the numerical algorithm

Condition (4.9), that must be fulfilled to determine the existence of an invariant cone in the phase portrait of a 2 d.o.f. mechanical system described by the equations of motion in the form (4.1), cannot be generally solved with an analytical procedure. In fact, equation (4.9) defines a nonlinear eigenvalue problem, because the matrix exponentials depend on the eigenvectors, through the intersection time intervals $t^{\pm}(\boldsymbol{x})$. Moreover, the switching relations from which the intersection times can be computed is still nonlinear in terms of the initial position $\boldsymbol{x}$, on the switching manifold. Hence, a numerical approach is necessary for the solution of this problem.

The starting point for the design of this numerical algorithm is the choice of the terms that are considered *a priori* known in equation (4.9). In particular, assuming that both $(-)$ and $(+)$ subsystems are stable, so that they can be described by matrix exponentials in the form (3.38), the total number of parameters is equal to eight, namely $a_{1,2}^{\pm}$ and $\beta_{1,2}^{\pm}$. Moreover, in this approach also the quantities t^{-} and t^{+} are considered additional "free

parameters", that can be fixed through the switching rules, imposing the fulfilment of the two relations (4.5) rewritten below

$$\begin{aligned} t^-(\boldsymbol{x}) &= \inf\left\{t>0 : \boldsymbol{e}_1 \cdot e^{\boldsymbol{A}^- t}\boldsymbol{x} = 0\right\}, \\ t^+(\boldsymbol{\xi}) &= \inf\left\{t>0 : \boldsymbol{e}_1 \cdot e^{\boldsymbol{A}^+ t}\boldsymbol{\xi} = 0\right\}. \end{aligned} \tag{5.1}$$

Let's observe that equations (5.1) must be added to the set of equations (4.9), to close the problem when t^- and t^+ are considered additional unknown and not simple variables being functions of the starting point $\boldsymbol{x}$.

In this numerical algorithm, the eight parameters in the matrix exponential are assumed to be *a priori* fixed, while the quantities t^- and t^+ are considered the only unknowns of the problem,[1] since the relations between the intersection time and the eigenvector can simply be deduced by the definition of the Poincaré halfmaps (4.4), rewritten below for the sake of simplicity,

$$\boldsymbol{\xi} = e^{\boldsymbol{A}^- t^-}\boldsymbol{x}, \qquad\qquad \boldsymbol{\eta} = e^{\boldsymbol{A}^+ t^+}\boldsymbol{\xi}.$$

The aim of this algorithm is the determination of the couples $\{t^-, t^+\}$ that fulfil all the nonlinear equations (4.9) and (5.1) of the problem. In a further step, from the couples of time intervals, the eigenvalues and eigenvectors of equation (4.9) can be determined, completely describing the geometry of the invariant cone. Too many equations seems to be present in the problem for only two unknowns $t^\pm$, if both equations (4.9) and (5.1) need to be imposed. However, the reduced 3×3 formulation of the Po-

[1] Actually, this assumption on the known and unknown parameters may be misunderstood, leading the Reader to refer to this procedure as a *check approach* and not as a *design approach*, see Section 5.1.1. On the contrary, this is not true, since it is simply an operative choice of the parameters, yielding a more general solution to the problem. In fact, together with the geometrical, mechanical, and load parameters, two further variables must be considered in the mathematical model, namely t^- and t^+, describing the actual "shape" of the invariant cone. While the numerical values of the eight parameters of the structure, $a^\pm_{1,2}$ and $\beta^\pm_{1,2}$, can easily be fixed on the basis of physical constraints, the choice of the two time intervals is more complex, since fixing their values means that only the existence of a *specific* invariant cone is sought. For this reason, the described strategy has been considered more convenient: the search for the presence of an invariant cone is free and a *generic* invariant manifold can be detected, while the structural parameters can be chosen in such a way they span a proper range of values, in a sort of numerical bifurcation analysis.

incaré map can be used to avoid the introduction of the same constraint more than once.

First of all, let's rewrite the equations of the problem in such a way the intermediate point $\boldsymbol{\xi}$ becomes the fundamental unknown, describing the whole geometry of the cone, hence

$$\boldsymbol{x} = (e^{\boldsymbol{A}^- t^-})^{-1}\boldsymbol{\xi}, \qquad \boldsymbol{\eta} = e^{\boldsymbol{A}^+ t^+}\boldsymbol{\xi}, \qquad e^{\boldsymbol{A}^+ t^+}\boldsymbol{\xi} = \mu(e^{\boldsymbol{A}^- t^-})^{-1}\boldsymbol{\xi}, \tag{5.2}$$

where the first and the second formulas are simply a new definition of Poincaré halfmaps as functions of the coordinates of the intermediate points $\boldsymbol{\xi}$, while the third expression represents a condition analogous to (4.9), which must be solved to find the invariant cone. For the sake of convenience, let's introduce the following compact notation

$$\boldsymbol{Q}^- = (e^{\boldsymbol{A}^- t^-})^{-1}, \qquad \boldsymbol{Q}^+ = e^{\boldsymbol{A}^+ t^+},$$

so that the formulas in (5.2) can be rewritten as

$$\boldsymbol{x} = \boldsymbol{Q}^-\boldsymbol{\xi}, \qquad \boldsymbol{\eta} = \boldsymbol{Q}^+\boldsymbol{\xi}, \qquad \boldsymbol{Q}^+\boldsymbol{\xi} = \mu\boldsymbol{Q}^-\boldsymbol{\xi}.$$

The intersection time intervals $t^\pm$ are now free parameters, that must fulfil the additional equations (5.1), which can also be rewritten as a function of the intermediate point $\boldsymbol{\xi}$ as

$$\begin{aligned} t^- &= \inf\left\{t > 0 : \boldsymbol{e}_1 \cdot (e^{\boldsymbol{A}^- t})^{-1}\boldsymbol{\xi} = 0\right\} = \inf\left\{t > 0 : \boldsymbol{e}_1 \cdot \boldsymbol{Q}^-\boldsymbol{\xi} = 0\right\}, \\ t^+ &= \inf\left\{t > 0 : \boldsymbol{e}_1 \cdot e^{\boldsymbol{A}^+ t}\boldsymbol{\xi} = 0\right\} = \inf\left\{t > 0 : \boldsymbol{e}_1 \cdot \boldsymbol{Q}^+\boldsymbol{\xi} = 0\right\}. \end{aligned} \tag{5.3}$$

As pointed out from a theoretical perspective in Chapter 4, the Poincaré map are defined on points belonging to the switching manifold Σ, so the explicit formulation of the map can be written in different ways, on the basis of the chosen reference frame. At this step, in which all the theoretical properties have been defined and an explicit calculation of the position of the cone must be performed, the local reference system is the best choice, to have the lower possible number of equations. Therfore, the points $\boldsymbol{x}$, $\boldsymbol{\xi}$, and $\boldsymbol{\eta}$ can be rewritten as

$$\boldsymbol{x} = [0, x_2, x_3, x_4]^{\mathrm{T}}, \quad \boldsymbol{\xi} = [0, \xi_2, \xi_3, \xi_4]^{\mathrm{T}}, \quad \boldsymbol{\eta} = [0, \eta_2, \eta_3, \eta_4]^{\mathrm{T}},$$

as explained in formulas (4.6), while, using a block-matrix notation, the Poincaré halfmaps become

$$\begin{bmatrix} 0 \\ \hat{\boldsymbol{x}} \end{bmatrix} = \begin{bmatrix} \boldsymbol{Q}_{11}^{-} & \boldsymbol{Q}_{12}^{-} \\ \boldsymbol{Q}_{21}^{-} & \boldsymbol{Q}_{22}^{-} \end{bmatrix} \begin{bmatrix} 0 \\ \hat{\boldsymbol{\xi}} \end{bmatrix} \tag{5.4}$$

and

$$\begin{bmatrix} 0 \\ \hat{\boldsymbol{\eta}} \end{bmatrix} = \begin{bmatrix} \boldsymbol{Q}_{11}^{+} & \boldsymbol{Q}_{12}^{+} \\ \boldsymbol{Q}_{21}^{+} & \boldsymbol{Q}_{22}^{+} \end{bmatrix} \begin{bmatrix} 0 \\ \hat{\boldsymbol{\xi}} \end{bmatrix}, \tag{5.5}$$

where, since the original problem is 4-dimensional, the block matrices are $\boldsymbol{Q}_{11}^{\pm} \in \mathbb{R}$, $\boldsymbol{Q}_{12}^{\pm} \in \mathbb{R}^{1\times 3}$, $\boldsymbol{Q}_{21}^{\pm} \in \mathbb{R}^{3\times 1}$ and $\boldsymbol{Q}_{22}^{\pm} \in \mathbb{R}^{3\times 3}$, while $\hat{\boldsymbol{x}}$, $\hat{\boldsymbol{\xi}}$ and $\hat{\boldsymbol{\eta}}$ are the reduced coordinate vectors introduced in formula (4.7).

Let's now observe that the equations in the first row of (5.4) and (5.5) are identical to the conditions (5.3), that have been introduced to be able to consider $t^{\pm}$ as free parameters of the system. The only difference is that in the former equations the 'inf' operator is not present, therefore they are fulfilled also when the intersection time intervals are not as lower as possible. Since they impose essentially the same constraint on the solution, only the first row of (5.4) and (5.5) can be considered and conditions (5.3) can be neglected, being aware that the final solutions in terms of the couples $\{t^{-}, t^{+}\}$ must be filtered, in order to reject those that do not show the lowest possible intersection time intervals.

Furthermore, using the block notation above and considering the two first rows of (5.4) and (5.5) as two separate conditions, an invariant cone exists if the following equations are fulfilled

$$\begin{cases} \boldsymbol{Q}_{12}^{-}\hat{\boldsymbol{\xi}} = 0, \\ \boldsymbol{Q}_{12}^{+}\hat{\boldsymbol{\xi}} = 0, \\ \boldsymbol{Q}_{22}^{+}\hat{\boldsymbol{\xi}} = \mu \boldsymbol{Q}_{22}^{-}\hat{\boldsymbol{\xi}}, \end{cases} \tag{5.6}$$

where one must note that the matrices $\boldsymbol{Q}_{ij}^{\pm} = \boldsymbol{Q}_{ij}^{\pm}(t^{\pm}, a_{1,2}^{\pm}, \beta_{1,2}^{\pm})$ depends on the mechanical parameters and on the intersection time intervals.

From the first and second linear (and scalar) relations of (5.6), two components of the vector $\hat{\boldsymbol{\xi}}$ can be obtained as functions of the third one,

namely

$$\begin{cases} \boldsymbol{Q}_{12}^{-}\hat{\boldsymbol{\xi}} = 0 \\ \boldsymbol{Q}_{12}^{+}\hat{\boldsymbol{\xi}} = 0 \end{cases} \longrightarrow \begin{cases} \xi_2 = \xi_2(\xi_4, t^{\pm}, a_{1,2}^{\pm}, \beta_{1,2}^{\pm}) \\ \xi_3 = \xi_3(\xi_4, t^{\pm}, a_{1,2}^{\pm}, \beta_{1,2}^{\pm}) \end{cases}. \tag{5.7}$$

Moreover, the relation between $\xi_{2,3}$ and ξ_4 is known to be linear, due to the structure of the first and second equations of (5.6), hence

$$\begin{aligned} \xi_2(\xi_4, t^{\pm}, a_{1,2}^{\pm}, \beta_{1,2}^{\pm}) &= \xi_4 \cdot h_2(t^{\pm}, a_{1,2}^{\pm}, \beta_{1,2}^{\pm}), \\ \xi_3(\xi_4, t^{\pm}, a_{1,2}^{\pm}, \beta_{1,2}^{\pm}) &= \xi_4 \cdot h_3(t^{\pm}, a_{1,2}^{\pm}, \beta_{1,2}^{\pm}), \end{aligned} \tag{5.8}$$

where the two functions h_2 and h_3 of the structural parameters have been introduced. According to the results obtained in (5.7) and (5.8), the intermediate point $\hat{\boldsymbol{\xi}}$ can now be expressed as

$$\hat{\boldsymbol{\xi}} = \xi_4 \begin{bmatrix} h_2 \\ h_3 \\ 1 \end{bmatrix} = \xi_4 \, \hat{\boldsymbol{m}}(t^{\pm}, a_{1,2}^{\pm}, \beta_{1,2}^{\pm}), \tag{5.9}$$

where the vector $\hat{\boldsymbol{m}}$ has been introduced, containing the dependencies to the parameters and the time intervals.

The third and most important equation of (5.6) can now be imposed, considering the assumption in (5.9), so that

$$\boldsymbol{Q}_{22}^{+}\hat{\boldsymbol{m}}(t^{-}, t^{+}) = \mu \boldsymbol{Q}_{22}^{-}\hat{\boldsymbol{m}}(t^{-}, t^{+}), \tag{5.10}$$

where the term $\hat{\xi}_4$ can be simplified and, for the sake of convenience, the only dependency on $t^{\pm}$ have been written explicitly. Let's observe that the condition (5.10) simply represents the fact that the two vectors

$$\begin{aligned} \hat{\boldsymbol{x}} &= \boldsymbol{Q}_{22}^{-}\hat{\boldsymbol{m}}(t^{-}, t^{+}) \\ \hat{\boldsymbol{\eta}} &= \boldsymbol{Q}_{22}^{+}\hat{\boldsymbol{m}}(t^{-}, t^{+}) \end{aligned} \tag{5.11}$$

must be parallel, while the ratio of their norms must be equal to $||\hat{\boldsymbol{\eta}}||/||\hat{\boldsymbol{x}}|| = \mu$. These simple conditions on the starting and ending points can be written in terms of components, so that

$$\frac{\eta_2(t^{-}, t^{+})}{x_2(t^{-}, t^{+})} = \frac{\eta_3(t^{-}, t^{+})}{x_3(t^{-}, t^{+})} = \frac{\eta_4(t^{-}, t^{+})}{x_4(t^{-}, t^{+})} = \mu \tag{5.12}$$

and these two nonlinear equations (in particular the first and the second, since the value of μ is not known) can be solved in the two unknowns t^- and t^+.

Finally, when all the possible couples $\{t^-, t^+\}$ that represent the two intersection time intervals are detected, the detected invariant cones can be considered completely described, since the starting, intermediate, and ending points of the Poincaré maps can be computed from (5.11) and (5.9), together with the value of μ from the last equation of (5.12).

Due to the nonlinearity of problem (5.12), a general definition of the number of couples $\{t^-, t^+\}$ that can be found for a specific mechanical system is not achievable. Actually, due to the nature of the matrix exponentials (3.38) involved in the problem, multiple solutions of (5.12) are expected, because of the presence of trigonometric terms in $t^{\pm}$. For this reason, a proper algorithm has been used to solve the set of nonlinear equations (5.12), capable of detecting all the solution of a set of nonlinear equations in a given domain of the unknowns, (it is the method called `FindAllCrossings2D` in [85]) . Once a specific couple $\{t^-, t^+\} = \{\tilde{t}^-, \tilde{t}^+\}$ is found and it is classified as a valid solution, on the basis of the feasibility condition that will be described in the next Sections 5.1.3 and 5.2, all the theoretical results presented in Chapter 4 can then be applied, since the existence of a given cone $\{\tilde{\mu}, \tilde{\boldsymbol{x}}\} = \{\mu(\tilde{t}^-, \tilde{t}^+), \boldsymbol{x}(\tilde{t}^-, \tilde{t}^+)\}$ has been proved.

As a final remark, one must note that the solutions in terms of starting, intermediate, and ending points of the Poincaré halfmaps are indeterminate, due to the presence of the coefficient ξ_4 in equation (5.9), as expected since it is a nonlinear eigenvector problem. The absolute value of this term is arbitrary, due to the scale property on the intersection time intervals, however, the sign must be chosen on the basis of the initial convention in the Poincaré map. When the Poincaré map has been defined in equation (4.9), a certain order in the evolution of the map has been assumed, in particular at point $\boldsymbol{x}$ the orbit enters in the negative subdomain, while at point $\boldsymbol{\xi}$ the trajectory enters in the positive one. Hence, the final results must match this initial hypothesis, so the sign of the term ξ_4 must be chosen in such a way the orbits enters in the correct subspace, i.e. the term x_3 must be negative.

5.1.3 Feasibility of the solution: crossing condition

The fundamental assumption, on which the previous numerical method for the determination of an invariant cone is based, is the fact that the orbits are assumed to always cross the switching manifold. In Section 4.2, this problem has been deeply investigated and the solution from a computational point of view is now exposed below.

The equations (5.6) described above, which are imposed for the detection of an invariant cone in the phase portrait of a piecewise-linear dynamical system, do not take into consideration any crossing condition, so the main outputs of the numerical method, the couples $\{t^-, t^+\}$, must be filtered *a posteriori*, in order to reject the solutions producing a wrong crossing behaviour.

From a numerical perspective, the conditions expressed in (4.18), according to which an invariant cone can be defined *feasible*, can be rewritten as

$$x_3\xi_3 = (\boldsymbol{e}_3 \cdot \boldsymbol{Q}^-\boldsymbol{\xi})(\boldsymbol{e}_3 \cdot \boldsymbol{\xi}) < 0,$$
$$x_3\eta_3 = (\boldsymbol{e}_3 \cdot \boldsymbol{Q}^-\boldsymbol{\xi})(\boldsymbol{e}_3 \cdot \boldsymbol{Q}^+\boldsymbol{\xi}) > 0.$$

As reported in Section 4.2, a solution presenting a vanishing x_3, ξ_3, or η_3 is neglected in this numerical investigation, since a singular critical case has been encountered and the concept of Poincaré map is not well-defined in this special case, when the orbit representing the solution is tangent to the Poincaré section. Hence, the invariant cones described by vectors with a vanishing third component cannot be considered valid, according to this analysis.

5.2 The estimation of the time domain for the computation of the solution

The problem of the existence of an invariant cone in the phase portrait of a piecewise-linear mechanical system has been approached by solving numerically the generalised eigenvalue problem (4.9), reduced to the set of equations (5.6). The unknowns of these conditions are the intersection time intervals t^- and t^+, which have been defined in formulas (5.3). Moreover, the latter expressions have been traduced in (5.6), dropping the 'inf' operator, to be able to directly solve the problem. Therefore, some spu-

rious solution couples $\{t^-, t^+\}$ have been introduced, since, in principle, invariant cones that fulfil (5.6) could be found, but with wrong intersection times, as can be seen in Figure 5.1 in a conceptual sketch.

A wide number of possible wrong solutions can be originated from the adopted numerical algorithm (only the simplest ones are depicted in Figure 5.1), and this issue comes from the attempt to identify *a priori* the presence of an invariant cone. In fact, the solution of a nonlinear system can generally be found only following the evolution of the motion step by step. On the contrary, the presented numerical strategy is capable of detecting the presence of a cone with a simpler approach that does not involve the explicit integration of the equations of motion for the identification of the correct switching of the system. However, the disadvantage of this *design approach* is the presence of spurious solutions that must be discarded, since the evolution of the system is not directly followed in this procedure.

The elimination of the unfeasible solutions can only be done *a posteriori*, due to the complex form of the intersection conditions expressed by the first row of the equations (5.4) and (5.5), which can be explicitly written in terms of the generic intermediate point $\boldsymbol{\xi}$ as

$$\frac{\beta_1^{\pm}\beta_2^{\pm}a_1^{\pm}a_2^{\pm}\left(\cos\beta_2^{\pm}t^{\pm}-\cos\beta_1^{\pm}t^{\pm}\right)}{\beta_1^{\pm}\beta_2^{\pm}\left(a_1^{\pm}-a_2^{\pm}\right)}\xi_2+\frac{a_1^{\pm}\beta_2^{\pm}\sin\beta_1^{\pm}t^{\pm}-a_2^{\pm}\beta_1^{\pm}\sin\beta_2^{\pm}t^{\pm}}{\beta_1^{\pm}\beta_2^{\pm}\left(a_1^{\pm}-a_2^{\pm}\right)}\xi_3 + \frac{a_1^{\pm}a_2^{\pm}\left(\beta_1^{\pm}\sin\beta_2^{\pm}t^{\pm}-\beta_2^{\pm}\sin\beta_1^{\pm}t^{\pm}\right)}{\beta_1^{\pm}\beta_2^{\pm}\left(a_1^{\pm}-a_2^{\pm}\right)}\xi_4=0.$$

Since the conditions above have the same structure for both t^- and t^+, the superimposed '$\pm$' can now be dropped (being aware that the results below are valid for both systems), obtaining the transcendental equation

$$\beta_1\beta_2a_1a_2\left(\cos\beta_2t-\cos\beta_1t\right)\xi_2+\left(a_1\beta_2\sin\beta_1t-a_2\beta_1\sin\beta_2t\right)\xi_3 + a_1a_2\left(\beta_1\sin\beta_2t-\beta_2\sin\beta_1t\right)\xi_4=0. \quad (5.13)$$

One must note that the values of t for which the equation above is fulfilled depend on the initial conditions (which is represented here by the intermediate point $\boldsymbol{\xi}$). Hence, the reason why the link between the intersection time intervals and the points of the Poincaré map cannot be determined explicitly is the strongly nonlinear nature of equation (5.13).

However, this problem in the definition of the intersection time intervals as functions of the intermediate point $\boldsymbol{\xi}$ can be overcome, adopting the following strategy. For each possible solution $\{t^-, t^+\}$ of equations (5.6), obtained by the application of the numerical algorithm exposed in Section 5.1.2, the components of the intermediate point $\boldsymbol{\xi}$ can be computed. Then, using these values of the components of $\boldsymbol{\xi}$, equation (5.13) can be solved in t with well-known numerical techniques. In particular, the lowest positive solution for the time intervals $t^\pm$ is determined, which must then be compared to the initial assumption on the couple $\{t^-, t^+\}$. If at least one solution $t^\pm$ obtained by solving equation (5.13) is lower than the value of the considered time interval obtained using the numerical procedure for the detection of the invariant cone, then the couple $\{t^-, t^+\}$ must be neglected, since the cone identified by the algorithm does not consider the first intersections in the solution of the dynamical system. On the contrary, if the results of (5.6) and (5.13) agree, the detected invariant cone can be considered valid. Hence, with this procedure, only the feasible cones can be extracted from the entire set of solutions of problem (5.6).

The discussion above is based on the assumption that *all* the solutions $\{t^-, t^+\}$ can be found solving (5.6), which is certainly a strong hypothesis since we are dealing with numerical techniques. In particular, the solutions of problem (5.12) are obtained in a given time domain $t^\pm \in [0, t^\pm_{\max}]$, which cannot be an infinite domain, due to the numerical nature of the problem. Therefore, two possible issues can be identified: i) if a too small time domain is chosen, possible feasible invariant cones may not appear in the solution of (5.6), and ii) if a too big time domain is chosen, lots of efforts are spent in searching the solutions of (5.6) in areas of the domain in which the solution is not present, hence the computational time can be so high that the solution of the problem cannot be reached.

These two problems are now investigated, with the aim of defining some bounds on the time interval domain, so that all the possible correct *"first" intersections* can be found inside this bounded range of time values. In particular, for any choice of the structural parameters $a^\pm_{1,2}$ and $\beta^\pm_{1,2}$, the target is the attempt to find some special values of ξ_2, ξ_3, and ξ_4 that can

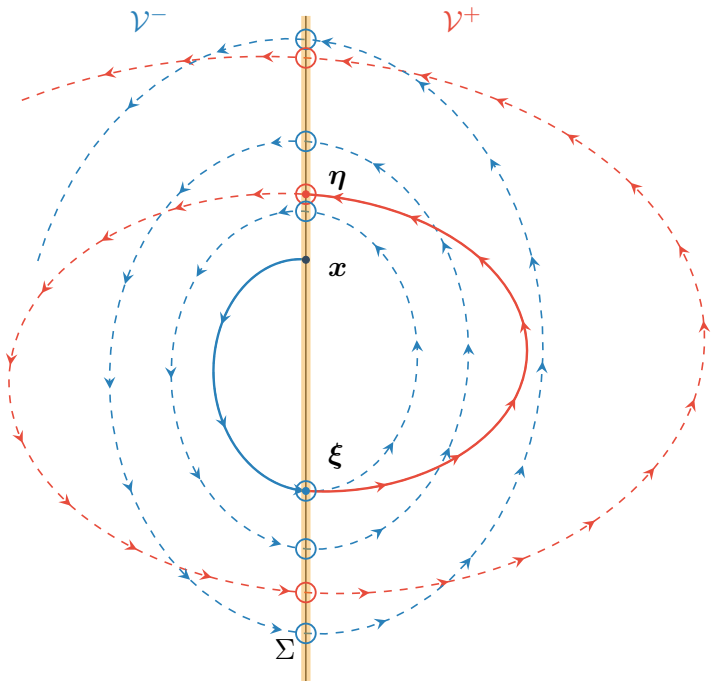

wrong solution: ξ is not the first intersection of the blue orbit with the switching manifold

wrong solution: η is not the first intersection of the red orbit with the switching manifold

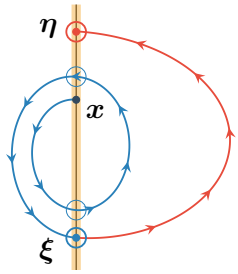

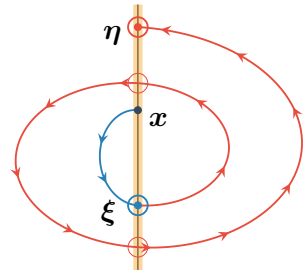

Figure 5.1: Pictorial 2D sketch of the 4D phase portrait for a piecewise dynamical system, evidencing the presence of possible wrong solutions in the described numerical algorithm, which must be discarded *a posteriori*. As can be seen in the picture on the top, multiple intersection points between the blue/red orbits and the switching manifold Σ are generally present and the computational procedure can find all these configurations, however, only the first intersection has a precise meaning and must be considered as a correct solution. In the two figures on the bottom, two examples of wrong solutions are described in detail.

be substituted into (5.13), so that the associated lowest positive solution [2] in terms of time intervals is as great as possible. In this way, provided that these values of ξ_2, ξ_3, and ξ_4 exist, the lowest positive intersection time defined by the solution of equation (5.6) for any other choice of values $\boldsymbol{\xi}$ is surely lower than the bound value defined before.

The starting point is the equation (5.13), which defines the switching condition and creates a link between the time interval t and the initial condition $\boldsymbol{\xi}$, that must now be investigated. In particular, let's observe that, since the intermediate point $\boldsymbol{\xi}$ belongs to the invariant cone, the possible values of ξ_2, ξ_3, and ξ_4 do not have to be selected in the entire phase space. On the contrary, they can be chosen, for example, only on the sphere with radius $||\boldsymbol{\xi}|| = 1$, because it is well-known, from Section 4.1.2, that the intersection time intervals are constant values for orbits lying on the invariant cone.

Thus, for the sake of simplicity, equation (5.13) can be condensed in the following form

$$\mathcal{A}\left(\cos\beta_2 t - \cos\beta_1 t\right) + \mathcal{B}\sin\beta_2 t + \mathcal{C}\sin\beta_1 t = 0, \tag{5.14}$$

where the coefficients

$$\mathcal{A} = \beta_1\beta_2 a_1 a_2 \xi_2, \quad \mathcal{B} = -a_2\beta_1\left(\xi_3 - a_1\xi_4\right), \quad \mathcal{C} = a_1\beta_2\left(\xi_3 - a_2\xi_4\right), \tag{5.15}$$

have been introduced. Let's now transform the left-hand-side of (5.14) in such a way the sine function is the only trigonometric function present in the equation, obtaining

$$\mathcal{R}_1\sin\left(\beta_1 t + \phi_1\right) = -\mathcal{R}_2\sin\left(\beta_2 t + \phi_2\right), \tag{5.16}$$

where the following parameters

$$\mathcal{R}_1 = \sqrt{\mathcal{A}^2 + \mathcal{C}^2}, \ \mathcal{R}_2 = \sqrt{\mathcal{A}^2 + \mathcal{B}^2}, \ \tan\phi_1 = -\frac{\mathcal{A}}{\mathcal{C}}, \ \tan\phi_2 = \frac{\mathcal{A}}{\mathcal{B}}, \tag{5.17}$$

have been defined. Then, let's substitute the unknown t with the new variable τ, such that

$$t = \frac{\tau}{\beta_2} - \frac{\phi_2}{\beta_2} \qquad \rightarrow \qquad \tau = \beta_2 t + \phi_2, \tag{5.18}$$

[2] Let's observe that we are investigating the evolution of the system for increasing time $t > 0$, hence all the solutions of the time intervals $t^{\pm}$, associated with the invariant cone, are assumed to be positive values.

in order to transform the fundamental equation (5.16) into

$$\sin\tau = -\frac{\mathcal{R}_1}{\mathcal{R}_2}\sin\left[\frac{\beta_1}{\beta_2}\tau - \frac{\beta_1}{\beta_2}\phi_2 + \phi_1\right].$$

After the last substitution of the following parameters

$$\alpha = -\frac{\mathcal{R}_1}{\mathcal{R}_2}, \quad \omega = \frac{\beta_1}{\beta_2}, \quad \phi = \phi_1 - \omega\phi_2, \tag{5.19}$$

the equation that represents the intersection times is finally reduced to

$$\sin\tau = \alpha\sin\left[\omega\tau + \phi\right]. \tag{5.20}$$

Now, the aim is finding an estimation of the greatest value, say $\tau_{\max}$, of the smallest positive solution of (5.20) in terms of τ, as a function of the parameters α, ω and ϕ. For this estimation, it is crucial to understand whether or not these coefficients have some bounds. The ratio ω is independent of the initial conditions so its value is defined by the structural parameters, in the range $\omega \in [0, +\infty)$. On the contrary, α and ϕ depend on the initial conditions $\boldsymbol{\xi}$, so, in principle, they could have some bound, since the intermediate point is assumed to be on the unit sphere in the phase space. In particular, trivial bounds for the phase ϕ can be found, i.e. $\phi \in [0, 2\pi)$, because of the periodicity of the sine function. Moreover, some calculations on the possible values of α can be performed, which are described in Appendix B, so the range for this coefficient is $\alpha \in (-\infty, 0)$.

To find a coarse estimation of $\tau_{\max}$ from (5.20), the two functions

$$y(\tau) = \sin\tau,$$
$$y(\tau) = \alpha\sin(\omega\tau + \phi),$$

have been plotted in a plane $0\tau y$, as depicted in Figure 5.2, being aware that the solution of (5.20) can be found as the intersection points between the two curves. As can be seen in Figure 5.2, the following two cases have been considered separately: $|\alpha| \leq 1$ (*case 1*) and $|\alpha| > 1$ (*case 2*).

When *case 1* is considered for a particular value of α, such that $|\alpha| \leq 1$, the function $y = \sin\tau$ (red curve) is taken as a reference and the function $y = \alpha\sin(\omega\tau + \phi)$ (blue curve) is plotted varying the parameters ω and ϕ. The blue curves have an amplitude lower than 1, so it is clearly visible that

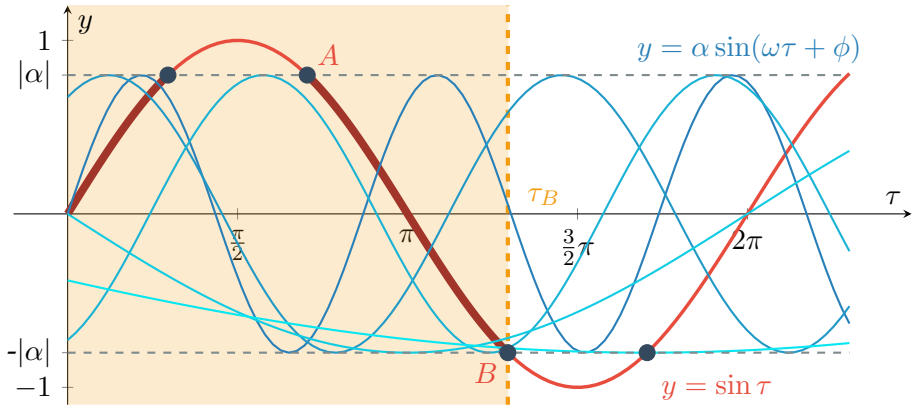

(a) *case 1*

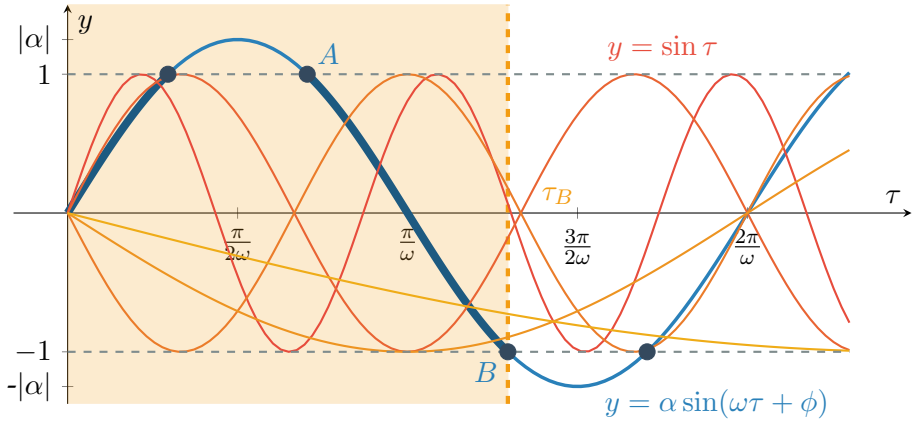

(b) *case 2*

Figure 5.2: Plot of the functions $y = \sin\tau$ (red lines) and $y = \alpha\sin(\omega\tau + \phi)$ (blue lines) for different values of the parameters α, ω, and ϕ. In Figure 5.2a (*case 1*, $|\alpha| \leq 1$) the red function $y = \sin\tau$ has been considered as a reference, while the parameters ω and ϕ of the blue function are changed in order to find the intersection point between the red and blue curves, having the maximum value of τ. In Figure 5.2a (*case 2*, $|\alpha| > 1$) the blue function $y = \alpha\sin(\omega\tau + \phi)$ has been considered as a reference (with $\phi = 0$, the worst possible configuration) and the parameter ω is changed in order to find the intersection between the red and blue curves, having the maximum value of τ. The first crossing point between the red and blue curve is always in the orange areas, so τ_B is a good bound for the time interval.

the intersections between the functions must be in the segments of the red curve associated with $|y| \leq |\alpha|$ (these segments will be called *crossing areas* and they have been underlined with a greater thickness in the red curve). Furthermore, the segment of the red curve between the points A and B covers all the values of y in the range between $-|\alpha|$ and $|\alpha|$, hence all the intersections with $\tau > \tau_B$ cannot be the first crossing points. Therefore, the value τ_B can be considered a good bound for the given value of α.

Analogous considerations can be done for *case 2*, but now the role of the curves is inverted: the blue function $y = \alpha \sin(\omega\tau + \phi)$ is considered the reference plot and it fixed, while the red curve $y = \sin\tau$ varies with respect to parameters ω and ϕ, for a given value of α. One must note that in Figure 5.2b, the values on the τ-axis contain the parameter ω, so, in this way, the blue curve can always be represented in the same way and the red curve changes as a function of ω. For the same reasons exposed for *case 1*, the maximum value of τ that can be assumed as a bound is τ_B. One must note that now the phase ϕ can be different from zero, so this case is more complex with respect to the previous one, due to the fact that the reference blue curve can be plotted in different ways, i.e. it can translate horizontally along τ-axis, on the basis of this parameter. However, the worst case is when $\phi = 0$, in fact, if ϕ were negative, the value of τ_B would increase, but the first intersection would certainly be in the crossing area different from AB, because the red curves always pass through the origin (so, in this case, the estimation of τ_B would be meaningless). On the contrary, if ϕ were positive, the point B would obviously translate to lower values of τ, leading to an estimation of τ_B that is not the worst condition.

The value of τ_B clearly depends on α, so now this parameter must be tuned to have the highest value of the intersection time. The value $\alpha = -1$ is obviously related to the worst condition, in fact, for both cases, the distance along the τ-axis between the points A and B decreases when α is different from -1, therefore the value of τ_B decreases itself.

For the reasons described above, the maximum value of τ that can be assumed as a bound in the numerical algorithm for the detection of invariant cones, can be estimated as

$$\tau_{\max} = \max\left\{\tau_{B,1}, \tau_{B,2}\right\} = \max\left\{\frac{3}{2}\pi, \frac{3\pi}{2\omega}\right\} = \max\left\{\frac{3}{2}\pi, \frac{3\beta_2}{2\beta_1}\pi\right\},$$

where $\tau_{B,1}$ and $\tau_{B,2}$ are the values of τ_B for *case 1* and *case 2*, respectively.

Using the definition (5.18) for the variable τ, the maximum time interval associated with the first crossing is

$$t_{\max} = \max_{\phi_2} \left\{ \frac{\tau_{\max}}{\beta_2} - \frac{\phi_2}{\beta_2} \right\},$$

where another $\max$ operator has been introduced to take into account that t varies with respect to the angle ϕ_2 and the worst condition must be identified. Let's observe that $\phi_2 \in [0, \pi]$, because of the periodicity of the tangent trigonometric function, which defines the angle ϕ_1 and ϕ_2. The dependency of $t_{\max}$ on the parameter ϕ_2 can be simplified, observing that this relation is linear, hence the maximum value of t can be reached for the minimum or maximum value of ϕ_2, leading to the following definition

$$t_{\max} = \max \left\{ \frac{\tau_{\max}}{\beta_2}, \frac{\tau_{\max}}{\beta_2} - \frac{\pi}{\beta_2} \right\}.$$

However, the parameter β_2 can always be assumed positive (it is the imaginary part of one eigenvalue of the dynamical system), so the worst condition is clearly for the value $\phi_2 = 0$, hence

$$t^{\pm}_{\max} = \frac{\tau_{\max}}{\beta_2^{\pm}} = \max \left\{ \frac{3\pi}{2\beta_2^{\pm}}, \frac{3\pi}{2\beta_1^{\pm}} \right\},$$

where also the dependency of the subdomain has been introduced in this last formula.

Finally, the numerical procedure exposed in Section 5.1.2 can now be used to compute the solution couples $\{t^-, t^+\}$, within a time interval domain $[0, t^-_{\max}] \times [0, t^+_{\max}]$. One must note that this estimation of the maximum time interval does not assure that in this domain *all* the couples $\{t^-, t^+\}$ found by the algorithm are feasible solutions. In fact, some of them could eventually be a second intersection with the switching manifold, since in general there could be a crossing area for values $\tau < \tau_A$, see Figure 5.2, where a first intersection may occur. Therefore, the numerical check on the first intersection introduced in the first part of Section 5.2 must be performed.

5.3 Conclusions

The problem of detecting invariant cones in a 4-dimensional phase space associated with a 2 d.o.f. piecewise-smooth mechanical system is now completely solved, since a numerical method has been developed and described in Section 5.1.2. This computational algorithm has been deeply investigated and it is the basis for the numerical results obtained in the next Chapter 6. The most relevant issues in this numerical approach have been described and solved in Section 5.1.3 and 5.2, where the conditions of crossing and the estimate of the lowest intersection time intervals for the two subsystems have been investigated.

CHAPTER 6

Numerical results and simulations

"A mathematician plays a game and invents the rules. A physicist plays a game whose rules are dictated by Nature. As time goes by it is more and more evident that the rules the mathematician finds appealing are precisely those Nature has chosen."

Paul A. M. Dirac

A numerical algorithm has been developed in Chapter 5, to detect the presence of invariant cones in the phase portrait of piecewise-linear systems. Once mechanical and geometrical parameters are assigned, the only unknowns of the problem are the intersection time intervals t^- and t^+, from which the geometrical description of the possible cone can be derived (i.e. the points $\boldsymbol{x}$, $\boldsymbol{\xi}$ and $\boldsymbol{\eta}$), together with the stability of the considered fixed point (given by the multiplier μ).

The aforementioned numerical procedure is employed in the present Chapter to detect the existence of an invariant cone for some specific sets of design parameters for the reference discontinuous structure composed of a doubly circular profile, introduced in Section 3.2. In the cases exposed below, the algorithm provides the existence of several invariant cones, but only the unstable one is described, revealing a multiplier $\mu > 1$. Let's remark that, according to this numerical method, the computation of the invariant cone can be performed *a priori*, without the explicit integration of the equations of motion, hence the instability can be deduced without

the determination of the evolution in time of the generalised coordinates.

The presence of an invariant cone in a given mechanical system is then checked, integrating the Initial Value Problem defining the mathematical model of the mechanical system, in which the initial conditions are assumed to belong to the invariant set, namely $\boldsymbol{y}_0 = \boldsymbol{x}$. The plots of the time evolution of the Lagrangian generalised coordinates and the phase portraits have been obtained through a Runge-Kutta scheme on the linear or nonlinear set of first order ODEs, see [12, 79, 91].

The numerical algorithm for the detection of the invariant cones has been tested and validated through several numerical simulations, showing in all cases an excellent agreement in results obtained with different methods. The attractivity of the considered cone was also checked, through perturbations in the initial conditions obtained from the computational procedure, and all the examples have confirmed the theoretical predictions on the attractivity of the invariant set, exposed in Section 4.3.3.

As a final remark, all the numerical analyses presented below refer to the non-dimensional formulation defined by equations (3.19) and (3.22). However, the numerical method described in Chapter 5 has been developed using a general notation that is not specific for the non-dimensional case. For this reason, all the quantities that appear in the following numerical outcomes must be considered in this sense, including all the generalised coordinates $\overline{\xi}$ and $\overline{\phi}$ and the intersection time intervals $t^{\pm}$, which actually has to be read as $\tau^{\pm}$, since they refer to the non-dimensional time variable.

6.1 Linearised behaviour of the non-smooth structure

6.1.1 Numerical solution of the reference mechanical system

Let's consider the piecewise structure with a doubly circular profile described in Section 3.2 and let's assume the following values for the mechanical and geometrical non-dimensional parameters

$$\zeta_+ = \frac{R_+}{l} = 0.6, \quad k = \frac{k_1 l^2}{k_2} = 0.3, \quad \gamma = \frac{Fl}{k_2} = 0.06,$$
$$\sigma = \frac{y_s}{l} = 0, \qquad \Theta = \frac{\rho l^3}{T^2 k_2} = 1, \quad \chi = \frac{\zeta^-}{\zeta^+} = 6.$$

This example will be used as a reference, because it contains all the most relevant features of this kind of unstable structural behaviours. For the above geometry and loading conditions, an attractive invariant cone exists for the piecewise-linear system, revealing an unstable equilibrium configuration located in the origin of the phase space. This cone is defined by the following initial conditions

$$\boldsymbol{y}_0 = \boldsymbol{x} = \left[\overline{\xi}(0), \overline{\phi}(0), \dot{\overline{\xi}}(0), \dot{\overline{\phi}}(0)\right] = \xi_4 \left[0, 0.008541, 0.372225, -0.928103\right],$$

where the value of the parameter ξ_4 must be fixed according to what have been reported at the end of Section 5.1.2. In particular, the modulus can be set to 1 and the sign must be chosen according to the general hypothesis that the orbit passing through point $\boldsymbol{x}$ must enter in the $(-)$ subdomain, hence $\xi_4 = -1$. For this specific case, the fixed point is unstable, since the multiplier is $\mu = 1.0799962$, while the intersection time intervals (calculated using the algorithm for the detection of the invariant cone and then confirmed by the numerical integration of the equations of motion) are

$$t^- = 0.637107, \qquad \text{and} \qquad t^+ = 2.981694.$$

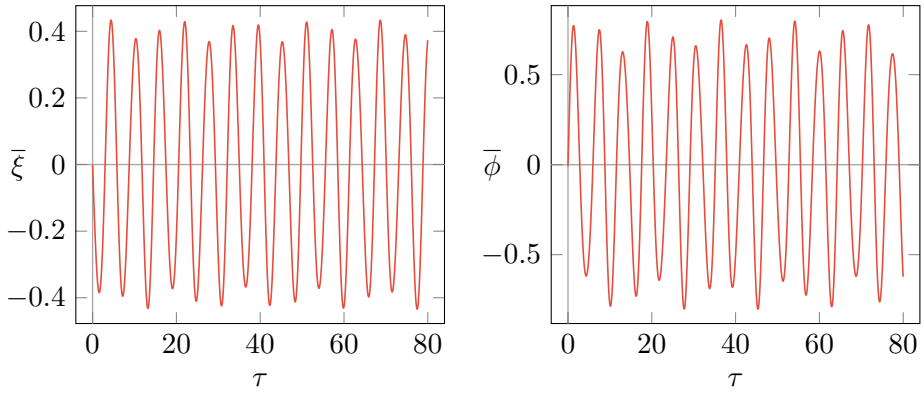

Figure 6.1: Time evolution of the non-dimensional generalised coordinates $\overline{\xi}$ and $\overline{\phi}$ as a function of the non-dimensional time τ, when only the linearised $(+)$ subsystem is analysed. The plots reveal a stable behaviour of the linearised positive subsystem.

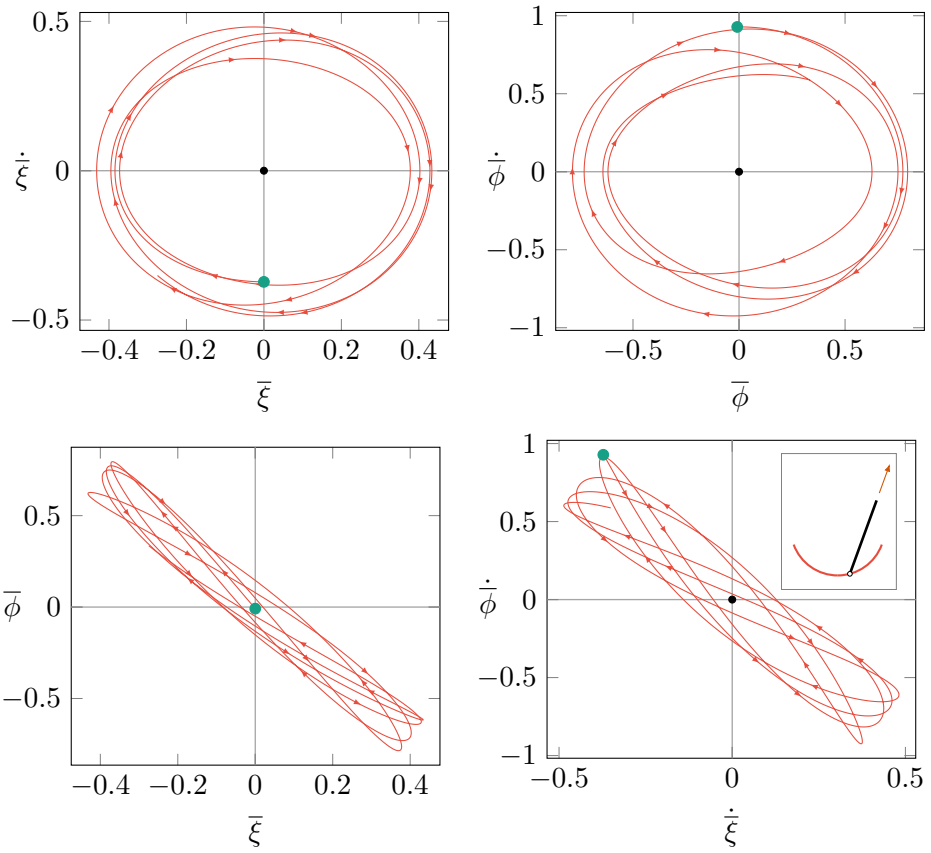

Figure 6.2: Phase portraits for the single linearised $(+)$ subsystem near the equilibrium configuration (black dot) located in the origin. The initial conditions of the plotted orbit (green dot) are those defining the unstable invariant cone for the piecewise-smooth system. The plots show a stable behaviour of the linearised positive subsystem.

The flutter critical loads for the single smooth subsystem that compose the complete piecewise structure can be calculated from equations (3.47) and (3.48), as

$$\gamma_{fl}^{-} = -1.83477, \qquad \text{and} \qquad \gamma_{fl}^{+} = 0.774567,$$

for the $(-)$ and $(+)$ subsystem, respectively. Therefore the subsystems are both stable when considered separately, since the external load is $\gamma = 0.06$, which is located in the stable region of the bifurcation parameter. The stability of each smooth subsystem can be observed in the results plotted in Figures 6.1 and 6.3, where the time evolution of the generalised coordinates is depicted, as well as in Figures 6.2 and 6.4 in terms of the evolution of the orbits in the phase space.

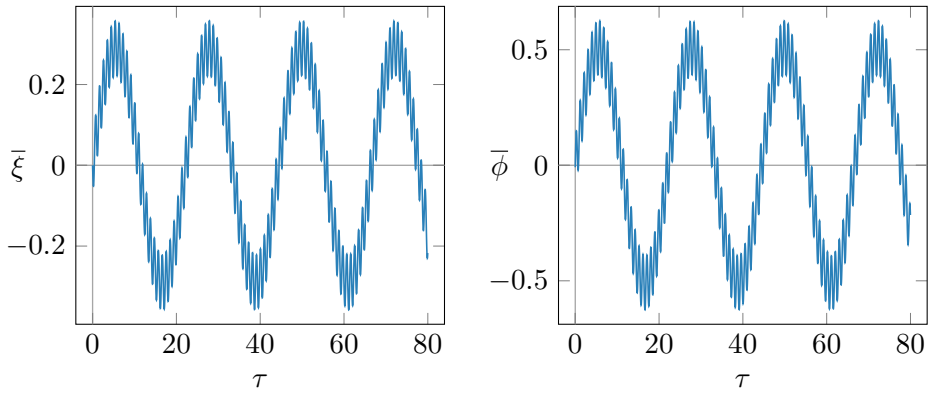

Figure 6.3: Time evolution of the non-dimensional generalised coordinates $\overline{\xi}$ and $\overline{\phi}$ as a function of the non-dimensional time τ, when only the linearised $(-)$ subsystem is analysed. The plots reveal a stable behaviour of the linearised negative subsystem.

The phase portraits refer to the linearised solution in the vicinity of the origin, where the equilibrium point is located. It is clearly visible that the orbit with initial conditions in the neighbourhood of the equilibrium point evolves in time still remaining in the neighbourhood of the origin, revealing a stable behaviour of these linearised dynamical systems.

Although the two subsystems forming the piecewise-linear structure are separately stable, the combination of them clearly reveals an unstable

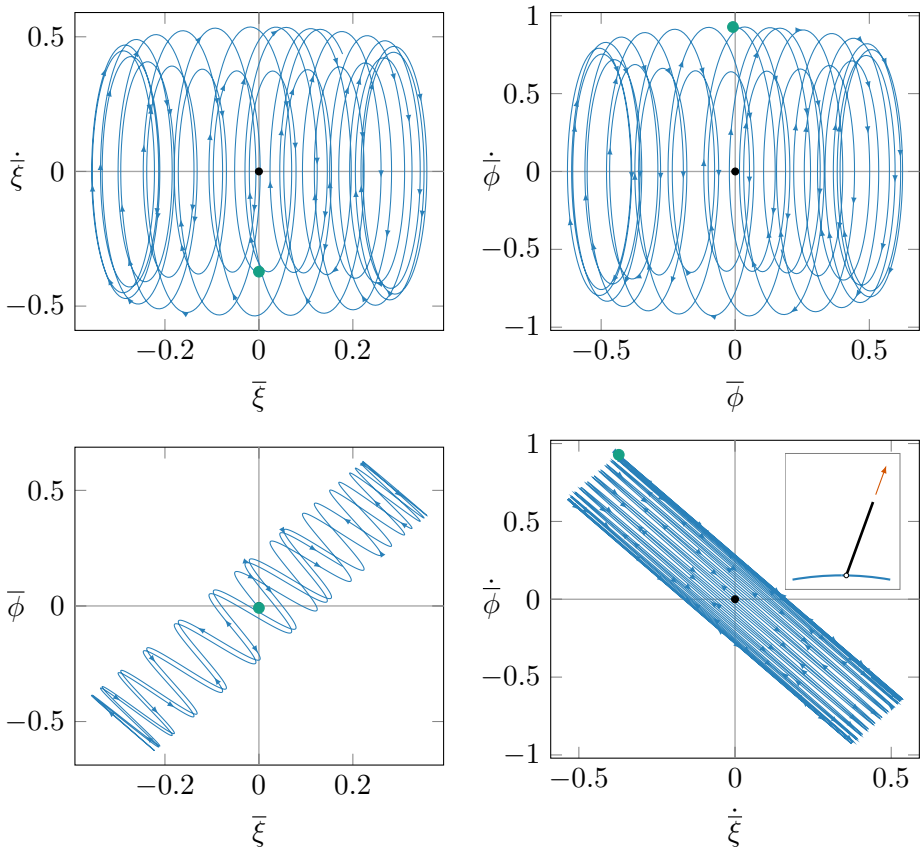

Figure 6.4: Phase portraits for the single linearised $(-)$ subsystem near the equilibrium configuration (black dot) located in the origin. The initial conditions of the plotted orbit (green dot) are those defining the unstable invariant cone for the piecewise-smooth system. The plots show a stable behaviour of the linearised positive subsystem.

behaviour, as can be appreciated from the following outcomes. The motion of the piecewise structure is sketched in Figure 6.5, for $\tau \in [0, 50]$. It is clearly visible that the displacement of the rigid bar evolves in time so that the vertical equilibrium configuration with the hinged support in the discontinuity of the profile is left.

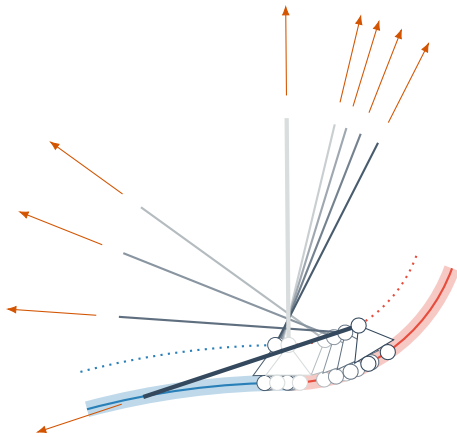

Figure 6.5: A sketch of the motion of the linearised piecewise system with a doubly circular profile, for a non-dimensional time $\tau \in [0, 50]$, with initial conditions near the straight equilibrium configuration. As can be seen from the positions of the rigid bar at given times (from light grey at $\tau = 0$ to black at $\tau = 50$), the undeformed configuration with $(\xi, \phi) = (0, 0)$ is unstable.

Furthermore, the evolution in time of the non-dimensional generalised coordinates $\overline{\xi}(\tau)$ and $\overline{\phi}(\tau)$, plotted in Figure 6.6, reveals an exponential increase of the amplitude. This evolution in time is analogous to the behaviour of a smooth mechanical system undergoing flutter instability, hence, this case can be considered a *flutter-like* instability for piecewise systems, originated by stable subsystems.

The unstable invariant cone can be seen in the 2D and 3D phase portraits, see Figure 6.8 and 6.7. The complete cone cannot be visualised, since it is a 3D hypersurface embedded in a 4D space, however, the projections of the hyper-cone can be plotted and this "decomposed" behaviour can be appreciated. In particular, one can observe that the orbits with initial conditions in the neighbourhood of the origin evolves spiralling out, leading

to an unstable behaviour. Since the cone is also attractive, a set of initial conditions can be found, with non-zero measure, so that this unexpected "theoretical" behaviour becomes a realistic evolution of a physical system.

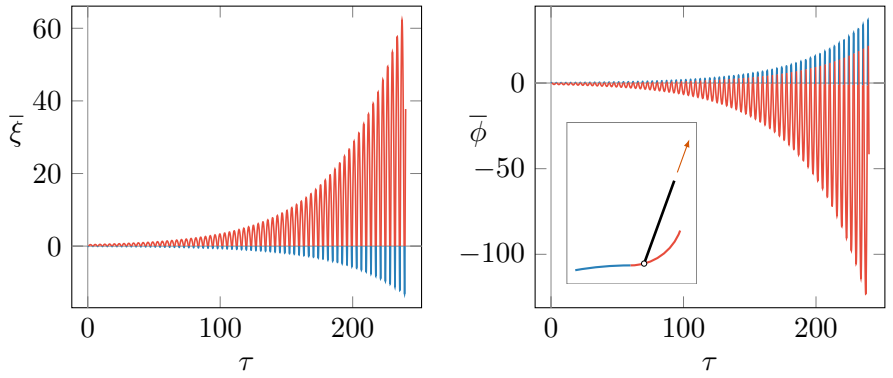

Figure 6.6: Time evolution of the non-dimensional generalised coordinates $\overline{\xi}$ and $\overline{\phi}$ as a function of the non-dimensional time τ, for the structure with a doubly circular profile. An exponential growth of the amplitude of the generalised coordinates denotes a *flutter-like* instability for the piecewise-linear model.

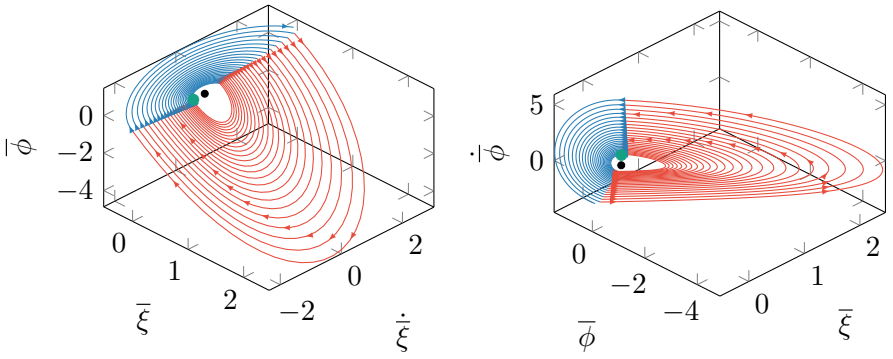

Figure 6.7: A 3D representation of the phase portraits near the equilibrium configuration (black dot) located in the origin, for the structure with a doubly circular profile. The initial conditions of the plotted orbit (green dot) define an unstable invariant cone spiralling out from the origin, denoting a *flutter-like* instability for the piecewise-linear model.

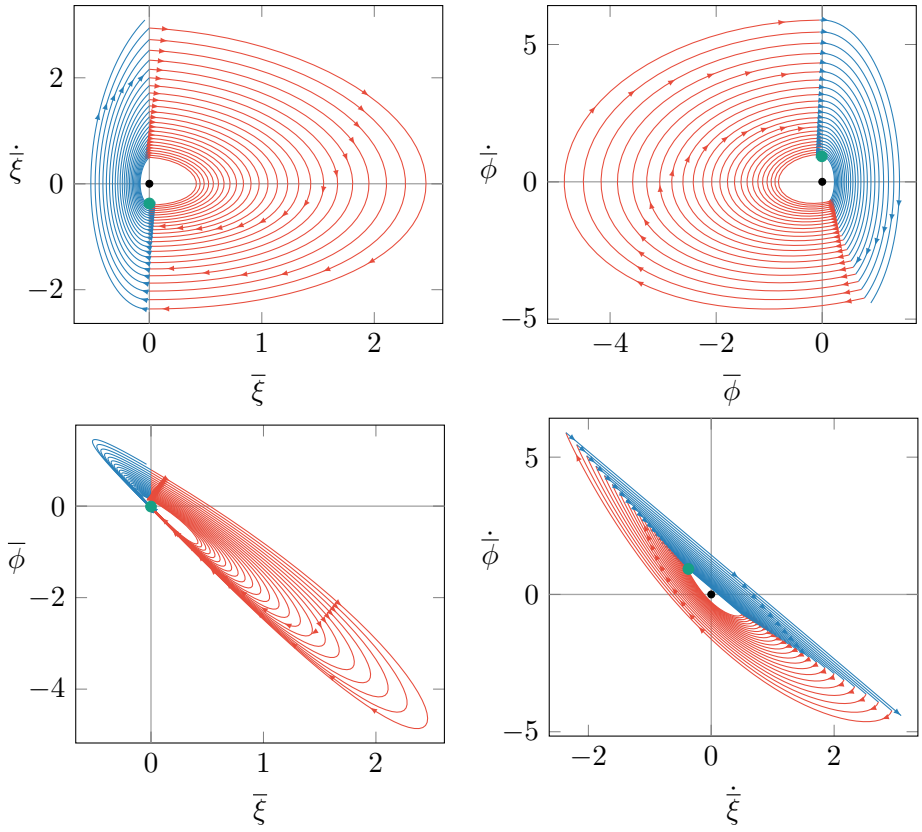

Figure 6.8: A 2D representation of the phase portraits near the equilibrium configuration (black dot) located in the origin, for the structure with a doubly circular profile. The initial conditions of the plotted orbit (green dot) are those defining the unstable invariant cone, which is clearly visible from the orbit that spirals out from the origin, denoting a *flutter-like* instability for the piecewise-linear model.

6.1.2 Invariant cone for other combinations of parameters: tensile and compressive follower forces

The reference problem considered in the previous Section 6.1.1 is an example of instability related to the discontinuity present in the structure. Considering other parameter combinations, the phase portraits are generally different from those examined in 6.1.1. However, in all cases, they can be considered topological equivalent, see Definition 15 in Section 2.1.5, hence the form of instability is actually the same.

It is interesting to note that non-smooth structures reveal an unstable behaviour both for tensile and compressive follower forces, a property that is not common in smooth systems. This particular aspect will be outlined in the following example, where the set of design parameters

$$\zeta_+ = 0.5 \quad k = 0.1 \quad \sigma = 0 \quad \Theta = 1 \quad \chi = 2,$$

has been considered, together with the two load parameters

$$\gamma^A = -1.5 \qquad \text{and} \qquad \gamma^B = 0.75,$$

where γ^A (γ^B) represents a compressive (tensile) follower force. For this combination of mechanical parameters, the critical flutter loads for $(-)$ and $(+)$ subsystems are

$$\gamma_{fl}^- = -2.62091 \qquad\qquad \gamma_{fl}^+ = 1.10455$$

so both the subsystems are stable.

When the case with *compressive* load is considered, the unstable invariant cone is described by the vector of initial conditions

$$\boldsymbol{y}_0^A = \boldsymbol{x}^A = \left[\overline{\xi}(0), \overline{\phi}(0), \dot{\overline{\xi}}(0), \dot{\overline{\phi}}(0)\right] = [0, -0.005946, -0.608652, 0.793415]$$

and the associated multiplier is equal to $\mu^A = 2.481825$, denoting a high growth rate of the modulus of the phase vector $\boldsymbol{y}(t)$ after each time period $t^- + t^+$, namely about 248%, if compared to that of the reference solution described in Section 6.1.1, which was only 7.99%. The intersection time intervals calculated for this case are

$$t_A^- = 9.79729, \qquad\qquad t_A^+ = 1.595401.$$

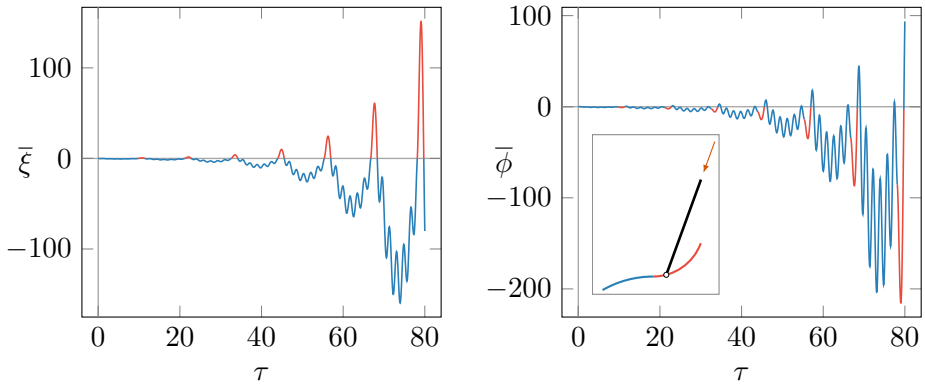

Figure 6.9: Time evolution of the non-dimensional generalised coordinates $\overline{\xi}$ and $\overline{\phi}$ as a function of the non-dimensional time τ, for the structure with a doubly circular profile subjected to the compressive load $\gamma^A = -1.5$. An exponential growth of the amplitude of the generalised coordinates is clearly visible, denoting a *flutter-like* instability for the piecewise-linear model. In this specific case the orbit remains for a longer time in the negative subspace, revealing a more irregular path, with respect to the reference solution exposed in Section 6.1.1.

For the case of *tensile* follower force, the initial condition that leads to the presence of an unstable invariant cone is

$$\boldsymbol{y}_0^B = \boldsymbol{x}^B = \left[\overline{\xi}(0), \overline{\phi}(0), \dot{\overline{\xi}}(0), \dot{\overline{\phi}}(0)\right] = [0, 0.086944, -0.360442, 0.928721]\,,$$

while the multiplier is equal to $\mu^B = 2.486877$, very closed to the value for the compressive load, hence the growth rate of the modulus of the solution $\boldsymbol{y}(t)$ after each cycle is almost the same for these two cases. The intersection time intervals are

$$t_B^- = 0.311784, \qquad t_B^+ = 4.132277.$$

The time evolution and phase portraits for the piecewise structure subjected to compressive and tensile forces is depicted in Figures 6.9 and 6.10 for the load γ^A and in Figures 6.11 and 6.12 for γ^B. As can be seen from the phase portraits, the second case with tensile load is clearly similar to the reference solution, with an obvious higher growth rate due to the difference in the multiplier μ. On the contrary, the phase portraits depicted in

Figure 6.10, referring to the case of a compressive follower force, are more irregular with respect to the reference solution. However, despite the irregularity in the trajectories, these two cases are topology equivalent.

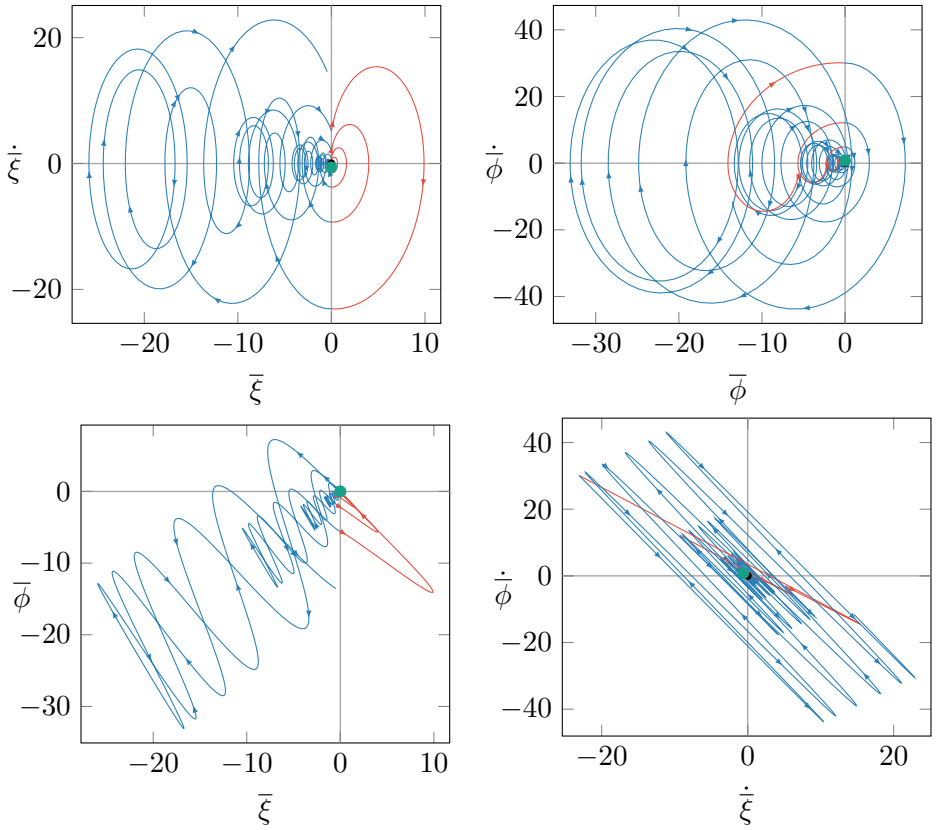

Figure 6.10: Phase portraits near the equilibrium configuration (black dot) located in the origin, for the structure with a doubly circular profile subjected to the compressive load $\gamma^A = -1.5$. The initial conditions of the plotted orbit (green dot) are those defining the unstable invariant cone, which is clearly visible from the orbit that spirals out from the origin, denoting a *flutter-like* instability for the piecewise-linear model. In this specific case the orbit remains for a longer time in the negative subspace, revealing a more irregular path, with respect to the reference solution exposed in Section 6.1.1.

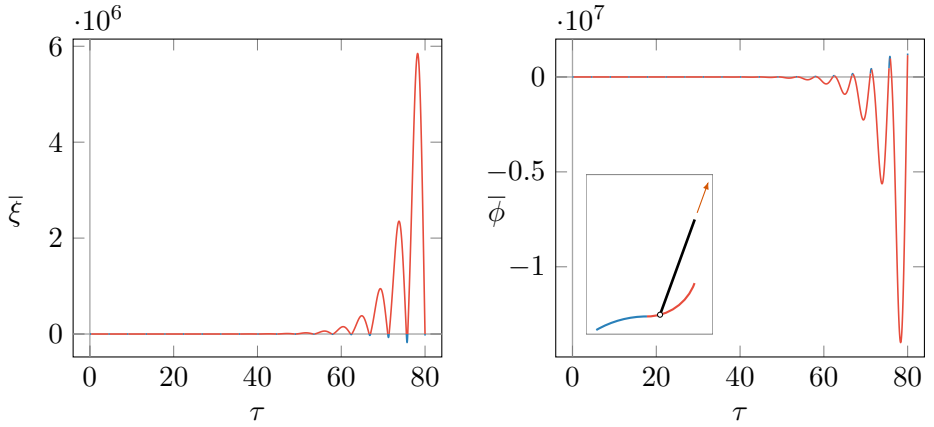

Figure 6.11: Time evolution of the non-dimensional generalised coordinates $\overline{\xi}$ and $\overline{\phi}$ as a function of the non-dimensional time τ, for the structure with a doubly circular profile subjected to the tensile load $\gamma^B = 0.75$. An exponential growth of the amplitude of the generalised coordinates is clearly visible, denoting a *flutter-like* instability for the piecewise-linear model.

6.2 Nonlinear solution of the non-smooth structure

6.2.1 Numerical solution of the reference mechanical system

All the theoretical and numerical results concerning the existence of an invariant cone are based on the assumption that the subsystems that compose the structure have been linearised. As presented in Section 2.1.3 and 4.4, the linearisation of the equations of motion in the neighbourhood of an equilibrium configuration is a classical strategy for determining whether or not the considered fixed point is stable, since, through Theorem 2 described in Section 2.1.3, the stability of a smooth nonlinear system can be deduced by the linearised one.

Unfortunately, this strategy cannot be adopted for the analysis of non-conservative piecewise systems, thus the characterisation of an equilibrium configuration for a nonlinear piecewise-smooth system becomes a cumbersome task, from a theoretical point of view.

However, Weiss *et al.* [86] discovered a possible extension of the classical approach to non-smooth system, as was explained in Section 4.4. In

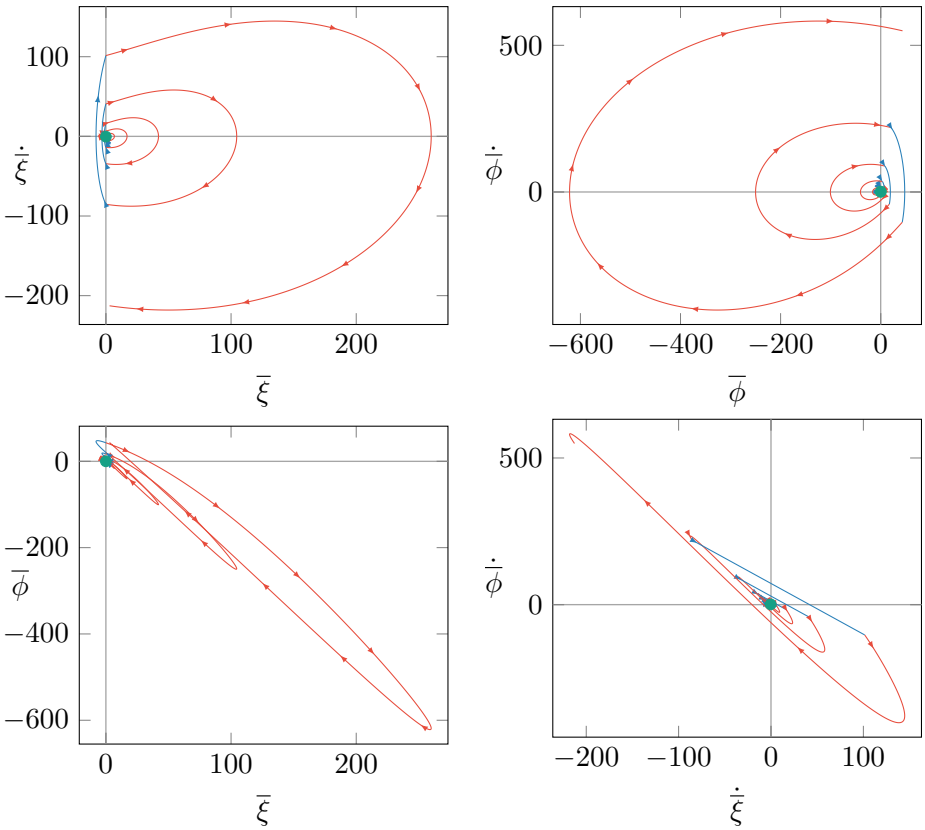

Figure 6.12: Phase portraits near the equilibrium configuration (black dot) located in the origin, for the structure with a doubly circular profile subjected to the compressive load $\gamma^B = 0.75$. The initial conditions of the plotted orbit (green dot) are those defining the unstable invariant cone, which is clearly visible from the orbit that spirals out from the origin, denoting a *flutter-like* instability for the piecewise-linear model.

particular, if an invariant cone for the piecewise-linear case is detected, then a *cone-like* invariant set can be found near the equilibrium configuration, which is a sort of deformed cone presenting the same properties of the original invariant manifold defined in piecewise-linear systems.

The reference structure studied in its linearised formulation in Section 6.1.1 is now analysed, integrating the set of nonlinear equations of motion (3.22). In particular, the behaviour of the nonlinear system near the origin is investigated and a comparison with the linearised case is presented, that confirms the theoretical results in [86].

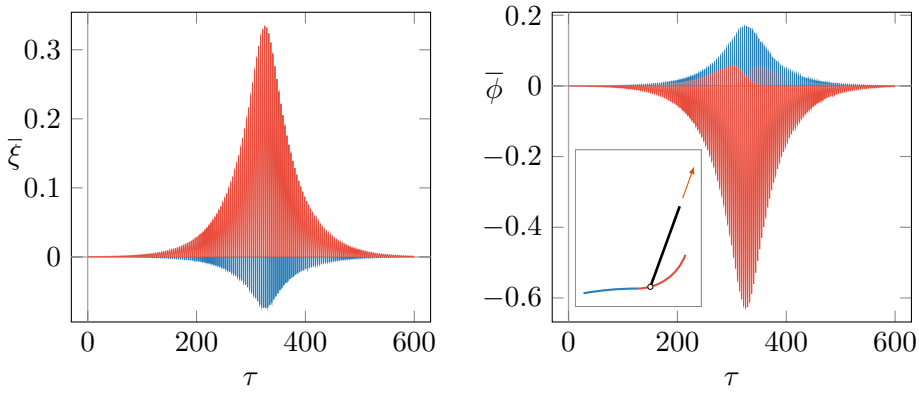

Figure 6.13: Time evolution of the non-dimensional generalised coordinates $\overline{\xi}$ and $\overline{\phi}$ as a function of the non-dimensional time τ, for the nonlinear model of the structure with a doubly circular profile. An exponential growth of the amplitude of the generalised coordinates is clearly visible for about $\tau < 300$ and then the amplitude exponentially decreases. This behaviour is repeated in time producing a phenomenon similar to beats. The equilibrium configuration is unstable, since the peak values are always reached, also decreasing the modulus of initial conditions.

The solution of the nonlinear system is depicted in Figures 6.13 and 6.14, where the initial conditions are assumed to be identical to those obtained in the linearised case, i.e. $\boldsymbol{y}_0 = \boldsymbol{x}$, since the connection between the invariant sets in the linear and nonlinear case is investigated. Regarding this specific aspect, one must note that the initial conditions must be carefully chosen to fulfil the condition of the theorem given by Weiss *et al.* [86].

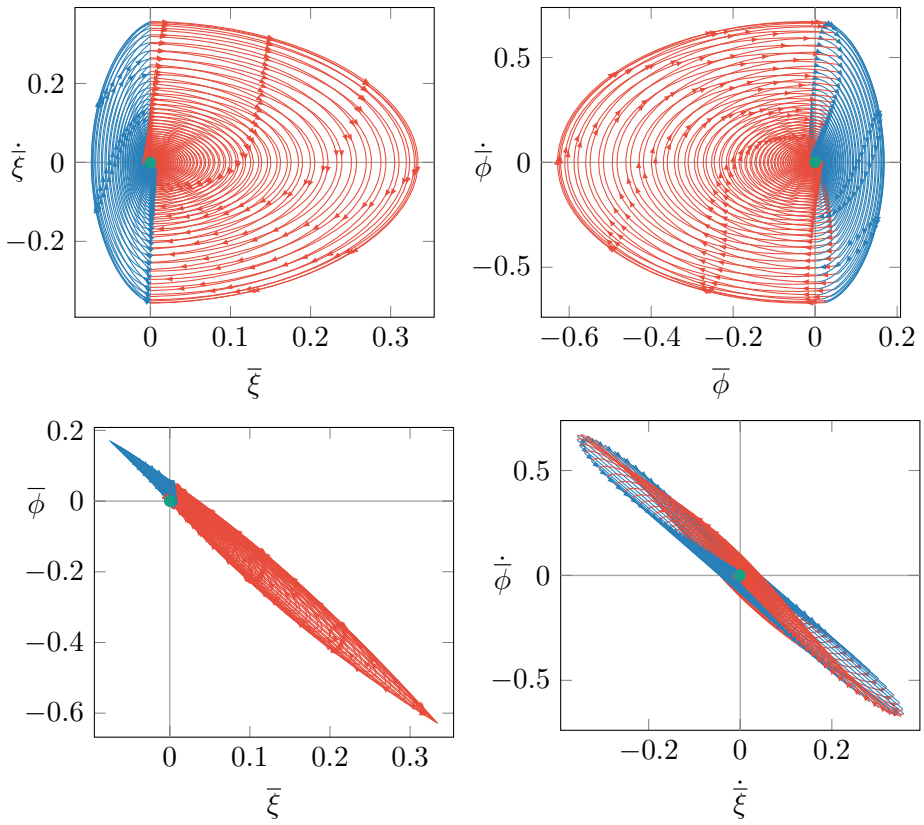

Figure 6.14: Phase portraits near the equilibrium configuration (black dot) located in the origin, for the structure with a doubly circular profile and in case of nonlinear mathematical model. The initial conditions of the plotted orbit (green dot) are those defining the unstable invariant cone for the linearised system. The beat-like behaviour in time of the system reveals an invariant cone that spirals out and in, alternatively.

In particular, the value of the scale parameter ξ_4, which is meaningless in the linearised analysis, plays now a crucial role, therefore it must be tuned to have a solution which is really closed to the equilibrium configuration. Specifically, the solution represented in Figures 6.13 and 6.14 are obtained assuming $\xi_4 = 0.001$, so that the initial conditions are

$$\boldsymbol{y}_0 = 0.001 \times [0, -0.008541, -0.372225, 0.928103] \,.$$

The evolution of the generalised coordinates in the non-dimensional time τ reveals an exponential growth for small values of τ that can be associated with the presence of an unstable cone-like invariant set. However, the orbits do non reach a limit cycle as in classical Hopf bifurcation of smooth mechanical system, but the solution collapses with an exponential decay, producing a series of oscillations analogous to the physical phenomenon of beats (in fact the behaviour plotted in 6.13 is repeated if a greater time domain is considered in the integration).

Even though there exists an exponential decay, the solution can be considered unstable, since the peak value of about $\xi = 0.3$ and $\phi = -0.6$ in the plot in Figure 6.13 is always reached, also in simulations with a lower value of the modulus ξ_4 of the initial conditions. This implies, according to Definition 8 in Section 2.1.3, that it is not possible to decrease the radius of the Liapunov ball in which initial conditions are chosen, to obtain a bounded evolution of the orbit, so the system can be considered unstable near the equilibrium configuration located in the origin.

6.2.2 Invariant cone for other combinations of parameters: tensile and compressive follower forces

Analogous investigations of those presented in Section 6.2.1 have been performed on the structures seen in Section 6.1.2, in case of compressive and tensile loads. As pointed out in the previous example, the choice of ξ_4 for which the system can be considered close to the origin plays an essential role. In this case, this scale parameter has been assumed equal to $\xi_4 = 10^{-6}$, hence the initial condition for the compressive and tensile load are, respectively

$$\boldsymbol{y}_0^A = 10^{-6} \times [0, -0.005946, -0.608652, 0.793415] \,,$$
$$\boldsymbol{y}_0^B = 10^{-6} \times [0, 0.086944, -0.360442, 0.928721] \,.$$

The behaviour of these cases is qualitatively different from that reported in Section 6.2.1 since the beats are not present for these nonlinear structures. As for the compressive load case (γ^A), the evolution of the mechanical system seems to reach a sort of limit cycle, so that the orbits approach a complex manifold. As in the previous Section, this behaviour can be considered unstable, since a reduction in the modulus of initial conditions does not affect the peak values of $\overline{\xi}$ and $\overline{\phi}$. For the tensile load case (γ_B), the solution evolves spiralling out from the origin and then an abrupt deviation appears, revealing the instability of the system.

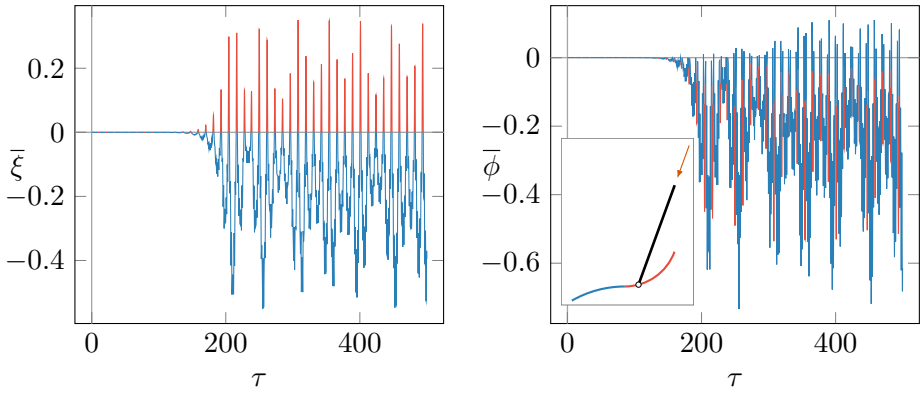

Figure 6.15: Time evolution of the non-dimensional generalised coordinates $\overline{\xi}$ and $\overline{\phi}$ as a function of the non-dimensional time τ, for the structure with a doubly circular profile subjected to the compressive load $\gamma^A = -1.5$. An exponential growth of the amplitude of the generalised coordinates is clearly visible for about $\tau < 220$ in the nonlinear model, then the orbit follows a sort of irregular path with a fixed maximum amplitude.

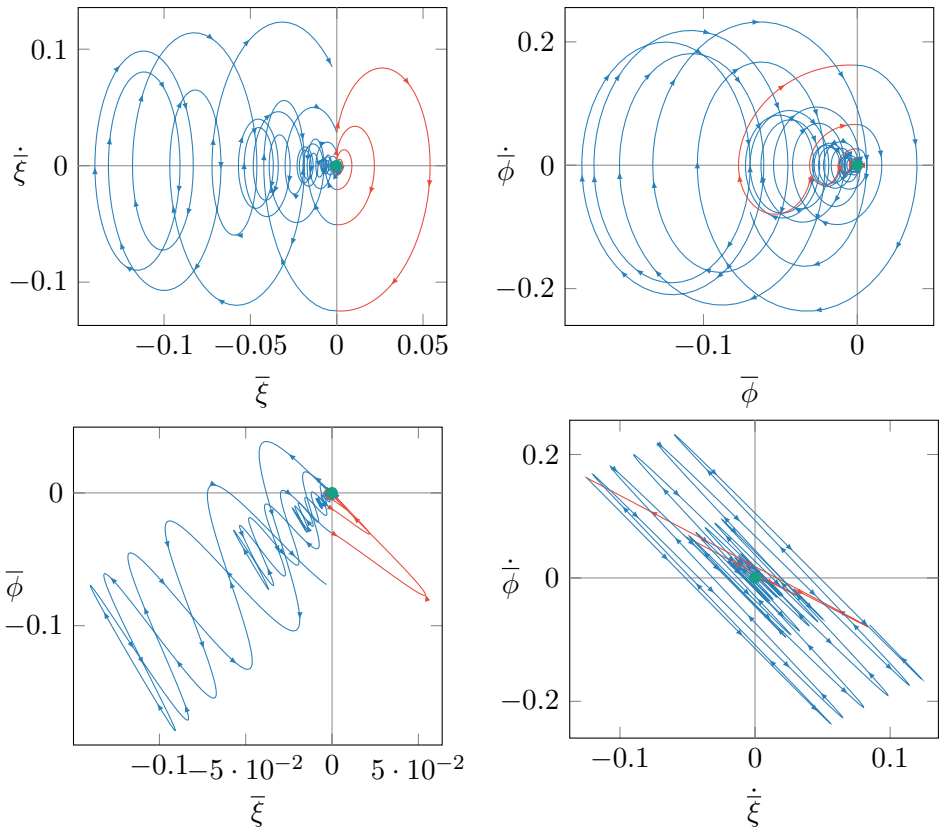

Figure 6.16: Phase portraits near the equilibrium configuration (black dot) located in the origin, for the structure with a doubly circular profile subjected to the compressive load $\gamma^A = -1.5$. The initial conditions of the plotted orbit (green dot) are those defining the unstable invariant cone for the linearised system. A sort of invariant cone is visible, describing the first part of the time evolution of the system.

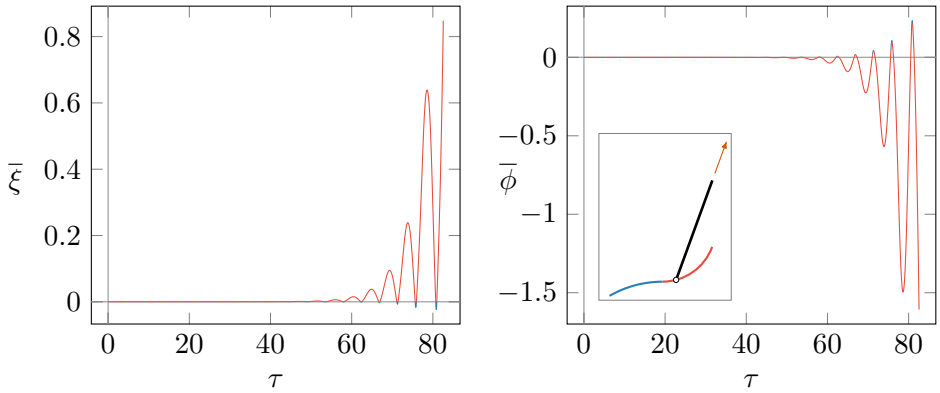

Figure 6.17: Time evolution of the non-dimensional generalised coordinates $\overline{\xi}$ and $\overline{\phi}$ as a function of the non-dimensional time τ, for the structure with a doubly circular profile subjected to the compressive load $\gamma^B = 0.75$. An exponential growth of the amplitude of the generalised coordinates is clearly visible.

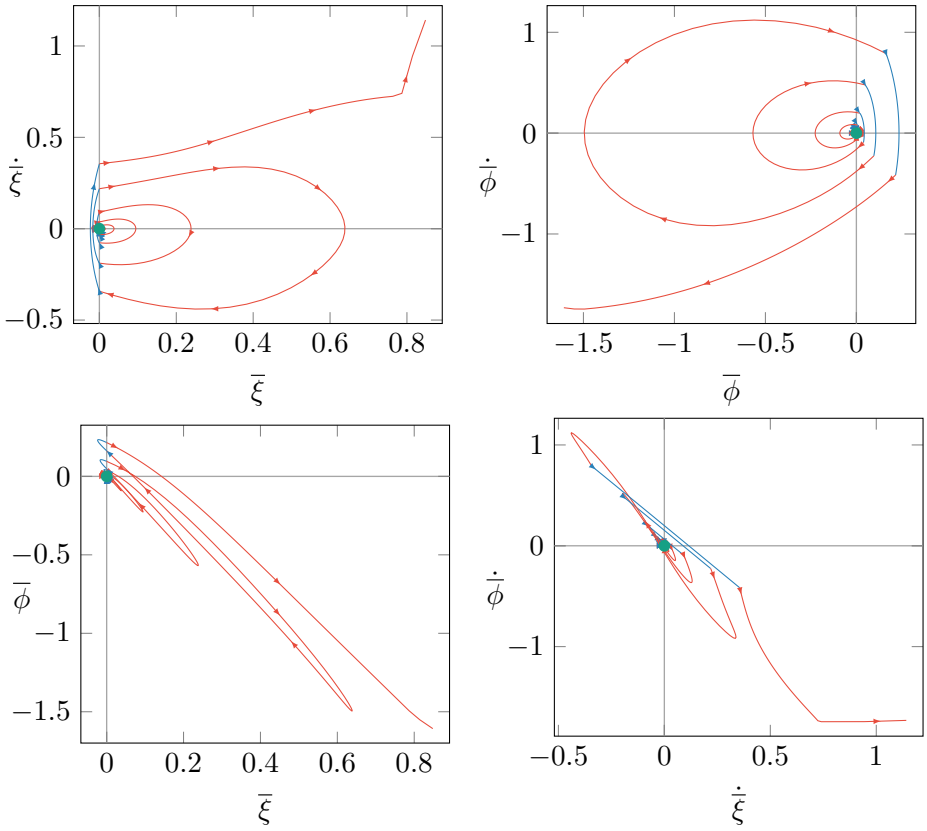

Figure 6.18: Phase portraits near the equilibrium configuration (black dot) located in the origin, for the structure with a doubly circular profile subjected to the compressive load $\gamma^B = 0.75$. The initial condition of the plotted orbit (green dot) are those defining the unstable invariant cone in the linearised model. A sort of invariant cone is visible in the first part of the evolution, then an abrupt divergence appears, leading to an unstable behaviour.

6.3 Design of piecewise system through instability domains

In smooth mechanical systems, the stability of an equilibrium configuration can easily be determined through standard theoretical procedures, that generally allow the determination of ranges of parameters revealing a given behaviour for the system. A bifurcation analysis, described in Section 2.1.5, can be performed from an analytical perspective, determining when the system is stable or unstable on the basis of the bifurcation parameters that have been assumed (typically, for mechanical systems, a classical choice for a bifurcation parameter is the load).

In Chapter 5, this kind of purely theoretical approach has been demonstrated to be unfeasible in the cases treated in this Thesis, due to the complexity of piecewise-smooth dynamics. However, a semi-analytical approach can be adopted to identify the presence of an invariant cone, derived by the necessary criterion of instability shown in Chapter 4. The determination of design parameter domains that can be associated with a specific behaviour for the system is generally impossible for piecewise dynamics, from an analytical point of view. On the contrary, this problem can be solved by adopting a numerical perspective, testing a finite number of sets of parameters and determining the features of the possible cones.

For this purpose, instability domains can be defined using the numerical algorithm derived in Chapter 5, which can identify *a priori* the presence of a cone and the stability of the equilibrium configuration. The instability domain depicted in Figure 6.19 is an example of this approach, which refers to the reference example described in Section 6.1.1, assuming

$$\zeta_+ = 0.5757, \quad k = 0.301722, \quad \sigma = 0, \quad \Theta = 1.$$

Two non-dimensional design parameters have been considered, namely χ describing the ratio of the radii of curvature and γ associated with the load. These design parameters can assume a finite set of numerical values, describing for example a 2-dimensional grid, as can be seen in the picture, while all the other parameters are fixed. The aforementioned numerical procedure is adopted, where the free parameters are chosen as the point (χ, γ) of the grid, and for each point, the presence of an invariant cone is investigated. The red dots denote the values of χ and γ for which an unstable invariant cone can be detected, on the contrary, for the blue points,

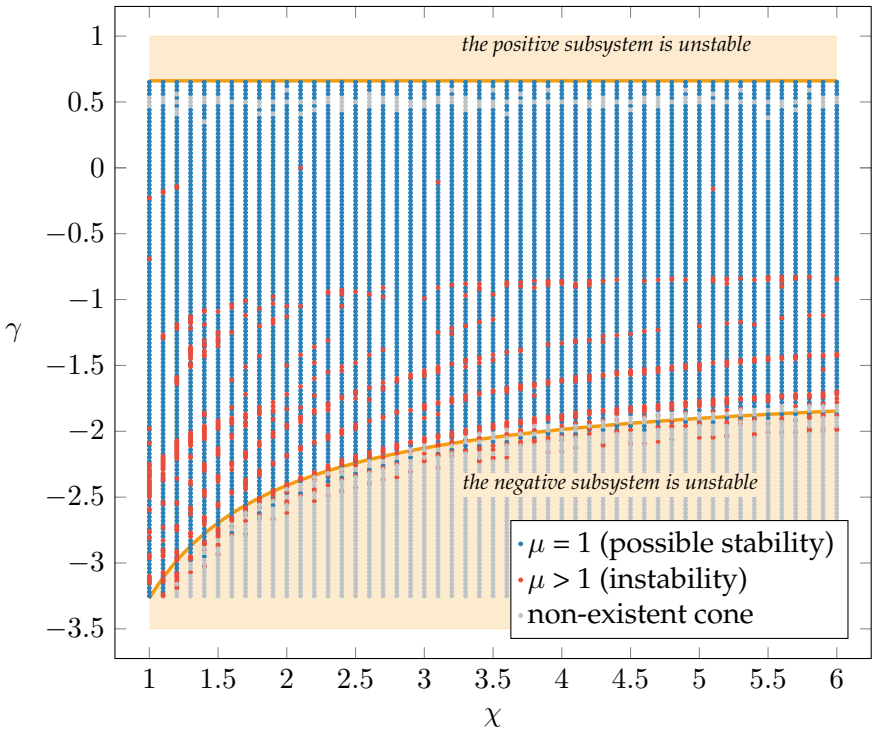

Figure 6.19: Instability domain, describing the presence of invariant cones in the reference structure. The parameters χ (ratio of the radii of curvature) and γ (non-dimensional follower load) are chosen in a given finite set of values (the grid of points in the plot), while the remaining parameters are equal to $\zeta_+ = 0.5757$, $k = 0.301722$, $\sigma = 0$, $\Theta = 1$. The red dots denote the presence of an unstable invariant cone with $\mu > 1$ that implies the instability of the linearised piecewise-smooth system, while the blue dots represent parameter combinations for which a cone with $\mu = 1$ is detected, which does not actually imply that the solution is stable. The grey dots denote the absence of a cone, according to the numerical method adopted for the detection of this invariant set. The points of the grid in the orange areas must be neglected since in these regions one of the two subsystems suffers flutter instability and the fundamental hypothesis on the stability of both subsystems is violated.

all invariant cones with $\mu = 1$ have been determined. The grey points are associated with mechanical parameters for which the numerical algorithm does not identify the presence of any invariant cone.

One must observe that this numerical procedure can be adopted only for stable positive and negative subsystems, hence the points of the grid which do not fulfil this condition must be discarded. In the analysed case, the dots in the orange area reveals an unstable flutter behaviour in one of the systems, so only the points outside these regions must be considered as correct solutions.

Actually, only in the red dots, a clearly defined behaviour can be found, since the absence of an unstable cone does not necessarily imply that the system is stable. Moreover, also unstable cones with a definition more complex than (4.9) may be present in the system, denoted by blue points, for example, the invariant sets for which more than two cycles are necessary to appreciate the periodicity of the solution.

Although this discrete approach cannot be exhaustive for an overall comprehension of the problem and cannot lead to an accurate design, some regions with the desired unstable behaviour can be determined, i.e. the red bands for a negative value of the load γ. This numerical technique and the graphical outcomes as Figure 6.19 can be fruitful tools for the correct design of 2 d.o.f. mechanical systems.

6.4 Conclusions

The algorithm for the detection of an invariant cone has been used for the analysis of the structure with a doubly circular profile. The most important features of the solutions of this specific piecewise system have been shown in a reference example, for which the presence of the invariant manifold has been confirmed by the explicit integration of the equations of motion. Moreover, the investigation of a mechanical system presenting an unstable behaviour both for compressive and tensile follower forces has been performed, which is an unusual condition for smooth structure.

These analyses have been extended to the nonlinear case, so the non-smooth mathematical model for the mechanical system has been studied to determine the presence of a cone-like invariant set. The unstable behaviour of the cones in the linearised formulation is then confirmed in the

nonlinear regime, hence this unexpected instability phenomenon becomes realistic and feasible for real applications.

Finally, a conceptual tool for the design of piecewise 2 d.o.f. mechanical systems has been presented, which allows the definition of the region in the design parameter space where this instability behaviour can be present.

PART II

Cloaking of flexural waves in Kirchhoff-Love plates

CHAPTER 7

Invisibility cloak for a Kirchhoff-Love Plate

"Facts which at first seem improbable will, even on scant explanation, drop the cloak which has hidden them and stand forth in naked and simple beauty"

Galileo Galilei

The theory of transformation elastodynamics is exposed in the present Chapter, in order to introduce the problem of modelling an invisibility cloak for flexural waves in thin elastic plates, with the aim of shielding a hole from vibrations. The case of an invisibility cloak for a square hole is analysed in depth and the theoretical transformations that allow the determination of the elastic parameters of the cloak is described. Moreover, a Finite Element model is developed, according to the classical approach of Galerkin. The aim of this Thesis is the definition of an approximated invisibility cloak, neglecting the unrealistic presence of prestress and the investigated numerical procedure is a fundamental tool for the determination of a correct design.

7.1 Theoretical background

7.1.1 Transformation elastodynamics for thin plates

The definition of a flexural cloak for a homogeneous, isotropic Kirchhoff-Love plate, defined on a two-dimensional domain $\mathcal{K}$, is based on a transformation, say χ, that maps a two-dimensional subdomain $\mathcal{C}^0 \subset \mathcal{K}$ to the

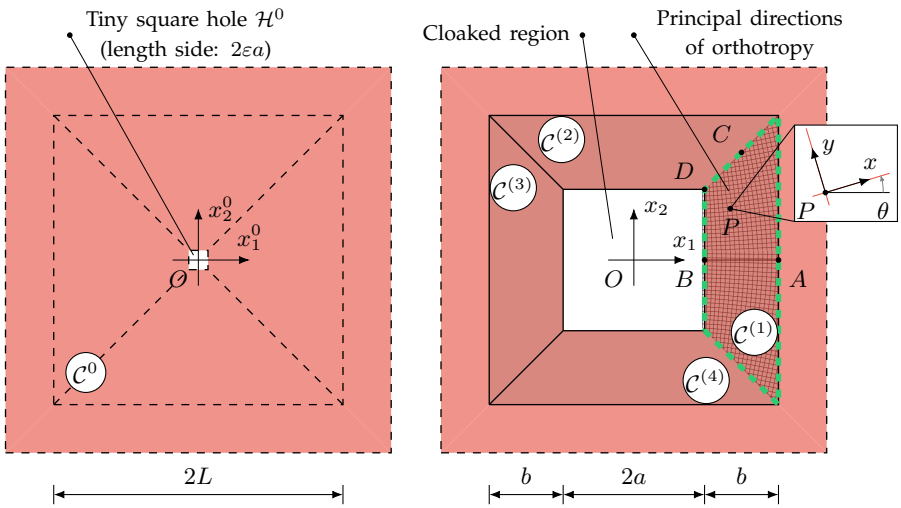

(a) *undeformed domain* **(b)** *deformed domain*

Figure 7.1: Sketch of a square 1cloak studied in [25]: (a) undeformed domain $\mathcal{C}^0$ where the plate is isotropic and homogeneous; (b) transformed domain $\mathcal{C}$, where the four trapezoids composing the cloak are numbered. The principal directions of orthotropy are represented with thin lines (the local axes at a generic point P are labelled x and y as depicted). The perimeter of trapezoid $\mathcal{C}^{(1)}$ is marked with a dashed green line.

domain $\mathcal{C}$ where the meta-plate is to be constructed, namely [1]

$$\chi_k : \mathcal{C}^0 \to \mathcal{C}, \qquad x_K^0 \to x_k = \chi_k(x_K^0).$$

The map is such that the transformed equation in the latter is still the governing equation for flexural waves supported by a Kirchhoff-Love plate, which is, in general, non-homogeneous and anisotropic. In our case, $\mathcal{C}^0$ is a square deprived of a tiny hole $\mathcal{H}^0$ in the centre (see Figure 7.1a) that is mapped to a collection of four trapezoids $\mathcal{C}^{(i)}$ $(i = 1, \dots, 4)$ (Figure 7.1b), such that $\mathcal{C} = \bigcup \mathcal{C}^{(i)}$. The length of one side of the external boundary of both $\mathcal{C}^0$ and $\mathcal{C}$ is equal to $2L$ whereas that of $\mathcal{H}^0$ is equal to $2\varepsilon a$, where ε is

[1] Uppercase and lowercase indices, both ranging between 1 and 2, are referred to reference and transformed domains, respectively, whereas a 0 in either super- or sub-script position indicates that the quantity concerned is evaluated in the reference configuration.

a small parameter. [2]

In both configurations, the exterior domain $\mathcal{K} \setminus \mathcal{C}^0 \equiv \mathcal{K} \setminus \mathcal{C}$ is occupied by the initial, homogeneous structure that possesses constant thickness H, mass density per unit volume ρ^0 and bending stiffness $D^0 = EH^3/[12(1-\nu^2)]$, where E is the Young's modulus of the material and ν its Poisson's ratio. The governing equation of the homogeneous isotropic Kirchhoff-Love plate (neglecting the presence of a distribute load per unit area) takes the form

$$D^0 \nabla_0^4 w + \sigma^0 \ddot{w} = 0, \tag{7.1}$$

where $w(x_K^0, t)$ is the transverse displacement, ∇_0^4 is the biharmonic operator in $\mathcal{C}^0$ and $\sigma^0 = \rho^0 H$ is the mass density per unit area. For the relevant case of a plate resting on a homogeneous substrate modelled as a bed of independent linear springs (Winkler model), a term $k_W^0 w$ is to be added on the left-hand side of equation (7.1), where k_W^0 is the subgrade coefficient. We emphasise that in equation (7.1), D^0 and σ^0 are independent of the position, since the plate is homogeneous.

The function $\chi_k(x_K^0)$ is assumed to be invertible, a requisite that is met if its evaluation in the inner boundary of the cloak is non-singular as in the case under study. After having recalled that uppercase indices refer to points belonging to $\mathcal{C}^0$ and that a comma indicates partial differentiation, the gradient of the transformation $x_{i,K}$, its Jacobian $J(x_h) = \det x_{i,K}$ and the tensor [3]

$$g_{ij}(x_h) = x_{i,P} x_{j,P}/J$$

are instrumental in defining the properties of the cloak.

In order to have a complete overview on the established theory of meta-plate cloaks, we remind that the local governing equation of a non-homogeneous anisotropic Kirchhoff-Love plate subject to in-plane prestress takes the form [59, 84]

$$m_{ij,ij} + n_{ij} w_{,ij} - s_i w_{,i} = \sigma \ddot{w}, \tag{7.2}$$

where σ is the mass density per unit area, m_{ij} represents the set of moments per unit length whilst n_{ij} and s_i have been introduced to model

[2] ε plays the role of regularisation parameter for the construction of a *near cloak* [50] in which the material properties at the inner boundary of the cloak are not singular.

[3] The summation over the repeated index is implied throughout the paper.

membrane forces and in-plane body forces per unit length, respectively, in equilibrium through fulfilment of the condition

$$n_{ij,j} + s_i = 0. \tag{7.3}$$

The next step is the introduction of the constitutive equations that connect m_{ij} to the generalised curvature $w_{,kl}$, i.e. $m_{ij} = -D_{ijkl}w_{,kl}$, where $D_{ijkl}(x_h)$ is the stiffness tensor which may depend on the position. The substitution into equation (7.2) yields

$$D_{ijkl}w_{,ijkl} + 2D_{ijkl,i}w_{,jkl} + \left(D_{ijkl,ij} - n_{kl}\right)w_{,kl} + s_l w_{,l} = -\sigma\ddot{w}, \tag{7.4}$$

an equation used by [25] to identify the different terms corresponding to the transformation and to confirm that the flexural displacement of a Kirchhoff-Love plate under an arbitrary coordinate mapping may be interpreted as a generalised plate.

Before the application of the domain transformation defining the cloak, the differential equation (7.1) governing the isotropic homogeneous problem must be rewritten in a form analogous to (7.4), namely

$$D^0_{pqrt}w_{,pqrt} + \sigma^0\ddot{w} = 0,$$

where for an isotropic homogeneous plate, the stiffness term can be computed as

$$D^0_{pqrt} = \frac{Eh^3}{12(1-\nu^2)}\left[\nu\delta_{pq}\delta_{rt} + \frac{1-\nu}{2}(\delta_{pr}\delta_{qt} + \delta_{pt}\delta_{qr})\right].$$

The identification of terms shows that the stiffness tensor of the transformed plate corresponds to

$$D_{ijkl}(x_h) = D^0_{pqrt}J^{-1}g_{ip}g_{jq}g_{kr}g_{lt}, \tag{7.5}$$

the in-plane body forces to

$$s_l(x_h) = D^0_{pqrt}\Big[\left(J^{-1}g_{ip}g_{jq,i}g_{kr}g_{lt}\right)_{,j} - J^{-1}g_{jq}\left(g_{lp}g_{kr,i}g_{it} + g_{kp}g_{lr,i}g_{it}\right)_{,j} + \frac{1}{2}J^{-1}g_{jq}g_{it}\left(g_{lp,j}g_{kr,i} + g_{kp,j}g_{lr,i}\right)\Big]_{,k}, \tag{7.6}$$

and the transformed density per unit area turns out to be $\sigma(x_h) = \rho^0 H/J$. When the Winkler foundation is involved, the subgrade coefficient transforms similarly to the density, i.e.

$$k_W(x_p) = \frac{k_W^0}{J}, \tag{7.7}$$

a quantity that is now dependent on the position.

Focusing on the square cloak transformation sketched in Figure 7.1 and, in particular, on trapezoid $\mathcal{C}^{(1)}$, $\chi^{(1)}(x_K^0 \boldsymbol{e}_K) = (\alpha x_1^0 + c)\boldsymbol{e}_1 + (\alpha x_2^0 + c x_2^0/x_1^0)\boldsymbol{e}_2$,

$$g_{ij}^{(1)} = \begin{bmatrix} \alpha & 0 \\ \dfrac{x_2 \alpha c}{x_1(c - x_1)} & \dfrac{x_1 \alpha}{x_1 - c} \end{bmatrix},$$

and $J^{(1)} = x_1 \alpha^2/(x_1 - c)$, where

$$\alpha = \frac{b/L}{1 - \varepsilon a/L}, \qquad c = \frac{a - \varepsilon a}{1 - \varepsilon a/L},$$

and $\{\boldsymbol{e}_1, \boldsymbol{e}_2\}$ is the orthonormal basis associated with both coordinate systems $Ox_1^0 x_2^0$ and $Ox_1 x_2$; a is the half-length of the side of the square hole to be cloaked and $b = L - a$ is the "cloak thickness". This information defines the six independent components of the stiffness tensor D_{ijkl}, the prestress n_{ij} and the in-plane body forces s_i in the four subdomains. For trapezoid $\mathcal{C}^{(1)}$, all these quantities can be computed explicitly. In particular, the six independent flexural stiffness coefficients for trapezoid $\mathcal{C}^{(1)}$ of the cloak are

$$D_{1111}^{(1)} = \alpha^2 \left(1 - \frac{c}{x_1}\right) D^0, \qquad D_{2222}^{(1)} = \frac{\alpha^2 \left(c^2 x_2^2 + x_1^4\right)^2}{(x_1 - c)^3 x_1^5} D^0,$$

$$D_{2211}^{(1)} = \frac{\alpha^2 \left(c^2 x_2^2 + \nu x_1^4\right)}{(x_1 - c) x_1^3} D^0, \qquad D_{1212}^{(1)} = \alpha^2 \frac{c^2 x_2^2 + (1 - \nu) x_1^4}{2 (x_1 - c) x_1^3} D^0,$$

$$D_{1112}^{(1)} = -\alpha^2 c \frac{x_2}{x_1^2} D^0, \qquad D_{2212}^{(1)} = -\frac{\alpha^2 c x_2 \left(c^2 x_2^2 + x_1^4\right)}{(x_1 - c)^2 x_1^4} D^0,$$

while the membrane forces and in-plane body forces are, respectively,

$$n_{11}^{(1)} = \frac{2\alpha^2 c}{x_1^2 (x_1 - c)} D^0, \qquad n_{22}^{(1)} = -\frac{2\alpha^2 c \left((2 - \nu) x_1^4 + 8 c x_2^2 x_1 - 3 c^2 x_2^2\right)}{x_1^4 (x_1 - c)^3} D^0,$$

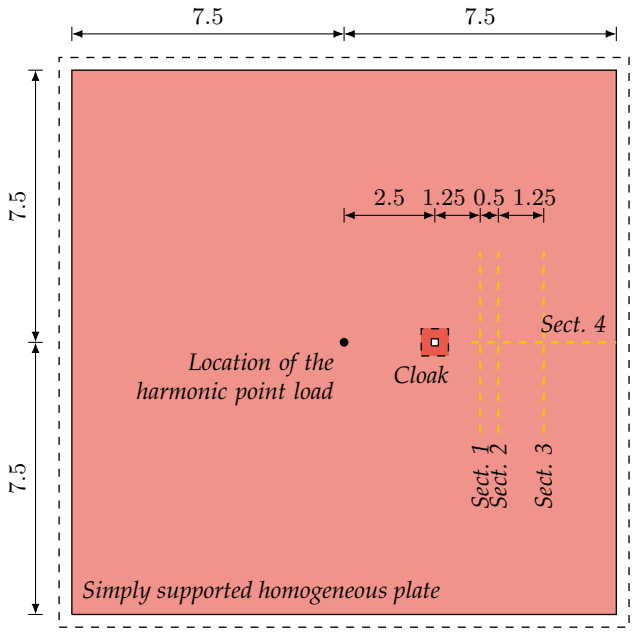

(a) *Geometry of the plate*

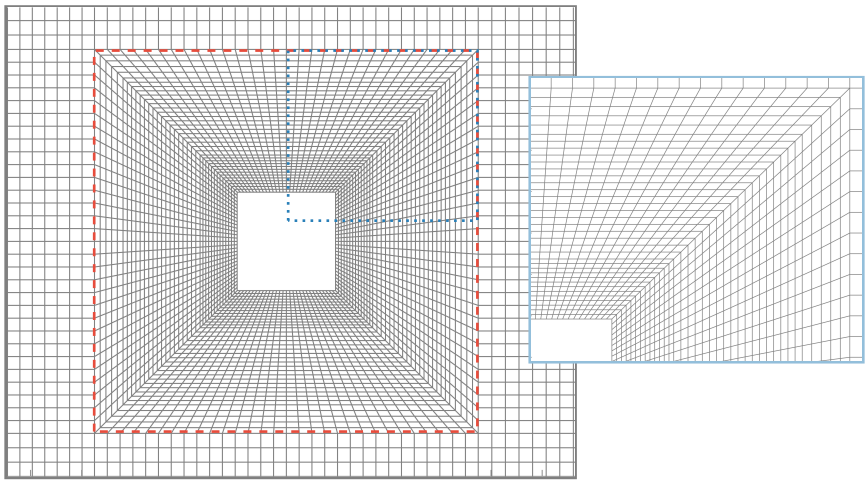

(b) *Mesh adopted for the simulation*

Figure 7.2: a) Geometry of the studied plate where it is visible the point where the time-varying load is enforced (dimensions in m) and the sections considered in Figure 8.2; b) detail of the mesh, the external boundary of the cloak is marked with a dashed red line.

and

$$n_{12}^{(1)} = \frac{2\alpha^2 c x_2 \left(3x_1 - 2c\right)}{\left(x_1 - c\right)^2 x_1^3} D^0, \quad s_1^{(1)} = 0, \quad s_2^{(1)} = \frac{24\alpha^2 c x_2}{\left(x_1 - c\right)^3 x_1^2} D^0.$$

For the other parts of the cloak, they can be easily inferred by taking into account the relevant symmetries. Note that α is dimensionless while $[c] = [\mathrm{L}]$.

For the same trapezoid $\mathcal{C}^{(1)}$, to reach the orthotropic principal directions at a point P, the angle $\theta(x_1, x_2)$ (anticlockwise in the domain $x_2 > 0$, see Figure 7.1b) is now introduced. In particular, this angle identifies the principal axis x (respectively y) moving from x_1 (respectively x_2). Its value is

$$\theta = \frac{1}{4} \arccos \left[-\frac{Q}{Q + 2(D_{1111} - D_{2222})(D_{2221} - D_{1112})} \right], \tag{7.8}$$

where

$$Q = (D_{1111} + D_{2222} - 2D_{1122} - 4D_{1212})(D_{1112} + D_{2221}).$$

In the new local system Pxy, the constitutive relationships assume the form

$$\begin{aligned} m_{xx} &= -D_{xxxx} w_{,xx} - D_{xxyy} w_{,yy}, \\ m_{yy} &= -D_{xxyy} w_{,xx} - D_{yyyy} w_{,yy}, \\ m_{xy} &= -D_{xyxy} w_{,xy}, \end{aligned} \tag{7.9}$$

where the new stiffness moduli contained therein can be deduced in terms of the aforementioned D_{ijkl} and, according to formula (7.8), they can be computed as

$$\begin{aligned} D_{xxxx} &= D_{1111} \cos^4\theta + 2(D_{1122} + 2D_{1212}) \sin^2\theta \cos^2\theta + \\ &\quad D_{2222} \sin^4\theta + 2(D_{1112} \cos^2\theta + D_{2221} \sin^2\theta) \sin 2\theta; \\ D_{yyyy} &= D_{1111} \sin^4\theta + 2(D_{1122} + 2D_{1212}) \sin^2\theta \cos^2\theta + \\ &\quad D_{2222} \cos^4\theta - 2(D_{1112} \sin^2\theta + D_{2221} \cos^2\theta) \sin 2\theta; \\ D_{xxyy} &= D_{1122} + (D_{1111} + D_{2222} - 2(D_{1122} + 2D_{1212})) \sin^2\theta \cos^2\theta + \\ &\quad (D_{2221} - D_{1112}) \cos 2\theta \sin 2\theta; \\ D_{xyxy} &= D_{1212} + (D_{1111} + D_{2222} - 2(D_{1122} + 2D_{1212})) \sin^2\theta \cos^2\theta + \\ &\quad (D_{2221} - D_{1112}) \cos 2\theta \sin 2\theta. \end{aligned}$$

Interestingly, as shown in [25], the twisting stiffness D_{xyxy} brought about by the transformation *vanishes* in all points of the transformed domain. This is a particular feature of the cloak under investigation that must be properly addressed in a meaningful design. It is worth recalling that in an isotropic plate with compact cross-section, $D_{xyxy} = D^0(1-\nu)$.

As a final remark, the cloak is subjected to traction-free boundary conditions in the inner free boundary and to continuity conditions at the interface between itself and the outer homogeneous plate.

7.2 Finite Element model for the analysis of the cloak

With the aim of performing numerical simulations of the transient dynamic behaviour of a square cloak via the Finite Element Method (FEM), a *weak form* of the governing equations is now obtained.

The formulation can be derived by multiplying equation (7.4) by the test function $v(x_1, x_2)$ and using the Galerkin method [78, 91] . After the application of the divergence theorem to the generic subdomain Ω of the entire plate and usage of the equilibrium equations (7.3), the final expression for the weak form becomes

$$\int_\Omega v_{,ij} D_{ijkl} w_{,kl}\, d\Omega - \int_\Omega v_{,l} n_{kl} w_{,k}\, d\Omega + \int_\Omega \sigma v \ddot{w}\, d\Omega + \int_\Omega k_W v w\, d\Omega$$
$$- \int_\Gamma \left\{ m_{\hat{n}\hat{n}} v_{,\hat{n}} - v\left(t_{\hat{n}} + m_{\hat{n}\hat{s},\hat{s}}\right) \right\} ds + \int_\Gamma \left\{ n_{\hat{n}\hat{s}} v w_{,\hat{n}} + n_{\hat{n}} v w_{,\hat{s}} \right\} ds = 0,$$
$$\forall v \in H_0^2(\Omega), \quad (7.10)$$

where also the term involving k_W is now taken into account. In expression (7.10), $(\cdot)_{,\hat{n}}$ and $(\cdot)_{,\hat{s}}$ are the directional derivatives along the normal unit vector $\hat{\boldsymbol{n}}$ and tangent unit vector $\hat{\boldsymbol{s}}$ of the boundary Γ of Ω; $m_{\hat{n}}$, $m_{\hat{n}\hat{s}}$ are the bending and twisting moments per unit length along Γ, respectively, whereas $n_{\hat{n}}$, $n_{\hat{n}\hat{s}}$ describe the in-plane internal actions along the normal and tangent unit vectors; $t_{\hat{n}}$ is the specific shear force on the boundary and $H_0^2(\Omega)$ is the suitable Sobolev space. It should be noted that in the standard procedure leading to the weak form (7.10), the terms $D_{ijkl,i}$ and $D_{ijkl,ij}$ naturally disappear by integrating by part. The analysed plate is composed of various subdomains with different stiffness properties represented by the terms D_{ijkl}: the uncloaked region $\mathcal{K} \setminus \mathcal{C}$ possesses a homoge-

neous stiffness D^0 whereas the cloak is described by the parameters D_{ijkl} given in (7.5).

Geometric and analytical approximations are performed to achieve the *discretised formulation*, by dividing the entire domain into a finite subset of elements, i.e. $\Omega \approx \bigcup_{e=1}^{n_e} \Omega_e$, where n_e is the number of the elements, and substituting unknown and test functions with the linear combinations

$$w(\xi,\eta,t) = N_p(\xi,\eta,t)u_p(t), \qquad v(\xi,\eta,t) = N_q(\xi,\eta,t)v_q,$$

respectively, where $N_p(\xi,\eta,t)$ and $N_q(\xi,\eta,t)$ are the so-called shape functions, defined on the spatial domain Ω_e, and indices p, q range within a suitable interval as specified later. For each Finite Element, the final discretised formulation can be written as

$$\sum_{p=1}^{n_p}\sum_{q=1}^{n_q} v_q \left\{ \int_{\Omega_e} N_{q,ij} D_{ijkl} N_{p,kl} u_p \, d\Omega + \int_{\Omega_e} \sigma N_q N_p \ddot{u}_p \, d\Omega \right.$$
$$\left. + \int_{\Omega_e} k_W N_q N_p u_p \, d\Omega - \int_{\Gamma_e} \left[m_{\hat{n}\hat{n}} N_{q,\hat{n}} - N_q \left(t_{\hat{n}} + m_{\hat{n}\hat{s},\hat{s}} \right) \right] ds \right\} = 0, \quad \forall v_q, \tag{7.11}$$

where n_p and n_q are the number of the shape functions that discretise w and v, respectively. Moreover, in equation (7.11), all the terms related to the in-plane prestress have been neglected, since the aim of this work is the definition of a reasonable cloak, without the presence of unrealistic components as a non-homogeneous membrane load, see Chapter 1.2.1.

A parametric representation is implemented in the code: the shape functions are defined in the local coordinate system $O\xi\eta$ of the master element

$$\hat{\Omega}_e = \left\{ (\xi,\eta) \subseteq \mathbb{R}^2 : -1 \leq \xi \leq 1, -1 \leq \eta \leq 1 \right\},$$

which is mapped into each element of the mesh using appropriate coordinate transformations. Since an isoparametric representation is not possible for thin plate elements unless a previous distortion of the mesh (see for example [75]), a subparametric representation has been adopted, so the *bilinear* shape functions that are used for the transformation of the master element are different from the *hermitian* ones used for the analytical approximation of the unknown.

The structured mesh employed in the numerical analyses is composed of quadrangular elements with four nodes in the corner of each element,

whose generalised displacements are

$$\left\{ w^{(k)} \quad w^{(k)}_{,\xi} \quad w^{(k)}_{,\eta} \quad w^{(k)}_{,\xi\eta} \right\}, \quad k = 1, 2, 3, 4, \tag{7.12}$$

leading to ($n_p = n_q =$) 16 degrees of freedom for each Finite Element, see [45, 77, 78, 91].

Finally, after substitution and integration of the aforementioned shape functions in equation (7.11) and the assembly operation over all the Finite Elements of the mesh, the set of algebraic equations used for the spatial approximation of this problem can be written as

$$\boldsymbol{M}\ddot{\boldsymbol{u}}(t) + \boldsymbol{K}\boldsymbol{u}(t) = \boldsymbol{f}(t), \tag{7.13}$$

where $\boldsymbol{M}$ and $\boldsymbol{K}$ are the mass matrix and the stiffness matrix, respectively; $\boldsymbol{u}(t)$ is the vector of the degrees of freedom whereas $\boldsymbol{f}(t)$ is the vector of generalised external loads.

The approximation in the time domain is performed with the single-step time-integration algorithm *Generalized-α method*, see [21, 22], which is an evolution of the well-known Newmark method that is frequently used for transient dynamical analysis in mechanics [44, 45, 77, 91]. According to this method, equation (7.13) is written as

$$\boldsymbol{M}\ddot{\boldsymbol{u}}(t_n) + \boldsymbol{C}\dot{\boldsymbol{u}}(t_n) + \boldsymbol{K}\boldsymbol{u}(t_n) = \boldsymbol{f}(t_n), \tag{7.14}$$

where a generic damping matrix $\boldsymbol{C}$ has been introduced for the sake of generality and the time-domain discretisation

$$\boldsymbol{T} = \{0, t_1, t_2, \ldots, t_n, \ldots, t_N = T_{\max}\}, \quad t_{n+1} = t_n + \Delta t_n,$$

is performed, with respect to the time-domain $T = [0,\, T_{\max}]$.

The Taylor's expansions of the solution $\boldsymbol{u}(t_{n+1}) \equiv \boldsymbol{u}_{n+1}$ and its first time derivative $\dot{\boldsymbol{u}}(t_{n+1}) \equiv \dot{\boldsymbol{u}}_{n+1}$ are given by

$$\begin{aligned} \boldsymbol{u}_{n+1} &= \boldsymbol{u}_n + \Delta t_n \dot{\boldsymbol{u}}_n + (1-\theta_2)\,\frac{\Delta t_n^2}{2}\ddot{\boldsymbol{u}}_n + \theta_2 \frac{\Delta t_n^2}{2}\ddot{\boldsymbol{u}}_{n+1}, \\ \dot{\boldsymbol{u}}_{n+1} &= \dot{\boldsymbol{u}}_n + (1-\theta_1)\,\Delta t_n \ddot{\boldsymbol{u}}_n + \theta_1 \Delta t_n \ddot{\boldsymbol{u}}_{n+1}, \end{aligned} \tag{7.15}$$

where θ_1 and θ_2 are positive real parameters that define the integration scheme. Formulae (7.15) are substituted into equation (7.14) calculated in

the intermediate time value $t_{n+1-\alpha_f} = (1-\alpha_f)\, t_{n+1} + \alpha_f t_n$, thus obtaining

$$\boldsymbol{M}\left[(1-\alpha_m)\,\ddot{\boldsymbol{u}}_{n+1} + \alpha_m \ddot{\boldsymbol{u}}_n\right] + \boldsymbol{C}\left[(1-\alpha_f)\,\dot{\boldsymbol{u}}_{n+1} + \alpha_f \dot{\boldsymbol{u}}_n\right] + \\ + \boldsymbol{K}\left[(1-\alpha_f)\,\boldsymbol{u}_{n+1} + \alpha_f \boldsymbol{u}_n\right] = \boldsymbol{f}_{n+1-\alpha_f},$$

where α_f and α_m are two additional parameters that will be specified later.

The following implicit scheme can be used to achieve the solution $\ddot{\boldsymbol{u}}_{n+1}$, namely

$$\ddot{\boldsymbol{u}}_{n+1} = \mathcal{A}^{-1}\Bigg[\boldsymbol{f}_{n+1-\alpha_f} - \boldsymbol{K}\boldsymbol{u}_n - \Big(\boldsymbol{C} + \boldsymbol{K}\,(1-\alpha_f)\,\Delta t_n\Big)\dot{\boldsymbol{u}}_n + \\ - \left(\boldsymbol{M}\alpha_m + \boldsymbol{C}\,(1-\alpha_f)\,(1-\theta_1)\,\Delta t_n + \boldsymbol{K}\,(1-\alpha_f)\,(1-\theta_2)\,\frac{\Delta t_n^2}{2}\right)\ddot{\boldsymbol{u}}_n\Bigg], \tag{7.16}$$

where

$$\mathcal{A} = \left[\boldsymbol{M}\,(1-\alpha_m) + \boldsymbol{C}\,(1-\alpha_f)\,\theta_1 \Delta t_n + \boldsymbol{K}\,(1-\alpha_f)\,\theta_2 \frac{\Delta t_n^2}{2}\right].$$

Equations (7.15) and (7.16) are employed to calculate the complete solution at each time step t_n.

The Generalized-α method is completely described by the four parameters α_m, α_f, θ_1, θ_2 that define the stability and the convergence properties of the time-integration scheme. They can be written as a function of the asymptotic spectral radius $\rho_\infty \in [0,1]$ which is related to the numerical damping in the high-frequency limit as

$$\alpha_m = \frac{2\rho_\infty - 1}{\rho_\infty + 1}, \qquad \alpha_f = \frac{\rho_\infty}{\rho_\infty + 1},$$
$$\theta_1 = \frac{1}{2} - \alpha_m + \alpha_f, \qquad \theta_2 = \frac{1}{2}\,(1 - \alpha_m + \alpha_f)^2.$$

It is worth mentioning that equation (7.13) can be profitably employed to perform time-harmonic simulations once a harmonic form for $\boldsymbol{u}(t)$ and $\boldsymbol{f}(t)$ is introduced.

The mass matrix can generally be computed in different ways: the consistent mass matrix $\boldsymbol{M}_C$ is obtained directly from the weak formulation (7.11), so the inertia contribution is assigned to each node via the

shape function; the lumped mass matrix $\boldsymbol{M}_L$ is a diagonal matrix obtained condensing the mass of each element in its nodes via equilibrium. In the ensuing simulations we considered a mixed mass matrix $\boldsymbol{M} = (1-\alpha_l)\boldsymbol{M}_C + \alpha_l \boldsymbol{M}_L$, where $\alpha_l \in [0,1]$, see [44, 91].

7.3 Main features of the Finite Element code

The previously described computational model has been used for the creation of a Finite Element code, written using the software Matlab. The development of an in-house code allows a better comprehension of the model, since all the details of the problem must be investigated in depth. However, the two most important advantages are the possibility of not being constrained to the limit of commercial software and of possibly extending the "core" of the program to deal with more complicated problems, representing evolutions of the original one.

The structure of the code can be divided into three main parts:

- *pre-processing*: in this part, the geometry and the mesh are defined, together with all the mechanical parameters and loads. Furthermore, the choice of the shape functions determines the stiffness and mass matrices of the single Finite Element, namely, $\boldsymbol{K}_{\text{EF}}$ and $\boldsymbol{M}_{\text{EF}}$, which are then assembled into the global matrices that must be inverted to find the solution of the problem. Finally, the essential and natural boundary conditions are imposed to the problem.

- *processing*: this is the main part of the program, since the set of algebraic equations obtained in the passage from the mathematical to the computational model are solved and the vector of d.o.f. is explicitly determined. With the present code, it is possible to perform static, modal, and time-harmonic analysis, however the subroutine used for the current investigations concerns the transient explicit dynamical analysis through the Generalised-α method.

- *post-processing*: the principal unknown field is determined, according to equation $(7.12)_1$ and all the derived unknown fields are obtained. Then, the behaviour of the investigated quantities is plotted in 2D or 3D plots or in the 1D section cuts.

As mentioned before, one of the advantages of this kind of routine is its extendibility. For this reason, the present code has been developed in a "modular" way, to support further extensions. For example, the code is structured in such a way that the weak form can be substituted to deal with more complex problems, or new general Finite Elements can be added to the library of elements, simply defining the suitable shape functions. Hence, the modularity introduced in the programming is a fundamental feature of the present Finite Element code.

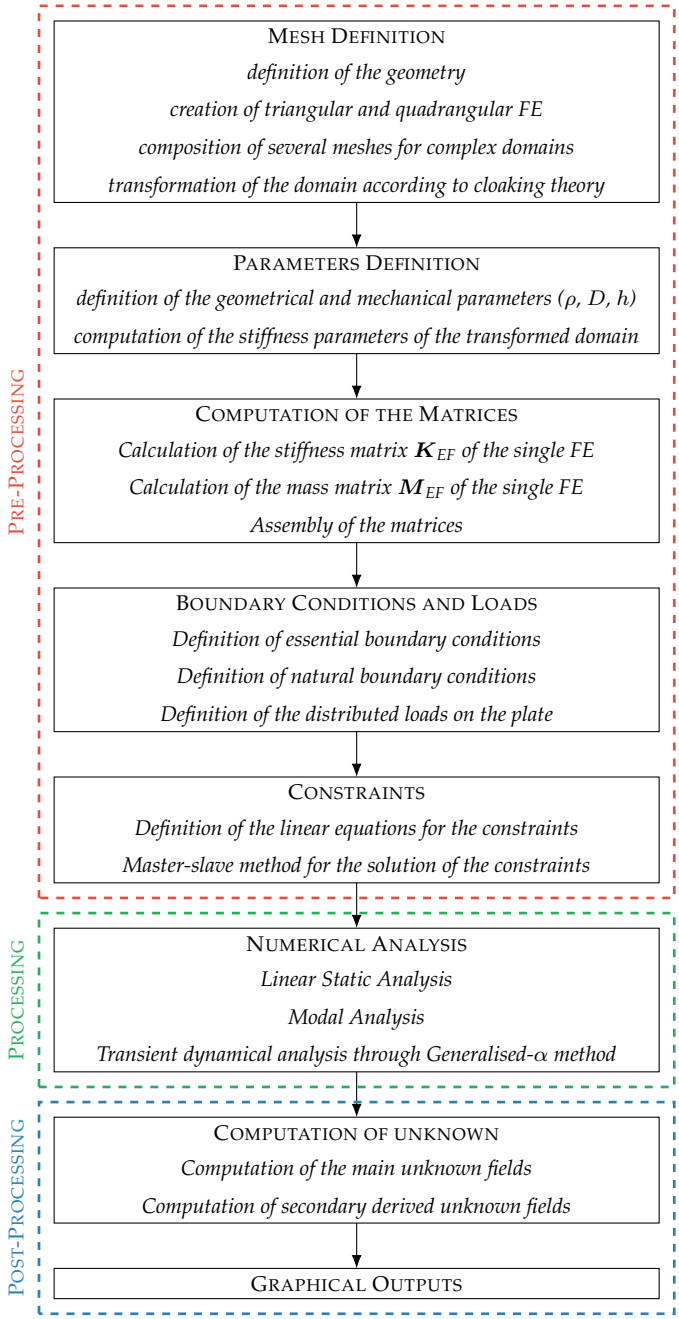
PRE-PROCESSING
MESH DEFINITION
definition of the geometry
creation of triangular and quadrangular FE
composition of several meshes for complex domains
transformation of the domain according to cloaking theory
PARAMETERS DEFINITION
definition of the geometrical and mechanical parameters (ρ, D, h)
computation of the stiffness parameters of the transformed domain
COMPUTATION OF THE MATRICES
Calculation of the stiffness matrix $\boldsymbol{K}_{EF}$ of the single FE
Calculation of the mass matrix $\boldsymbol{M}_{EF}$ of the single FE
Assembly of the matrices
BOUNDARY CONDITIONS AND LOADS
Definition of essential boundary conditions
Definition of natural boundary conditions
Definition of the distributed loads on the plate
CONSTRAINTS
Definition of the linear equations for the constraints
Master-slave method for the solution of the constraints
PROCESSING
NUMERICAL ANALYSIS
Linear Static Analysis
Modal Analysis
Transient dynamical analysis through Generalised-α method
POST-PROCESSING
COMPUTATION OF UNKNOWN
Computation of the main unknown fields
Computation of secondary derived unknown fields
GRAPHICAL OUTPUTS

CHAPTER 8

Numerical simulations and results

"Science is the study of what is, Engineering builds what will be. The scientist merely explores that which exists, while the engineer creates what has never existed before"

Theodore von Kármán

The Finite Element code analysed in Chapter 7 has been employed for the investigation of a specific numerical example, which will be described below. The considered solution refers to a specific geometry, shown in Figure 7.2, which will be taken as a reference in the following examples. Then, some elastic and load parameters in the problem are changed, in order to perform a sensitivity analysis and define how the solution is perturbed by these variations.

The main purpose of this Thesis is the definition of a *realistic* invisibility cloak and this practical perspective leads to neglect the most unrealistic component of the cloak (e.g. the inhomogeneous prestress) or to consider other phenomena (e.g. the interaction with a Winkler soil). The definition of a "quality measure" for the performance of the cloak is essential for a quantitative determination of the quality of the approximated cloak.

Finally, a simple example of a possible real invisibility cloak is presented, which is the starting point for further investigation in this topic.

8.1 Numerical result for the approximated invisibility cloak

8.1.1 Description of the reference geometry

Using the code described above, we studied the transient propagation of flexural waves in a simply-supported square plate, in which a square hole is cloaked with respect to out-of-plane vibration generated by a point force varying sinusoidally. With reference to Figure 7.2, the homogeneous plate in $\mathcal{C}^0$ is a steel one ($E = 210$ GPa, $\nu = 0.3$, $\rho^0 = 7800\,\mathrm{kg/m^3}$) with thickness $H = 1$ mm and bending stiffness $D^0 = 19.23$ Nm. The outer side of the cloak is such that $L = 0.75$ m while $a = 0.1923$ m, $b = 0.5577$ m and $\varepsilon a = 0.025$ m. [1] When a Winkler-like soil comes into play in the analysis, the stiffness of the elastic substratum is represented by $k_W^0 = 0.5 \times 10^6$ $\mathrm{N/m^3}$, qualitatively corresponding to that of a silicone material [5, 35].

The boundary conditions on the outer perimeter are those of a simply supported plate, namely null transversal displacement $w|_{\partial\mathcal{K}} = 0$, null rotation $w_{,\hat{s}}|_{\partial\mathcal{K}} = 0$ and null bending moment $m_{\hat{n}\hat{n}}|_{\partial\mathcal{K}} = 0$. The distance between the centre of the plate and the centre of the cloaked square hole is equal to 2.5 m. A harmonic transversal point force $F(t) = \bar{F}\cos(\omega t)$ is applied at the centre of the plate where we assumed $\bar{F} = 100$ N and ω varying from 50 rad/s to 600 rad/s. The information of the point load is contained in the vector load $\boldsymbol{f}(t)$ in the right-hand-side of (7.13) and (7.14).

The mesh that we used for the transient analysis is composed of ($n_e =$) 83340 quadrangular elements with 335864 total degrees of freedom; the elements are rectangular and regular outside the area of the cloak whereas the mesh is refined and composed of trapezoidal elements inside the area of the cloak. Each trapezoid of the cloak $\mathcal{C}^{(i)}$ is composed of 1080 Finite Elements.

We performed a transient dynamical analysis with the Generalized-α method, see Section 7.2, for which we chose $\rho_\infty = 1$ to neglect numerical damping, therefore the method reduces to a second order and unconditionally stable algorithm with $\alpha_m = \alpha_f = \theta_1 = \theta_2 = 1/2$,

[1] With this set of parameters, it turns out that for the trapezoid $\mathcal{C}^{(1)}$ the stiffnesses for the four representative points sketched in Figure 7.1b are displayed in Table 8.3. The minimum value D_{1111} is achieved along the whole inner boundary whereas the maximum D_{2222} is at point D.

which is equivalent to the constant-average acceleration method [78]. This choice of the parameters of the numerical algorithm leads to a stable scheme for any time interval, so we considered a time domain $T = [0, 200$ ms$]$ with $\Delta t_n = 1$ ms. We assumed homogeneous initial condition, so $\boldsymbol{u}(t = 0) = \boldsymbol{u}_0 = \mathbf{0}$ and $\dot{\boldsymbol{u}}(t = 0) = \dot{\boldsymbol{u}}_0 = \mathbf{0}$. The initial value of $\ddot{\boldsymbol{u}}_0$ (necessary in the first step) has been calculated assuming the initial condition on $\boldsymbol{u}_0$ and $\dot{\boldsymbol{u}}_0$ and solving equation (7.14) for $t = 0$. In the time-domain integration we neglected the contribution of the damping matrix, i.e. $\boldsymbol{C} = \mathbf{0}$, and we assumed $\alpha_l = 0.5$.

The performance of the cloak is now assessed with reference to the following case studies:

(i) a cloak possessing all properties of the Theoretical Transformation Without Prestress (TTWP) is analysed first. As recalled in the Introduction 1.2.1, the prestress is ruled out as it is not realistic to assume the distribution of initial stress n_{ij} and in-plane body forces s_i foreseen by the transformation. For this cloak, however, the local twisting stiffness D_{xyxy} vanishes in the whole domain $\mathcal{C}$;

(ii) a cloak is investigated, possessing all properties of the TTWP but with a different amount of torsional stiffness D_{xyxy}, to evaluate the influence of this parameter. This case is significant as every constructed meta-plate cloak would be equipped with a certain amount of twisting stiffness;

(iii) same as (ii), but with the goal of estimating the role of the coupling bending stiffness D_{xxyy};

(iv) a cloak with the properties predicted by the TTWP is then studied, but resting on a substrate modelled as a Winkler foundation whose position-dependent subgrade modulus obeys relationship (7.7).

For all case studies, the displacement maps and the other relevant quantities that are illustrated are computed at a time t compatible with a propagation of the wavefront located downline of the region of the cloak, but not significantly disturbed by secondary waves reflected at the boundary of the plate.

8.1.2 Performance of the cloak

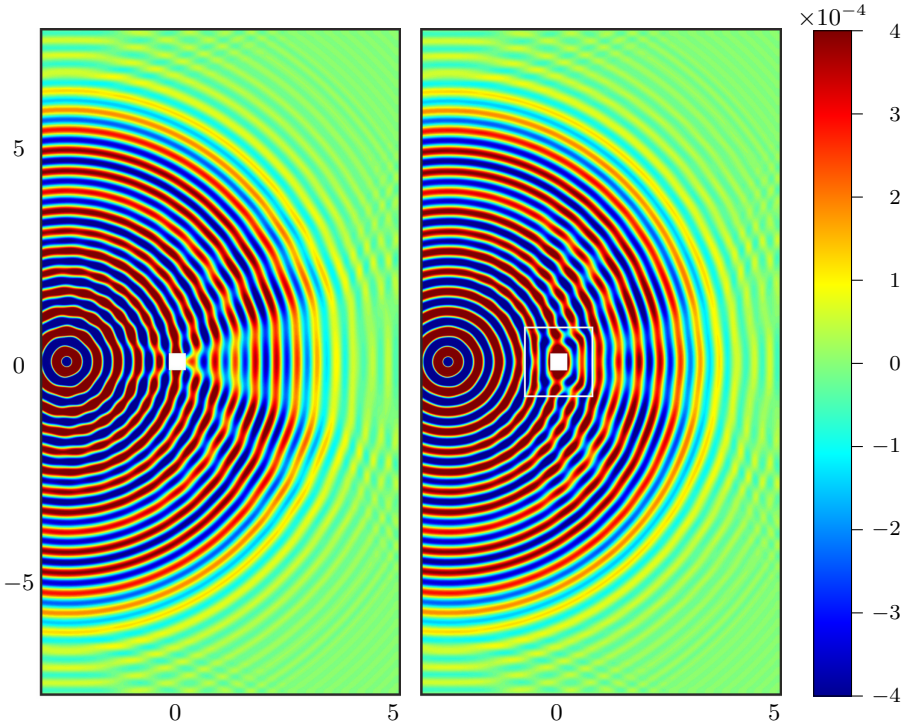

(a) *Uncloaked square hole* **(b)** *Cloaked square hole (TTWP)*

Figure 8.1: Displacement map w (in m) computed numerically at $t = 155$ ms for $\omega = 300$ rad/s: a) uncloaked square hole; b) performance of a cloak obtained through the Theoretical Transformation Without Prestress (TTWP). The square-shaped white contour sketched in b) indicates the external boundary of the cloak.

The displacement map of a TTWP cloak computed at $t = 155$ ms for $\omega = 300$ rad/s is displayed in Figure 8.1b, to be compared with that reported in Figure 8.1a for a plate with an uncloaked hole. In the latter diagram, a wake is evident just on the right-hand side of the hole as well as a perturbed wave pattern on the left-hand side due to reflection caused by the hole. Those two features have been eliminated by the cloak that is able to regularise the wavefront emerging from the device into the ex-

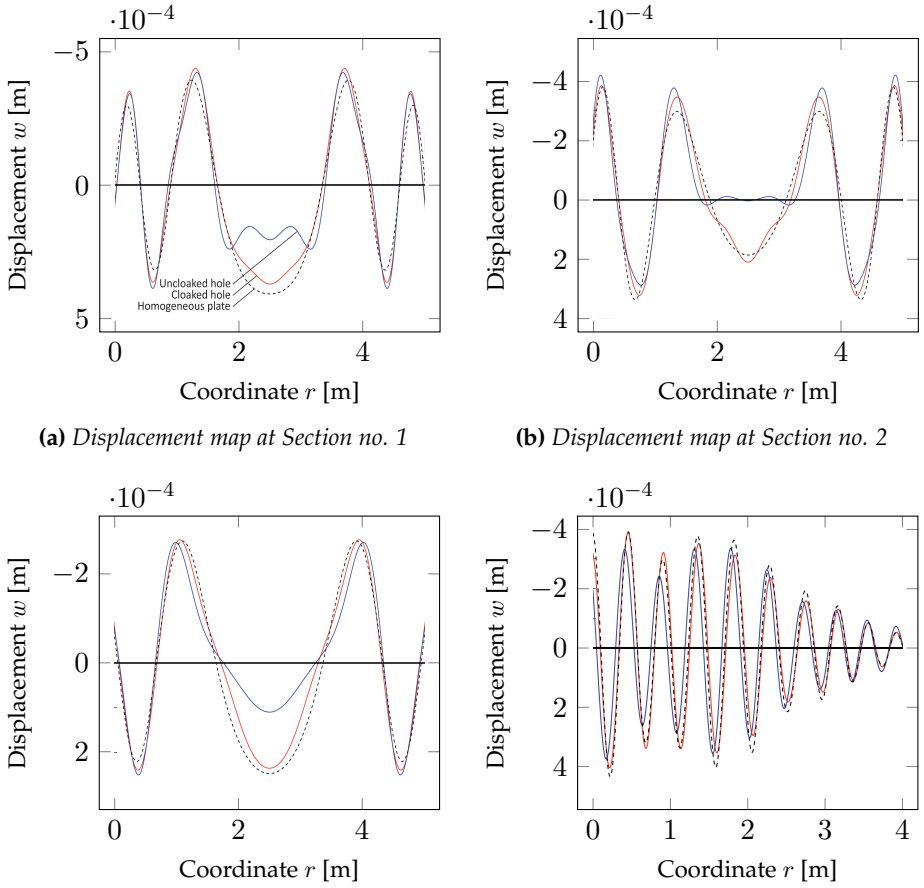

(a) *Displacement map at Section no. 1*

(b) *Displacement map at Section no. 2*

(c) *Displacement map at Section no. 3*

(d) *Displacement map at Section no. 4*

Figure 8.2: Displacement map w (in m) computed at $t = 155$ ms for $\omega = 300$ rad/s along the four Sections sketched in Figure 7.2. Comparison between solutions for a cloaked (TTWP–red line) and an uncloaked (blue line) hole. The dashed line represents the response of a homogeneous plate without the hole.

pected circular pattern and minimise back scattering. A cloak following the transformation with prestress, see equations (7.5)-(7.6), would have produced a circular wavefront matching that of a homogeneous plate as presented by [25].

In order to appraise more in detail the quality of the cloaking, Figure 8.2 reports the out-of-plane displacement w for the four sections plotted in Figure 7.2; the first three sections are transverse with respect to the propagation of the wave, at a distance from the centre of the hole of 1.25 m (Section no. 1), 1.75 m (Section no. 2) and 3 m (Section no. 3); the fourth one runs longitudinally from a point at 0.25 m just outside the right-hand boundary of the cloak to the external side of the plate. In all plots, the red line, which describes the displacements of the TTWP cloak, follows quite well the dashed line representing the response of the square, holeless, homogeneous plate $\mathcal{K}$. Figure 8.2d shows that the approximate cloak is able to reproduce quite satisfactorily the phase of the wave of the homogeneous plate/perfect cloak at points in the region just after the cloaked region, to confirm the remark on Figure 8.1b that the TTWP cloak is able to reconstruct the circular wavefront.

In order to measure quantitatively the *quality* of the cloak we adopt the index [25]

$$\mathcal{Q} = \frac{\int_{\varsigma} |w^{\mathrm{FE}}(r) - w^{\mathrm{Hom}}(r)|^2 \, dr}{\int_{\varsigma} |w^{\mathrm{Hom}}(r)|^2 \, dr}, \tag{8.1}$$

that is computed along the relevant section ς that is described by the coordinate r. Perfection corresponds to $\mathcal{Q} = 0$. In equation (8.1), the terms w^{FE} are the displacements computed by the numerical model for the non-homogeneous case under investigation and w^{Hom} corresponds to the solution for the homogeneous plate. With reference to the four sections displayed in Figure 8.2, it turns out that the quality indices are those reported in Table 8.1, showing that the cloaked solutions are on average 5.95 times more effective than the uncloaked ones, therefore a good result is in any case obtained.

The effect of an amount of twisting stiffness on the displacement map of a cloak TTWP is displayed in Figure 8.3 where several increasing values of the parameter D_{xyxy} are analysed. The plot on the far left of the first row is the one reported in Figure 8.1b. The detrimental effect of this parameter is readily observed. A quality factor can also be computed for the

Section	$\mathcal{Q}^{\text{cl}}$	$\mathcal{Q}^{\text{uncl}}$
1	0.0340	0.1149
2	0.0296	0.1701
3	0.0270	0.1389
4	0.0329	0.3071

Table 8.1: Quality index for the four sections reported in Figure 8.2 .

displayed cases. For Section no. 2, $\mathcal{Q}$ increases from 0.1241 (second panel) to 1.348 (far right panel) showing a constant worsening in the response of the meta-plate. In Section 8.2, a strategy to minimise the twisting stiffness of a fibre-composite microstructured plate is illustrated.

A similar analysis can be reiterated for the coupling stiffness D_{xxyy}. This term plays an unexpected important role as revealed by the simulations reported in Figure 8.4 where TTWP meta-plates are implemented, but possessing a D_{xxyy} whose point-wise value corresponds to 90%, 50% and 10% of the theoretical one. Unexpected because, on the one hand, in a rational microstructured plate design where the principal bending stiffnesses D_{xxxx} and D_{yyyy} are matched first, the coupling term simply results as an outcome of the choices made previously; on the other hand, the mathematical transformation generally predicts values of this parameter that are remarkably larger than those that can be reasonably reachable for an orthotropic plate (see Section 8.2, where the list of theoretical stiffnesses are reported for two selected cases). The three panels displayed in the figure clearly demonstrate the relevance of the coupling bending stiffness in assuring an accurate behaviour of the cloak.

The last picture of this Section, namely Figure 8.5, refers to a TTWP cloak subjected to point-loads pulsating at different ω, to show that the approximate model is behaving well for a quite broad range of frequencies. The time of computation t differs from one picture to the other in order to compare a similar displacement pattern. For all displayed cases, the meta-plate is able to reconstruct satisfactorily the circular wavefront.

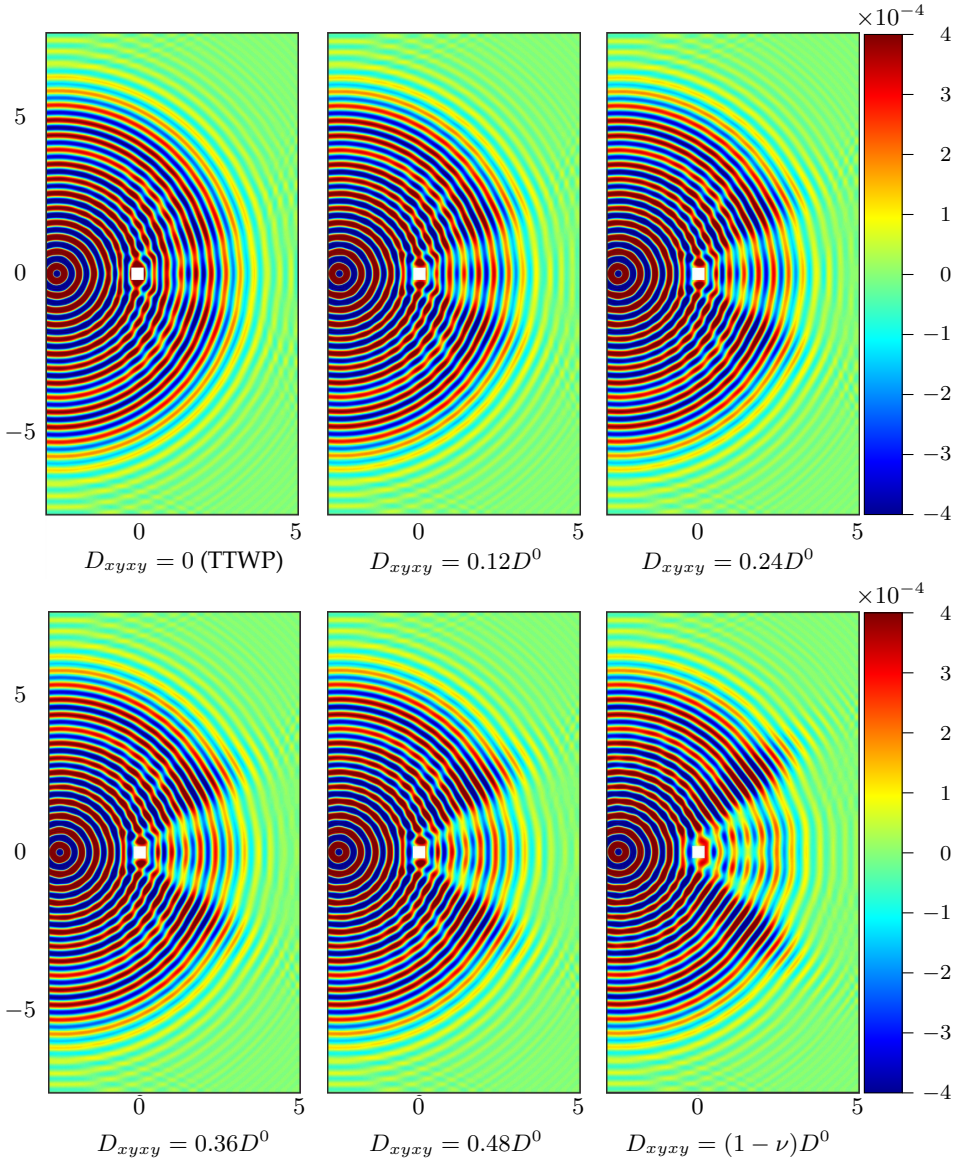

Figure 8.3: Displacement map w (in m) computed numerically at $t = 155$ ms for $\omega = 300$ rad/s carried out for increasing twisting stiffness D_{xyxy}. The detrimental effect on the cloaking performance of an increase in this parameter is clearly evident.

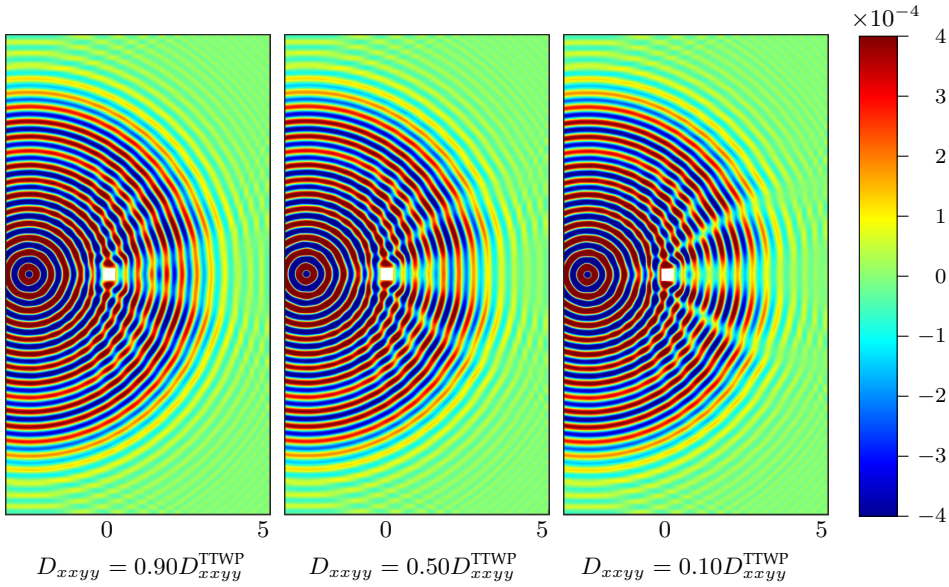

Figure 8.4: Displacement map w (in m) computed numerically at $t = 140$ ms for $\omega = 300$ rad/s carried out for decreasing coupling bending stiffness D_{xxyy}. D^{TTWP}_{xxyy} indicates the value of the variable predicted by the theoretical transformation. The damaging effect on the cloaking performance of a decrease in this parameter is clearly evident.

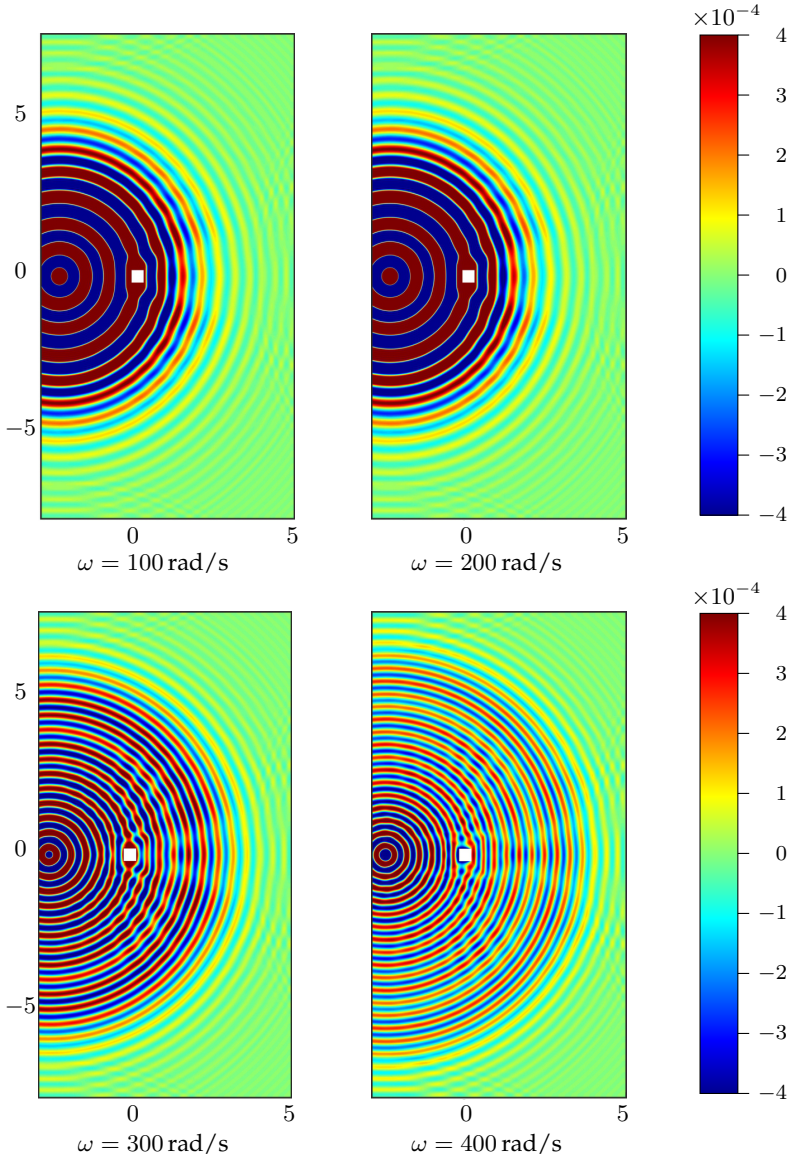

Figure 8.5: Displacement maps w (in m) computed numerically at frequencies $\omega = 100,\ 200,\ 300,\ 400$ rad/s (at different times t in order to compare a similar displacement pattern) for a TTWP cloak.

8.1.3 Flexural cloaks on Winkler substrates

In real applications, cloaks are likely grounded to a substrate which also provides the support of the object to hide. The cloaking features of a plate resting on a Winkler foundation is analysed in Figure 8.6 for $\omega = 300$ rad/s at $t = 145$ ms. In Figure 8.6b, the TTWP cloak rests on a bed of springs whose subgrade modulus is constant ($k_W = k_W^0$). This assumption clearly worsens the performance of the device with respect to the uncloaked hole case depicted in Figure 8.6a. Conversely, the position-dependent stiffness $k_W(x_p)$, whose value in $\mathcal{C}$ follows equation (7.7), guarantees a satisfactory behaviour of the device, as it can be noted that the wavefront reconstructs correctly after the transformed domain. Similarly to the simply-supported plate, solutions along two sections (i.e. no. 2 and no. 4 in Figure 7.2a) are studied in Figure 8.7. The quality index for the two sections are $\mathcal{Q}_2^{\text{cl}} = 0.0134$, $\mathcal{Q}_2^{\text{uncl}} = 0.1719$ and $\mathcal{Q}_4^{\text{cl}} = 0.0164$, $\mathcal{Q}_4^{\text{uncl}} = 0.3304$, respectively. Again, the behaviour of the perfect cloak, both in phase and amplitude, is captured remarkably well by the approximate one with position-dependent subgrade modulus. This shows that a correct design of a flexural cloak resting on a substrate requires the presence of a variable subgrade modulus that follows the provision of the theoretical transformation.

As a final remark of this Section, one must note that the employed geometrical, elastic and loading conditions correspond to a chosen prototype geometry, but the scale of the dimensions, and the load intensity and frequency can be changed to obtain an identical behaviour on a different scaled structure subjected to different load conditions.

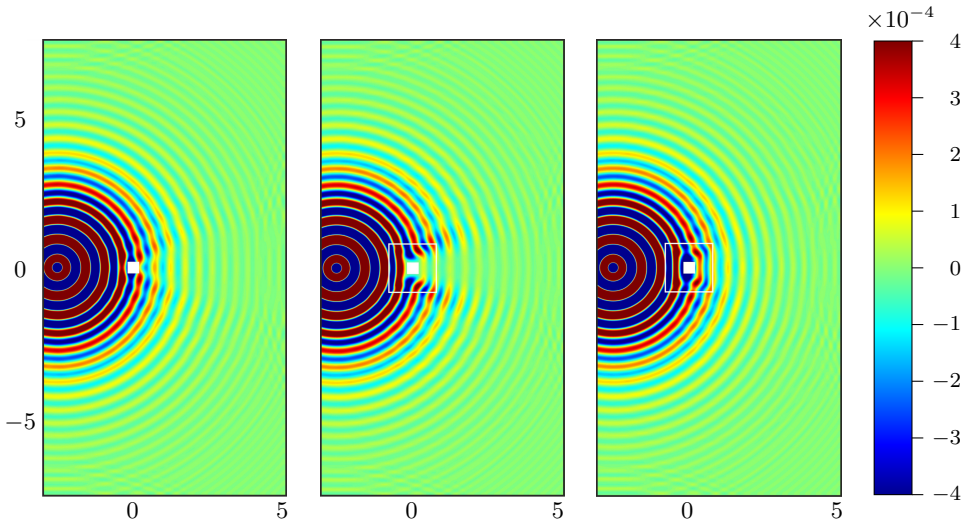

(a) *Uncloaked square hole; Winkler foundation (constant k_w)*

(b) *Cloaked square hole (TTWP); Winkler foundation (constant k_w)*

(c) *Cloaked square hole (TTWP); Winkler foundations (k_w follows eq. (7.7))*

Figure 8.6: Displacement maps w (in m) computed numerically at $t = 145$ ms for $\omega = 300$ rad/s. a) Uncloaked square hole where the plate rests on a Winkler foundation with $k_W^0 = 0.5 \cdot 10^6$ N/m^3; b) hole cloaked by a plate obtained through the TTWP resting on a Winkler foundation with a constant $k_W = k_W^0$; c) same as b), but with a position-dependent subgrade module whose value follows equation (7.7). The square-shaped white contour indicates the external boundary of the cloak.

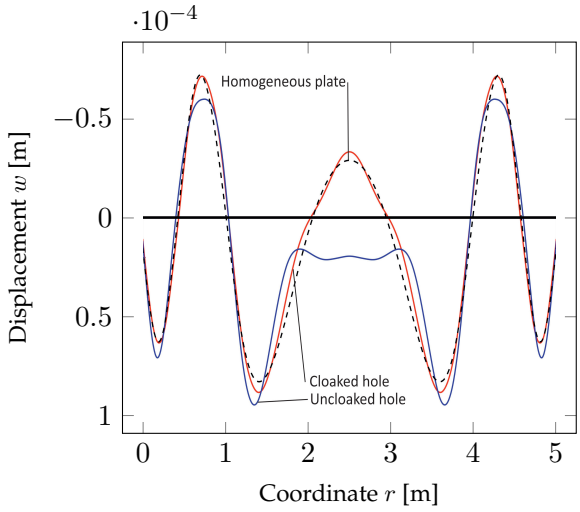

(a) *Displacement map at Section no. 2*

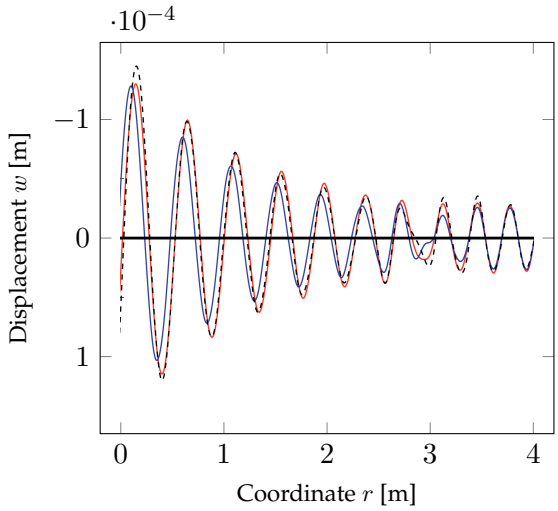

(b) *Displacement map at Section no. 4*

Figure 8.7: Displacement map w (in m) at $t = 145$ ms for $\omega = 300$ rad/s along Sections no. 2 (a) and no. 4 (b) in Fig. 7.2, for a plate resting on a Winkler soil with $k_W^0 = 0.5 \cdot 10^6$ N/m^3. Comparison between solutions for a cloaked hole (red line, TTWP with position-dependent subgrade module, eq. (7.7)) and an uncloaked one (blue line) . The dashed line represents the response of a homogeneous plate without the hole.

8.2 An example of a microstructured plate cloak

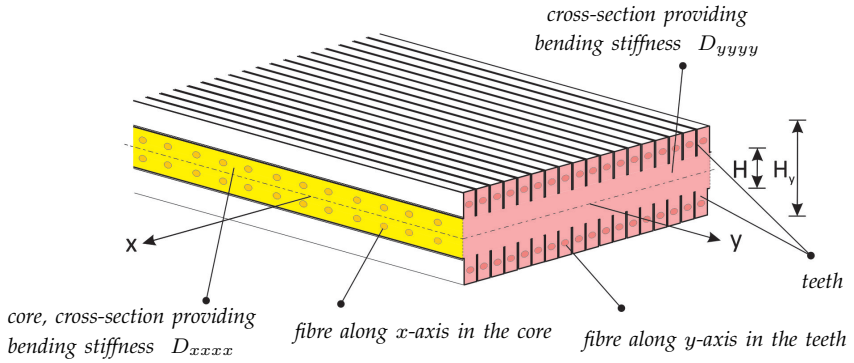

Figure 8.8: Local microstructure of the meta-plate for cloaking flexural waves. The yellow (resp. pink) cross section provides the bending stiffness D_{xxxx} (resp. D_{yyyy}). Axes x and y correspond to the local principal directions of orthotropy. The teeth density is n/H.

A design based on a microstructured meta-plate is here proposed with the aim of matching locally the principal bending stiffnesses D_{xxxx} and D_{yyyy}, and limiting the twisting stiffness D_{xyxy}. The exercise is conducted by assuming a high-performance fibre-reinforced material whose epoxy matrix (shortened as 'ep'; material parameters: $E_{\rm ep} = 3.4$ GPa, $\nu_{\rm ep} = 0.3$, $\rho_{\rm ep} = 1200$ kg/m^3) is stiffened by long boron fibres (shortened as 'B'; material parameters: $E_{\rm B} = 380$ GPa, $\nu_{\rm B} = 0.13$, $\rho_{\rm B} = 2600$ kg/m^3) [48, 70].

As can be seen in Figure 8.8, the meta-plate is such that the cross-section orthogonal to axis x is compact (and corresponds to the 'core', indicated with 'c') with its thickness matching the height H and fibres aligned along axis x. On the contrary, the cross-section orthogonal to axis y features a set of tiny rectangular appendices, in the number of n over a length equal to H, on both the outer sides, called 'teeth' (shortened as 't'). The total height of core and teeth is H_y.

The reason for selecting rectangular appendices lies in the stringent requirement of limiting the twisting stiffness. The slenderness of the teeth may lead to instability on the side of the plate in compression, however this issue is not further addressed here. Fibres are here aligned along

axis y only in the teeth. Along both directions, fibres are locally measured out (their volume fractions are spatially-varying design variables that are however capped at 0.8) to allow the relevant cross-section to reach the needed bending stiffness.

In the spirit of the Kirchhoff-Love theory for plates, the core material is subjected to a plane-stress state, therefore the linear elastic constitutive equations read

$$\begin{aligned}
\sigma_{xx} &= \frac{E_{\mathrm{c}1}}{1-\nu^{\mathrm{c}}_{xy}\nu^{\mathrm{c}}_{yx}}\varepsilon_{xx} + \frac{\nu^{\mathrm{c}}_{xy}E_{\mathrm{c}2}}{1-\nu^{\mathrm{c}}_{xy}\nu^{\mathrm{c}}_{yx}}\varepsilon_{yy},\\
\sigma_{yy} &= \frac{E_{\mathrm{c}2}}{1-\nu^{\mathrm{c}}_{xy}\nu^{\mathrm{c}}_{yx}}\varepsilon_{yy} + \frac{\nu^{\mathrm{c}}_{xy}E_{\mathrm{c}2}}{1-\nu^{\mathrm{c}}_{xy}\nu^{\mathrm{c}}_{yx}}\varepsilon_{xx},\\
\tau_{xy} &= G_{\mathrm{c}}\gamma_{xy},
\end{aligned}$$

whereas the teeth undergo a uniaxial stress (i.e. $\sigma^{\mathrm{t}}_{yy} = E_{\mathrm{t}}\varepsilon_{yy}$). All constitutive parameters of the composite in both core and teeth follow the rule of mixtures applied to composite materials, [2] however more sophisticated models (e.g. Halpin-Tsai model described in [40]) can be adopted for their estimation.

The effective stiffnesses D^{clk}_{ijkl} appearing in the cloak moment/curvature constitutive equations (defined in equation (7.9))

$$\begin{aligned}
m_{xx} &= -D^{\mathrm{clk}}_{xxxx}w_{,xx} - D^{\mathrm{clk}}_{xxyy}w_{,yy},\\
m_{yy} &= -D^{\mathrm{clk}}_{yyyy}w_{,yy} - D^{\mathrm{clk}}_{xxyy}w_{,xx},\\
m_{xy} &= -D^{\mathrm{clk}}_{xyxy}w_{,xy},
\end{aligned}$$

can be calculated by applying the standard methodology of integrating

[2] In particular, $E_{\mathrm{c}1}$, ν^{c}_{xy} follow the weighted average $(\cdot)_\xi = (\cdot)_{\mathrm{B}}c^\xi_{\mathrm{B}} + (\cdot)_{\mathrm{ep}}c^\xi_{\mathrm{ep}}$, whereas $E_{\mathrm{c}2}$, G_{c} and G_{t} obey the harmonic average $1/(\cdot)_\xi = c^\xi_{\mathrm{B}}/(\cdot)_{\mathrm{B}} + c^\xi_{\mathrm{ep}}/(\cdot)_{\mathrm{ep}}$, with $\xi \in \{\mathrm{c},\mathrm{t}\}$; $\nu^{\mathrm{c}}_{yx} = \nu^{\mathrm{c}}_{xy}E_{\mathrm{c}2}/E_{\mathrm{c}1}$.

locally stresses across the plate thickness. The integration leads to

$$\begin{aligned} D^{\mathrm{clk}}_{xxxx} &= D^0 R \frac{E_{\mathrm{c}1}}{E_{\mathrm{c}2}}, \\ D^{\mathrm{clk}}_{xxyy} &= D^0 R \nu^{\mathrm{c}}_{xy}, \\ D^{\mathrm{clk}}_{xyxy} &= G_{\mathrm{c}} \frac{H^3}{6} + G_{\mathrm{t}} \frac{H_y - H}{6} \left(\frac{H}{n}\right)^2, \\ D^{\mathrm{clk}}_{yyyy} &= D^0 \left[R + (1-\nu^2) \frac{E_{\mathrm{t}}}{E} \left[\left(\frac{H_y}{H}\right)^3 - 1 \right] \right], \end{aligned} \tag{8.2}$$

where $R = (E_{\mathrm{c}2}/E)(1-\nu^2)/(1-\nu^{\mathrm{c}}_{xy}\nu^{\mathrm{c}}_{yx})$.

Point [m]	**Theoretical requirement**			**Design parameters**			**Cloak parameters**	
	$\frac{D_{yyyy}}{D^0}$	$\frac{D_{xxxx}}{D^0}$	$\frac{D_{xxyy}}{D^0}$	$c^{\mathrm{c}}_{\mathrm{B}}$	$c^{\mathrm{t}}_{\mathrm{B}}$	$\frac{H_y}{H}$	$\frac{D^{\mathrm{clk}}_{xxyy}}{D^0}$	$\frac{D^{\mathrm{clk}}_{xyxy}}{D^0}$
A* (0.75, 0.00)	1.115	0.7207	0.897	0.4318	0.766	1.23	0.0059	0.0201
B* (0.10, 0.00)	71.385	0.1802	3.586	0.1006	0.796	3.81	0.0047	0.0186
C** (0.425, 0.425)	1.737	0.5565	0.983	0.3312	0.799	1.32	0.0054	0.0175
D* (0.10, 0.10)	183.2	0.1802	5.74	0.1006	0.799	5.19	0.0047	0.0217

Table 8.2: Microstructural parameters of the boron/epoxy cloak for the transformation whose parameters are $a = 0.1$ m, $b = 0.65$ m, $\varepsilon a = 0.025$ m, $L = 0.75$ m. The calculations are for $n = 5$. *: at this point, the principal system of orthotropy is aligned with Ox_1x_2; **: at this point, the principal directions of orthotropy are rotated of an angle $\theta_C = 0.343$ rad $(19°632)$ with respect to Ox_1x_2.

Point [m]	Theoretical requirement			Design parameters			Cloak parameters	
	$\frac{D_{yyyy}}{D^0}$	$\frac{D_{xxxx}}{D^0}$	$\frac{D_{xxyy}}{D^0}$	$c_{\mathrm{B}}^{\mathrm{c}}$	$c_{\mathrm{B}}^{\mathrm{t}}$	$\frac{H_y}{H}$	$\frac{D_{xxyy}^{\mathrm{clk}}}{D^0}$	$\frac{D_{xyxy}^{\mathrm{clk}}}{D^0}$
A* (0.75, 0.00)	1.300	0.455	0.769	0.269	0.770	1.23	0.0051	0.0158
B* (0.1923, 0.00)	591.7	0.059	5.92	0.0263	0.799	7.66	0.0045	0.0261
C** (0.4712, 0.4712)	3.370	0.260	0.936	0.150	0.787	1.53	0.0048	0.0143
D* (0.1923, 0.1923)	1938	0.059	10.71	0.0263	0.799	11.37	0.0045	0.0342

Table 8.3: Microstructural parameters of the boron/epoxy cloak for the transformation whose parameters are $a = 0.1923$ m, $b = 0.5577$ m, $\varepsilon a = 0.025$ m, $L = 0.75$ m. The calculations are for $n = 5$. *: at this point, the principal system of orthotropy is aligned with Ox_1x_2; **: at this point, the principal directions of orthotropy are rotated of an angle $\theta_C = 0.282$ rad $(16°171)$ with respect to Ox_1x_2.

With reference to the square transformation displayed in Figure 7.1b, the properties of the two cross-sections of the microstructured plate can be defined as follows:

1) the function $c_{\mathrm{B}}^{\mathrm{c}}(x_1, x_2)$ is computed through equation $(8.2)_1$ in which $D_{xxxx}(x_1, x_2)$ replaces the current entry on the left-hand side of the equation. The resulting expression is a cubic in the unknown. For the typical involved parameter $D_{xxxx}(x_1, x_2)$, there is always a solution in the range $0 < c_{\mathrm{B}}^{\mathrm{c}} \leq 0.8$;

2) equation $(8.2)_4$ can now be employed to compute H_y (or alternatively $c_{\mathrm{B}}^{\mathrm{t}}(x_1, x_2)$) in which $D_{yyyy}(x_1, x_2)$ appears on the left-hand side of the equation. In a practical case, the usual choice is to set $c_{\mathrm{B}}^{\mathrm{t}} = 0.8$ and then H_y is to be calculated;

3) the teeth density n/H should be selected so that the twisting stiffness can be estimated via equation $(8.2)_3$.

Eventually, the coupling term D_{xxyy}^{clk} can be computed through equation $(8.2)_2$.

The outcome of the design is shown in Tables 8.2 and 8.3 with reference to two transformations whose parameters are (both with $L = 0.75$ m): (i) $a = 0.1$ m, $b = 0.65$ m and $\varepsilon a = 0.025$ m, and (ii) $a = 0.1923$ m, $b = 0.5577$ m and $\varepsilon a = 0.025$ m (i.e. the one studied in the numerical simulations). It can be noted that in all control points listed in the tables, the value of D^{clk}_{xxyy} is orders of magnitude smaller than the theoretical one.

CHAPTER 9

Conclusions

"A new scientific truth does not triumph by convincing its opponents and making them see the light, but rather because its opponents eventually die, and a new generation grows up that is familiar with it."

Max Planck

9.1 Instability of piecewise-smooth systems

The problem of the stability of piecewise-smooth dynamical systems subject to non-conservative follower forces has been investigated. In particular, the counterintuitive and unexpected behaviour of special piecewise-linear systems, which are unstable even though each subsystem composing the entire structure is stable, has been proved to be possible also in 2 d.o.f. mechanical systems.

Moreover, a sufficient instability criterion has been found for 2 d.o.f. piecewise mechanical structures, associated with the presence of an invariant cone in the phase portrait of the given system. Furthermore, several properties of the aforementioned invariant manifold have been proved in the specific case of 2 d.o.f. mechanical structures, that lead to a link between the presence of an unstable equilibrium configuration and the attractivity of the invariant cone. This latter feature is crucial to state that the unstable behaviour, previously found only as a theoretical example, can also be an effective realistic phenomenon that can be observed in experiments and the real world. Furthermore, a new physical interpretation

of this form of instability has been found, revealing the practical reason why this evolution can be achieved. In fact, the bounded oscillations in time of the mechanical energy of each stable subsystem (a necessary feature deriving from the non-conservative follower force) can be "summed up" in such a way the mechanical energy for the entire composed structure reveals an exponential growth, leading to a *flutter-like* instability for the piecewise system. Hence, the presence of a non-conservative source has been proved to be crucial for the achievement of this unexpected behaviour.

A numerical method has been developed for the determination of an invariant cone in the phase portrait of a given 2 d.o.f. piecewise-linear mechanical system. In this way, the problem can be solved *a priori*, without any specific calculation of the solution and, primarily, without following the evolution in time to understand when the switching to another subdomain occurs. On the contrary, a specific invariant cone can be determined through this numerical method and a set of different mechanical systems can be studied in a sort of bifurcation analysis, such that a semi-analytical criterion of instability can be defined.

A 2 d.o.f. structure composed of a rigid bar subject to a follower force and constrained to move, without damping, on a doubly circular profile has been investigated in depth and several numerical analyses have been performed, to determine the unstable evolution in time in the neighbourhood of the equilibrium point. In particular, the presence of the predicted invariant cone has been verified through the explicit integration of the equations of motion and an extension from piecewise-linear to nonlinear system has been shown from a numerical point of view.

The three initial questions, exposed in the Introduction 1.1 and motivating the investigation of this topic, have been answered above. Concerning the fourth question, it has been partially neglected and it actually represents the starting point for new research, since the goal of this work has been the theoretical investigation of this phenomenon. Despite the adopted strong mathematical approach, the idea that motivated this work has been the translation of the purely theoretical results present in the literature to more useful instruments for future mechanical applications. In the "researcher dilemma" between studying the theoretical problem in depth and with only a few conceptual examples or, on the contrary, obtaining a simpler overview on the hard mathematical topic preferring a more prac-

tical approach, the former way has been followed, without a few doubts.

However, the computational approach presented in Chapter 5 is sufficiently general to deal with a great number of different 2 d.o.f. mechanical systems. New piecewise structures can be found and analysed, in order to obtain the same unexpected instability. Moreover, the mathematical model can be extended to cover other physical phenomena (such as internal and external dumping, viscosity, plasticity...) or more complex structures with more than 2 degrees of freedom. Furthermore, other forms of instability can be investigated, e.g. those leading to "higher order" invariant cones, for which the Poincaré map is defined by more than two half-maps. Also the numerical tools can be extended and improved to reduce the computational time.

This strong mathematical approach leads to a theoretical background that allows possible future extensions of this work for real application. From a practical perspective, the unusual behaviour exposed in this Thesis can be used when the goal is obtaining an unstable structure, e.g. in energy harvesting or soft actuators. In these cases, instability can be achieved also when the subsystems are stable, hence the domain of the design parameters is enlarged and this fact provides greater freedom to the engineers in the design of piecewise structures.

9.2 Cloaking of flexural waves

The engineering of a meta-structural cloak for elastic flexural waves based on transformation elastodynamics is an exceptional challenge that theoretically would require the implementation of unfeasible compressive prestresses and in-plane body forces to warrant equilibrium. Therefore, reasonable assumptions should be adopted that are however grounded on the following main points: (i) the meta-plate has a locally orthotropic response with (ii) an almost vanishing twisting stiffness, (iii) spatially-varying bending stiffnesses and (iv) density. In addition, the structure invariably would interact with a substrate.

With the aim of dealing with a fully open simulation tool, a FE code is developed and implemented with the specific purpose of studying transient wave propagation in locally orthotropic Kirchhoff-Love plates. A subparametric technique is adopted for spatial discretization, whereas the

approximation in the time domain is performed with the single-step time-integration algorithm Generalized-α method.

The performance of a prototype meta-plate square cloak based on the approximate assumption of null prestress is then assessed parametrically by focusing especially on the role of the twisting stiffness and the coupling bending stiffness. The reason is that while the local principal bending rigidities can be matched quite easily in a microstructured plate, for those two parameters the process is much more difficult.

The simulations show that for an effective cloaking response, the twisting stiffness should be lower than 10% of the bending one for the homogeneous plate, while for the coupling bending stiffness a departure of 10% from the theoretical value already worsens with some evidence the performance of the meta-plate.

A second contribution of this work consists in the extension of the general theory of thin-plate cloaks to comprise interaction of the meta-structure with an elastic substrate via Winkler-foundation model. The conclusion is that the subgrade modulus transforms similarly to the mass density of the plate. The numerical simulations confirm this finding and clearly show that a constant modulus beneath the cloak jeopardizes dramatically the functionality of the structure.

The Finite Element tool can be further expanded to embed inelastic responses of plate and substrate, thus enabling simulations of approximate supported meta-plates subjected to transient waves arising from seismic shocks.

APPENDIX A

Canonical Jordan form

Let's consider a $n \times n$ matrix $\boldsymbol{A} \in \mathbb{C}^{n \times n}$ and a scalar $\lambda_j \in \mathbb{C}$. Each non-trivial vector $\boldsymbol{v}_j \in \mathbb{C}^n$ that fulfils the equation

$$\boldsymbol{A}\boldsymbol{v}_j = \lambda_j \boldsymbol{v}_j, \tag{A.1}$$

is called an *eigenvector* of $\boldsymbol{A}$, while the associated scalar λ_j is called *eigenvalue* of $\boldsymbol{A}$. The solution of (A.1) in terms of eigenvalues can be obtained imposing that the characteristic polynomial $\mathcal{P}(\lambda)$ of the matrix $\boldsymbol{A}$ vanishes, i.e.

$$\begin{aligned}\mathcal{P}(\lambda) &= \det\left[\boldsymbol{A} - \lambda \boldsymbol{I}\right] = \\ &= (\lambda - \lambda_1)^{r_1} (\lambda - \lambda_2)^{r_2} \cdots (\lambda - \lambda_m)^{r_m} = \prod_{h=1}^{m} (\lambda - \lambda_h)^{r_h} = 0.\end{aligned}$$

The problem (A.1) admits n eigenvalues but, in general, only $m \leq n$ of them have distinct values. The exponent r_h is called the *algebraic multiplicity* of the eigenvalue λ_h, while the number γ_h of linearly independent eigenvectors $\boldsymbol{v}_{h,s}$, with $s = 1, 2, \ldots \gamma_h$, that can be associated with λ_h, is called *geometric multiplicity* of the h-th eigenvalue.

The geometric multiplicity is always not greater than the algebraic multiplicity, i.e. $\gamma_h \leq r_h$, and, in particular, if $r_h \neq \gamma_h$, the matrix $\boldsymbol{A}$ is called *defective*. However, for any eigenvalue λ_h, a set of $(r_h - \gamma_h)$ *generalised eigenvectors* can be found, that are obtained by solving the iterative

problem

$$
\begin{aligned}
(\boldsymbol{A} - \lambda_h \boldsymbol{I})\, \boldsymbol{v}_{h,s}^{(1)} &= 0, \\
(\boldsymbol{A} - \lambda_h \boldsymbol{I})\, \boldsymbol{v}_{h,s}^{(2)} &= \boldsymbol{v}_{h,s}^{(1)}, \\
(\boldsymbol{A} - \lambda_h \boldsymbol{I})\, \boldsymbol{v}_{h,s}^{(3)} &= \boldsymbol{v}_{h,s}^{(2)}, \\
&\vdots
\end{aligned}
$$

while the set of eigenvectors and generalised eigenvectors is called the *Jordan chain*.

A $n \times n$ matrix $\boldsymbol{A} \in \mathbb{C}^{n \times n}$ can generally be written in the *canonical Jordan form* as

$$\boldsymbol{A} = \boldsymbol{U} \overline{\boldsymbol{A}} \boldsymbol{U}^{-1},$$

where $\boldsymbol{U}$ is an invertible $n \times n$ matrix and $\overline{\boldsymbol{A}}$ is the block matrix

$$\overline{\boldsymbol{A}} = \begin{bmatrix} \boldsymbol{J}_1 & \boldsymbol{0} & \cdots & \boldsymbol{0} \\ \boldsymbol{0} & \boldsymbol{J}_2 & \cdots & \boldsymbol{0} \\ \vdots & \vdots & \vdots & \vdots \\ \boldsymbol{0} & \boldsymbol{0} & \cdots & \boldsymbol{J}_m \end{bmatrix},$$

where each sub-matrix $\boldsymbol{J}_h$, for $h = 1, 2, \ldots m$, is called *Jordan blocks*. The dimension of the h-th Jordan block is equal to the algebraic multiplicity r_h of the h-th eigenvalue λ_h of the matrix $\boldsymbol{A}$, while the number m of the blocks is equal to the number of distinct eigenvalues. Each Jordan block $\boldsymbol{J}_h$ can be written as

$$\boldsymbol{J}_h = \begin{bmatrix} \boldsymbol{J}_{h,1} & \boldsymbol{0} & \cdots & \boldsymbol{0} \\ \boldsymbol{0} & \boldsymbol{J}_{h,2} & \cdots & \boldsymbol{0} \\ \vdots & \vdots & \vdots & \vdots \\ \boldsymbol{0} & \boldsymbol{0} & \cdots & \boldsymbol{J}_{h,p} \end{bmatrix},$$

where the sub-matrices $\boldsymbol{J}_{h,s}$, for $s = 1, 2, \ldots, p$, are called *Jordan sub-blocks*. The number p of Jordan sub-block in each $\boldsymbol{J}_h$ Jordan block is equal to the geometric multiplicity γ_h of the h-th eigenvalue λ_h of the matrix $\boldsymbol{A}$. More-

over, each sub-block $\boldsymbol{J}_{h,s}$ can be written as

$$\boldsymbol{J}_{h,s} = \begin{bmatrix} \lambda_h & 1 & 0 & \cdots & 0 & 0 \\ 0 & \lambda_h & 1 & \cdots & 0 & 0 \\ 0 & 0 & \lambda_h & \cdots & 0 & 0 \\ \vdots & \vdots & \vdots & \vdots & \vdots & \vdots \\ 0 & 0 & 0 & \cdots & \lambda_h & 1 \\ 0 & 0 & 0 & \cdots & 0 & \lambda_h \end{bmatrix}$$

and the dimension of each sub-block $\boldsymbol{J}_{h,s}$ is equal to the dimension of the Jordan chain of generalised eigenvectors that can be determined from the eigenvector $\boldsymbol{v}_{h,s}$.

The diagonalisation of a matrix is clearly a particular case of reduction to the Jordan canonical form, in fact, when the matrix is not defective and the algebraic and geometric multiplicities coincide for each eigenvalue λ_h, each sub-block $\boldsymbol{J}_{h,s}$ can be reduced to a 1×1 sub-matrix whose value is λ_h, and each matrix $\boldsymbol{J}_h$ is simply diagonal, as well as the matrix $\overline{\boldsymbol{A}}$.

The matrix $\boldsymbol{U}$, defined above for the transformation in the canonical Jordan form, contains in each column the eigenvectors belonging to the Jordan chain, associated with all the eigenvectors.

APPENDIX B

Estimation of time domain for invariant cone

The calculation of the time domain presented in Section (5.2) is crucial for the solution of the computational problem regarding the existence of invariant cones. Equation (5.20), rewritten here for the sake of convenience,

$$\sin\tau = \alpha \sin\left[\omega\tau + \phi\right], \tag{B.1}$$

must be solved in order to find a proper estimate of the bounds of the computational domain in which the numerical procedure is able to detect the presence of invariant cones. Let's observe that the values of ω, α and ϕ must be spanned in the proper ranges in which they are defined, in order to find the lowest positive solution of (B.1) in terms of τ, which is as great as possible.

While the determination of the range in which ω and ϕ must be chosen is simple, the dependency of α from the intermediate point $\boldsymbol{\xi}$ makes this problem not trivial. According to definitions (5.15), (5.17), and (5.19) performed in Section (5.20), the amplitude α can be studied as a function of $\boldsymbol{\xi}$, written as

$$\alpha = -\frac{\mathcal{R}_1}{\mathcal{R}_2} = -\sqrt{\frac{a_1^2\beta_2^2\left[a_2^2\beta_1^2\xi_2^2 + (\xi_3 - a_2\xi_4)^2\right]}{a_2^2\beta_1^2\left[a_1^2\beta_2^2\xi_2^2 + (a_1\xi_4 - \xi_3)^2\right]}}.$$

Recalling that the point $[\xi_2, \xi_4, \xi_4]$ is on a unit sphere in $\mathbb{R}^3$ (i.e. the intersection between the unit sphere in $\mathbb{R}^4$ and the switching manifold $\xi_1 = 0$), the coordinate ξ_2 can be defined as

$$\xi_2^2 + \xi_3^2 + \xi_4^2 = 1 \qquad \rightarrow \qquad \xi_2^2 = 1 - \xi_3^2 - \xi_4^2,$$

while the variable ξ_3 and ξ_4 can be further rewritten in polar coordinates as

$$\begin{cases} \xi_3 = \gamma \cos\theta \\ \xi_4 = \gamma \sin\theta \end{cases}, \qquad \gamma \in [0,1], \quad \theta \in [0, 2\pi].$$

Now, the amplitude α depends on the two variables γ and θ, but the problem can be split into two single-variable analysis, assuming a certain fixed value of θ and studying the function of γ

$$\alpha(\gamma) = -\alpha_0 \sqrt{\frac{(v_1 - u_1)\gamma^2 + u_1}{(v_2 - u_2)\gamma^2 + u_2}}, \tag{B.2}$$

where we have introduced the non-negative coefficients

$$u_1 = a_2^2\beta_1^2, \qquad u_2 = a_1^2\beta_2^2, \qquad \alpha_0 = \sqrt{\frac{a_1^2\beta_2^2}{a_2^2\beta_1^2}},$$
$$v_1 = (\cos\theta - a_2 \sin\theta)^2, \quad v_2 = (-\cos\theta + a_1 \sin\theta)^2.$$

Studying the behaviour of function (B.2) in the given domain $\gamma \in [0,1]$, one can conclude that no vertical asymptotes are present in the range $0 \leq \gamma \leq 1$, while the only stationary point is at $\gamma = 0$. Therefore, the function $\alpha(\gamma)$ is monotone in γ and this property implies that α can be considered bounded by the extreme value $\alpha(0)$ and $\alpha(1)$, hence

$$\alpha \in \left[\min\left\{ -1, -\alpha_0 \sqrt{\frac{v_1}{v_2}} \right\}, \max\left\{ -1, -\alpha_0 \sqrt{\frac{v_1}{v_2}} \right\} \right].$$

Furthermore, the ratio $\sqrt{v_1/v_2}$ clearly depends on the angle θ, therefore the amplitude α can actually be considered bounded only if this ratio has proper bounds. In particular, it can be explicitly written as

$$\sqrt{\frac{v_1(\theta)}{v_2(\theta)}} = \sqrt{\frac{(\cos\theta - a_2 \sin\theta)^2}{(-\cos\theta + a_1 \sin\theta)^2}} = \left| \frac{(\cos\theta - a_2 \sin\theta)}{(-\cos\theta + a_1 \sin\theta)} \right| \geq 0,$$

and it is clearly visible that this function is superiorly unbounded in the domain $\theta \in [0, 2\pi]$. Therefore the amplitude α is always negative and it belongs to the range $\alpha \in (-\infty, 0]$.

Bibliography

[1] V. Acary and B. Brogliato. *Numerical Methods for Nonsmooth Dynamical Systems: Applications in Mechanics and Electronics*.

[2] A. I. Ahamed and M. Lakshmanan. "Discontinuity Induced Hopf and Neimark-Sacker Bifurcations in a Memristive Murali - Lakshmanan - Chua Circuit". *International Journal of Bifurcation and Chaos* 27.6 (2017), p. 1730021. DOI: 10.1142/S021812741730021X.

[3] T. Apostol. *Multi Variable Calculus and Linear Algebra, with Applications to Differential Equations and Probability*. New York, NY: John Wiley & Sons, 1969.

[4] D. Bigoni, D. Misseroni, G. Noselli, and D. Zaccaria. "Effects of the constraint's curvature on structural instability: tensile buckling and multiple bifurcations". *Proceedings of the Royal Society A: Mathematical, Physical and Engineering Sciences* 468.2144 (2012), pp. 2191–2209. DOI: 10.1098/rspa.2011.0732.

[5] D. Bigoni, M. Gei, and A. B. Movchan. "Dynamics of a prestressed stiff layer on an elastic half space: filtering and band gap characteristic of periodic structural models derived from long-wave asymptotics". *Journal of the Mechanics and Physics of Solids* 56 (2008), pp. 2494–2520. DOI: 10.1016/j.jmps.2008.02.007.

[6] D. Bigoni, O. N. Kirillov, D. Misseroni, G. Noselli, and M. Tommasini. "Flutter and divergence instability in the Pflüger column: Experimental evidence of the Ziegler destabilization paradox". *Journal of the Mechanics and Physics of Solids* 116 (2018), pp. 99–116. DOI: 10.1016/j.jmps.2018.03.024.

[7] D. Bigoni and G. Noselli. "Experimental evidence of flutter and divergence instabilities induced by dry friction". *Journal of the Mechanics and Physics of Solids* 59.10 (2011), pp. 2208–2226. DOI: 10.1016/j.jmps.2011.05.007.

[8] V. Bolotin. *Nonconservative Problems of the Theory of Elastic Stability*. 1st ed. New York, NY: Pergamon Press, 1963.

[9] B. Brogliato. *Nonsmooth Mechanics*. Red. by E. D. Sontag and M. Thoma. Communications and Control Engineering. London: Springer London, 1999. DOI: 10.1007/978-1-4471-0557-2.

[10] M. Brun, D. J. Colquitt, I. S. Jones, A. B. Movchan, and N. V. Movchan. "Transformation cloaking and radial approximations for flexural waves in elastic plates". *New Journal of Physics* 16 (2014), p. 093020. DOI: 10.1088/1367-2630/16/9/093020.

[11] M. Brun, S. Guenneau, and A. B. Movchan. "Achieving control of in-plane elastic waves". *Applied Physics Letters* 94 (2009), p. 061903. DOI: 10.1063/1.3068491.

[12] J. C. Butcher. *Numerical methods for ordinary differential equations*. 2nd ed. Chichester, England ; Hoboken, NJ: Wiley, 2008.

[13] N. V. Butenin, Y. I. Neimark, and Fufàev, N.A. *Introducion a la Toeria de Oscilaciones no lineales*. Moscow: Mir, 1987.

[14] V. Carmona, E. Freire, E. Ponce, and F. Torres. "Bifurcation of invariant cones in piecewise linear homogeneous systems". *International Journal of Bifurcation and Chaos* 15.8 (2005), pp. 2469–2484. DOI: 10.1142/S0218127405013423.

[15] V. Carmona, E. Freire, E. Ponce, and F. Torres. "On simplifying and classifying piecewise-linear systems". *IEEE Transactions on Circuits and Systems I: Fundamental Theory and Applications* 49.5 (2002), pp. 609–620. DOI: 10.1109/TCSI.2002.1001950.

[16] V. Carmona, E. Freire, E. Ponce, and F. Torres. "The continuous matching of two stable linear systems can be unstable". *Discrete & Continuous Dynamical Systems - A* 16.3 (2006), pp. 689–703. DOI: 10.3934/dcds.2006.16.689.

[17] V. Carmona and F. Fernández-Sánchez. "Integral characterization for Poincaré half-maps in planar linear systems". *Journal of Differential Equations* 305 (2021), pp. 319–346. DOI: 10.1016/j.jde.2021.10.010.

[18] V. Carmona, E. Freire, and S. Fernández-García. "Periodic orbits and invariant cones in three-dimensional piecewise linear systems". *Discrete & Continuous Dynamical Systems - A* 35.1 (2015), pp. 59–72. DOI: 10.3934/dcds.2015.35.59.

[19] Y. Chen, J. Hu, and G. L. Huang. "A design of active elastic metamaterials for control of flexural waves using the transformation method". *Journal of Intelligent Materials Systems and Structures* 27 (2016), pp. 1337–1347. DOI: 10.1177/1045389X15590273.

[20] R. Chiappinelli. "What Do You Mean by "Nonlinear Eigenvalue Problems"?" *Axioms* 7.2 (2018), p. 39. DOI: 10.3390/axioms7020039.

[21] J. Chung and G. Hulbert. "A family of single-step Houbolt time integration algorithms for structural dynamics". *Computer Methods in Applied Mechanics and Engineering* 118 (1994), pp. 1–11. DOI: 10.1016/0045-7825(94)90103-1..

[22] J. Chung and G. Hulbert. "A Time Integration Algorithm for Structural Dynamics with Improved Numerical Dissipation: The Generalized-alpha Method". *Journal of Applied Mechanics* 60 (1993), pp. 371–375. DOI: 10.1115/1.2900803.

[23] L. Clarke, Y. Ledyaev, R. Stern, and P. Woelenski. *Nonsmooth Analysis and Control Theory*. Springer New York, 1998.

[24] A. Climente, D. Torrent, and J. Sanchez-Dehesa. "Analysis of flexural wave cloaks". *AIP Advances* 6 (2016), p. 121704. DOI: 10.1063/1.4968611.

[25] D. J. Colquitt et al. "Transformation elastodynamics and cloaking for flexural waves". *Journal of the Mechanics and Physics of Solids* 72 (2014), pp. 131–143. DOI: 10.1016/j.jmps.2014.07.014.

[26] A. Darabi, A. Zareei, M.-R. Alam, and M. J. Leamy. "Experimental Demonstration of an Ultrabroadband Nonlinear Cloak for Flexural Waves". *Physical Review Letters* 121 (2018), p. 174301. DOI: 10.1103/PhysRevLett.121.174301.

[27] M. Di Bernardo, ed. *Piecewise-smooth dynamical systems: theory and applications*. Applied mathematical sciences 163. London: Springer, 2008.

[28] Y. Do, S. D. Kim, and P. S. Kim. "Stability of fixed points placed on the border in the piecewise linear systems". *Chaos, Solitons & Fractals* 38.2 (2008), pp. 391–399. DOI: 10.1016/j.chaos.2006.11.022.

[29] K. Efstathiou, X. Liu, and H. W. Broer. "The Boundary-Hopf-Fold Bifurcation in Filippov Systems". *SIAM Journal on Applied Dynamical Systems* 14.2 (2015), pp. 914–941. DOI: 10.1137/140988887.

[30] M. Farhat, S. Guenneau, and S. Enoch. "Ultrabroadband elastic cloaking in thin plates". *Physical Review Letters* 103 (2009), p. 024301. DOI: 10.1103/PhysRevLett.103.024301.

[31] M. Farhat, S. Guenneau, S. Enoch, and A. B. Movchan. "Cloaking bending waves propagating in thin elastic plates". *Physical Review B* 79 (2009), p. 033102. DOI: 10.1103/PhysRevB.79.033102.

[32] A. F. Filippov. *Differential Equations with Discontinuous Righthand Sides*. Ed. by F. M. Arscott. Red. by M. Hazewinkel. Vol. 18. Mathematics and Its Applications. Dordrecht: Springer Netherlands, 1988. DOI: 10.1007/978-94-015-7793-9.

[33] E. Freire, E. Ponce, F. Rodrigo, and F. Torres. "Bifurcation Sets of Continuous Piecewise Linear Systems with Two Zones". *International Journal of Bifurcation and Chaos* 08.11 (1998), pp. 2073–2097. DOI: 10.1142/S0218127498001728.

[34] G. Futhazar, W. J. Parnell, and A. N. Norris. "Active cloaking of flexural waves in thin plates". *Journal of Sound and Vibration* 356 (2015), pp. 1–19. DOI: 10.1016/j.jsv.2015.06.023.

[35] M. Gei. "Elastic waves guided by a material interface". *European Journal of Mechanics-A/Solids* 27 (2008), pp. 328–345. DOI: 10.1016/j.euromechsol.2007.10.002.

[36] D. Giaouris, S. Maity, S. Banerjee, V. Pickert, and B. Zahawi. "Application of Filippov Method for the Analysis of Subharmonic Instability in dc-dc Converters". *International Journal of Circuit Theory and Applications* 37.8 (2009), pp. 899–919. DOI: 10.1002/cta.505.

[37] P. Glendinning. "Less Is More I: A Pessimistic View of Piecewise Smooth Bifurcation Theory". *Extended Abstracts Spring 2016*. Ed. by A. Colombo, M. Jeffrey, J. T. Lázaro, and J. M. Olm. Vol. 8. Cham: Springer International Publishing, 2017, pp. 71–75. DOI: 10.1007/978-3-319-55642-0_13.

[38] C. Glocker. *Set-Valued Force Laws*. Berlin, Heidelberg: Springer Berlin Heidelberg, 2001. DOI: 10.1007/978-3-540-44479-4.

[39] J. Guckenheimer and P. Holmes. *Nonlinear Oscillations, Dynamical Systems, and Bifurcations of Vector Field*. 1st ed. Applied mathematical sciences 42. Springer, 1983.

[40] J. C. Halpin and J. L. Kardos. "Halpin-Tsai equations: a review". *Polymer Engineering and Science* 16 (1976), pp. 344–352. DOI: 10.1002/pen.760160512.

[41] H. A. Hosham. "Bifurcation of limit cycles in piecewise-smooth systems with intersecting discontinuity surfaces". *Nonlinear Dynamics* 99.3 (2020), pp. 2049–2063. DOI: 10.1007/s11071-019-05400-z.

[42] H. A. Hosham. "Bifurcations in four-dimensional switched systems". *Advances in Difference Equations* 2018.1 (2018), p. 388. DOI: 10.1186/s13662-018-1850-1.

[43] H. A. Hosham. "Cone-like Invariant Manifolds for Nonsmooth Systems". PhD thesis. Universitat zu Koln, 2011.

[44] T. Hughes. *The Finite Element Method - Linear Static and Dynamic Finite Element Analysis*. Prentice Hall., 1987.

[45] F. Imbert. *Analyse des Structures par Elements Finis*. Cepadues Editions, 1979.

[46] A. Johann, H.-P. Kruse, F. Rupp, and S. Schmitz, eds. *Recent Trends in Dynamical Systems: Proceedings of a Conference in Honor of Jürgen Scheurle*. Vol. 35. Springer Proceedings in Mathematics & Statistics. Basel: Springer Basel, 2013. DOI: 10.1007/978-3-0348-0451-6.

[47] T. Kalmár-Nagy, R. Csikja, and T. A. Elgohary. "Nonlinear analysis of a 2-DOF piecewise linear aeroelastic system". *Nonlinear Dynamics* 85.2 (2016), pp. 739–750. DOI: 10.1007/s11071-016-2719-z.

[48] A. Kaw. *Mechanics of Composite Materials*. Taylor & Francis Group, 2006.

[49] O. N. Kirillov. *Nonconservative stability problems of modern physics*. De Gruyter studies in mathematical physics 14. Berlin ; Boston: Walter de Gruyter GmbH & Co., KG, 2013.

[50] R. V. Kohn, H. Shen, M. S. Vogelius, and M. I. Weinstein. "Cloaking via change of variables in electric impedance tomography". *Inverse Problems* 24 (2008), p. 015016. DOI: 10.1088/0266-5611/24/1/015016.

[51] T. Küpper and H. Hosham. "Reduction to invariant cones for non-smooth systems". *Mathematics and Computers in Simulation* 81.5 (2011), pp. 980–995. DOI: 10.1016/j.matcom.2010.10.004.

[52] T. Küpper. "Invariant cones for non-smooth dynamical systems". *Mathematics and Computers in Simulation* 79.4 (2008), pp. 1396–1408. DOI: 10.1016/j.matcom.2008.03.010.

[53] Y. A. Kuznetsov, S. Rinaldi, and A. Gragnani. "One-Parameter Bifurcations in Planar Filippov Systems". *International Journal of Bifurcation and Chaos* 13.8 (2003), pp. 2157–2188. DOI: 10.1142/S0218127403007874.

[54] Y. A. Kuznetsov. *Elements of Applied Bifurcation Theory*. 2nd ed. Vol. 112. Applied mathematical sciences. New York: Springer-Verlag, 1998.

[55] C. Lanczos. *The Variational Principle of Mechanics*. 4th ed. Dover Books on Physics. Toronto: Dover Publications Inc.

[56] R. Leine and D. van Campen. "Bifurcation phenomena in non-smooth dynamical systems". *European Journal of Mechanics - A/Solids* 25.4 (2006), pp. 595–616. DOI: 10.1016/j.euromechsol.2006.04.004.

[57] R. I. Leine and H. Nijmeijer. *Dynamics and Bifurcations of Non-Smooth Mechanical Systems*. Red. by F. Pfeiffer and P. Wriggers. Vol. 18. Lecture Notes in Applied and Computational Mechanics. Berlin, Heidelberg: Springer Berlin Heidelberg, 2004. DOI: 10.1007/978-3-540-44398-8.

[58] H. Leipholz. *Stability Theory*. Wiesbaden: Vieweg+Teubner Verlag, 1987. DOI: 10.1007/978-3-663-10648-7.

[59] S. Lekhnitskii, S. Tsai, and T. Cheron. *Anisotropic Plates*. New York: Gordon and Breach, 1968.

[60] M. Liu and W. D. Zhu. "Nonlinear tranformation-based broadband cloaking for flexural waves in elastic thin plates". *Journal of Sound and Vibration* 445 (2019), pp. 270–287. DOI: 10.1016/j.jsv.2018.12.025.

[61] J. Llibre, D. D. Novaes, and M. A. Teixeira. "Limit Cycles Bifurcating from the Periodic Orbits of a Discontinuous Piecewise Linear Differentiable Center with Two Zones". *International Journal of Bifurcation and Chaos* 25.11 (2015), p. 1550144. DOI: 10.1142/S0218127415501448.

[62] J. Llibre, D. D. Novaes, and M. A. Teixeira. "On the birth of limit cycles for non-smooth dynamical systems". *Bulletin des Sciences Mathématiques* 139.3 (2015), pp. 229–244. DOI: 10.1016/j.bulsci.2014.08.011.

[63] J. Llibre and M. A. Teixeira. "Periodic orbits of continuous and discontinuous piecewise linear differential systems via first integrals". *São Paulo Journal of Mathematical Sciences* 12.1 (2018), pp. 121–135. DOI: 10.1007/s40863-017-0064-x.

[64] J. Llibre and M. A. Teixeira. "Piecewise linear differential systems with only centers can create limit cycles?" *Nonlinear Dynamics* 91.1 (2018), pp. 249–255. DOI: 10.1007/s11071-017-3866-6.

[65] J. Llibre and M. A. Teixeira. "Piecewise linear differential systems without equilibria produce limit cycles?" *Nonlinear Dynamics* 88.1 (2017), pp. 157–164. DOI: 10.1007/s11071-016-3236-9.

[66] G. W. Milton, M. Briane, and J. R. Willis. "On cloaking for elasticity and physical equations with a transformation invariant form". *New Journal of Physics* 8 (2006), p. 248. DOI: 10.1088/1367-2630/8/10/248.

[67] D. Misseroni, G. Noselli, D. Zaccaria, and D. Bigoni. "The deformation of an elastic rod with a clamp sliding along a smooth and curved profile". *International Journal of Solids and Structures* 69-70 (2015), pp. 491–497. DOI: 10.1016/j.ijsolstr.2015.05.004.

[68] D. Misseroni, D. J. Colquitt, A. B. Movchan, N. V. Movchan, and I. S. Jones. "Cymatics for the cloaking of flexural vibrations in a structures plate". *Scintific Reports* 6 (2016), p. 23929. DOI: 10.1038/srep23929.

[69] D. Misseroni, A. B. Movchan, and D. Bigoni. "Omnidirectional flexural invisibility of multiple interacting voids in vibrating elastic plates". *Proceedings of the Royal Society A* 475 (2019), p. 2229. DOI: 10.1098/rspa.2019.0283.

[70] A. Mroz. "Stability analysis of a plane, rectangular, boron-epoxy laminated plate basing on strength properties determined by different methods". *Mechanics and Mechanical Engineering* 15 (2011), pp. 161–181.

[71] L. Ning, Y.-Z. Wang, and Y.-S. Wang. "Active control cloak of the elastic wave metamaterial". *International Journal of Solids and Structures* 202 (2020), pp. 126–135. DOI: 10.1016/j.ijsolstr.2020.06.009.

[72] A. N. Norris and A. L. Shuvalov. "Elastic cloaking theory". *Wave Motion* 48 (2011), pp. 525–538. DOI: 10.1016/j.wavemoti.2011.03.002.

[73] J. O'Neill, O. Selsil, R. C. McPhedran, A. B. Movchan, and N. V. Movchan. "Active cloaking of inclusions for flexural waves in thin elastic plates". *The Quarterly Journal of Mechanics and Applied Mathematics* 68 (2015), pp. 263–288. DOI: 10.1093/qjmam/hbv007.

[74] T. S. Parker and L. O. Chua. *Practical Numerical Algorithms for Chaotic Systems*. New York, NY: Springer New York, 1989. DOI: 10.1007/978-1-4612-3486-9.

[75] J. Petera and J. Pittman. "Isoparametric Hermite Elements". *International Journal for Numerical Methods in Engineering* 3 (1994), pp. 3489–3519. DOI: 10.1002/nme.1620372006.

[76] K. B. Petersen and M. S. Pedersen. *The Matrix Cookbook*. 2021.

[77] M. Petyt. *An introduction to the Finite Element Method*. Cambridge University Press, 1990.

[78] J. Reddy. *An introduction to the Finite Element Method*. 2nd ed. McGraw-Hill, 1993.

[79] R. Seydel. *Practical Bifurcation and Stability Analysis*. Vol. 5. Interdisciplinary Applied Mathematics. New York, NY: Springer New York, 2010. DOI: 10.1007/978-1-4419-1740-9.

[80] D. J. Simpson. "A compendium of Hopf-like bifurcations in piecewise-smooth dynamical systems". *Physics Letters A* 382.35 (2018), pp. 2439–2444. DOI: 10.1016/j.physleta.2018.06.004.

[81] D. J. Simpson, D. S. Kompala, and J. D. Meiss. "Discontinuity induced bifurcations in a model of Saccharomyces cerevisiae". *Mathematical Biosciences* 218.1 (2009), pp. 40–49. DOI: 10.1016/j.mbs.2008.12.005.

[82] D. J. W. Simpson. *Bifurcations in piecewise-smooth continuous systems*. World Scientific series on nonlinear science. Series A, Monographs and treatises v. 70. New Jersey: World Scientific, 2010.

[83] N. Stenger, M. Wilhelm, and M. Wegener. "Experiments on elastic cloaking in thin plates". *Physical Review Letters* 108 (2012), p. 014301. DOI: 10.1103/PhysRevLett.108.014301.

[84] S. Timoshenko and S. Woinowsky-Krieger. *Theory of plates and shells*. McGraw-Hill, New York, 1959.

[85] S. Wagon, ed. *Mathematica in Action*. New York, NY: Springer New York, 2010. DOI: 10.1007/978-0-387-75477-2.

[86] D. Weiss, T. Küpper, and H. Hosham. "Invariant manifolds for nonsmooth systems". *Physica D: Nonlinear Phenomena* 241.22 (2012), pp. 1895–1902. DOI: 10.1016/j.physd.2011.07.012.

[87] D. Weiss, T. Küpper, and H. Hosham. "Invariant manifolds for non-smooth systems with sliding mode". *Mathematics and Computers in Simulation* 110 (2015), pp. 15–32. DOI: 10.1016/j.matcom.2014.02.004.

[88] S. Wiggins. *Introduction to Applied Nonlinear Dynamical Systems and Chaos*. Texts in Applied Mathematics 2. New York, NY: Springer-Verlag, 1989.

[89] A. Zareei and M.-R. Alam. "Broadband cloaking of flexural waves". *Physical Review E* 95 (2017), p. 063002. DOI: 10.1103/PhysRevE.95.063002.

[90] H. Ziegler. *Principles of Structural Stability*. 2nd ed. Basel: Birkhäuser Basel, 1977. DOI: 10.1007/978-3-0348-5912-7.

[91] O. Zienkiewicz and R. Taylor. *The Finite Element Method*. 6th ed. Elsevier, 2005.

[92] Y. Zou, T. Kupper, and W.-J. Beyn. "Generalized Hopf Bifurcation for Planar Filippov Systems Continuous at the Origin". *Journal of Nonlinear Science* 16.2 (2006), pp. 159–177. DOI: 10.1007/s00332-005-0606-8.

In the realm of Mechanics, an increasing interest of researchers and engineers is being revealed in the analysis of unexpected mechanical features that dynamical systems may exhibit, concerning both discrete and continuous models for real structures.
In this Thesis, two completely different topics are investigated, from two different perspectives. The first part deals with the theoretical analysis of discrete mechanical systems presenting a lack of smoothness in the governing differential equations. In particular, it is proven that a piecewise-smooth mechanical system composed of two stable subsystem may exhibit an unstable behaviour and this unexpected and counterintuitive phenomenon has been associated to presence of a non-conservative follower force. A theoretical explanation of this feature has been provided, through the presence of invariant cones in the phase space of the piecewise-smooth mechanical system. Moreover, a numerical procedure has been developed for the detection of this invariant set, leading to the definition of instability criteria for this specific case.
In the second part, a computational Finite Element model based on the Galerkin Method has been developed for the investigation of continuous thin elastic plates, with the aim of shielding a void with respect to flexural waves, using a particular kind of metamaterial that behaves as an "invisibility cloak". An in-house Finite Element code has been created and the role of different parameters has been investigated in depth, through the numerical analyses performed on a square cloak.Finally, a conceptual design of a meta-structural plate has been proposed, leading to an approximated but realistic invisibility cloak.